



24649091

MICHIGAN STATE UNIVERSITY LIBRARIES



3 1293 00612 2596



This is to certify that the

dissertation entitled

Nonlinear Seismic Analysis of Steel Arch Bridges

presented by

Chung-Ming Lee

has been accepted towards fulfillment
of the requirements for

Ph. D. degree in Civil Engineering

Major professor

Date May 1, 1990

PLACE IN RETURN BOX to remove this checkout from your record.
TO AVOID FINES return on or before date due.

DATE DUE	DATE DUE	DATE DUE
FEB 08 1992 049	_____	_____
APR 25 1992	_____	_____
Jul 4 2	_____	_____
_____	_____	_____
_____	_____	_____
_____	_____	_____
_____	_____	_____

MSU Is An Affirmative Action/Equal Opportunity Institution

6119

NONLINEAR SEISMIC ANALYSIS OF STEEL ARCH BRIDGES

BY

Chung-Ming Lee

A DISSERTATION

**Submitted to
Michigan State University
in partial fulfillment of the requirements
for the degree of**

DOCTOR OF PHILOSOPHY

Department of Civil and Environmental Engineering

1990

6059867

ABSTRACT

NONLINEAR SEISMIC ANALYSIS OF STEEL ARCH BRIDGES

By

Chung-Ming Lee

This study presents a method for the nonlinear seismic analysis of steel arch bridges. The effects of either geometric or material nonlinearity have been taken into account. The effects of such nonlinearities enter in the analysis through the computation of the "resistance" of the arch ribs.

The elasto-plastic resistance of a curved beam element has been derived using the plastic potential theory as applied to stress resultants. For geometric nonlinearity, a twelve degrees of freedom incremental stiffness matrix was also derived. A computer program was prepared for the implementation of the time history analysis.

Three bridge models: Medium Span Bridge, Short Span Bridge and Long Span Bridge, based on three prototype bridges, Cold Springs Canyon Bridge (700 ft), South Street Bridge (193 ft) and New River Gorge Bridge (1700 ft), respectively, were used to obtain the numerical results. Three-dimensional models were employed to consider the nonlinear inelastic effects. Results for nonlinear elastic solution were based on two-dimensional models. The ground motion used was the artificially generated motion CIT-A2 with different amplification factors applied to induce nonlinear effects.

From time histories, it is seen that even for the nonlinear cases the responses were generally dominated by the "fundamental modes" (either in-plane or out-of-plane) except at those points where the fundamental modal response is small. The history curves of nonlinear elastic responses exhibited different periods of vibration. In general, the dominant period increased by 5% to 10% from that of the linear solution.

For the maximum force responses involving material nonlinearity, plasticity limited the magnitude of the internal force response to that as defined by the yield function. It follows that if plastic deformations are allowed, the design forces may be reduced from that which would be required if the design is to be done on a linearly elastic basis.

Time histories of work and energy distribution indicated that the dissipated damping energy (for a 1.5% damping ratio) is over 70% of the work done for all models. When the damping ratio was varied from 0.25% to 5%, the percentage of damping energy to work done changed from 50% to 96%. These observations emphasize the importance of damping in the response.

ACKNOWLEDGEMENTS

The writer wishes to express his gratitude to his academic advisor, Dr. Robert K. Wen, Professor of Civil and Environmental Engineering, Michigan State University, for his supervision and encouragement and also to members of the writer's guidance committee, Dr. George E. Mase, Dr. David H. Yen and Dr. Parviz Soroushian for their help.

Appreciation is extended to the Division of Engineering Research and the Department of Civil and Environmental Engineering at Michigan State University as well as the National Science Foundation for their generous support. The writer also owes his appreciation to his parents, Pi-Yao Lee and Chang S. J. Lee, for their financial support. Special thanks is also due his wife, Huang Shin-Hwei Lee, for her patience and spiritual support.

TABLE OF CONTENTS

	Page
LIST OF TABLES	vii
LIST OF FIGURES	viii
CHAPTER I: INTRODUCTION	1
1.1 GENERAL	1
1.2 OBJECT AND SCOPE	2
1.3 PREVIOUS STUDIES	6
1.4 NOTATION	10
CHAPTER II: ANALYSIS AND METHOD OF SOLUTION	16
2.1 GENERAL	16
2.2 EQUATIONS OF MOTION	17
2.3 METHOD OF SOLUTION	18
2.4 USE OF CONSTRAINTS AMONG NODAL DEGREES OF FREEDOM	22
2.5 RESISTANCE OF STRUCTURAL ELEMENTS	24
2.5.1 General	24
2.5.2 Linear Resistance of Curved Beam Elements	25
2.5.3 Nonlinear Elastic Resistance of Curved Beam Elements	26
2.5.4 Elasto-Plastic Resistance of Curved Beam Elements	27
2.5.4.1 General	27
2.5.4.2 Plastic Potential Function	28
2.5.4.3 Plastic Deformation of Member Ends	29
2.5.4.4 Tangent Stiffness Matrix of Member	31
2.5.4.5 Elastic Return	31
2.5.4.6 Incremental Resistance and Deformations of Elasto-Plastic Element	32
2.6 PLASTIC WORK DENSITIES AND DUCTILITY FACTORS	36
2.6.1 Plastic Work Densities	36
2.6.2 Ductility Factors	38
2.7 WORK AND ENERGY DISTRIBUTION CHECK	39
CHAPTER III: APPLICATIONS AND NUMERICAL RESULTS	50
3.1 GENERAL	50
3.2 COMPUTER PROGRAM	50
3.3 MODELS OF BRIDGE AND GROUND MOTION USED	51
3.4 MATERIAL NONLINEAR PROBLEMS	53

	Page
3.4.1 General	53
3.4.2 Typical Displacement Time Histories	53
3.4.2.1 Medium Span Bridge (MSB)	54
3.4.2.2 Short Span Bridge (SSB)	55
3.4.2.3 Long Span Bridge (LSB)	56
3.4.3 Maximum Displacements	56
3.4.4 Typical Force Time Histories	58
3.4.4.1 Medium Span Bridge (MSB)	58
3.4.4.2 Short Span Bridge (SSB)	59
3.4.4.3 Long Span Bridge (LSB)	59
3.4.5 Maximum Forces and Force Reduction Factors	61
3.4.6 Typical Work and Energy Distribution Time Histories	62
3.4.7 Variation of Energy Distribution with Different Damping Ratio	64
3.4.8 Inelastic Responses Versus Linear Response Factor	64
3.5 GEOMETRIC NONLINEAR PROBLEMS	66
3.5.1 General	66
3.5.2 Typical Displacement Time Histories	66
3.5.2.1 Medium Span Bridge (MSB)	66
3.5.2.2 Short Span Bridge (SSB)	67
3.5.2.3 Long Span Bridge (LSB)	68
3.5.3 Maximum Displacements	68
3.5.4 Typical Force Time Histories	69
3.5.4.1 Medium Span Bridge (MSB)	69
3.5.4.2 Short Span Bridge (SSB)	70
3.5.4.3 Long Span Bridge (LSB)	70
3.5.5 Maximum Forces	71
3.5.6 Typical Work and Energy Distribution Time Histories	71
3.5.7 Instability Effects	71
 CHAPTER IV: SUMMARY AND CONCLUSION	 195
4.1 SUMMARY	195
4.2 CONCLUSION	197
 LIST OF REFERENCES	 200
 APPENDIX: PROPERTIES OF BRIDGE MODELS	 204

LIST OF TABLES

Table 3-1.	Natural Periods of Vibration	73
Table 3-2.	Elastic and Inelastic Maximum Displacements of MSB ...	74
Table 3-3.	Elastic and Inelastic Maximum Displacements of SSB ...	75
Table 3-4.	Elastic and Inelastic Maximum Displacements of LSB ...	76
Table 3-5.	Elastic and Inelastic Maximum End Forces of MSB	77
Table 3-6.	Elastic and Inelastic Maximum End Forces of SSB	77
Table 3-7.	Elastic and Inelastic Maximum End Forces of LSB	78
Table 3-8.	Maximum Responses for Various Values of Damping Ratio	79
Table 3-9.	Linear and Nonlinear Elastic Maximum Displacements of MSB	80
Table 3-10.	Linear and Nonlinear Elastic Maximum Displacements of SSB	80
Table 3-11.	Linear and Nonlinear Elastic Maximum Displacements of LSB	81
Table 3-12.	Linear and Nonlinear Elastic Maximum End Forces of MSB	82
Table 3-13.	Linear and Nonlinear Elastic Maximum End Forces of SSB	82
Table 3-14.	Linear and Nonlinear Elastic Maximum End Forces of LSB	82
Table 3-15.	Maximum Displacements for Different Values of Initial Load	83

LIST OF FIGURES

Figure 2-1.	Arch Bridge Considered	42
Figure 2-2.	Nodal Coordinates for Deck and Arch Ribs Nodes	42
Figure 2-3.	Constraint for Infinitely Large Axial Stiffnesses ...	43
Figure 2-4.	Treatment of "Rigid Column" in Mixed Nodal Coordinates system	43
Figure 2-5.	Typical Curved Beam Element	44
Figure 2-6.	Curved Beam Element End Displacements	45
Figure 2-7.	Spherical Yield Surface	45
Figure 2-8.	Member End Forces Corresponding to Displacement Changes	46
Figure 2-9.	Preliminary Definitions and Basic Operations	47
Figure 2-10.	Definition of Cross-Section	48
Figure 2-11.	Typical Member End Force Path For An Elasto-Plastic Element	49
Figure 3-1.	Medium Span Bridge Model (A "True" Three-Dimensional Model)	84
Figure 3-2.	Short Span Bridge Model (A "True" Three-Dimensional Model)	85
Figure 3-3.	Long Span Bridge Model (A "One-Plane" Model)	86
Figure 3-4.	Medium Span Bridge Model (Two-Dimensional Model)	87
Figure 3-5.	In-Plane Mode Shapes for MSB	88
Figure 3-6.	Out-of-Plane Mode Shapes for MSB and SSB	89
Figure 3-6.	(Continued) Out-of-Plane Mode Shapes for MSB and SSB	90
Figure 3-7.	In-Plane Mode Shapes for SSB	91

Figure 3-8.	In-Plane Mode Shapes for LSB	92
Figure 3-9.	Out-of-Plane Mode Shapes for LSB	93
Figure 3-10.	In-Plane Mode Shapes for Two-Dimensional MSB Model	94
Figure 3-11.	CIT-A2 Ground Motion	95
Figure 3-12.	Time Intervals with Inelastic Response (MSB)	96
Figure 3-13.	Time Intervals with Inelastic Response (SSB)	97
Figure 3-14.	Time Intervals with Inelastic Response (LSB)	98
Figure 3-15.	Node 5 Horizontal (X) Displacement Time History for MSB	99
Figure 3-16.	Node 17 Horizontal (X) Displacement Time History for MSB	100
Figure 3-17.	Node 31 Horizontal (X) Displacement Time History for MSB	101
Figure 3-18.	Node 5 Vertical (Y) Displacement Time History for MSB	102
Figure 3-19.	Node 17 Vertical (Y) Displacement Time History for MSB	103
Figure 3-20.	Node 31 Vertical (Y) Displacement Time History for MSB	104
Figure 3-21.	Node 5 Lateral (Z) Displacement Time History for MSB	105
Figure 3-22.	Node 17 Lateral (Z) Displacement Time History for MSB	106
Figure 3-23.	Node 31 Lateral (Z) Displacement Time History for MSB	107
Figure 3-24.	Node 11 Horizontal (X) Displacement Time History for SSB	108
Figure 3-25.	Node 13 Horizontal (X) Displacement Time History for SSB	109
Figure 3-26.	Node 23 Horizontal (X) Displacement Time History for SSB	110
Figure 3-27.	Node 11 Vertical (Y) Displacement Time History for SSB	111

Figure 3-28.	Node 13 Vertical (Y) Displacement Time History for SSB	112
Figure 3-29.	Node 23 Vertical (Y) Displacement Time History for SSB	113
Figure 3-30.	Node 11 Lateral (Z) Displacement Time History for SSB	114
Figure 3-31.	Node 13 Lateral (Z) Displacement Time History for SSB	115
Figure 3-32.	Node 23 Lateral (Z) Displacement Time History for SSB	116
Figure 3-33.	Node 12 Horizontal (X) Displacement Time History for LSB	117
Figure 3-34.	Node 18 Horizontal (X) Displacement Time History for LSB	118
Figure 3-35.	Node 24 Horizontal (X) Displacement Time History for LSB	119
Figure 3-36.	Node 12 Vertical (Y) Displacement Time History for LSB	120
Figure 3-37.	Node 18 Vertical (Y) Displacement Time History for LSB	121
Figure 3-38.	Node 24 Vertical (Y) Displacement Time History for LSB	122
Figure 3-39.	Node 12 Lateral (Z) Displacement Time History for LSB	123
Figure 3-40.	Node 18 Lateral (Z) Displacement Time History for LSB	124
Figure 3-41.	Node 24 Lateral (Z) Displacement Time History for LSB	125
Figure 3-42.	Member 1 End J (Node 5) Axial Force Time History for MSB	126
Figure 3-43.	Member 16 End I (Node 31) Axial Force Time History for MSB	127
Figure 3-44.	Member 1 End J (Node 5) In-Plane Bending Time History for MSB	128
Figure 3-45.	Member 16 End I (Node 31) In-Plane Bending Time History for MSB	129

Figure 3-46.	Member 1 End J (Node 5) Out-of-Plane Bending Time History for MSB	130
Figure 3-47.	Member 16 End I (Node 31) Out-of-Plane Bending Time History for MSB	131
Figure 3-48.	Member 9 End J (Node 11) Axial Force Time History for SSB	132
Figure 3-49.	Member 13 End I (Node 23) Axial Force Time History for SSB	133
Figure 3-50.	Member 9 End J (Node 11) In-Plane Bending Time History for SSB	134
Figure 3-51.	Member 13 End I (Node 23) In-Plane Bending Time History for SSB	135
Figure 3-52.	Member 9 End J (Node 11) Out-of-Plane Bending Time History for SSB	136
Figure 3-53.	Member 13 End I (Node 23) Out-of-Plane Bending Time History for SSB	137
Figure 3-54.	Member 5 End I (Node 12) Axial Force Time History for LSB	138
Figure 3-55.	Member 10 End J (Node 24) Axial Force Time History for LSB	139
Figure 3-56.	Member 5 End I (Node 12) In-Plane Bending Time History for LSB	140
Figure 3-57.	Member 10 End J (Node 24) In-Plane Bending Time History for LSB	141
Figure 3-58.	Member 5 End I (Node 12) Out-of-Plane Bending Time History for LSB	142
Figure 3-59.	Member 10 End J (Node 24) Out-of-Plane Bending Time History for LSB	143
Figure 3-60.	Member 4 End I (Node 10) Out-of-Plane Bending Time History for LSB	144
Figure 3-61.	Member 5 End J (Node 14) Out-of-Plane Bending Time History for LSB	145
Figure 3-62.	Work and Energy Distribution Time History for MSB (Linear Elastic)	146
Figure 3-63.	Work and Energy Distribution Time History for MSB (Inelastic)	147

Figure 3-64.	Work and Energy Distribution Time History for SSB (Linear Elastic)	148
Figure 3-65.	Work and Energy Distribution Time History for SSB (Inelastic)	149
Figure 3-66.	Work and Energy Distribution Time History for LSB (Linear Elastic)	150
Figure 3-67.	Work and Energy Distribution Time History for LSB (Inelastic)	151
Figure 3-68.	Work and Energy Distribution Time History for MSB (2-D Model) with 0.0% Damping Ratio (Inelastic)	152
Figure 3-69.	Work and Energy Distribution Time History for MSB (2-D Model) with 0.25% Damping Ratio (Inelastic)	153
Figure 3-70.	Work and Energy Distribution Time History for MSB (2-D Model) with 0.5% Damping Ratio (Inelastic)	154
Figure 3-71.	Work and Energy Distribution Time History for MSB (2-D Model) with 1.0% Damping Ratio (Inelastic)	155
Figure 3-72.	Work and Energy Distribution Time History for MSB (2-D Model) with 2.0% Damping Ratio (Inelastic)	156
Figure 3-73.	Work and Energy Distribution Time History for MSB (2-D Model) with 3.0% Damping Ratio (Inelastic)	157
Figure 3-74.	Work and Energy Distribution Time History for MSB (2-D Model) with 5.0% Damping Ratio (Inelastic)	158
Figure 3-75.	Inelastic Responses Versus Linear Response Factor for MSB	159
Figure 3-76.	Inelastic Responses Versus Linear Response Factor for SSB	160
Figure 3-77.	Inelastic Responses Versus Linear Response Factor for LSB	161
Figure 3-78.	Node 3 Horizontal (X) Displacement Time History for MSB	162



Figure 3-64.	Work and Energy Distribution Time History for SSB (Linear Elastic)	148
Figure 3-65.	Work and Energy Distribution Time History for SSB (Inelastic)	149
Figure 3-66.	Work and Energy Distribution Time History for LSB (Linear Elastic)	150
Figure 3-67.	Work and Energy Distribution Time History for LSB (Inelastic)	151
Figure 3-68.	Work and Energy Distribution Time History for MSB (2-D Model) with 0.0% Damping Ratio (Inelastic)	152
Figure 3-69.	Work and Energy Distribution Time History for MSB (2-D Model) with 0.25% Damping Ratio (Inelastic)	153
Figure 3-70.	Work and Energy Distribution Time History for MSB (2-D Model) with 0.5% Damping Ratio (Inelastic)	154
Figure	Work and Energy Distribution Time History for MSB (2-D Model) with 1.0% Damping Ratio (Inelastic)	155
Figure	Work and Energy Distribution Time History for MSB (2-D Model) with 2.0% Damping Ratio (Inelastic)	156
Figure	Work and Energy Distribution Time History for MSB (2-D Model) with 3.0% Damping Ratio (Inelastic)	157
Figure	Work and Energy Distribution Time History for MSB (2-D Model) with 4.0% Damping Ratio (Inelastic)	158
Figure	Work and Energy Distribution Time History for MSB (2-D Model) with 5.0% Damping Ratio (Inelastic)	159
Figure		
Figure		

Figure 3-79.	Node 5 Horizontal (X) Displacement Time History for MSB	163
Figure 3-80.	Node 3 Vertical (Y) Displacement Time History for MSB	164
Figure 3-81.	Node 5 Vertical (Y) Displacement Time History for MSB	165
Figure 3-82.	Node 9 Horizontal (X) Displacement Time History for SSB	166
Figure 3-83.	Node 21 Horizontal (X) Displacement Time History for SSB	167
Figure 3-84.	Node 9 Vertical (Y) Displacement Time History for SSB	168
Figure 3-85.	Node 21 Vertical (Y) Displacement Time History for SSB	169
Figure 3-86.	Node 12 Horizontal (X) Displacement Time History for LSB	170
Figure 3-87.	Node 18 Horizontal (X) Displacement Time History for LSB	171
Figure 3-88.	Node 24 Horizontal (X) Displacement Time History for LSB	172
Figure 3-89.	Node 12 Vertical (Y) Displacement Time History for LSB	173
Figure 3-90.	Node 18 Vertical (Y) Displacement Time History for LSB	174
Figure 3-91.	Node 24 Vertical (Y) Displacement Time History for LSB	175
Figure 3-92.	Member 1 End J (Node 3) Axial Force Time History for MSB	176
Figure 3-93.	Member 4 End I (Node 7) Axial Force Time History for MSB	177
Figure 3-94.	Member 1 End J (Node 3) In-Plane Bending Time History for MSB	178
Figure 3-95.	Member 4 End I (Node 7) In-Plane Bending Time History for MSB	179
Figure 3-96.	Member 2 End J (Node 9) Axial Force Time History for SSB	180

Figure 3-97.	Member 6 End I (Node 21) Axial Force Time History for SSB	181
Figure 3-98.	Member 2 End J (Node 9) In-Plane Bending Time History for SSB	182
Figure 3-99.	Member 6 End I (Node 21) In-Plane bending Time History for SSB	183
Figure 3-100.	Member 5 End I (Node 12) Axial Force Time History for LSB	184
Figure 3-101.	Member 10 End J (Node 24) Axial Force Time History for LSB	185
Figure 3-102.	Member 5 End I (Node 12) In-Plane Bending Time History for LSB	186
Figure 3-103.	Member 10 End J (Node 24) In-Plane Bending Time History for LSB	187
Figure 3-104.	Work and Energy Distribution Time History for MSB (Linear Elastic)	188
Figure 3-105.	Work and Energy Distribution Time History for MSB (Nonlinear Inelastic)	189
Figure 3-106.	Work and Energy Distribution Time History for SSB (Linear Elastic)	190
Figure 3-107.	Work and Energy Distribution Time History for SSB (Nonlinear Inelastic)	191
Figure 3-108.	Work and Energy Distribution Time History for LSB (Linear Elastic)	192
Figure 3-109.	Work and Energy Distribution Time History for LSB (Nonlinear Inelastic)	193
Figure 3-110.	"Instability" Effects for LSB	194

CHAPTER I
INTRODUCTION

1.1 GENERAL

Bridges form vital links in land transportation systems. The recent Loma Prieta Earthquake caused the collapse of more than a mile of elevated highway (essentially bridge-like structures) on I-880 and serious damage to the Bay Bridge in San Francisco. It again bespeaks the importance of seismic effects on the safety of bridges. Actually, significant damage to bridges had occurred in the 1971 San Fernando earthquake and highlighted the need for reassessment of existing seismic design practice for bridges. A series of studies had since been conducted on the safety of highway bridges under earthquake loads. Those studies have been reported for long multiple span highway bridges ([16], [35], [36], and [37]), suspension bridges ([1], [2], [3], [4], [5], and [17]), and steel deck-type arch highway bridges ([10], [11], [12], and [13]).

The study reported here represents an effort to develop a method of analysis for the nonlinear behavior of arch bridges subjected seismic loading. The two nonlinearities of structural behavior are "material nonlinearity" that originates from the plasticity of the material, and "geometric nonlinearity" (nonlinear elastic effects) which represents the effects of the distortion of the structure on its response.

1.2 OBJECT AND SCOPE

The major objective of the study is to present a method of analysis for the seismic response of arch bridges that takes into account the effects of geometric nonlinearity or material nonlinearity. Included in this objective is the development of a computer program that carries out the necessary computations for the analysis.

The second objective is to use the computer program to obtain certain numerical results based on a reasonable modelling of several real steel deck-type arch bridges subjected to earthquake motions. Included in this objective is the interpretation of the numerical results with a view to greater understanding of the seismic behavior of such bridges. It is hoped that the analysis and the computer program developed may serve as tools for further research in this area, and the numerical results presented may point to directions leading to the development of improved design procedure for such structures.

In Chapter II the structural system is introduced and the method of analysis is presented. For the analysis, the mass matrix is formulated by the lumped mass approach and the damping matrix is of the Rayleigh type. The structure system model features "mixed nodal coordinate systems": cartesian coordinates for deck nodes and curvilinear coordinates for arch rib nodes. In consequence, no coordinate transformations are needed for the beam elements as their element coordinates are the same as the system nodal coordinates. Another means employed to make the computational procedure more effective is the use of constraints that correspond to the assumption that the axial stiffnesses of certain members are infinitely large, thus reducing the number of degrees of freedom.

The effects of either geometric or material nonlinearity are included in the analysis. The computational procedures of the nonlinear "resistance" for both nonlinearities are derived. For material nonlinearity, a method of analysis is developed for the elasto-plastic resistance of a curved beam element based on the "plastic hinge" concept. The yield function is based on three stress resultants: P (axial force), M_y (in-plane bending moment) and M_x (out-of-plane bending moment). For geometric nonlinearity, a twelve degrees of freedom incremental stiffness matrix is derived.

For the solution of the equations of motion, the method is one of a step-by-step numerical integration in the time domain coupled with a Newton-Raphson scheme implying an outer loop of iteration for the equilibrium of the system. For each elasto-plastic element, an inner loop of iteration is needed because of the material nonlinearity. Measures of the inelastic response such as "curvature ductility factors" and "plastic work densities" are defined. As a check on the validity of the procedure, a work and energy balance for the system is considered. A computer program is prepared to implement the three-dimensional nonlinear seismic analysis described above.

In Chapter III three real steel deck-type arch bridges: the Cold Springs Canyon Bridge (CSCB) in California, the South Street Bridge (SSB) in Connecticut, and the New River Gorge Bridge (NRGB) in West Virginia are chosen to be the prototypes for the medium span bridge (MSB), the short span bridge (SSB), and the long span bridge (LSB) used for numerical studies. The bridges are modelled by using curved beam elements for the arch ribs, straight beam and truss elements for the deck system, columns, and bracing systems. It should be noted that while

CSCB and SSB each has two ribs with a solid box cross-section, NRGB has a single box rib with each side a truss.

"True" three-dimensional models for MSB and SSB and "one-plane" three-dimensional model [12] for LSB are used to consider material nonlinearity. For studies on geometric nonlinearity, only motions in the vertical plane of the rib(s) are considered and simplified two-dimensional models used.

The ground motion used is the artificially generated motion CIT-A2 [18] with amplification factors applied to induce nonlinear effects. Nonlinear behavior due to material inelasticity is presented first, followed by behavior due to geometric nonlinearity.

For comparison purposes, numerical results of the linear response are also obtained. The time history curves are presented for displacements (horizontal-X, vertical-Y, and lateral-Z), and for internal forces (axial force P, in-plane bending moment M_y , and out-of-plane bending moment M_x) at selected points.

From time histories, it can be seen that even for the nonlinear cases the responses were generally dominated, as expected, by the "fundamental modes" (either in-plane or out-of-plane) except at those points where the fundamental modal response is small. However, the higher modes, up to the fourth mode, can be significant. For example, the response of the vertical displacement time history at the crown point for LSB was primarily in the second and fourth in-plane mode. This fourth in-plane mode is overall the ninth mode (i.e., counting in-plane and out-of-plane modes together) for the LSB model.

For the displacement time history curves, the wave patterns for the linear elastic and nonlinear inelastic cases are quite similar. But

the wave patterns for geometric nonlinear case differ more (about 9% for the fundamental mode and lower for higher modes) because of the changes in the natural periods due to stiffness differences. The maximum displacement responses, obtained by considering either material or geometric nonlinearity, are not much different from those of the linearly elastic analysis. For all models, the maximum displacement was about 1% of the arch height in the horizontal direction, 2.5% in the vertical direction. In the lateral direction, the maximum displacement was about 8% of the arch height for MSB and 3% for SSB and LSB.

Although the wave patterns of the internal force (stress resultants) time histories are quite similar between the elastic and inelastic cases, the magnitudes of the maximum internal forces differed considerably. If inelastic behavior is allowed in the structural system, because of the definition of yield function, the internal forces (P , M_y and M_x) are bounded by the fully plastic values (P_0 , M_{y0} and M_{x0}). The maximum values of such forces were about 20% less than those obtained from a linearly elastic analysis. This "force reduction" was realized at a price of plastic deformations in the structure. This led to the consideration that, if one is willing to accept such plastic deformations, the structure could be "designed" with a "reduced load." For the geometric nonlinear cases, the wave patterns of internal force time histories, as in the case of displacement time histories, differed from the linear elastic ones. However, there is no appreciable difference in the maximum values of the internal forces obtained from the linear elastic and nonlinear elastic solutions.

During an earthquake energy is fed through the base of the structure. It is instructive to know how the energy is distributed in

the structural system during the earthquake loading. The work and energy balance equation of the system is written by setting the work done by the support reactions and by gravity loads equal to the sum of the recoverable strain energy, irrecoverable (plastic) strain energy, kinetic energy, and the energy dissipated by damping. From the work and energy distribution time histories, the dissipated damping energy (for a 1.5% damping ratio) was over 70% of the work done for all cases. When the damping ratios were varied from 0.25% to 5%, the percentages of damping energy to work done changed from 50% to 96%. In the inelastic analyses, about 15% of the work done was dissipated by irrecoverable strain energy.

1.3 PREVIOUS STUDIES

Response of arch ribs (with no deck system) to earthquake shaking was reported by Thakkar and Arya [33]. The study was limited to linearly elastic behavior of a single rib subjected to in-plane motion only. A study of the in-plane strength of deck arch bridges under longitudinal ground motion was reported by Kuranishi and Nakajima [19].

Dusseau and Wen ([10] and [11]) have reported the elastic seismic responses of two existing arch bridges: the Cold Springs Canyon Bridge (CSCB) in California and the South Street Bridge (SSB) in Connecticut. Free vibration characteristics were studied. Seismic responses in all three dimensions were estimated from a "normalized rock spectra" [16] using an input ground acceleration level of 0.50 g and 0.09 g, respectively for the California bridge and Connecticut bridge. Dusseau and Wen ([12], [13]) have also studied the effects of unequal motion at the supports of three deck arch bridges: CSCB, SSB, and New

River Gorge Bridge (NRGB) in West Virginia. In using time history analysis with step-by-step numerical integration, a "one-plane model" was introduced to decrease the number of degrees of freedom. In this model a transverse cross-section of the arch rib(s) is modelled as that of a single beam element. Thus for a two rib bridge, in lateral response, each rib would act as a flange of a beam.

A key factor in the nonlinear dynamic analysis of a bridge is the structural stiffness. Studies on the material nonlinear static behavior of a beam-column member by various investigators have been discussed in a treatise by Chen and Atsuta [6]. In particular, the yield surface for a cross-section and the behavior of a segment have been described in some detail. For elasto-plastic statical problems the concept of plastic potential theory using stress resultants as generalized stresses has been adopted by Hodge [15], Morris and Fenves [21], and others.

A method for the small displacements analysis of three-dimensional inelastic frames subjected to static loads has been described by Morris and Fenves [22]. The elements are assumed to be elastic-plastic and to yield at generalized plastic hinges, the behavior of which is governed by four dimensional curved yield surfaces. To insure that the point representing the end forces on any element does not travel outside the yield surface, when such a point reaches the surface it is drawn back a small distance and constrained to move tangent to the surface.

The dynamic response of three dimensional frames with elasto-plastic elements has been studied by Nigam [23]. The elements are assumed to yield at generalized plastic hinges governed by two

dimensional circular yield surfaces. For each load increment the increments in member end forces at each plastic hinge are constrained to move in the tangent plane to yield surface, and a new tangent stiffness is formulated for each load step. Nigam's formulation of the problem was not in matrix algebra, and consequently the equations involved are somewhat complex. A concise and general matrix form was presented by Porter and Powell [26].

A more general form of the stiffness of a beam element was derived by Wen and Farhoomand [38]. They carried out dynamic analysis of three dimensional frames in which the yielded regions were assumed to have finite length. The elasto-plastic elements are assumed to be governed by a four dimensional parabolic or elliptic plastic potential function. An iterative procedure was described that would keep the force vector on the curved yield surface during yielding. To keep the force point on the yield surface during yielding, several approaches including iterative procedures [38] and one-step approximate force corrections [29] have been proposed.

Cheng and Kitipitayangkul [7] adopted a different approach from the plastic potential theory to handle the elasto-inelastic analysis of building frames. The force-deformation relationship for each pair of generalized stress and strain was taken to be of the Ramberg-Osgood hysteretic type. However, the yield values of the various generalized stresses were governed by appropriate interaction equations such as given by Tebedge and Chen [31]. The effect of torsional moment was also included in the interactive behavior on the basis of Von Miss' yield criterion as was used in Ref. [21]. Powell and his co-workers [28] had employed two and three parallel elements to represent a single element

and thus strain hardening effects may be considered.

A number of investigators (See, for example, in [30], [19], and [42]) had formulated and analyzed the nonlinear problem at the stress, rather than stress-resultant level. Such approach, although more refined than the stress-resultant formulation, generally requires considerably more computational resource for a given physical problem.

For the consideration of geometric nonlinearities, the tangent stiffness matrix may be formed by adding the initial and geometric stiffness matrices. Many studies have been reported on the subject (e.g., [8], [24], [27], [32], and [40]). Among them Oran [24] has presented the nonlinear elastic tangent stiffness matrix of a straight beam element which is exact within the framework of the elastic beam-column theory. The expressions involve the axial force as a parameter that requires iterations for its determination. A nonlinear elastic tangent stiffness matrix based on a finite element approach [40] has been shown to be quite accurate for problems that do not involve very large displacements (for example, of the order of the dimension of the structure itself). It would cover the great majority of civil engineering structures.

A method of analysis for investigating the stability of complex structures has been described by Toridis and Khozeimeh [34]. The general approach is based on the finite element method and incremental numerical solution techniques. This incremental loading approach has been used with no equilibrium check. In the incremental solution process, the stiffness properties of the structure are continuously updated in order to properly account for large changes in the geometry of the structure (i.e., to take into account the effect of the geometry of the deformed

structure on the instantaneous stiffness matrix).

Both material and geometric nonlinearities were considered for the frame structures by Porter and Powell [26]. The geometric nonlinearity was considered in two-dimensional problems and only static loads were applied. The elasto-plastic stiffness and geometric stiffness of straight member have been derived. A general computational procedure has been described for the collapse load analysis of statically loaded plane frames and the analysis of dynamically loaded inelastic frames.

For arch buckling analysis, the linear and incremental stiffness matrices of a curved beam element deformable in three dimensional space have been described by Wen and Lange [39]. In developing a nonlinear curved beam element of general shape, the geometry of the curved axis of the element is represented by a fourth-order polynomials in terms of the inclination angle with the tangent at a member end, and the displacement functions are approximated by cubic polynomials in the same variable. The linear stiffness matrix $[k]$ and the first and second order incremental stiffness matrices, $[n1]$ and $[n2]$ were derived by differentiating the strain energy.

1.4 NOTATION

The notations shown below has been used in this report:

- A - cross-sectional area;
- B - width of the cross-section;
- b_2, b_3, b_4 - curved beam element geometry coefficients;
- $[C]$ - viscous damping matrix;
- c - subscript denoting "constrained";
- D - depth of the cross-section;

E	- Young's modulus of elasticity;
E_D	- energy dissipated by damping;
E_K	- kinetic energy;
E_{SE}	- recoverable strain energy;
E_{SP}	- irrecoverable (plastic) strain energy;
e	- superscript denoting "elastic part";
e	- subscript denoting "elastic part";
Δe_S	- incremental strain energy;
F_e	- maximum force by elastic analysis;
F_{ie}	- maximum force by inelastic analysis;
F_y	- yield stress;
g	- gravitational acceleration;
h	- time interval;
I_x	- moment of inertia about the x-axis;
I_y	- moment of inertia about the y-axis;
$[J]$	- Jacobian matrix;
$[k_t]$	- elasto-plastic tangent stiffness matrix;
$[k]; [k_0]$	- linear elastic stiffness matrix;
$[k_e]$	- elastic stiffness matrix;
$[M]$	- lumped mass matrix of the entire structure;
M_x	- bending moment about x-axis;
M_y	- bending moment about y-axis;
M_{x0}	- fully plastic bending moment about x-axis;
M_{y0}	- fully plastic bending moment about y-axis;
$[m]$	- lumped mass matrix of an element;
$[n1]$	- first order incremental stiffness matrix;
$[n2]$	- second order incremental stiffness matrix;

- P - axial force;
- P_0 - fully plastic axial force;
- p - superscript denoting "plastic part";
- p - subscript denoting "plastic part";
- (P) - external load vector;
- $(P)_s$ - external static load (dead load) vector;
- (Q) - member end force vector;
- (dq) - incremental displacement vector;
- R - radius of curvature;
- R_{Xi} - X component of reaction at support i;
- R_{Yi} - Y component of reaction at support i;
- R_{Zi} - Z component of reaction at support i;
- R_1, R_2 - radii of curvature at ends of an element;
- (R) - resistance vector;
- S_{xx} - section modulus about the x-x axis;
- S_{yy} - section modulus about the y-y axis;
- s - longitudinal axis of curved beam element;
- T - superscript denoting matrix transposition;
- t - time;
- t_f - thickness of flange;
- t_w - thickness of web;
- t_0, t_1 - beginning and end time of the time interval h;
- U_{Rx} - ground displacement component in x direction for node R;
- U_{Ry} - ground displacement component in y direction for node R;
- U_{Rz} - ground displacement component in z direction for node R;
- u - subscript denoting "unconstrained";
- u - ground motion component;

- u, v, w - displacements along x, y, z axes, respectively;
- (Δu) - incremental support or ground displacement vector;
- V_D, V_E - vertical displacement at node D and E;
- V_{hx} - hinge volume for M_x ;
- V_{hy} - hinge volume for M_y ;
- $V_{h\Delta}$ - hinge volume for P;
- (v) - relative displacement vector;
- (Δv) - incremental relative displacement vector;
- $(\Delta \dot{v})$ - incremental relative velocity vector;
- $(\Delta \ddot{v})$ - incremental relative acceleration vector;
- W_G - work done by gravity loads;
- W_R - work done by support reactions;
- (w) - total displacement vector for unconstrained degrees of freedom;
- w_{xp} - plastic work done by M_x in time interval h ;
- w_{yp} - plastic work done by M_y in time interval h ;
- $w_{\Delta p}$ - plastic work done by P in time interval h ;
- \bar{w}_p - dimensionless plastic work quantity;
- w_0 - strain energy per unit volume of material at yield;
- (Δw) - incremental displacement vector;
- $(\Delta \dot{w})$ - incremental velocity vector;
- $(\Delta \ddot{w})$ - incremental acceleration vector;
- X, Y, Z - cartesian coordinate system;
- X_g, Y_g, Z_g - ground displacement components in cartesian coordinates;
- x, y, z - curvilinear coordinate system;
- ΔX_i - incremental horizontal ground displacement at support i ;
- ΔY_i - incremental vertical ground displacement at support i ;

- ΔY_j - incremental vertical displacement of node point j;
- ΔZ_i - incremental lateral ground displacement at support i;
- α_i - parameters used for definition of displacement functions;
- α, β - constants for Rayleigh type damping matrix;
- $[\Gamma]$ - transformation matrix;
- ϵ - tolerance for yield function;
- ϵ_y - yield strain;
- $\{\epsilon_1\}$ - tolerance vector of force or moment;
- $\{\epsilon_2\}$ - tolerance vector of displacement or rotation;
- ϵ_3 - scalar tolerance of work;
- θ - angle that the tangent at the node makes with the global X-axis;
- $\theta_x, \theta_y, \theta_z$ - rotations about x, y, z axes, respectively;
- θ_{xp} - plastic rotation about x-axis;
- θ_{yp} - plastic rotation about y-axis;
- Δ_p - plastic axial displacement;
- λ - flow constant, a positive scalar;
- $\{\lambda\}$ - transformation matrix;
- $\mu_{\phi x}$ - curvature ductility factors for out-of-plane bending;
- $\mu_{\phi y}$ - curvature ductility factors for in-plane bending;
- μ_{Δ} - ductility factors for axial strain;
- Φ - yield function;
- Φ_e - linear response factor;
- ϕ - angle of the tangent measured with respect to the tangent at a reference end (Fig. 2-5);
- Δ - incremental operator;
- ∇ - prefix denoting "gradient";

- () - column vector;
- [] - row vector;
- [] - rectangular matrix;
- ($\dot{\quad}$) - $d(\quad)/dt$;
- ($\ddot{\quad}$) - $d^2(\quad)/dt^2$;

CHAPTER II
ANALYSIS AND METHOD OF SOLUTION

2.1 GENERAL

For purposes of analysis, the bridge structure is modelled by finite elements: truss, straight beam, and curved beam elements. A three-dimensional version of the model is shown in Figure 2-1. Generally, the bridge consists of two arch ribs (modelled by curved beam elements) and a deck (by straight beam elements) and columns (by truss elements) between the ribs and deck. The cross-beams between the ribs and the deck girders are modelled by straight beam elements. The other bracings are modelled by truss elements.

For the analysis, mass is lumped at the nodes. The system equation consists of the equations of motion for the unconstrained degrees of freedom of the nodes. These degrees of freedom are described in cartesian coordinates for the nodes on the deck, and curvilinear coordinates for nodes on the ribs. Thus there are two kinds of nodal coordinates: one cartesian, the other curvilinear (See Figure 2-2).

The analysis considers response due to either geometric or material nonlinearity that are associated with the curved beam elements. The straight beam and truss elements are presumed to be linearly elastic. The method of analysis is one of a step-by-step numerical integration in the time domain. Within a time increment, the method of solution is essentially one of the Newton-Raphson type which calls for

an "outer loop" of iteration for the dynamic equilibrium of the nodal degrees of freedom. In the case of elasto-plastic behavior an "inner loop" of iteration is necessary to satisfy the constitutive equation of the element involved.

In this Chapter, in addition to the method of analysis and solution, certain measures of the inelastic responses, i.e., "plastic work densities" and "ductility factors", are presented. The computation of work and energy balance is also described.

2.2 EQUATIONS OF MOTION

Let $\{w_u\}$ denote the unconstrained degrees of freedom (generally those of the interior nodes of the structure) and $\{w_c\}$ the constrained degrees of freedom (generally those of the external nodes or supports that are constrained to be equal to prescribed ground displacements). As noted previously, for a node on the deck, the equation of motion is written in the usual cartesian coordinates, and for a node on the ribs, it is written in curvilinear coordinates; See Figure 2-2. The assembled set of equations of motion or dynamic equilibrium may be written as follows:

$$\begin{bmatrix} [M_{uu}] & [M_{uc}] \\ [M_{cu}] & [M_{cc}] \end{bmatrix} \begin{Bmatrix} \{\ddot{w}_u\} \\ \{\ddot{w}_c\} \end{Bmatrix} + \begin{bmatrix} [C_{uu}] & [C_{uc}] \\ [C_{cu}] & [C_{cc}] \end{bmatrix} \begin{Bmatrix} \{\dot{w}_u\} \\ \{\dot{w}_c\} \end{Bmatrix} + \begin{Bmatrix} \{R_u\} \\ \{R_c\} \end{Bmatrix} = \begin{Bmatrix} \{P_u\} \\ \{P_c\} \end{Bmatrix} \quad (2-1)$$

in which the $[M]$'s are mass submatrices, the $[C]$'s are damping submatrices, $\{R_u\}$ and $\{R_c\}$ are resistances resulting from deformations of structural elements, $\{P_u\}$ and $\{P_c\}$ are external loads. The subscripts "u" and "c" denote "unconstrained" and "constrained"; the superscripts of "dots" denote time derivatives.

For lumped mass inertia, the cross submatrices $[M_{uc}]$ and $[M_{cu}]$ are null. It is assumed also that damping is due entirely to the velocities associated with the unconstrained degrees of freedom, i.e., $[C_{uc}] = [C_{cu}] = [0]$. Writing $[M]$ for $[M_{uu}]$, $[C]$ for $[C_{uu}]$, $\{R\}$ for $\{R_u\}$, $\{P\}$ for $\{P_u\}$, and $\{w\}$ for $\{w_u\}$, the equations of motion for the unconstrained degrees of freedom are

$$[M]\{\ddot{w}\} + [C]\{\dot{w}\} + \{R\} - \{P\} = \{0\} \quad (2-2)$$

In an earthquake response problem, the real dynamic load $\{P\}$ is in general null. The driving mechanism is contained in the resistance term $\{R\}$ which depends on the end displacements of the structural members. For members that are connected to the ground, the displacements at those ends are constrained to be equal to that of the ground motion. As those member forces change, they would disturb the equilibrium of the structure.

The detailed procedure of analysis is given in the next section.

2.3 METHOD OF SOLUTION

The equations of motion for the unconstrained degrees of freedom may be represented as:

$$\{H\}^* = [M]\{\ddot{w}\} + [C]\{\dot{w}\} + \{R\} - \{P\} = \{0\} \quad (2-3)$$

For a numerical analysis of the problem, consider the solution involved in a typical time interval h from time t_0 to time $t_1 = t_0 + h$. The equations of motion will be integrated numerically using a stable scheme, e.g., the Newmark $\beta = 1/4$ method.

$$\begin{aligned} \{\dot{w}\}_1 &= \{\dot{w}\}_0 + (h/2)(\{\ddot{w}\}_0 + \{\ddot{w}\}_1) \\ \{w\}_1 &= \{w\}_0 + (h/2)(\{\dot{w}\}_0 + \{\dot{w}\}_1) \end{aligned} \quad (2-4)$$

in which the subscripts "0" and "1" denote the beginning and end of the

time interval. Substituting Eqs. 2-4 into Eq. 2-3 for $t = t_1$, one obtains

$$\begin{aligned} \{H^* (\{w\}_1)\} - [M][\{(\Delta w) - h (\dot{w})_0\}(4/h^2) - (\ddot{w})_0] + [C][2(\Delta w)/h \\ - (\dot{w})_0] + \{R\}_0 + \{\Delta R\} - \{P\}_0 - \{\Delta P\} = \{0\} \end{aligned} \quad (2-5)$$

in which the symbol Δ is used as a modifier signifying the change of the modified quantity from t_0 to t_1 ; thus, $\{\Delta w\} = \{w\}_1 - \{w\}_0$,

$$\{\Delta R\} = \{R\}_1 - \{R\}_0, \text{ and } \{\Delta P\} = \{P\}_1 - \{P\}_0.$$

In order to compute $\{\Delta w\}$, the Newton-Raphson method of iteration is employed. For the $(k+1)$ th iteration, the procedure calls for a solution of $\delta(\{\Delta w\})_{k+1} = \{\Delta w\}_{k+1} - \{\Delta w\}_k$ from the following linear equation

$$[J(\{H\}^*, \{\Delta w\})_k] \delta(\{\Delta w\})_{k+1} = -\{H\}^*_k \quad (2-6)$$

in which $[J(\{H\}^*, \{\Delta w\})_k]$ is the Jacobian matrix of $\{H\}^*$ with respect to $\{\Delta w\}$, i.e., its i - j entry = $\partial H^*_i / \partial \Delta w_j$ with H^*_i denoting the i th element of $\{H\}^*$ and Δw_j the j th element of $\{\Delta w\}$, evaluated at $\{\Delta w\} = \{\Delta w\}_k$, and $-\{H\}^*_k$ is evaluated from Eq. 2-5 with $\{\Delta w\} = \{\Delta w\}_k$. It follows from Eq. 2-5 that

$$[J(\{H\}^*, \{\Delta w\})] = [(4/h^2)[M] + 2[C]/h + [K]_{ww}] \quad (2-7)$$

in which $[K]_{ww} = \partial(\Delta R) / \partial(\Delta w)$ = the tangent stiffness matrix.

The solution procedure for the overall problem may thus proceed as follows:

1. Perform a linear static analysis under initial static load $\{P\}_s$.
2. At time $t = 0$, set $\{R\} = \{P\}_s$, i.e., initially the structure is in equilibrium with such static load as the dead load. Set $\{w(0)\} = \{0\}$, i.e., the datum of displacement corresponds to the initial static deflection due to $\{P\}_s$. The initial

velocity $\{\dot{w}(0)\}$ is presumed known (generally equal to null). The initial acceleration vector $\{\ddot{w}(0)\}$ may be thus computed from Eq. 2-3.

3. For each time step thereafter $\{\dot{w}\}_0$ and $\{\ddot{w}\}_0$ are known. Set $\{\Delta w\}_{k=0}$ equal to the null vector (i.e., $\{w(t_1)\}_{k=0} - \{w(t_0)\}$). For the $(k+1)$ th iteration, $[K]_{ww,k}$ - the tangent stiffness matrix corresponding to $\{\Delta w\}_k$ can be updated. (One may also choose to use the "modified Newton-Raphson method" which avoids such updating but generally at the expense of more iterations.) The incremental resistance vector $\{\Delta R\}_k$ are obtained from summing the incremental resistances of the structural elements.
4. Thus $\delta(\{\Delta w\})_{k+1}$ can be solved from the set of linear equations, Eq. 2-6, and $\{\Delta w\}_{k+1}$ is computed as $\{\Delta w\}_k + \delta(\{\Delta w\})_{k+1}$. Convergence is arrived at when $\{H\}_{k+1}^* \leq \{\epsilon_1\}$ and/or $\delta(\{\Delta w\})_{k+1} \leq \{\epsilon_2\}$ and/or $(\{H\}_{k+1}^*)^T \delta(\{\Delta w\})_{k+1} \leq \epsilon_3$ in which $\{\epsilon_1\}$ is a tolerance vector consisting of preset "small" quantities of force or moment, and $\{\epsilon_2\}$ is a preset tolerance vector of displacement or rotation, and ϵ_3 is a preset scalar tolerance having the dimension of work.

For seismic analysis, $\{\Delta P\} = \{0\}$. (The case when $\{\Delta P\}$ is not null but some prescribed incremental loading vector can be incorporated in the analysis without difficulty.) Thus, as mentioned previously, the driving mechanism of the system is contained in $\{\Delta R\}$ which depends on $\{\Delta w\}$ and $\{\Delta u\}$, the incremental support or ground displacement vector. When the system is linear $\{\Delta R\} = [K]_{ww} \{\Delta w\} + [K]_{wu} \{\Delta u\}$ in which $[K]_{ww}$

and $[K]_{wu}$ are linear stiffness matrices corresponding to the degrees of freedom as represented by the subscripts. When the system is nonlinear, the determination of (ΔR) becomes a major aspect of the problem. It is discussed in the Section 2.5. The preceding analysis is applicable to cases in which different supports may undergo different motions.

For the case of uniform ground motion (over space), one may use ground acceleration directly in lieu of ground displacement as input. The motion of the unconstrained degrees of freedom are measured relative to the ground translations (rotational ground motions are not considered herein). Corresponding to the i th element of $\{w\}$, w_i , define $v_i = w_i - u_i$ in which u_i is the ground motion component expressed in the same coordinate system as w_i . For a node, say, R, in the rib, the ground displacement components in curvilinear coordinates are (See Figure 2-4)

$$\begin{aligned} U_{Rx} &= X_g \sin \theta_R - Y_g \cos \theta_R \\ U_{Ry} &= -Z_g \\ U_{Rz} &= X_g \cos \theta_R + Y_g \sin \theta_R \end{aligned} \quad (2-8)$$

in which θ_R is the angle that the tangent at the node makes with the cartesian X-axis, and X_g , Y_g , and Z_g are the ground displacement components in the cartesian coordinates. Thus Eq. 2-3 may be written as

$$\{H\} = [M]\{\ddot{v}\} + [C]\{\dot{v}\} + \{R\} - \{P\} + [M]\{\ddot{u}\} + [C]\{\dot{u}\} = \{0\} \quad (2-9)$$

Taking damping as the Rayleigh type, i.e., $[C] = \alpha[M] + \beta[K]_0$, $[K]_0$ being the linear stiffness matrix, and dropping the term $[C]\{\dot{u}\}$ (signifying an assumption that damping is due only to those motions that are relative to the ground motion), and following the procedure described previously when $\{w\}$ was used as the dependent variable, one obtains

$$[J(\{H\}, \{\Delta v\})_k] \delta(\{\Delta v\})_{k+1} = -\{H\}_k$$

$$= \{B\}_0 + [B]_1 \{\Delta v\}_k - \{\Delta R\}_k \quad (2-10)$$

in which $[J(\{H\}, \{\Delta v\})_k]$ is the Jacobian matrix of $\{H\}$ with respect to $\{\Delta v\}$ evaluated at $\{\Delta v\} = \{\Delta v\}_k$, and

$$\begin{aligned} \{B\}_0 &= [M]\{\ddot{v}\}_0 + [(\alpha + 4/h)[M] + \beta[K]_0]\{\dot{v}\}_0 - \{R\}_0 + \{P\}_s \\ &\quad - [M]\{\ddot{u}\} \end{aligned} \quad (2-11)$$

$$[B]_1 = -\{[(4/h^2) + (2\alpha/h)][M] + (2/h)\beta[K]_0\} \quad (2-12)$$

The Newton-Raphson iteration would begin with $\{\Delta v\}_{k=0} = \{0\}$. The solution procedure is entirely analogous to that previously described.

2.4 USE OF CONSTRAINTS AMONG NODAL DEGREES OF FREEDOM

In order to decrease the number of degrees of freedom of the structural model, certain constraints may be introduced among the set of degrees of freedom at a given "transverse panel" of the bridge (e.g., nodes 5, 6, 7, 8 in Figure 2-1). The constraints correspond to the assumption that the axial stiffnesses of the straight beam and truss elements involved are infinitely large. Thus, (a) the transverse (Z) displacements of the floor beam ends (see Figure 2-3) at the deck are equal, (b) the transverse (y) displacements of the cross beam ends of the rib bracing system are equal, and (c) the vertical displacements at the ends of each column are equal.

For a constraint of equality between two degrees of freedom, one may be chosen as the "master", and the other "slave". In forming the system stiffness matrix, the stiffness pertaining to the slave degree of freedom is added to that of the master degree of freedom. This can be done routinely for case (a) and (b) as each case involves the same nodal coordinate system for the two end nodes.

For case (c) consider Figure 2-4. The nodal coordinates for the

deck nodes D and E are cartesian, and the rib nodes R and Q are curvilinear. The constraints correspond to the assumption of rigid column (with pinned ends) DR and EQ, or,

$$\begin{aligned} v_D &= -u_R \cos \theta_R + w_R \sin \theta_R \\ v_E &= -u_Q \cos \theta_Q + w_Q \sin \theta_Q \end{aligned} \quad (2-13)$$

in which θ_R and θ_Q are defined in Figure 2-4. Regarding u_R , w_R , u_Q and w_Q as the master degrees of freedom, in order to transfer the vertical stiffness of the deck stringer M, partition the degrees of freedom at the two ends of element M as $\{d^*\} = [\{d_1\} ; v_D \ v_E]^T$ in which $\{d_1\}$ consists of all degrees of freedom for the element except v_D and v_E . In terms of the master degrees of freedom, the degrees of freedom for member M is $\{d\} = [\{d_1\} ; u_R \ w_R \ u_Q \ w_Q]^T$. Using Eqs. 2-13 one can write $\{d^*\} = [\Gamma]\{d\}$, in which the displacement transformation matrix:

$$[\Gamma] = \left[\begin{array}{c|cccc} [I] & & & & [0] \\ \hline [0] & -\cos \theta_R & \sin \theta_R & 0 & 0 \\ [0] & 0 & 0 & -\cos \theta_Q & \sin \theta_Q \end{array} \right] \quad (2-14)$$

The stiffnesses of M expressed in degrees of freedom of $\{d\}$ is

$$[k] = [\Gamma]^T [k^*] [\Gamma] \quad (2-15)$$

in which $[k^*]$ is the usual beam stiffness in degrees of freedom $\{d^*\}$. Of course, $[k]$ is then assembled into the system stiffness matrix in the usual fashion.

The constraints also affect the mass matrix. Denoting by $\{\dot{d}^*\}$ and $[m^*]$ the "old" velocity vector and "old" mass matrix, and $\{\dot{d}\}$ and $[m]$ the "new" velocity vector and "new" mass matrix, let the old and new velocities be related by the transformation $\{\dot{d}^*\} = \{\lambda\}\{\dot{d}\}$. By equating the kinetic energy expressed in the old system to that expressed in the

new system, one has $[m] = (\lambda)^T [m^*] (\lambda)$.

Consider the effect of the lumped mass at D, m_D . In this case, $(\dot{d}^*) = \dot{v}_D$, $[m^*] = m_D$, $(\dot{d}) = [\dot{u}_R \ \dot{w}_R]^T$ and $(\lambda)^T = [-\cos\theta_R \ \sin\theta_R]$, one obtains

$$[m] = m_D \begin{bmatrix} \cos^2\theta_R & -\sin\theta_R \cos\theta_R \\ -\sin\theta_R \cos\theta_R & \sin^2\theta_R \end{bmatrix} \quad (2-16)$$

This submatrix is assembled into the system mass matrix (to rows and columns u_R and w_R). (Hence the system mass matrix is not diagonal.) For the other constraints involving the same coordinate systems, the masses of the slave degrees of freedom are added to those of the master degrees of freedom.

2.5 RESISTANCE OF STRUCTURAL ELEMENTS

2.5.1 GENERAL

In the preceding, a method of analysis has been developed for the linear and nonlinear response of a structure in three dimensional space. In the analysis, the structural resistance vector $\{R\}$ plays a key role as it is through this vector that the nonlinear behavior is accounted for in this study. However, the behavior of straight beam and truss elements is assumed to be linearly elastic during the entire loading period. The resistance is

$$\{R\} = [k] \{q\} \quad (2-17)$$

in which $\{q\}$ is the element displacement vector and $[k]$ is the usual linear elastic stiffness and need not be presented here. In the following, resistance of the curved beam elements, making up of the major components of the bridge, is discussed first for linear behavior

and then for nonlinear elastic and elasto-plastic behavior.

2.5.2 Linear Resistance of Curved Beam Elements

The curved beam finite element model used is illustrated in Figure 2-5, in which A and B denote the two end nodes, x, y, and z represent the curvilinear coordinates. The stiffness of this element has been presented in Ref. [39], in which the curved axis of the element was represented by a fourth order polynomials in ϕ , the angle of the tangent measured with respect to the tangent at end A. The coefficients of the polynomial are determined by end slopes and curvatures as well as the coordinates of end B. Thus at a common node of two elements, continuities of slopes and curvatures can be maintained. Four independent displacement functions are considered: u (radial), v (transverse), w (tangential) translations, and θ_z (twist about tangential axis), each represented by a third order polynomials in ϕ .

Each of the four displacement functions involve four coefficients. The sixteen coefficients were determined by eight degrees of freedom at each end. For example, at end A, the three translations, u_A , v_A , w_A and three rotations θ_{xA} , θ_{yA} , θ_{zA} plus $(d\theta_z/ds)_A$ and $(dw/ds)_A$. The last two degrees of freedom are "nonessential". The twelve essential degrees of freedom are illustrated in Figure 2-6.

In this work, the nonessential degrees of freedom are condensed out before assembling into the system stiffness matrix with the usual six degrees of freedom per node in three dimensional space behavior.

The linear elastic resistance is of course simply the linear elastic stiffness (k_0) multiplied by the end displacement vector.

2.5.3 Nonlinear Elastic Resistance of Curved Beam Elements

The resistance of a nonlinear elastic element may be written as (Ref. [20])

$$\{R\} = \left([k_0] + \frac{[n_1]}{2} + \frac{[n_2]}{3} \right) \{q\} \quad (2-18)$$

in which $[n_1]$ and $[n_2]$ are the first and second order incremental stiffness matrices. The matrices $[k_0]$, $[n_1]$, and $[n_2]$ are obtained as the second derivatives of the quadratic, cubic, and quartic parts, respectively, of the strain energy expression.

The incremental or nonlinear stiffness matrices $[n_1]$ and $[n_2]$ based on the interpolation functions and sixteen degrees of freedom mentioned previously are also given in Ref. [39]. In this study, the second order incremental stiffness matrix $[n_2]$ is not used because numerical experience showed that it would make the element too stiff with unacceptable errors. In order to fit into the twelve degrees of freedom per node scheme of analysis, the 16 by 16 $[n_1]$ matrix need be condensed to 12 by 12. Since it is linear in the displacement variables, the condensed matrix is valid only for the displacement state at which the condensation is executed. For a time history analysis, this means that a condensation is needed for every time increment.

In order to save computing time, this condensation is avoided by using a twelve degrees of freedom incremental stiffness matrix. It is based on third order polynomials for the radial and transverse displacements and first order polynomials for the tangential displacement and twist about the tangential axis. They are:

$$u = \alpha_1 + \alpha_2\phi + \alpha_3\phi^2 + \alpha_4\phi^3$$

$$\begin{aligned}
 v &= \alpha_5 + \alpha_6\phi + \alpha_7\phi^2 + \alpha_8\phi^3 \\
 w &= \alpha_9 + \alpha_{10}\phi \\
 \theta_z &= \alpha_{11} + \alpha_{12}\phi
 \end{aligned}
 \tag{2-19}$$

As mentioned previously, the nonlinear elastic stiffness matrix $[n_1]$ was derived as the second derivatives of the cubic part of the strain energy expression (now corresponding to the preceding interpolation functions). Numerical experience (Ref. [39]) also indicated that in general more accurate results would be obtained if the terms containing rotations were dropped. The rotation terms include rotation about y-axis = $(du/ds) + (w/R)$ and rotation about x-axis = (dv/ds) . This modified form of $[n_1]$ was used to obtain the numerical results presented in Section 3.5.

2.5.4 Elasto-Plastic Resistance of Curved Beam Elements

2.5.4.1 General

The elasto-plastic resistance is calculated using the plastic potential theory as applied to stress resultants (Ref. [15]). Material yielding is assumed to take place only at either or both ends of the member. This is warranted if there is no load between the ends, and the offset is small in comparison with the length of the chord. The part of the element between the two ends would remain linearly elastic.

Although the plastic potential function is defined individually for each end, the tangential stiffness is derived for the entire member. The incremental resistance and the elastic and plastic parts of the deformation are obtained by an iteration process. The details of the above are given in the following sections.

2.5.4.2 Plastic Potential Function

It is assumed that the material is "associative". Thus the plastic potential function and the "yield function" are the same. The yield function defines the combination of the force components necessary to initiate yielding at a cross-section. A shape factor of 1.0 is assumed for the end sections, i.e., the cross section is assumed to make an abrupt transition from a completely elastic state to a plastic state in which unrestricted plastic flow can occur. Thus plastic yielding is confined to an individual cross section with zero "hinge length." The yield function is assumed to remain the same as yielding progresses, i.e., there is no strain hardening.

For the numerical results presented herein, the yield function Φ for a cross-section is written as:

$$\Phi - \left(\frac{P}{P_0} \right)^2 + \left(\frac{M_y}{M_{y0}} \right)^2 + \left(\frac{M_x}{M_{x0}} \right)^2 - 1 = 0 \quad (2-20)$$

in which P is the axial force, M_y the bending moment in the plane of the rib, M_x the out-of-plane bending moment or moment about the radial axis, and P_0 , M_{y0} , M_{x0} are the fully plastic force components corresponding to P , M_y , M_x , respectively. For this study, they were computed as:

$$\begin{aligned} P_0 &= F_y A \\ M_{y0} &= F_y S_{yy} \\ M_{x0} &= F_y S_{xx} \end{aligned} \quad (2-21)$$

in which F_y is the yield stress, A , S_{yy} , S_{xx} are the cross-sectional area, section moduli about the y-y and x-x axis, respectively. This yield surface, though quite idealized, provides a convenient

approximation for the complex phenomenon of inelastic behavior in the three dimensional space.

Figure 2-7 shows the spherical yield surface. Thus, in accordance with the plastic potential theory, if the "force point" $(P/P_0, M_y/M_{y0}, M_x/M_{x0})$ is inside the surface, the section is regarded as linearly elastic. If it is on the yield surface, it is plastic. It cannot go outside the yield surface.

As mentioned previously, the force-deformation properties at the end sections are not entirely independent because the elastic parts of the responses are governed by the member elastic stiffness. The member elasto-plastic properties are described in the following.

2.5.4.3 Plastic Deformation of Member Ends

The displacement increment vector at a member end can be expressed as the sum of an elastic and a plastic part:

$$(dq) = (dq^e) + (dq^p) \quad (2-22)$$

in which (dq^e) is the vector of the elastic part of the member end displacement increments and (dq^p) is the vector of the plastic part of the increments.

The member end force increments are related to the elastic member end displacement increments as follows:

$$(dQ) = [k_e](dq^e) \quad (2-23)$$

in which (dQ) is the vector of member end force increments and $[k_e]$ is the elastic stiffness matrix.

Following Drucker's normality criterion (Ref. [9]), at a point on the yield surface the incremental plastic deformation vector has the direction of the outwardly directed normal.

$$\{dq^P\} = \lambda\{\nabla\Phi\} \quad (2-24)$$

in which λ is a positive scalar, called the flow constant, which defines the magnitude of the plastic deformation at the point (plastic hinge); and $\{\nabla\Phi\}$ (gradient of function Φ) is the outwardly direction normal vector at the point on the yield surface.

As the force vector can not extend beyond the yield surface, any force increment vector $\{dQ\}$ corresponding to a plastic deformation at the cross section must move on the surface (or on the tangent plane). This requirement is expressed by the normality condition.

$$\{\nabla\Phi\}^T\{dQ\} = 0 \quad (2-25)$$

in which the superscript T denotes "transpose". Substituting Eq. 2-23 into Eq. 2-25, one obtains

$$\{\nabla\Phi\}^T[k_e]\{dq^e\} = 0 \quad (2-26)$$

Then, from Eqs. 2-22, and 2-24, one has

$$\{\nabla\Phi\}^T[k_e]\{(\{dq\}) - \{dq^P\}\} = 0 \quad (2-27)$$

$$\{\nabla\Phi\}^T[k_e]\{(\{dq\}) - \lambda\{\nabla\Phi\}\} = 0 \quad (2-28)$$

Solve for λ :

$$\lambda = \frac{\{\nabla\Phi\}^T[k_e]\{dq\}}{\{\nabla\Phi\}^T[k_e]\{\nabla\Phi\}} \quad (2-29)$$

Substituting Eq. 2-29 into Eq. 2-24, one obtains the plastic part of the incremental displacement as:

$$\{dq^P\} = \frac{\{\nabla\Phi\}\{\nabla\Phi\}^T[k_e]}{\{\nabla\Phi\}^T[k_e]\{\nabla\Phi\}}\{dq\} \quad (2-30)$$

2.5.4.4 Tangent Stiffness Matrix of Member

The following sequence of equations can be obtained from Eqs.

2-23, 2-22, and 2-24

$$\{dQ\} = [k_e]\{dq^e\} \quad (2-31)$$

$$= [k_e](\{dq\} - \{dq^p\}) \quad (2-32)$$

$$= [k_e](\{dq\} - \lambda\{\nabla\Phi\}) \quad (2-33)$$

Then, from Eq. 2-30

$$\{dQ\} = [k_e](\{dq\} - \frac{\{\nabla\Phi\}\{\nabla\Phi\}^T[k_e]}{\{\nabla\Phi\}^T[k_e]\{\nabla\Phi\}}\{dq\}) \quad (2-34)$$

$$\{dQ\} = [k_e](\{I\} - \frac{\{\nabla\Phi\}\{\nabla\Phi\}^T[k_e]}{\{\nabla\Phi\}^T[k_e]\{\nabla\Phi\}})\{dq\} \quad (2-35)$$

Therefore, the elasto-plastic tangent stiffness matrix is

$$[k_t] = [k_e](\{I\} - \frac{\{\nabla\Phi\}\{\nabla\Phi\}^T[k_e]}{\{\nabla\Phi\}^T[k_e]\{\nabla\Phi\}}) \quad (2-36)$$

2.5.4.5 Elastic Return

As a structure is being deformed, a change in load distribution may cause one or more plastic hinges to unload and become elastic again. This phenomenon is referred to as an "elastic return." It occurs whenever there is a reversal in the direction of the incremental displacement at a plastic hinge. It follows from Eq. 2-24 that the elastic return at any plastic hinge is signalled by a negative flow constant λ at the hinge.

2.5.4.6 Incremental Resistance and Deformations of Elasto-Plastic Element

As mentioned earlier, a key step in the solution procedure is the calculation, for each member, of the new member end force vector (Q_2) and possible incremental plastic deformation vector for a given current force vector (Q_1) and incremental end displacement vector (dq).

In the Section 2.5.4.4, the tangential stiffness has been derived. The incremental member forces based on the tangent stiffness would necessarily violate the yield condition (going out of the yield surface). The technique of keeping the force point on the yield surface consists of essentially obtaining, by iteration, a "local secant stiffness". Corresponding to a given (dq), none, one or both ends may yield or return to elastic behavior. The details of the procedures to treat these complex behavior are given below (Ref. [41]).

Procedure described in this section combines two features. Firstly, following an iterative process, the new member force vector would be made to stay on the yield surface as required by the theory of plasticity. Secondly, the incremental displacement can be large enough so that the element may undergo the process of changing from a state of total elasticity to having one yielding end and then on to having both ends yielding. This feature allows the solution procedure to use constant load or time increment.

It is assumed that during a load or time increment the change of the displacement is linear and one may write

$$\{dq\} = \{dq_{ee}\} + \{dq_{ep}\} + \{dq_{pp}\} \quad (2-37)$$

in which (dq_{ee}) is the part of (dq) with both ends elastic, and (dq_{ep}) and (dq_{pp}) are those with one and two yielding ends, respectively. The

corresponding changes in the member end forces are illustrated in Figure 2-8, in which the notation should be self-explanatory. For example, Q_{1A} is the current force point and $Q_{2A,ee}$ is the force point at A at the end of (dq_{ee}) . The displacements would take place in the order as given on the right side of Eq. 2-37. However, any one or two of the three incremental terms may be null.

Consider the yield surface of a generic yielding end, say C, as shown in Figure 2-9(a). Let Q_{1C} denote the initial force point, $(Q_{2C}^*) = (Q_{1C}) + [k_{eC}](dq)$, in which $[k_{eC}]$ is a 6 by 12 stiffness matrix (partitioned from $[k_e]$, the element elastic stiffness matrix). The intersection of the vector $Q_{1C}-Q_{2C}^*$ and the yield surface, point $Q_{2C,g}^{**}$, is a "general penetration point," given by $(Q_{2C,g}^{**}) = (Q_{1C}) + \gamma_g [k_{eC}](dq)$ in which γ_g is solved from the yield function $\Phi((Q_{1C}) + \gamma_g [k_{eC}](dq)) = 0$. Illustrated in Figure 2-9(a) is also a "radial penetration point." It is the intersection of the vector $0-Q_{2C}^*$ and the yield surface, point $Q_{2C,r}^{**}$, given by $(Q_{2C,r}^{**}) = \gamma_r (Q_{2C}^*)$, in which γ_r is solved from $\Phi(\gamma_r (Q_{2C}^*)) = 0$.

When yielding takes place at only one end, the initial force point Q_{1C} is on the yield surface. Corresponding to an incremental displacement (Δq) , the force is $(Q_{2C}^*) = (Q_{1C}) + [k_C](\Delta q)$ in which the stiffness $[k_C]$ depends on the element elastic stiffness and the gradient of Φ at Q_{1C} . (See Eq. 2-36 and Refs. [22], [25] and [38]). Because of the convexity of the yield surface, Q_{2C}^* is necessarily not inside the surface. To keep Q_2 on the surface the following iteration procedure is used (See Figure 2-9(b)).

Let Q_{2C}^j denote the value of Q_{2C}^* for the jth iteration. For the first iteration, $(Q_{2C}^1) = (Q_{1C}) + [k_C^1](\Delta q)$ in which $[k_C^1]$ is based on

the gradient at Q_{1C} , i.e., $\nabla\Phi = \nabla\Phi(Q_{1C})$. For $j > 1$, compute $(Q_{2C}^j) = (Q_{1C} + [k_C^j](\Delta q))$ in which $[k_C^j]$ is based on $\nabla\Phi = \bar{\nabla}\Phi^j$ given as follows:

$$\bar{\nabla}\Phi^j = 0.5(\nabla\Phi^{j-1} + \bar{\nabla}\Phi^{j-1}) \quad \text{if } \Phi(Q_{2C}^{j-1}) > \epsilon \quad (2-38a)$$

$$\text{or } \bar{\nabla}\Phi^j = 0.5(\bar{\nabla}\Phi^1 + \bar{\nabla}\Phi^{j-1}) \quad \text{if } \Phi(Q_{2C}^{j-1}) < -\epsilon \quad (2-38b)$$

In the preceding, $\bar{\nabla}\Phi^1 = \nabla\Phi(Q_{1C})$ and $\nabla\Phi^{j-1}$ is the gradient at the radial penetration point for Q_{2C}^{j-1} , and ϵ is a tolerance. The iteration ends when $|\Phi(Q_{2C}^j)| \leq \epsilon$.

When there are two yielding ends, the procedure is the same except that the gradients at both ends should be simultaneously treated as described in the preceding for the formulation of the elasto-plastic stiffness, and the convergence criterion, of course, applies to both end force vectors.

The computation procedures of the incremental resistance and deformations of an elasto-plastic element are:

1. Using the elastic stiffness $[k_e]$, compute a tentative end force increment $(dQ^*) = [(dQ_A) (dQ_B)]^T = [k_e](dq)$, and a tentative new force point $(Q_2^*) = (Q_1) + (dQ^*)$. (The superscript "*" denotes "tentative".)
2. Compute the values of the yield functions for both ends corresponding to (Q_1) and (Q_2^*) : $\Phi_{A1} = \Phi_A(Q_{1A})$; $\Phi_{B1} = \Phi_B(Q_{1B})$; $\Phi_{A2} = \Phi_A(Q_{2A}^*)$; $\Phi_{B2} = \Phi_B(Q_{2B}^*)$.
3. Locate the general penetration points and compute the quantities (See Figure 2-9(a)): $L_A = \Phi_{A2} - \Phi_{A1}$; $\alpha_A = -\Phi_{A1}$; $\beta_A = L_A - \alpha_A$; and similarly for L_B , α_B , and β_B .

4. If $\beta_A \leq 0$ and $\beta_B \leq 0$, the element response is entirely elastic. Then, $(dq_{ee}) = (dq)$; $(dq_{ep}) = (dq_{pp}) = \text{null vector}$, $(Q_2) = (Q_2^*)$. The resistance computation ends.
5. Otherwise, compute $\gamma_1 = \text{minimum}(\alpha_A/L_A, \alpha_B/L_B)$. Assuming $\gamma_1 = \alpha_A/L_A$ (otherwise, switch the subscript from A to B), signifying that end A (or B) yields first. Compute:
 $(dq_{ee}) = \gamma_1(dq)$; $(Q_2) = (Q_1) + [k_e](dq_{ee})$ and
 $(\bar{dq}) = (1 - \gamma_1)(dq) = (dq_{ep}) + (dq_{pp})$.
6. Compute the gradient of yield surface at end A,
 $\nabla\Phi_A = \nabla\Phi_A^*((Q_{2A,ee}))$ and form the corresponding elasto-plastic tangent stiffness matrix $[k^*] = [[k_A^*] [k_B^*]]^T$.
7. Compute $(Q_{2,ep}^*) = [(Q_{2A,ep}^*) (Q_{2B,ep}^*)]^T$
 $= (Q_{2,ee}) + [k^*](\bar{dq})$. If $\Phi_B((Q_{2B,ep}^*)) > \epsilon$, go to step 9.
 Otherwise, end B is still elastic, and if
 $|\Phi_A((Q_{2A,ep}^*))| \leq \epsilon$, then (dq_{pp}) is null. Set
 $(dq_{ep}) = (1 - \gamma_1)(dq)$ and $(Q_2) = (Q_{2,ep}^*)$. The plastic part of (dq_{ep}) is $(dq_{ep,p}) = [(dq_{epA,p}) (dq_{epB,p})]^T$ with
 $(dq_{epB,p}) = \text{null}$, and $(dq_{epA,p}) = \lambda_A \nabla\Phi_A$ in which λ_A is the flow constant computed as usual (Eq. 2-29). The resistance computation ends.
8. If $|\Phi_A((Q_{2A,ep}^*))| > \epsilon$, compute $\bar{\nabla}\Phi_A$ as per Eqs. 2-38, update $[k^*]$ accordingly, and return to step 7.
9. Compute $\gamma_2^* = \alpha_B^*/L_B^*$ based on $(Q_{2B,ee})$ and $(Q_{2B,ep}^*)$ (corresponding to Q_{1C} and Q_{2C}^* in Figure 2-9(a)). Compute
 $(Q_{2,ep}^{**}) = (Q_{2,ee}) + [k^*]\gamma_2^*(dq)$. $(Q_{2B,ep}^{**})$ is thus on the yield surface.
10. If $|\Phi_A((Q_{2A,ep}^{**}))| \leq \epsilon$, set $\gamma_2 = \gamma_2^*$, $(Q_{2,ep}) = (Q_{2,ep}^{**})$.

$(dq_{ep}) = \gamma_2(1 - \gamma_1)(dq)$. The plastic part $(dq_{ep,p})$ is computed as usual. The part of (dq) remaining to be "accounted for" is $(dq_{pp}) = (dq) - (dq_{ee}) - (dq_{ep})$. Go to step 11. If $|\bar{\Phi}_A(Q_{2A,ep}^{**})| > \epsilon$, update $[k^*]$ using $\bar{\nabla}\bar{\Phi}_A$ computed as per Eqs. 2-38 (with $Q_{2A,ep}^{**}$ taking the place of Q_{2C}^*). Go to step 7.

11. Compute $(Q_{2,pp}^*) = (Q_{2,ep}) + [k^*](dq_{pp})$ in which $[k^*]$ is based on the gradients at $Q_{2,ep}$. Iterate as described previously to have $Q_{2,pp}$ on the yield surface for both ends.
12. The final stress point is $(Q_2) = (Q_{2,ep}) + [k^*](dq_{pp})$. The incremental plastic deformations in (dq_{pp}) , i.e., $(dq_{pp,p})$, consisting of $(dq_{ppA,p}) = \lambda_A \bar{\nabla}\bar{\Phi}_A$ and $(dq_{ppB,p}) = \lambda_B \bar{\nabla}\bar{\Phi}_B$ are computed as usual based on the latest gradients. The total incremental plastic deformation is $((dq_{ep,p}) + (dq_{pp,p}))$. The resistance computation ends.

2.6 PLASTIC WORK DENSITIES AND DUCTILITY FACTORS

The calculation of the plastic part of the incremental element displacements has been presented above. For purposes of interpreting the inelastic response characteristics of the structure, it is appropriate to further define the quantities "plastic work densities" and "ductility factors". They may be considered as approximate measures of "damage" to the structural elements.

2.6.1 Plastic Work Densities

It is assumed that all plastic work is due to the inelastic straining of the "longitudinal" fibers of the beam elements. Thus the

work would be done by the bending moments: M_x , M_y , and the axial force P . It is further assumed that the beam cross-section has the shape of a rectangular box with two axes of symmetry (See Figure 2-10.) Thus for each member end, the plastic work done by each of the stress resultants in the time interval h may be expressed respectively as:

$$w_{xp} = \sum_i M_{xi} \delta\theta_{xpi}$$

$$w_{yp} = \sum_i M_{yi} \delta\theta_{ypi}$$

$$w_{\Delta p} = \sum_i P_i \delta\Delta_{pi} \quad (2-39)$$

in which $\delta\theta_{xp}$, $\delta\theta_{yp}$, and $\delta\Delta_p$ denote the plastic part of the incremental rotations about x-x and y-y axis and the incremental axial displacement. The subscript "i" denotes the ith time interval.

Although in the mathematical analysis, the plastic length is assumed to have zero length, for purposes of engineering interpretation of the results, it is assumed that the plastic deformations are distributed for a finite length. Corresponding to the rotation in a principal plane that length is taken to be the depth of the cross-section in that plane. Consider the case $M_x \neq 0$ (signifying rotation in the principal plane y-z), $M_y = P = 0$. Assuming that there is no transition to fully plastic moment, i.e., all fibers across the web thickness t_w (see Figure 2-10) yield simultaneously, a "plastic hinge volume" for M_x may be defined as $V_{hx} = 2t_w DB$, in which D and B are respectively the depth and width of the section. Similarly, a plastic hinge volume for M_y is defined as $V_{hy} = 2t_f BD$, in which t_f is the thickness of the flange. For P , a plastic hinge volume, $V_{h\Delta}$ is taken to

be $V_{hx} + V_{hy}$. (If $D/B = t_f/t_w$, this volume corresponds to that of the cross-section area times a length equal to $(D + B)/2$.)

The strain energy per unit volume of material at yield is $w_0 = (1/2)F_y \epsilon_y$. The dimensionless measures of the various plastic work quantities may thus be represented as:

$$\begin{aligned}\bar{w}_{xp} &= w_{xp}/(V_{hx} w_0) \\ \bar{w}_{yp} &= w_{yp}/(V_{hy} w_0) \\ \bar{w}_{\Delta p} &= w_{\Delta p}/(V_{h\Delta} w_0)\end{aligned}\tag{2-40}$$

2.6.2 Ductility Factors

As alternative or additional measures of inelastic response, member end ductilities may be defined as follows. Corresponding to out-of-plane bending, the "curvature ductility factor" is

$$\mu_{\phi x} = 1 + \frac{\text{"inelastic curvature"}}{\text{elastic limit curvature}} = 1 + \frac{\theta_{xp}/B}{M_{x0}/(EI_x)}\tag{2-41}$$

in which θ_{xp} is the plastic rotation, B is the plastic hinge length for out-of-plane bending, M_{x0} , I_x are the elastic limit moment and moment of inertia about the x-axis, respectively, and E is the Young's modulus.

Similarly, for in-plane bending, the "curvature ductility factor" is

$$\mu_{\phi y} = 1 + \frac{\theta_{yp}/D}{M_{y0}/(EI_y)}\tag{2-42}$$

in which the meaning of the symbols are entirely analogous to those in the preceding expression. The "ductility factor" for axial strain, μ_{Δ} , is defined as the ratio of "plastic axial strain" to the elastic limit

strain. The former is taken as the plastic axial displacement, Δ_p , divided by its "hinge length." Taking the latter as $(D + B)/2$, one obtains

$$\mu_{\Delta} = \frac{2\Delta_p}{(B + D)\epsilon_y} \quad (2-43)$$

2.7 WORK AND ENERGY DISTRIBUTION CHECK

Considering work and energy balance, the following equation should hold for the system analyzed at all times:

$$W_R + W_G = E_{SE} + E_{SP} + E_K + E_D \quad (2-44)$$

in which W_R and W_G denote work done by support reactions and by gravity loads, respectively, E_{SE} is recoverable strain energy, E_{SP} is irrecoverable (plastic) strain energy, E_K is kinetic energy and E_D is energy dissipated by damping.

An examination of the variation of these quantities is instructive. Moreover, it can also serve as a check on the validity of the analysis and numerical computation. In the following for each time interval h , each work or energy item, with the exception of the kinetic energy, is computed as the product of force (taken as the average of those at the beginning and at the end of the time interval) and the incremental displacement. The total amount of a given kind of work or energy at a given time is of course obtained by summing the incremental quantities over all time intervals preceding it.

The incremental work done by the support reactions is

$$\Delta W_R = \sum_{i=1}^{NS} (R_{Xi} \Delta X_i + R_{Yi} \Delta Y_i + R_{Zi} \Delta Z_i) \quad (2-45)$$

in which R_{Xi} , R_{Yi} and R_{Zi} are the X, Y, Z components of the reaction and ΔX_i , ΔY_i , and ΔZ_i are the corresponding ground displacements at support i , and NS is the number of supports. The reactions at a support can be computed from summing the end forces of the structural members incident to that support.

The incremental work done by gravity loads is

$$\Delta W_G = \sum_{j=1}^{NN} M_j g \Delta Y_j \quad (2-46)$$

in which M_j is the lumped mass at a non-support node point j , g is the gravitational acceleration, ΔY_j is the incremental vertical displacement of node point j , and NN is the number of free nodes.

For a curved or straight beam element the displacement change $\{dq\}$ over h may be, in the general case, decomposed into:

$$\{dq\} = \{dq_{ee}\} + \{dq_{ep}\} + \{dq_{pp}\} \quad (2-47)$$

in which, as defined in Section 2.5.4.6, $\{dq_{ee}\}$ denotes that part of $\{dq\}$ for both ends being elastic, $\{dq_{ep}\}$ for one end elastic and the other end elasto-plastic, and $\{dq_{pp}\}$ for both ends plastic. The general case of force displacement change for a generic end, say end C, is illustrated in Figure 2-11 in which $\{Q_1\}$ denotes the force vector at the beginning of h , $\{Q_{2,ee}\}$, $\{Q_{2,ep}\}$ and $\{Q_{2,pp}\}$ denote the force vectors at the end of $\{dq_{ee}\}$, $\{dq_{ep}\}$ and $\{dq_{pp}\}$, respectively. The incremental strain energy Δe_S for the single member consists of an elastic part Δe_{Se} and a plastic part Δe_{Sp} ; i.e.,

$$\Delta e_S = \Delta e_{Se} + \Delta e_{Sp} \quad (2-48)$$

with

$$\Delta e_{Se} = 0.5 [(\{Q_1\} + \{Q_{2,ee}\})^T \{dq_{ee}\} + (\{Q_{2,ee}\} + \{Q_{2,ep}\})^T \{dq_{ep,e}\}]$$

$$+ ((Q_{2,ep}) + (Q_{2,pp}))^T (dq_{pp,e}) \quad (2-49)$$

$$\begin{aligned} \Delta e_{Sp} = & 0.5 [((Q_{2,ee}) + (Q_{2,ep}))^T (dq_{ep,p}) \\ & + ((Q_{2,ep}) + (Q_{2,pp}))^T (dq_{pp,p})] \end{aligned} \quad (2-50)$$

in which the third subscript "e" or "p" attached to (dq) denotes the "elastic part" or "plastic part", i.e.,

$$(dq_{ep}) = (dq_{ep,e}) + (dq_{ep,p}) \quad (2-51)$$

$$(dq_{pp}) = (dq_{pp,e}) + (dq_{pp,p}) \quad (2-52)$$

The incremental recoverable strain energy of the system is

$$\Delta E_{SE} = (\Delta e_{Se})_{CB} + (\Delta e_{Se})_{SB} + (\Delta e_{Se})_{TR} \quad (2-53)$$

in which the subscripts CB denote summing over all curved beam elements, SB over all straight beam elements, and

$$(\Delta e_{Se})_{TR} = \sum 0.5(Q_1 + Q_2)dq \quad (2-54)$$

denotes the incremental elastic strain energy due to all truss elements, with Q_1 and Q_2 representing the axial forces at the beginning and end of the time interval h , dq is the axial deformation changes taken place in the interval.

The incremental irrecoverable strain energy is

$$\Delta E_{SP} = (\Delta e_{Sp})_{CB} \quad (2-55)$$

The incremental kinetic energy over the time interval h is

$$\Delta E_K = 0.5((\dot{w})^T [m] (\dot{w}))_{t1} - 0.5((\dot{w})^T [m] (\dot{w}))_{t0} \quad (2-56)$$

The incremental energy dissipated by damping is

$$\Delta E_D = 0.5([C] (\dot{w}))_{t1} + ([C] (\dot{w}))_{t0}^T (\Delta w) \quad (2-57)$$

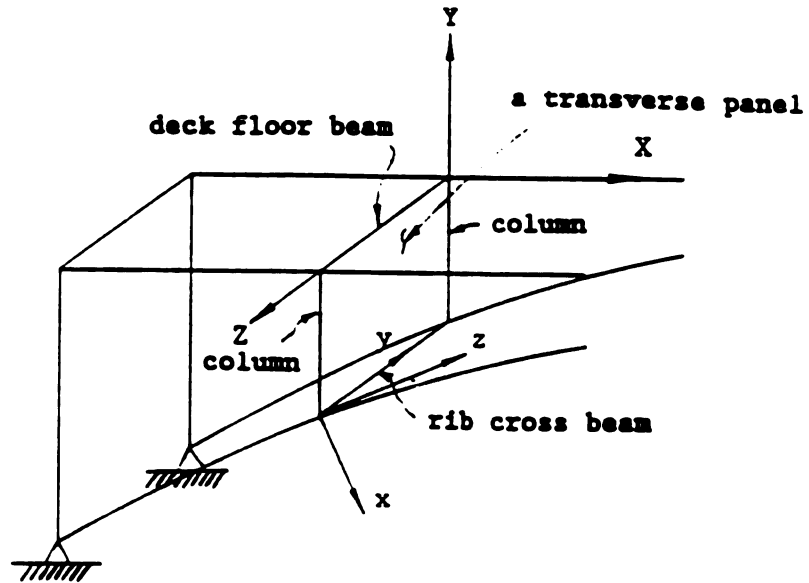


Figure 2-3. Constraint for Infinitely Large Axial Stiffnesses

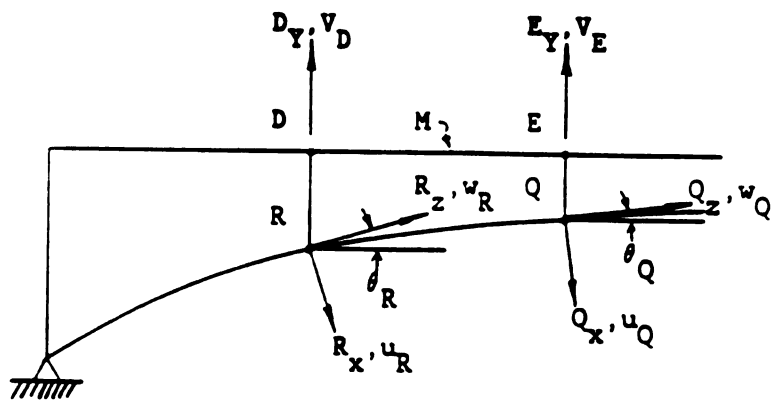


Figure 2-4. Treatment of "Rigid Column" in Mixed Nodal Coordinates System

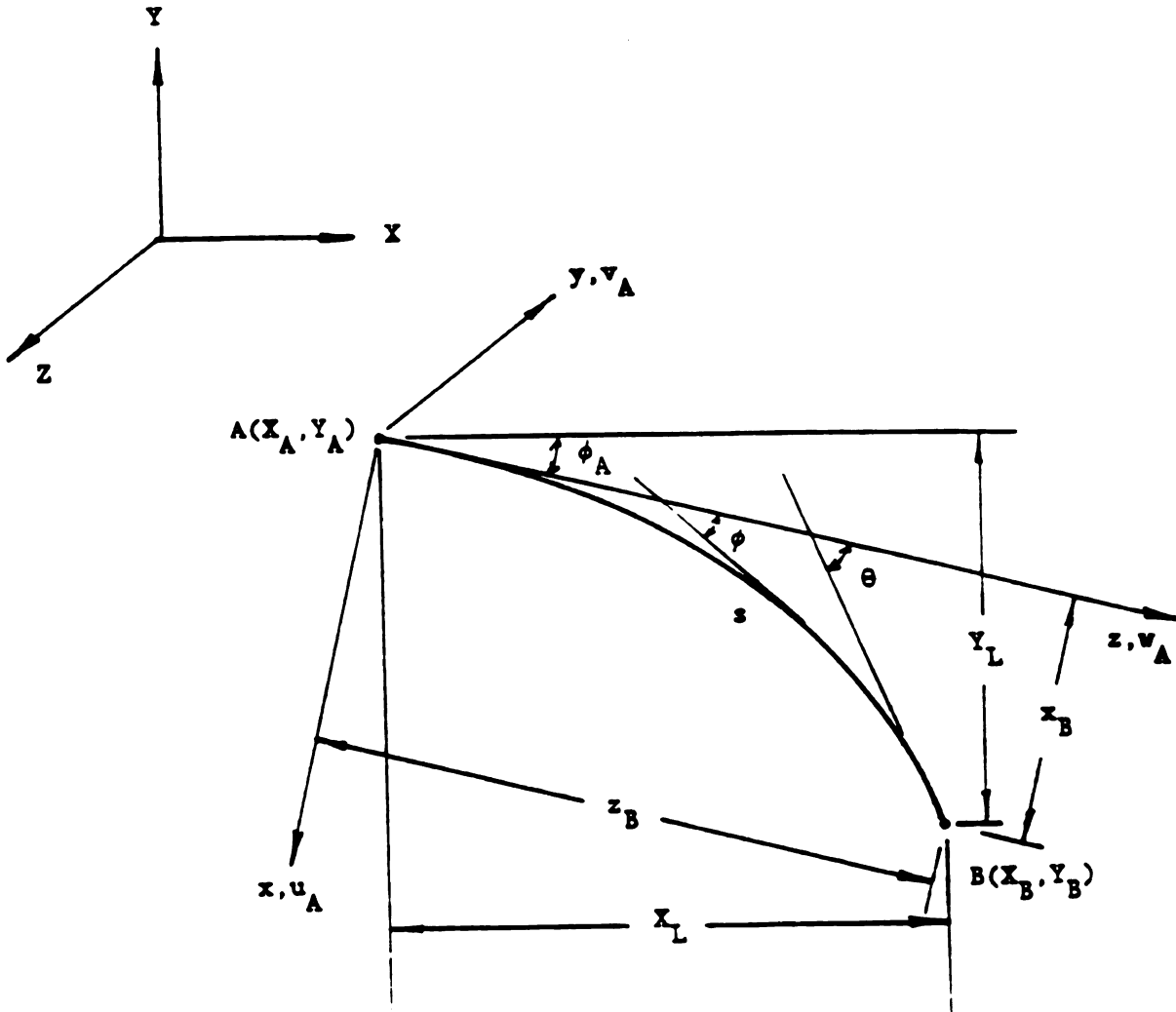


Figure 2-5. Typical Curved Beam Element

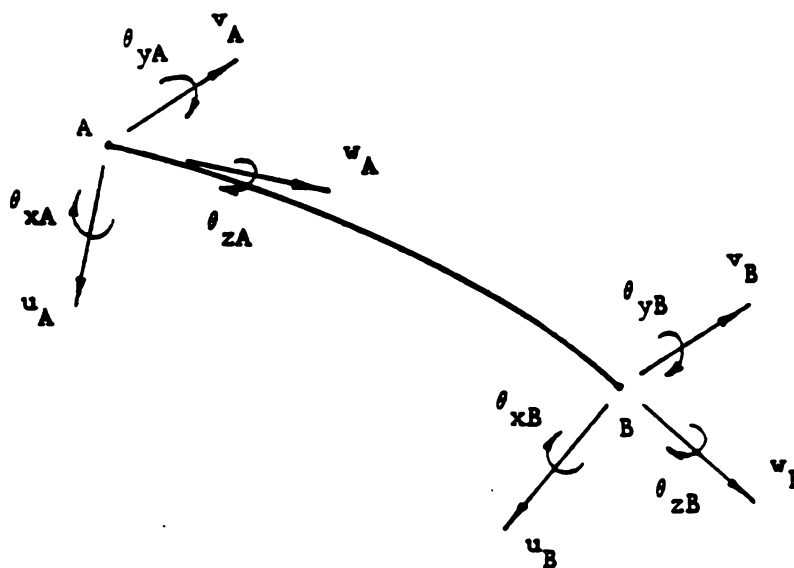


Figure 2-6. Curved Beam Element End Displacements

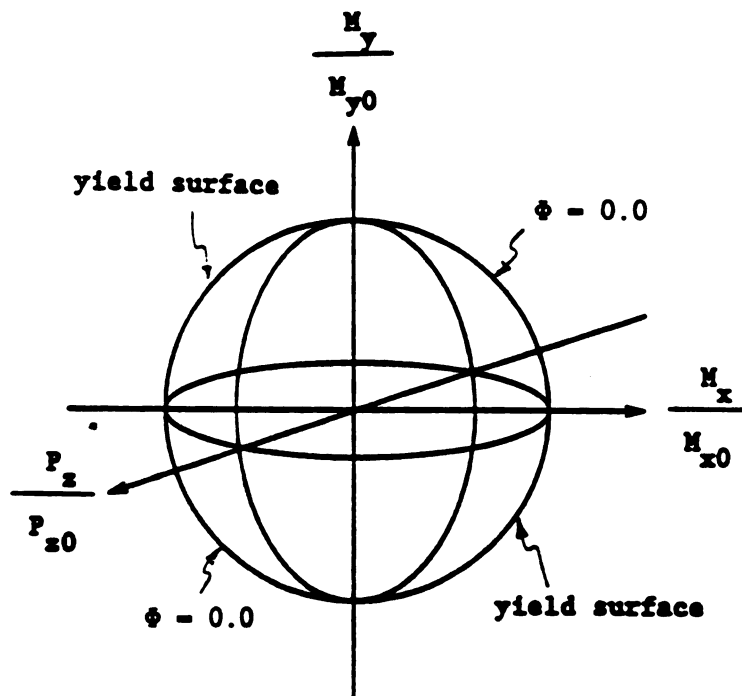


Figure 2-7. Spherical Yield Surface

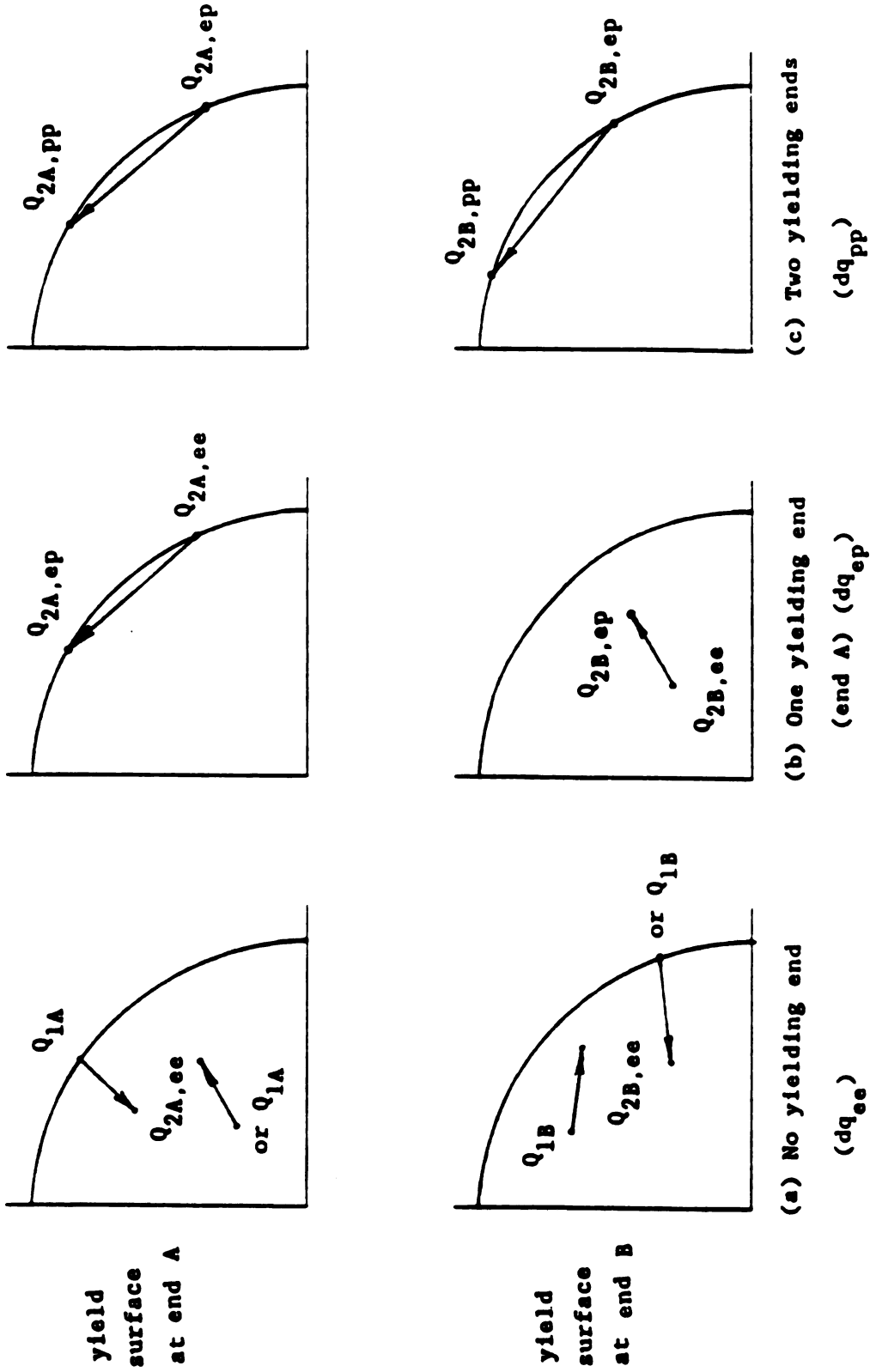


Figure 2-8. Member End Forces Corresponding to Displacement Changes

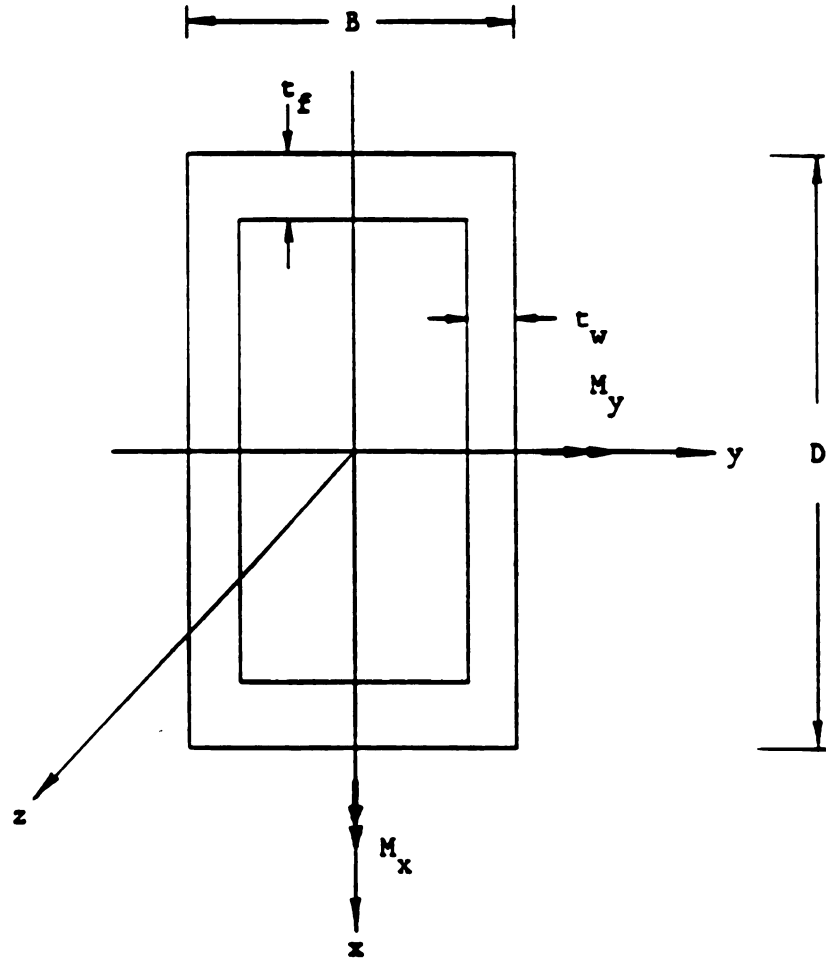


Figure 2-10. Definition of Cross-Section

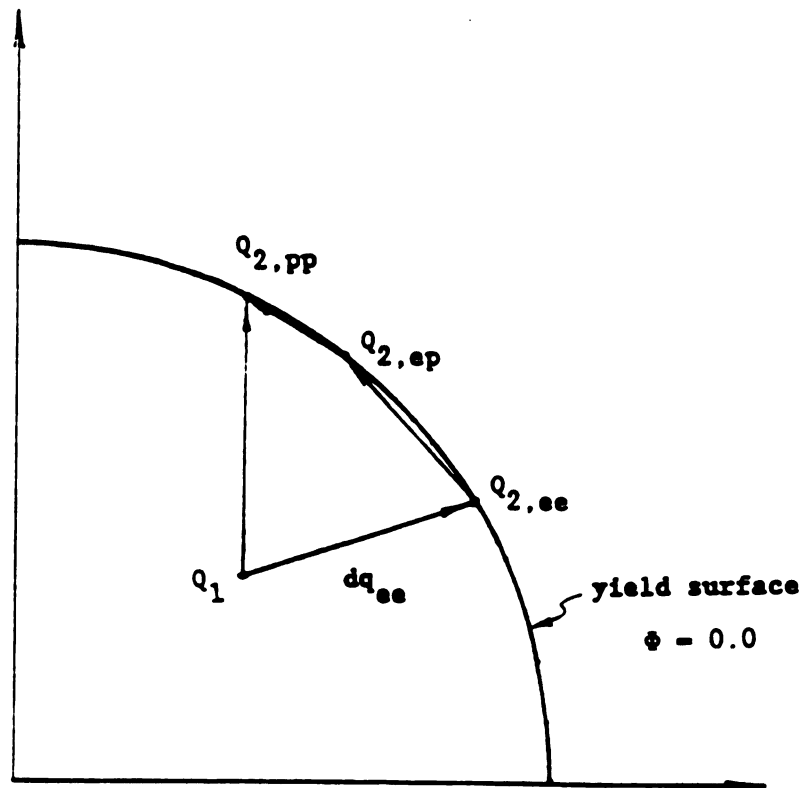


Figure 2-11. Typical Member End Force Path
For An Elasto-Plastic Element

CHAPTER III
APPLICATIONS AND NUMERICAL RESULTS

3.1 GENERAL

This chapter presents the numerical results based on the analyses described in the preceding chapter. The results were obtained by use of a computer program that incorporated the method of analysis presented. They cover three model bridges: one each of short span, medium span, and long span, and one ground motion.

Nonlinear behavior due to material inelasticity is presented first, followed by behavior due to geometric nonlinearity (nonlinearly elastic behavior). In each case, the time histories of displacements, internal forces (stress resultants) and energy distribution are discussed.

3.2 COMPUTER PROGRAM

The computer program was built from one based on linear analysis using straight beam elements (Ref. [12]). It consists of approximately 6000 lines of FORTRAN statements. The major additions are the nonlinear curved beam elements (material and geometric).

The bulk of the numerical results was obtained by use of the Supercomputer CYBER205 at Purdue University with the linear equations subroutine written for vector processing. After the National Science Foundation ceased to support the Purdue Supercomputer operation, the

computation was done on a VAX/VMS-11/750 computer at College of Engineering, Michigan State University. For a problem solved by both computers for comparison, the latter was 56 times slower than the supercomputer. However, the numerical results were within 2% of each other.

3.3 MODELS OF BRIDGE AND GROUND MOTION USED

Three existing steel deck-type arch bridges: the Cold Springs Canyon Bridge (CSCB) in California, the South Street Bridge (SSB) in Connecticut, and the New River Gorge Bridge (NRGB) in West Virginia with arch spans of 700, 193, and 1700 feet, respectively, were chosen to be the prototypes for the medium span bridge (MSB), the short span bridge (SSB), and long span bridge (LSB).

A complete real arch bridge system generally contains a large number of degrees of freedom. The expense for analysis of such a system can be kept within reasonable bounds in the case of a linear analysis. Because of the high cost of nonlinear analysis, it seemed necessary to use models that have fewer degrees of freedom than those used for linear analysis. For example, for the CSCB, the number of panels was reduced from eleven to eight. Nonlinear curved beam elements are used for the arch ribs. Straight beam and truss elements are used for the deck, columns, and cross bracing members. They are presumed to be entirely elastic.

"True" three-dimensional models with the two ribs modelled as distinct curved beam elements for MSB (Figure 3-1) and SSB (Figure 3-2), and "one-plane" three-dimensional model (Ref. [12]) with the two ribs (plus bracing) modelled as a single curved element for LSB (Figure 3-3)

were used to consider the inelastic effects (material nonlinearity). Yet a third type of model, i.e., a two-dimensional plane model (Figure 3-4) was used to study the nonlinear elastic effects. (Results for the three-dimensional models were obtained on the supercomputer and the latter two-dimensional models on the VAX.) A complete description of the properties and boundary conditions for these bridge models is given in APPENDIX.

There are two differences between the true three-dimensional model and the one-plane three-dimensional model. Firstly, the axial force in a rib of a true three-dimensional model would be approximated by the axial force and the bending stress effects in a one-plane three-dimensional model. Secondly, the bending response of the individual ribs in a true three-dimensional model cannot be produced in a one-plane three-dimensional model.

The natural periods of linear undamped vibration of the first four modes for out-of-plane and in-plane motions are listed in Table 3-1 and the mode shapes are shown in Figures 3-5, 3-6, 3-7, 3-8, 3-9 and 3-10. The fundamental out-of-plane natural periods are 3.032, 1.180, and 4.716 seconds for MSB, SSB, and LSB, respectively. The fundamental in-plane natural periods are 2.247, 1.065, 3.565, and 2.514 seconds for MSB, SSB, LSB, and the two-dimensional MSB model, respectively.

For this study, the basic ground motion used is an artificially generated motion, CIT-A2 (Figure 3-11) (Ref. [18]), which is intended to represent the ground motion near the epi-center of a magnitude 8 shock. It has a maximum acceleration of 0.39 g, a duration of approximately 120 seconds. In all cases, the first 45 seconds which covers the most intense part of the ground motion were used. The ground motion in all

three directions in space were used with the amplitude of the vertical motion being set equal to 75% of the two horizontal ones. The same ground motion was applied to all supports of the structure with no phase difference.

3.4 MATERIAL NONLINEAR PROBLEMS

3.4.1 General

For the material nonlinear studies, the three-dimensional bridge models were used with ground accelerations applied in all three directions. In order to induce inelastic response, an amplification factor (AF) was applied to the basic ground motion as described in Section 3.3. The typical amplification factors used were 2.0, 1.2, and 2.0 for MSB, SSB, and LSB, respectively. (Using AF = 1.2 for the SSB model induced as much inelastic response as that for the MSB model with AF = 2.0.)

Under the specified ground motion, Figures 3-12, 3-13, and 3-14 indicated for MSB, SSB, and LSB, respectively, the time intervals during which there was inelastic action (i.e., some elements yielding). One may observe that the first yielding occurred at 12.22 second for MSB, 7.54 second for SSB and 12.45 second for LSB. For the SSB even the AF used was 1.2 only, there were many members yielded within the duration of 45 seconds.

3.4.2 Typical Displacement Time Histories

In this section displacement time histories are presented for three nodes in each bridge model. For each node, three displacement components are plotted. They are X (horizontal), Y (vertical), and Z

(lateral; out-of-plane) displacement in the cartesian coordinates system.

3.4.2.1 Medium Span Bridge (MSB)

The three nodes selected for this bridge are: node 17, 31 and 5 (See Figure 3-1). Node 17 is at the crown of the front arch rib, node 5 is at the 1/8 span of the front arch rib, and node 31 is at the 7/8 span of the rear arch rib. The results indicate that at both node 5 and 31 there were yielding of the arch ribs.

The horizontal (X) displacement time histories for the three nodes are shown in Figures 3-15, 3-16, and 3-17. They indicate that the predominant period is approximately 2.2 seconds. The first in-plane undamped natural period had been calculated to be 2.247 seconds (See Table 3-1). Thus the response was then primarily in the first mode. There were also some contributions, though small, from the third mode (undamped natural period equal to 0.685 seconds). It may be noted that the second mode is symmetric (Figure 3-5) which would not be excited by the horizontal ground motion. Experience indicates that the effects of horizontal ground motion dominate over those of vertical ground motion. Because of antisymmetry in mode shapes, the horizontal displacement time histories of node 5 and 31 are in phase and almost equal. The wave patterns for the elastic and inelastic responses are quite similar.

The vertical (Y) displacement time histories are shown in Figures 3-18, 3-19, and 3-20. The predominant period is again approximately 2.2 seconds for time histories of nodes 5 and 31. As above, it indicates that the response was mostly in the first in-plane mode. Similarly, there were appreciable third mode contributions. These

vertical displacement time histories of node 5 and 31 are out-of-phase because of antisymmetry in mode shapes. The dominant period for node 17 is approximately 3.0 seconds which corresponds to the first out-of-plane mode. One can observe from Figure 3-5 that the vertical displacement is zero at the crown node in the first in-plane mode. Thus the displacements are apparently excited by the out-of-plane ground motion (See the first out-of-plane mode shapes in Figure 3-6). The wave patterns for the elastic and inelastic responses are similar too.

The lateral (Z) displacement time histories are shown in Figures 3-21, 3-22, and 3-23. The predominant period is approximately 3.0 seconds. It indicates that the response was primarily in the first out-of-plane mode. (Table 3-1 shown the first out-of-plane natural period to be 3.032 seconds.) One can also observe that the fourth mode with period equal to 0.942 seconds participated significantly in the overall response of node 5 (Figure 3-21) and node 31 (Figure 3-23). The lateral displacement time histories of node 5 and 31 are in phase and almost equal. The wave patterns for the elastic and inelastic responses are quite similar too.

3.4.2.2 Short Span Bridge (SSB)

For this bridge the nodes chosen for presenting displacement time histories are the two symmetric points: node 11 and 23. They are at the 2/7 and the 5/7 span of the rear rib (Figure 3-2), respectively. A third point chosen is node 13 at the 3/7 span of the front rib.

The displacement time histories in the X, Y, and Z direction for these nodes are shown in Figures 3-24 through 3-32. In general, they are similar in character to those presented above for the MSB. Hence, no

further discussion will be presented for them.

3.4.2.3 Long Span Bridge (LSB)

The displacement time histories for this bridge are shown in Figures 3-33 through 3-41. They refer to node 18 at the crown, node 12 at the 4/14 span of the arch rib, and node 24 at the 10/14 span of the arch rib (See Figure 3-3). Node 12 and 24 are symmetric points and there was yielding near them. These time history results are also similar in character to those presented for MSB, except for the following point.

For the vertical displacement time history of the crown point (node 18, See Figure 3-37), the response was primarily in the second in-plane mode (1.5 seconds) and fourth in-plane mode (1.1 seconds) as expected. Because the crown node has zero vertical displacement in the first and third in-plane modes (Figure 3-8). It differs from the response of MSB because, as mentioned previously, LSB is a one-plane model. The vertical displacement of the rib in that model corresponds to that of the center line of the bridge. That displacement is essentially unaffected by lateral ground motion. To deduce the actually vertical displacements along the edges of a cross-section of the bridge represented by a one-plane model, one needs to consider the torsional response.

3.4.3 Maximum Displacements

For the MSB model, the magnitudes of the maximum displacements at the above selected nodes (Section 3.4.2.1) and certain additional nodes are listed in Table 3-2. The odd numbers correspond to nodes on the ribs and the even numbers on the deck (Figure 3-1). The maximum

horizontal displacement occurring at the node next to a support amounts to 1.1% of the arch height (121.25 feet) for the linear elastic case and 1.13% for the inelastic case. The horizontal displacements in the deck are smaller. There are no significant differences between the vertical displacements in the ribs and deck. The maximum vertical displacement occurred at the mid-span and amounted to 2.02% of the arch height for elastic case and 2.12% for inelastic case. The maximum lateral rib displacement also occurred at the mid-span and is considerably larger, 8.13% of the arch height for elastic case and 7.6% for inelastic case. The deck nodes all had even larger lateral displacement. The maximum responses of the rear and front rib were approximately equal.

The maximum displacements for the SSB model are presented in Table 3-3. As before, the odd numbers are on the ribs and the even number are on the deck (Figure 3-2). There are no significant differences between the rib and deck for horizontal and vertical displacements. The maximum horizontal displacement was 1.58% of the arch height (28.398 feet) for the elastic case and 1.43% for the inelastic case. The corresponding maximum vertical displacements were 3.17% and 3.12%. The corresponding maximum lateral displacements were 3.48% and 3.29%. For this bridge, the inelastic displacement responses were smaller than the elastic responses. But the differences are relatively small.

The maximum displacements for the LSB model are listed in Table 3-4. The even numbers are on the rib and the odd numbers are on the deck (Figure 3-3). The maximum horizontal displacement was 0.98% of the arch height (370 feet) for the elastic case and 0.95% for the inelastic

case. The corresponding maximum vertical displacements were 1.65% and 1.61%. The corresponding maximum lateral displacements were 2.73% and 2.54%.

3.4.4 Typical Force Time Histories

In this section the force time histories are presented for two rib points in each bridge. At each point, three components are plotted: P_z (axial force), M_y (referred to as "in-plane bending" because the bending takes place in the plane of the rib), and M_x (referred to as "out-of-plane bending" because the bending causes deformation out of the plane of the rib).

3.4.4.1 Medium Span Bridge (MSB)

The two points selected are: end J of member 1 at node 5 (the 1/8 span of the front arch rib) and end I of member 16 at node 31 (the 7/8 span of the rear arch rib) (See Figure 3-1). They are symmetric points and yielding had been indicated in the inelastic analysis.

The P_z time histories are shown in Figures 3-42 and 3-43. The predominant period is approximately 3.0 seconds which indicates that the response was mostly in the first out-of-plane mode. In this mode, the two ribs essentially act as the two opposite flanges of a beam. One can also observe that the fourth in-plane mode (with a period equal to approximately 0.5 seconds.) participated significantly in the overall response. In this mode, the two ribs would respond identically. Because of the sign conventions used in the analysis (See Figure 2-6), the two time histories are seen to be in phase for the first out-of-plane mode and out-of-phase for the fourth in-plane mode. As it was the case for

displacement time histories, the wave patterns for the P_z forces for the elastic and inelastic responses are quite similar.

The in-plane rib bending moment time histories are shown in Figures 3-44 and 3-45. The predominant period is approximately 3.0 seconds which indicates that the response was again primarily in the first out-of-plane mode. (Note that in-plane bending of ribs may exist in an out-of-plane normal mode. See Figure 3-6) Similarly, there was substantial fourth in-plane mode contribution. The two time histories are in phase for the first out-of-plane mode and out-of-phase for the fourth in-plane mode.

The out-of-plane bending time histories are shown in Figures 3-46 and 3-47. The predominant period was measured as 3.0 seconds which indicates that the response was primarily in the first out-of-plane mode. The two time histories are out-of-phase.

3.4.4.2 Short Span Bridge (SSB)

The two points selected for this structure is end J of member 9 at node 11 (the 2/7 span of the rear arch rib) and end I of member 13 at node 23 (the 5/7 span of the rear arch rib) (See Figure 3-2).

The results are shown in Figures 3-48 through 3-53. In general, they are similar in character to those presented above for the MSB. Hence, no further discussion will be presented for them.

3.4.4.3 Long Span Bridge (LSB)

The points selected are end I of member 5 at node 12 (the 4/14 span of the arch rib) and end J of member 10 at node 24 (the 10/14 span of the arch rib) (See Figure 3-3). They are symmetric points and

yielding did occur at both points.

The axial force time histories are shown in Figures 3-54 and 3-55. The predominant period is approximately 1.1 seconds which indicates that the response was mostly in the fourth in-plane mode. It may be noted from Figure 3-8 that the fourth mode is the lowest mode in which the axial force dominates (over bending). The wave patterns for the elastic and the inelastic responses are quite similar.

The in-plane bending time histories are shown in Figures 3-56 and 3-57. The predominant period is approximately 3.5 seconds which indicates that the response was primarily in the first in-plane mode. There was also small contributions from higher modes. The two time histories are in phase for the first in-plane mode and out-of-phase for the higher modes.

The out-of-plane bending time histories are shown in Figures 3-58 and 3-59. The predominant period is approximately 0.5 seconds which indicates that the response was primarily in the higher mode. The two time histories are out-of-phase. The question arose why there was little first out-of-plane mode response. The time histories of out-of-plane bending at the two nodes (node 10 and 14) adjacent to node 12 were obtained and are shown in Figures 3-60 and 3-61. It can be seen that the responses at both nodes are mostly in the first out-of-plane mode. Thus it may be concluded that the selected points (node 12 and 24) are very close to points of inflection (zero moment) for out-of-plane bending in the fundamental out-of-plane mode.

3.4.5 Maximum Forces and Force Reduction Factors

The maximum values of the internal forces: P_z , M_y and M_x for the MSB model are listed in columns 3 and 4 of Table 3-5. It is seen that they differ considerably for the elastic and inelastic cases (although the time history wave patterns are quite similar for the two cases). It may be noted that the maximum values in the inelastic case are limited by the fully plastic values (See Eq. 2-20 and Table 3-5). No such limits exist in the elastic case.

For an elastic design, the design is generally carried out based on the maximum forces as indicated by the elastic analysis. For an inelastic design, if the designer would accept the "damage" due to plastic deformations, the design could be carried out based on the maximum force as indicated by the inelastic analysis. Assuming that the material needed is roughly proportional to the design force, it follows that savings in material are possible if the "inelastic force" is less than the "elastic force".

Let the term "force reduction factor" or simply "reduction factor," be defined as:

$$\text{reduction factor} = \frac{F_e - F_{ie}}{F_e} \quad (3-1)$$

in which, F_e = maximum force by elastic analysis and F_{ie} = maximum force by inelastic analysis. The factor may be regarded as a measure of possible material saving using inelastic design. Its values are listed in Table 3-5 for the data presented above. It is seen that they are of appreciable magnitude.

The largest reduction factor for the SSB (listed in Table 3-6) is 0.223 for in plane bending of member 9 end J. It is less than the

maximum values of 0.333 of the preceding MSB case. But the latter is based on a ground acceleration amplification factor $AF = 2.0$, while for the SSB model, $AF = 1.2$. Thus, the reduction factor per unit of AF is approximately the same for the two cases.

The largest reduction factor for the LSB (See Table 3-7) is 0.137 for in-plane bending of member 10 end J. It is smaller than the maximum reduction factors for either the MSB or SSB. It may also be noted that the values of the dimensionless response (displacements) for LSB model are also smaller than the other two bridges.

3.4.6 Typical Work and Energy Distribution Time Histories

The work and energy balance equation of the system was presented in Section 2.7 as:

$$W_R + W_G = E_{SE} + E_{SP} + E_K + E_D \quad (2-44)$$

in which, as noted in Chapter II, W_R and W_G denote work done by support reactions and by gravity loads, respectively, E_{SE} is recoverable strain energy, E_{SP} is irrecoverable (plastic) strain energy, E_K is kinetic energy and E_D is energy dissipated by damping. During an earthquake energy is fed through the base of the structure. It is instructive to know how the energy is distributed among the terms in the work and energy balance equation. There is no irrecoverable (plastic) strain energy for a linear elastic case, therefore, for that case the term E_{SP} should be deleted from the equation.

The equation representing work and energy distribution may be rewritten from Eq. 2-44 as follows:

$$1.0 = \frac{E_{SE}}{W} + \frac{E_{SP}}{W} + \frac{E_K}{W} + \frac{E_D}{W} \quad (3-2)$$

in which $W = W_R + W_G$. The equation becomes

$$1.0 = SE + KE + DE + PW \quad (3-3)$$

where $SE = E_{SE}/W$, $KE = E_K/W$, $DE = E_D/W$ and $PW = E_{SP}/W$ are presented in the figures of the work and energy distribution time histories. A spline technique was used in the graphs to connect the discrete points.

The work and energy distribution time histories of the MSB for the elastic and inelastic cases are shown in Figures 3-62 and 3-63. The elastic case has a greater percentage of dissipated damping energy compared to the inelastic case. The dissipated damping energy continued to increase to 87% of the work done for the elastic case and 74% for the inelastic case. For both cases the kinetic and recoverable strain energy remain relatively small throughout the whole 45 seconds and the elastic case has a greater percentage. For the inelastic case, 18% of the work done is shown to be dissipated by irrecoverable strain energy after about 20 seconds. From Figure 3-63, a decrease in PW can be noted. It is because of the fact that the ratio E_{SP}/W is plotted, i.e., a decrease signifies that the denominator, the work done, has increased faster than the numerator.

The work and energy distribution time histories of the SSB for the elastic and inelastic cases are shown in Figures 3-64 and 3-65. The dissipated damping energy continued to increase at an almost constant rate to 88% of the work done for the elastic case and 74% for the inelastic case. The percentages of the kinetic and recoverable strain energy were smaller than the corresponding percentages of MSB. According to Figure 3-65, 17% of the work done is shown to be dissipated by irrecoverable strain energy after about 15 seconds.

The work and energy distribution time histories of the LSB for

the elastic and inelastic cases are shown in Figures 3-66 and 3-67. The dissipated damping energy continued to increase at an almost constant rate to 85% of the work done for the elastic case and 75% for the inelastic case. The percentages of the kinetic and recoverable strain energy were larger than the corresponding percentages of MSB with the same amplification factor. For the inelastic case, 12% of the work done is shown to be dissipated by irrecoverable strain energy after about 23 seconds.

3.4.7 Variation of Energy Distribution with Different Damping Ratio

The results of the work and energy distribution time histories, obtained by using a two-dimensional model of MSB (Figure 3-4) with different damping ratios, are shown in Figures 3-68 through 3-74. The responses are listed in Table 3-8. It is seen that the inelastic responses and reduction factor decreased when the value of damping ratio was increased. The amplification factor used is 2.0 for all cases.

There is no inelastic effect when the damping ratio is equal to 5%. In that case, most (96%) of the work done was dissipated by damping. When the damping ratio is equal to 0.25%, 50% of the work done was dissipated by damping and 30% of the work done was dissipated by irrecoverable strain energy. The ratios of irrecoverable strain energy, kinetic energy and recoverable strain energy to the work done increased when the damping ratio decreased.

3.4.8 Inelastic Responses Versus Linear Response Factor

For a given bridge model and ground motion, one may carry out a linear elastic analysis. The quantity $\bar{\Phi}_e$, for the case of "spherical

plastic potential function," is defined as:

$$\bar{\Phi}_e = \left(\frac{P}{P_0} \right)^2 + \left(\frac{M_y}{M_{y0}} \right)^2 + \left(\frac{M_x}{M_{x0}} \right)^2 \quad (3-4)$$

(The yielding condition is defined by setting $\bar{\Phi}_e - 1 = 0$ (Eq. 2-20).) It is a function of time and position in the structure. Its value can be greater than 1. Let Φ_e be the maximum value of $\bar{\Phi}_e$ for all points and times considered in the linear analysis. It is called the linear response factor.

For the same bridge model and ground motion, an inelastic analysis may be carried out. The maximum inelastic response in terms total plastic work (Eq. 2-39), plastic work density (Eqs. 2-40) and ductility factor (Eqs. 2-41 through 2-43) may be computed. These inelastic response quantities may be used to represent measures of "damages" done to the structure due to inelasticity. They are plotted for the most severely strained member in the bridge MSB, in Figure 3-75 as a function of Φ_e .

It is seen that the inelastic response quantities generally increase with the linear response factor. This is expected. Following the concept of force reduction factor as discussed in Section 3.4.5, one might use such a graph as follows. If one would accept a certain level of "damage", for example, a curvature ductility factor about y-axis equal to 3.5, the corresponding curve in Figure 3-75 would indicate a linear response factor equal to 1.88. This factor may be used as a "load reduction factor" (to be applied to the "seismic load" based on linear behavior) or an allowable stress increase factor.

Similar curves are presented for the other two bridge models in Figures 3-76 and 3-77.

3.5 GEOMETRIC NONLINEAR PROBLEMS

3.5.1 General

In the preceding the nonlinear effects due to material inelasticity were considered. In this section numerical results on nonlinear elastic effects ("geometric nonlinearity") are presented. For simplicity, only in-plane behavior is studied. The same bridge models and earthquake loading considered previously are used with the exception that the MSB is simplified to a 4-panel model as depicted in Figure 3-4. The main feature of nonlinear elastic effects is that the axial compressive force in the arch ribs would lower the stiffness of the structure (analogous to the case of a beam-column). That would change the response characteristic and could even lead to instability.

3.5.2 Typical Displacement Time Histories

3.5.2.1 Medium Span Bridge (MSB)

For this bridge, typical displacement time histories are presented for node 3 (at the 1/4 point of the rib) and node 5 (at the crown).

The horizontal displacement time histories are shown in Figures 3-78 and 3-79 for both the linear and nonlinear analyses. The predominant period for the linear elastic case is approximately 2.5 seconds which corresponds to the first mode (Table 3-1). For the nonlinear elastic case, the measured period is approximately 2.8 seconds which represents approximately a 10% increase from the linear case. This, of course, is due to the effects of the decreased stiffness of the ribs resulting from dead load compression.

The vertical displacement time histories are shown in Figures

3-80 and 3-81. For the quarter point (node 3), the predominant period is that of the first mode (2.5 seconds) for the linear case. The crown point (node 5) has zero vertical displacement in the first mode (See Figure 3-10), which explains the fact that the response shows mainly a combination of second and third modes (1.15 and 0.50 seconds, respectively). For the nonlinear response, one can again notice an increase in the values of the dominant period. For the quarter point, it is approximately 10%, as for the preceding case of horizontal displacement. For the crown point, the change is from 1.15 seconds to 1.2 seconds representing an increase of about 5% in the second mode.

3.5.2.2 Short Span Bridge (SSB)

This bridge model has no node at the crown. The displacements of the two nodes symmetric with respect to it are considered. They are node 9 (at the 2/7 span) and node 21 (at the 5/7 span) (See Figure 3-2).

The horizontal displacement time histories are shown in Figures 3-82 and 3-83. For the linear elastic case, the predominant period is approximately 1.1 seconds which corresponds to the first mode. The period for the nonlinear elastic case is approximately 1.2 seconds which represents approximately a 9% increase. The responses of the two nodes are in phase.

The vertical displacement time histories are shown in Figures 3-84 and 3-85. The features of dominant periods of these responses are similar to those discussed above. The responses of the two nodes are out-of-phase.

3.5.2.3 Long Span Bridge (LSB)

For this bridge model, the displacements are considered at node 18 (the crown), and two nodes symmetric to it: node 12 (at the 4/14 span) and node 24 (at the 10/14 span) (See Figure 3-3).

The horizontal displacement time histories are shown in Figures 3-86, 3-87, and 3-88. Again, the response was primarily in the first mode (with a period of about 3.5 seconds). There was approximately a 8% increase of the dominant period for the nonlinear elastic case (3.8 seconds) from the linear elastic case.

The vertical displacement time histories are shown in Figures 3-89, 3-90 and 3-91. The responses of the two symmetric nodes, nodes 12 and 24, were mostly in the first mode and there was little contribution from higher modes. The response of the crown node, node 18, was primarily in the second mode (1.5 seconds) and fourth mode (1.1 seconds). The change in the dominant period is approximately a 7% increase for these nodal displacements.

3.5.3 Maximum Displacements

The maximum displacements are listed in Tables 3-9, 3-10 and 3-11 for MSB, SSB and LSB, respectively. The odd numbers represent nodes on the rib and the even numbers on the deck for MSB and SSB (Figures 3-4 and 3-2). For LSB, the even numbers are on the rib and the odd numbers are on the deck (Figure 3-3).

In Table 3-9, It can be seen that the maximum horizontal displacements for MSB are 0.77% of the arch height (121.25 feet) for the linear elastic case and 0.94% for the nonlinear elastic case. The maximum vertical displacements are 1.69% of the arch height for the

linear elastic case and 1.79% for the nonlinear elastic case.

As listed in Table 3-10, the maximum horizontal displacements for SSB are 1.56% of the arch height (28.398 feet) for the linear elastic case and 1.19% for the nonlinear elastic case. The corresponding maximum vertical displacements are 3.22% and 2.59%.

As listed in Table 3-11, the maximum horizontal displacements for LSB are 0.98% of the arch height (370 feet) for the linear elastic case and 0.92% for the nonlinear elastic case. The corresponding maximum vertical displacements are 1.65% and 1.6%.

3.5.4 Typical Force Time Histories

Two points in each bridge model are selected for presentation of force time histories. At each point, two components are plotted: P_z (axial force) and M_y (in-plane bending).

3.5.4.1 Medium Span Bridge (MSB)

The two points selected are end J of member 1 at node 3 (the 1/4 span of the arch rib) and end I of member 4 at node 7 (the 3/4 span of the arch rib) (See Figure 3-4). They are symmetric with respect to the crown.

The axial force time histories are shown in Figures 3-92 and 3-93. The predominant period is approximately 0.5 seconds which corresponds to the third mode. As was noted previously in Section 3.4.4.3, this dominance appears to be due to the fact that this third mode is the lowest mode in which axial force dominates (over bending) (See Figure 3-10). The wave patterns for the linear elastic and nonlinear elastic responses are quite similar.

The in-plane bending time histories are shown in Figures 3-94 and 3-95. In this case, it appears that the responses were mainly in the first and third modes. (These points, at which the responses are being considered, appear to be close to points of counter-flexure for the second mode.)

3.5.4.2 Short Span Bridge (SSB)

The two points selected are end J of member 2 at node 9 (the 2/7 span of the arch rib) and end I of member 6 at node 21 (the 5/7 span of the arch rib) (Figure 3-2). The results on this bridge are shown in Figures 3-96 through 3-99. They are generally similar in character to those presented in the preceding.

However, the in-plane bending response was primarily in its first mode. Unlike the preceding case of MSB, there was little contribution from the third mode. It should be noted that the points, at which the responses are being considered, do not quite correspond for the two bridge models.

3.5.4.3 Long Span Bridge (LSB)

The two points selected are end I of member 5 at node 12 (the 4/14 span of the arch rib) and end J of member 10 at node 24 (the 10/14 span of the arch rib) (See Figure 3-3). They are the same points from the same ("one-plane") model in Section 3.4.4.3 for material nonlinearity.

The results on this bridge are shown in Figures 3-100 through 3-103. It can be seen that the results are very close to those presented in Section 3.4.4.3. While in that section ground motions in three

directions were applied, here only in-plane motions are applied. These results thus suggest that the in-plane and out-of-plane responses were largely uncoupled for this ("one-plane") bridge model.

3.5.5 Maximum Forces

The maximum internal forces are listed in Tables 3-12, 3-13 and 3-14 for MSB, SSB, and LSB, respectively. There is no appreciable difference between linear elastic and nonlinear elastic solution.

3.5.6 Typical Work and Energy Distribution Time Histories

As was done in Section 3.4.6 for the case of material nonlinearity, the work and energy distribution time histories of the linear elastic and nonlinear elastic case of MSB, SSB, and LSB were calculated and are shown in Figures 3-104 through 3-109.

It may be seen that the differences between the linear and nonlinear elastic cases are very small for all three bridge models. The values of the ratios plotted for the kinetic and strain energy of SSB are larger than those of MSB and less than those of LSB. However, for both cases the kinetic and recoverable strain energy remain relatively small throughout the whole 45 seconds. This points to the importance of the role of damping.

3.5.7 Instability Effects

The results in Sec. 3.5.3 indicated that a consideration of the nonlinear elastic behavior increased the maximum displacement by 10% to 20% for MSB. But for the other two bridge models, such effects of the nonlinear behavior were much smaller (even negative). To consider

possible instability effects, the static buckling loads were computed as linear eigenvalue problems. They were found to be 4.415 D.L., 7.185 D.L. and 8.557 D.L. (D.L. stands for "dead load" for the respective models) for MSB, SSB and LSB, respectively.

The seismic responses were computed by increasing the initial load (initially applied static load) to be a factor times D.L.. No instability effects were observed until the initial load was closed to the static buckling load. This is illustrated in Table 3-15, in which are listed the maximum horizontal displacements at the crown for MSB and LSB, and at node 7 for SSB. It is seen that the maximum displacements remain quite moderate until the dead load placed almost reached the magnitude of the static buckling load. The responses for MSB and SSB became "infinite" at 99% of the buckling load. However, for LSB (See also Figure 3-110), even after the initial load exceeded the static buckling load the responses remained "finite" (but at larger rates of increase). The reason may lie in the difference in the boundary conditions between LSB and the other two bridge models (See Figures 3-2, 3-3 and 3-4.)

Table 3-1. Natural Periods of Vibration

Out-of-Plane				(second)
Mode No.	MSB	SSB	LSB	
1	3.032	1.180	4.716	
2	1.204	1.127	3.677	
3	1.174	0.379	2.612	
4	0.942	0.370	1.424	
In-Plane				(second)
Mode No.	MSB	SSB	LSB	
1	2.247	1.065	3.565	
2	1.276	0.484	1.534	
3	0.685	0.304	1.221	
4	0.469	0.242	1.094	
Two-Dimensional model of MSB (4 panels)				(second)
Mode No.	1	2	3	4
MSB	2.514	1.151	0.503	0.173

Table 3-2. Elastic and Inelastic Maximum Displacements of MSB

Nodal No.	Displacements(ft)		
	Horizontal	Vertical	Lateral
No. 5	1.082 (1.034)	1.637 (1.782)	0.856 (0.834)
No. 6	0.383 (0.359)	1.625 (1.795)	3.747 (3.528)
No. 7	1.237 (1.370)	1.867 (2.073)	0.856 (0.834)
No. 8	0.401 (0.376)	1.855 (2.049)	3.747 (3.528)
No. 17	0.455 (0.541)	2.437 (2.267)	7.772 (7.239)
No. 18	0.177 (0.169)	2.449 (2.267)	9.858 (9.215)
No. 19	0.456 (0.534)	2.389 (2.558)	7.772 (7.239)
No. 20	0.178 (0.173)	2.389 (2.571)	9.858 (9.215)
No. 29	1.334 (1.225)	2.073 (1.976)	0.867 (0.732)
No. 30	0.588 (0.552)	2.098 (2.001)	4.765 (4.401)
No. 31	1.124 (1.225)	1.843 (1.855)	0.867 (0.732)
No. 32	0.567 (0.531)	1.879 (1.843)	4.765 (4.401)

(.....) : Inelastic Displacement

Table 3-3. Elastic and Inelastic Maximum Displacements of SSB

Nodal No.	Displacements(ft)		
	Horizontal	Vertical	Lateral
No. 9	0.426 (0.378)	0.898 (0.835)	0.520 (0.503)
No. 10	0.388 (0.355)	0.900 (0.837)	0.987 (0.922)
No. 11	0.449 (0.400)	0.884 (0.884)	0.520 (0.503)
No. 12	0.386 (0.360)	0.886 (0.886)	0.987 (0.922)
No. 13	0.369 (0.334)	0.686 (0.771)	0.851 (0.804)
No. 14	0.383 (0.350)	0.689 (0.771)	0.950 (0.893)
No. 15	0.371 (0.339)	0.726 (0.830)	0.851 (0.804)
No. 16	0.383 (0.357)	0.729 (0.832)	0.950 (0.893)
No. 21	0.447 (0.400)	0.830 (0.853)	0.520 (0.487)
No. 22	0.386 (0.353)	0.835 (0.856)	0.987 (0.933)
No. 23	0.421 (0.407)	0.835 (0.766)	0.520 (0.487)
No. 24	0.388 (0.360)	0.837 (0.771)	0.987 (0.933)

(.....) : Inelastic Displacement

Table 3-4. Elastic and Inelastic Maximum Displacements of LSB

Nodal No.	Displacements(ft)		
	Horizontal	Vertical	Lateral
No. 12	3.619 (3.156)	6.068 (5.439)	5.365 (5.180)
No. 13	2.723 (2.560)	6.105 (5.476)	10.101 (9.250)
No. 18	2.868 (2.538)	2.320 (2.213)	8.658 (8.362)
No. 19	2.150 (2.146)	2.331 (2.224)	7.548 (7.141)
No. 24	3.530 (3.497)	5.883 (5.920)	5.365 (5.254)
No. 25	2.609 (2.560)	5.920 (5.957)	10.101 (9.398)

(.....) : Inelastic Displacement

Table 3-5. Elastic and Inelastic Maximum End Forces of MSB

Member End		Linear Elastic	Nonlinear Inelastic	Reduction Factor	Fully Plastic Force
1-J	P_z	8907	8635	0.031	10064.34
	M_y	40547	29584	0.270	30034.75
	M_x	4369	4989	-0.142	12169.45
16-I	P_z	9088	7890	0.132	10064.34
	M_y	43851	29344	0.331	30034.75
	M_x	4381	4077	0.069	12169.45

P_z : kips ; M_y : ft-kips ; M_x : ft-kips

Table 3-6. Elastic and Inelastic Maximum End Forces of SSB

Member End		Linear Elastic	Nonlinear Inelastic	Reduction Factor	Fully Plastic Force
9-J	P_z	2669	2455	0.080	4554.000
	M_y	7235	5623	0.223	5696.625
	M_x	185	193	-0.043	3112.313
13-I	P_z	2910	2637	0.094	4554.000
	M_y	6779	5577	0.177	5696.625
	M_x	185	247	-0.335	3112.313

P_z : kips ; M_y : ft-kips ; M_x : ft-kips

Table 3-7. Elastic and Inelastic Maximum End Forces of LSB

Member End		Linear Elastic	Nonlinear Inelastic	Reduction Factor	Fully Plastic Force
5-I	P_z	68350	67605	0.011	82849
	M_y	1667632	1554821	0.068	1634933
	M_x	322119	322119	0.000	2982580
10-J	P_z	66610	66610	0.000	82849
	M_y	1765728	1523757	0.137	1634933
	M_x	322119	283643	0.119	2982580

P_z : kips ; M_y : ft-kips ; M_x : ft-kips

Table 3-8. Maximum Responses for Various Values of Damping Ratio

Damping ratio (%)	Node 5 Displacement(ft)		Ductility Factor M_y	Plastic Work Density by M_y	Total Plastic Work
	Horizontal	Vertical			
0.25	0.558	0.825	17.560	527.33	11094
0.5	0.571	0.808	16.049	330.56	6772
1.0	0.761	0.764	14.591	140.72	2599
2.0	0.618	0.732	5.909	56.92	884
3.0	0.557	0.755	2.083	20.31	272
5.0	0.468	0.743	-----	-----	-----

Damping Ratio (%)	Member 1 End J					
	Axial Force (P_z)			In-Plane Bending (M_y)		
	Inelastic	Elastic	Reduction	Inelastic	Elastic	Reduction
0.25	9197	15420	0.404	48087	112430	0.572
0.5	8922	11841	0.246	48136	98802	0.513
1.0	7972	9982	0.201	48330	79334	0.391
2.0	6870	7724	0.110	44923	61325	0.263
3.0	6182	6499	0.049	45313	52565	0.138
5.0	5259	5259	0.000	43123	43123	0.000

P_z : kips ; M_y : ft-kips

Table 3-9. Linear and Nonlinear Elastic Maximum Displacements of MSB

Nodal No.	Linear Elastic (ft)		Nonlinear Elastic (ft)	
	Horizontal	Vertical	Horizontal	Vertical
3	0.918	1.831	1.135	2.037
4	0.409	1.879	0.409	2.086
5	0.650	0.955	0.833	1.135
6	0.663	0.968	0.663	1.146
7	0.935	2.001	1.062	2.134
8	0.832	2.049	0.832	2.170

Table 3-10. Linear and Nonlinear Elastic Maximum Displacements of SSB

Nodal No.	Linear Elastic (ft)		Nonlinear Elastic (ft)	
	Horizontal	Vertical	Horizontal	Vertical
5	0.443	0.912	0.329	0.684
6	0.389	0.914	0.312	0.687
7	0.378	0.525	0.278	0.491
8	0.386	0.528	0.307	0.491
11	0.437	0.849	0.338	0.733
12	0.389	0.852	0.312	0.736

Table 3-11. Linear and Nonlinear Elastic Maximum Displacements of LSB

Nodal No.	Linear Elastic (ft)		Nonlinear Elastic (ft)	
	Horizontal	Vertical	Horizontal	Vertical
12	3.619	6.068	3.414	5.920
13	2.723	6.105	2.542	5.920
18	2.868	2.320	2.642	2.301
19	2.150	2.331	1.865	2.309
24	3.530	5.883	3.230	5.587
25	2.609	5.920	2.290	5.624

Table 3-12. Linear and Nonlinear Elastic Maximum End Forces of MSB

Member End	Linear Elastic		Nonlinear Elastic	
	Axial Force P_z kips	In-Plane Bending M_y ft-kips	Axial Force P_z kips	In-Plane Bending M_y ft-kips
1-J	8633	67653	8564	71546
4-I	8784	68626	8756	69600

Table 3-13. Linear and Nonlinear Elastic Maximum End Forces of SSB

Member End	Linear Elastic		Nonlinear Elastic	
	Axial Force P_z kips	In-Plane Bending M_y ft-kips	Axial Force P_z kips	In-Plane Bending M_y ft-kips
2-J	2268	7064	2218	6152
6-I	2026	6551	2077	6665

Table 3-14. Linear and Nonlinear Elastic Maximum End Forces of LSB

Member End	Linear Elastic		Nonlinear Elastic	
	Axial Force P_z kips	In-Plane Bending M_y ft-kips	Axial Force P_z kips	In-Plane Bending M_y ft-kips
5-I	68350	1667632	68599	1623488
10-J	66610	1765728	69593	1554821

Table 3-15. Maximum Displacements for Different Values of Initial Load

MSB (Buckling Load = 4.415 D.L.)		SSB (Buckling Load = 7.185 D.L.)	
Initial Load	Node 5 Horizontal Displ.	Initial Load	Node 7 Horizontal Displ.
4.300 D.L.	0.3492 ft	7.000 D.L.	0.5992 ft
4.350 D.L.	0.4450 ft	7.100 D.L.	0.4089 ft
4.360 D.L.	0.4729 ft	7.150 D.L.	0.4742 ft
4.365 D.L.	0.4874 ft	7.155 D.L.	0.5311 ft
4.370 D.L.	2.0E+10 ft	7.160 D.L.	6.5031 ft
LSB (Buckling Load = 8.557 D.L.)			
Initial Load	Node 18 Horizontal Displ.	Initial Load	Node 18 Horizontal Displ.
8.45 D.L.	1.2136 ft	8.56 D.L.	2.7454 ft
8.46 D.L.	1.2506 ft	8.57 D.L.	3.7740 ft
8.47 D.L.	1.2987 ft	8.58 D.L.	5.2540 ft
8.48 D.L.	1.3579 ft	8.59 D.L.	7.2890 ft
8.49 D.L.	1.4356 ft	8.60 D.L.	9.5090 ft
8.50 D.L.	1.5281 ft	8.61 D.L.	13.801 ft
8.51 D.L.	1.6428 ft	8.62 D.L.	18.944 ft
8.52 D.L.	1.7760 ft	8.63 D.L.	25.567 ft
8.53 D.L.	1.9499 ft	8.64 D.L.	33.078 ft
8.54 D.L.	2.1645 ft	8.65 D.L.	43.290 ft
8.55 D.L.	2.4235 ft	8.66 D.L.	54.760 ft

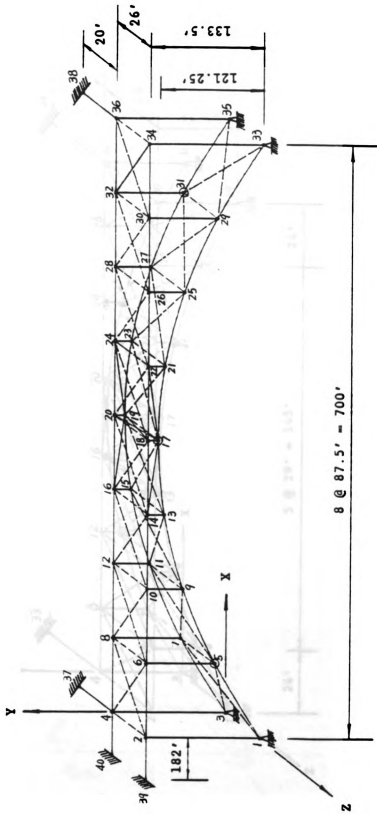


Figure 3-1. Medium Span Bridge (MSB) Model (A "True" Three-Dimensional Model)

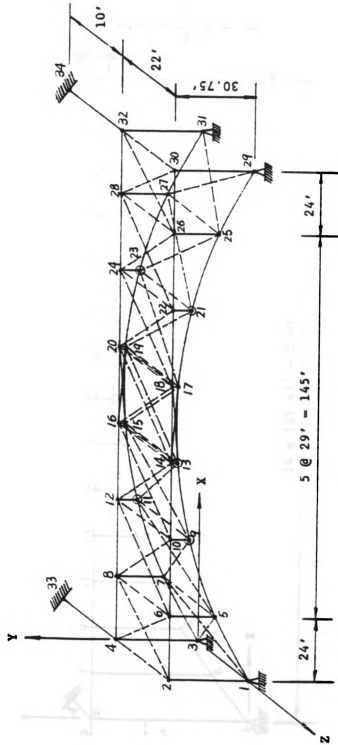


Figure 3-2. Short Span Bridge (SSB) Model (A "True" Three-Dimensional Model)

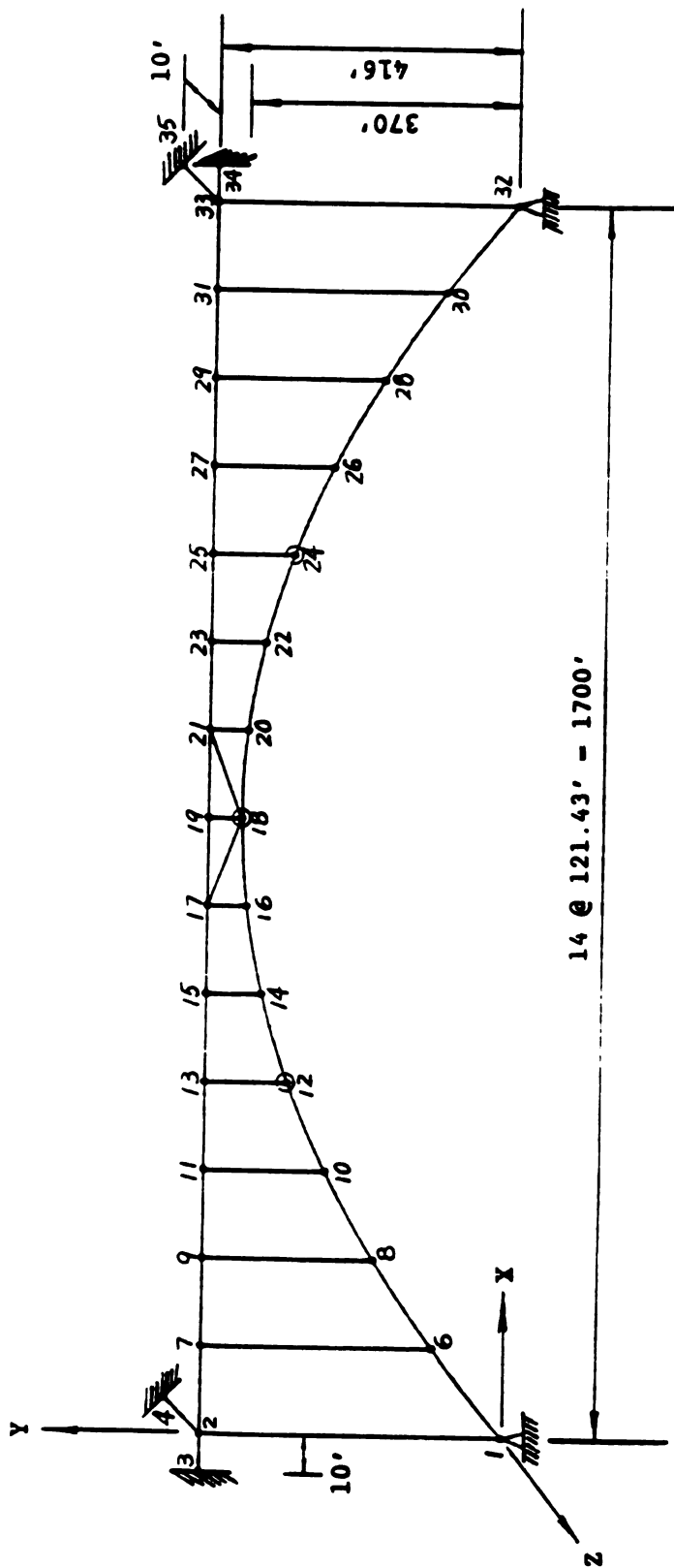


Figure 3-3. Long Span Bridge (LSB) Model (A "One-Plane" Model)

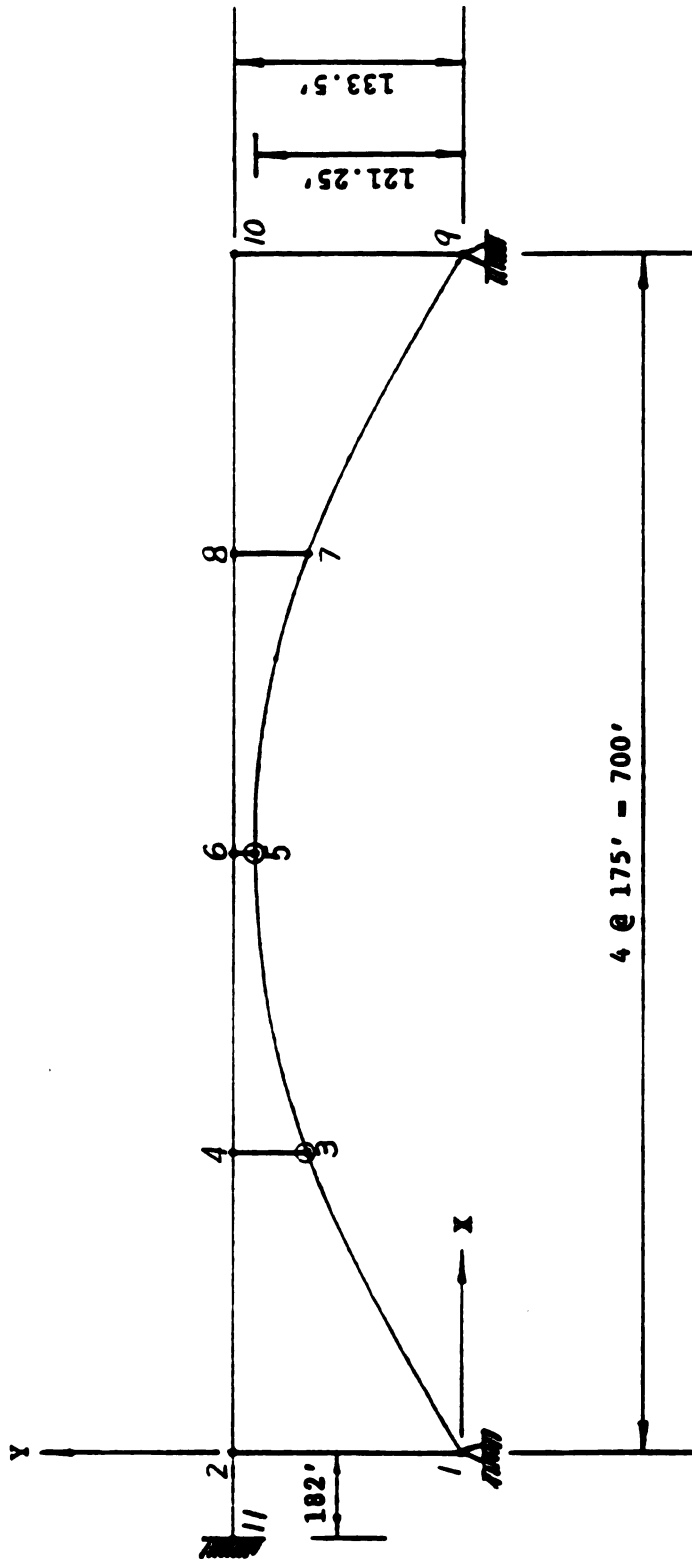
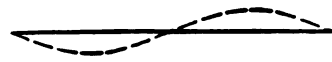


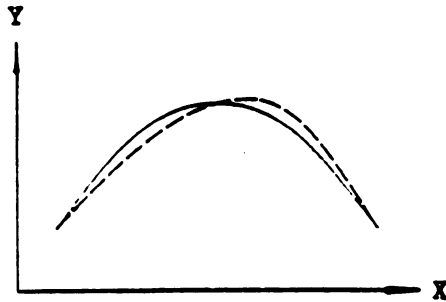
Figure 3-4. Medium Span Bridge Model (Two-Dimensional Model)



Front and Rear Deck

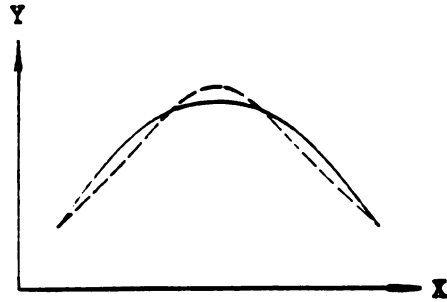


Front and Rear Deck



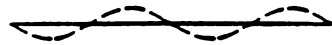
Front and Rear Rib

Mode 1 (2^*)



Front and Rear Rib

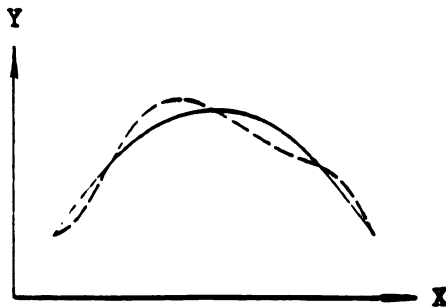
Mode 2 (3^*)



Front and Rear Deck

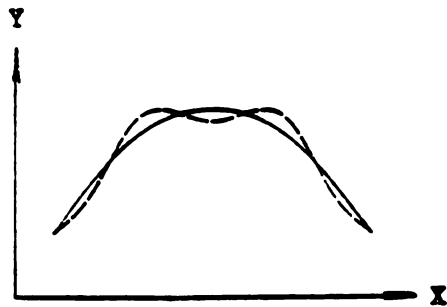


Front and Rear Deck



Front and Rear Rib

Mode 3 (8^*)

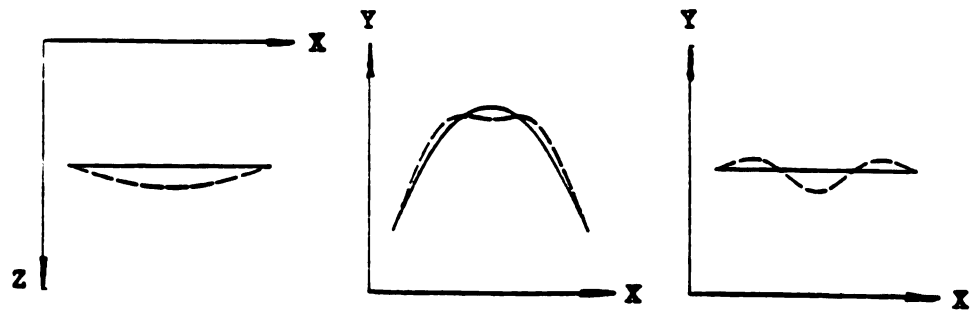


Front and Rear Rib

Mode 4 (12^*)

(* denotes overall mode number.)

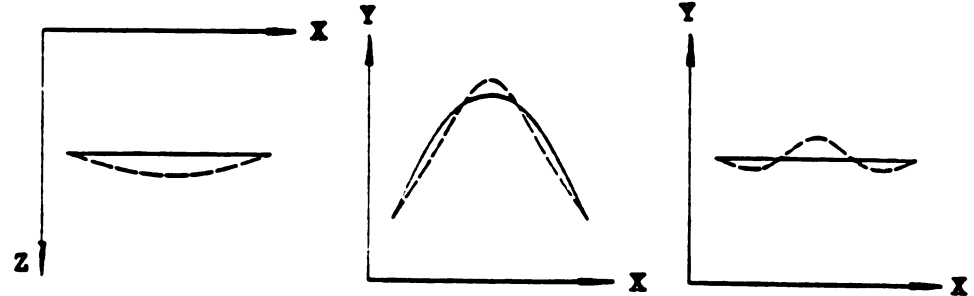
Figure 3-5. In-Plane Mode Shapes for MSB



Front and Rear Deck

Front Rib

Front Deck

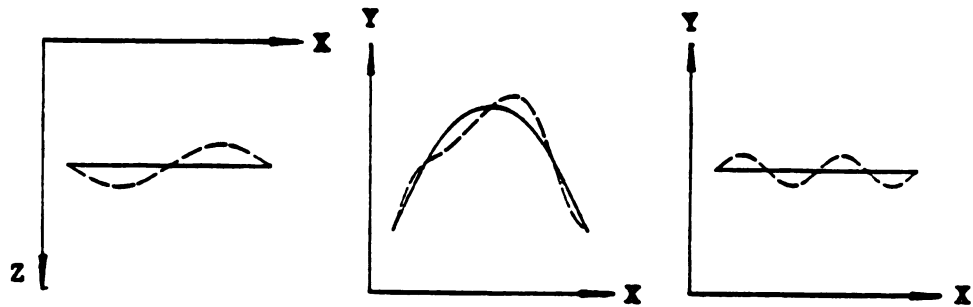


Front and Rear Rib

Rear Rib

Rear Deck

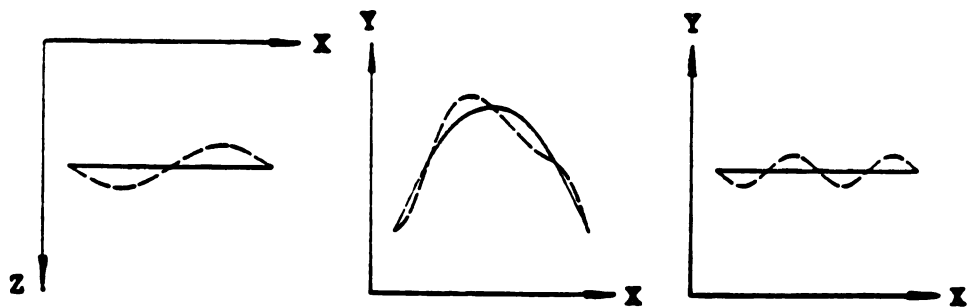
Mode 1 (1*)



Front and Rear Deck

Front Rib

Front Deck



Front and Rear Rib

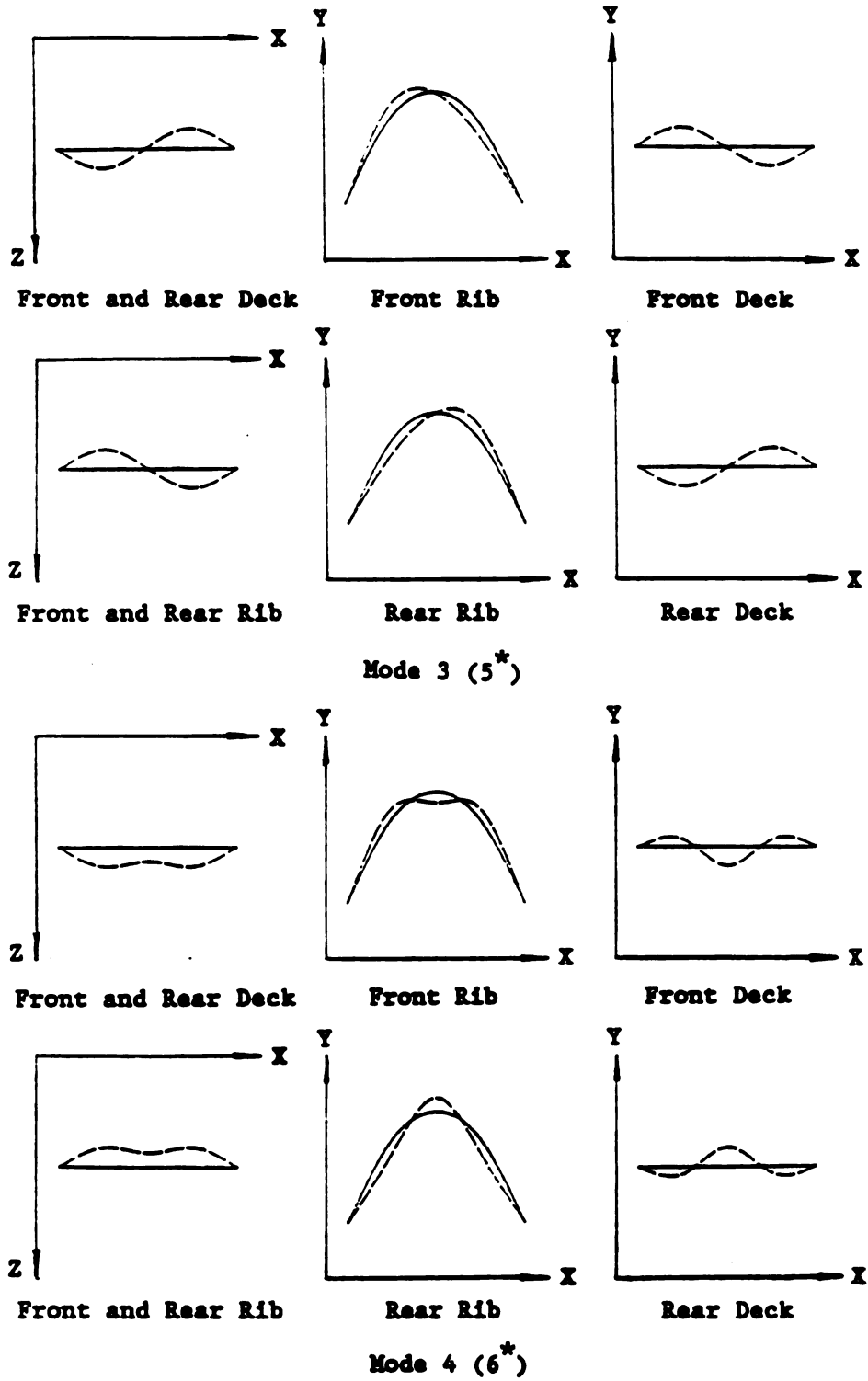
Rear Rib

Rear Deck

Mode 2 (4*-MSB; 3*-SSB)

(* denotes overall mode number.)

Figure 3-6. Out-of-Plane Mode Shapes for MSB and SSB



(* denotes overall mode number.)

(Continued)

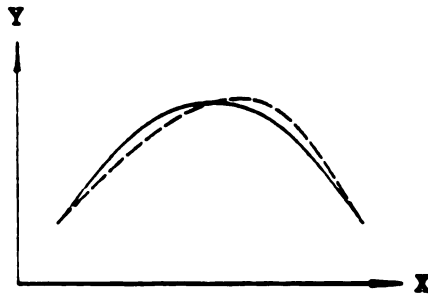
Figure 3-6. Out-of-Plane Mode Shapes for MSB and SSB



Front and Rear Deck

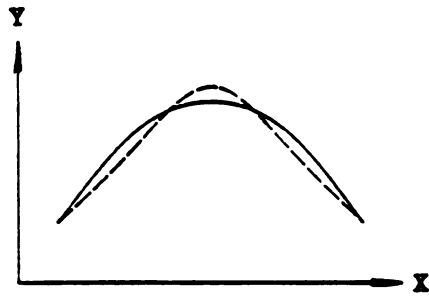


Front and Rear Deck



Front and Rear Rib

Mode 1 (2^{*})

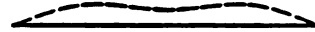


Front and Rear Rib

Mode 2 (4^{*})



Front and Rear Deck

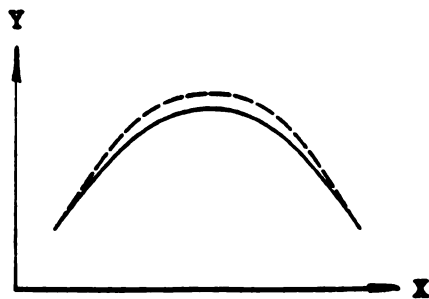


Front and Rear Deck



Front and Rear Rib

Mode 3 (7^{*})

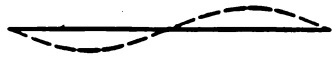


Front and Rear Rib

Mode 4 (9^{*})

(* denotes overall mode number.)

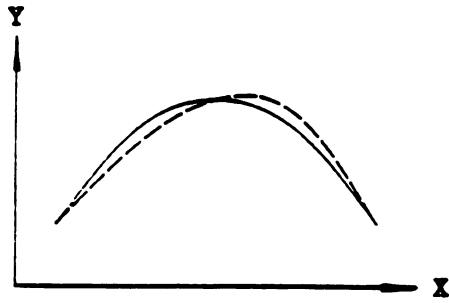
Figure 3-7. In-Plane Mode Shapes for SSB



Front and Rear Deck

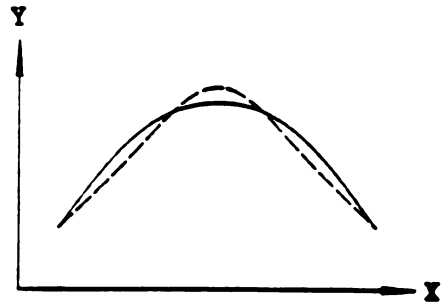


Front and Rear Deck



Front and Rear Rib

Mode 1 (2^{*})

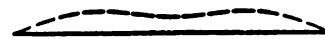


Front and Rear Rib

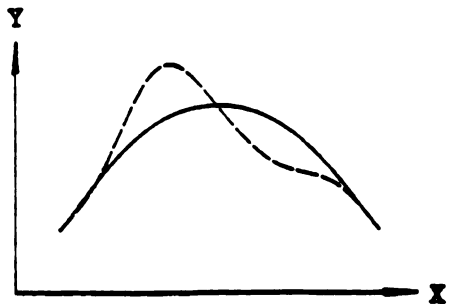
Mode 2 (5^{*})



Front and Rear Deck

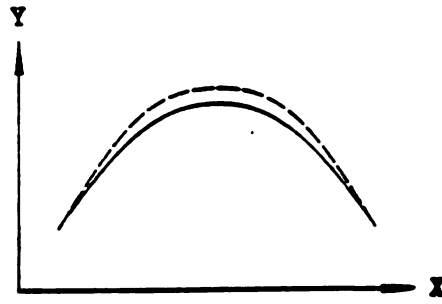


Front and Rear Deck



Front and Rear Rib

Mode 3 (8^{*})

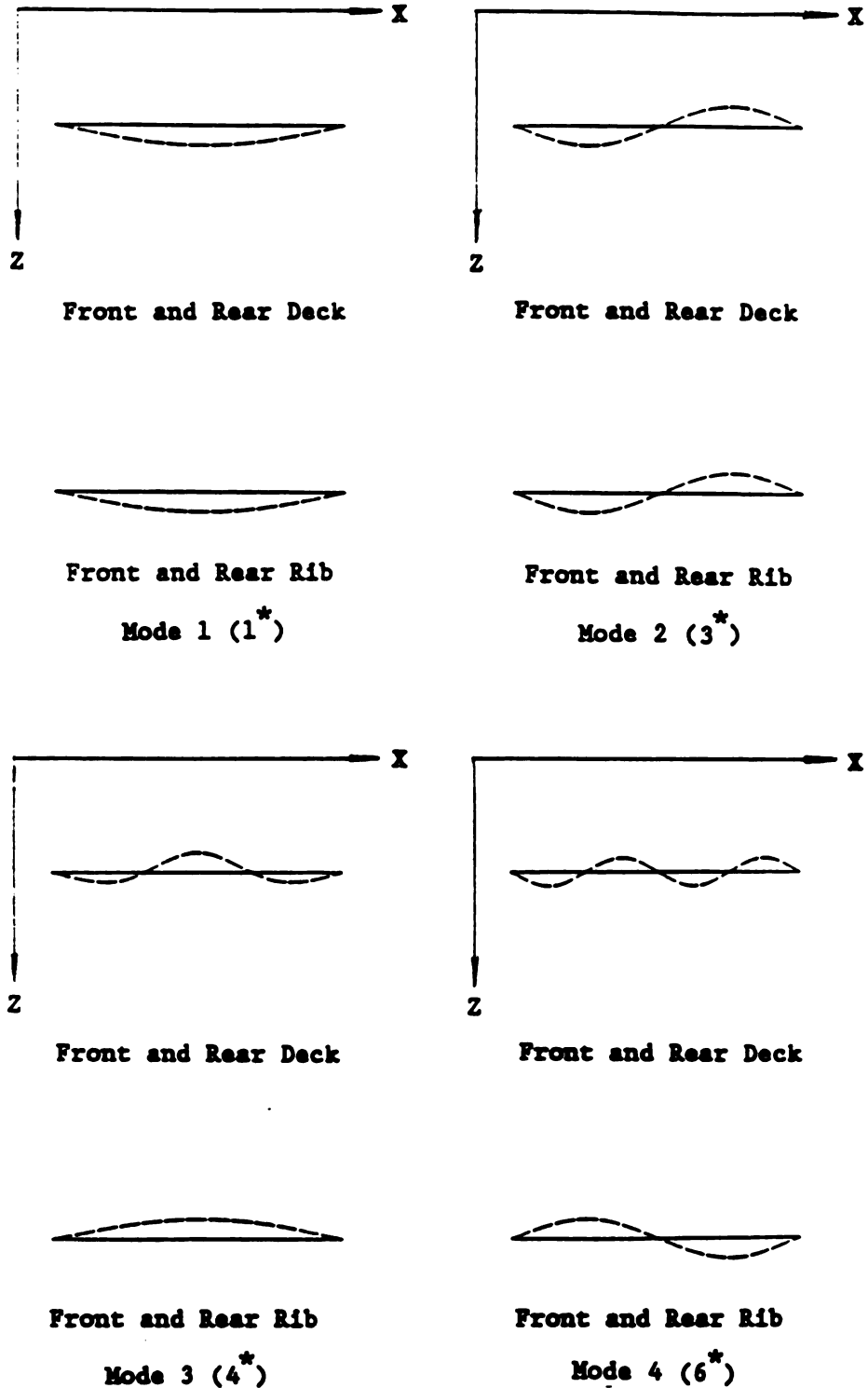


Front and Rear Rib

Mode 4 (9^{*})

(* denotes overall mode number.)

Figure 3-8. In-Plane Mode Shapes for LSB



(* denotes overall mode number.)

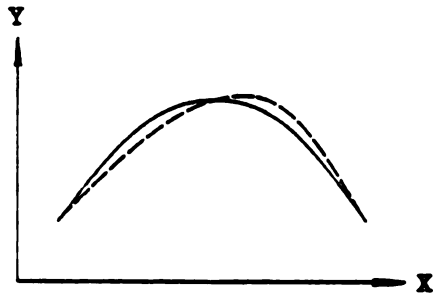
Figure 3-9. Out-of-Plane Mode Shapes for LSB



Front and Rear Deck

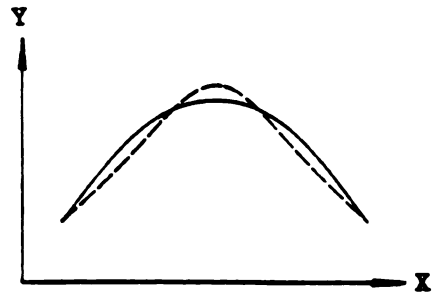


Front and Rear Deck



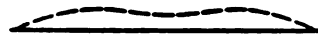
Front and Rear Rib

Mode 1



Front and Rear Rib

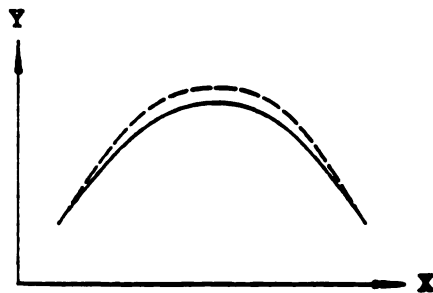
Mode 2



Front and Rear Deck



Front and Rear Deck



Front and Rear Rib

Mode 3



Front and Rear Rib

Mode 4

Figure 3-10. In-Plane Mode Shapes for Two-Dimensional MSB

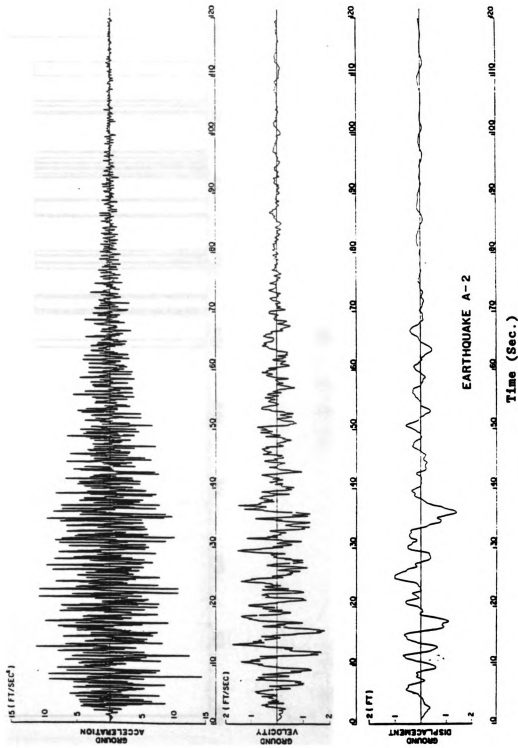


Figure 3-11. CIT-A2 Ground Motion

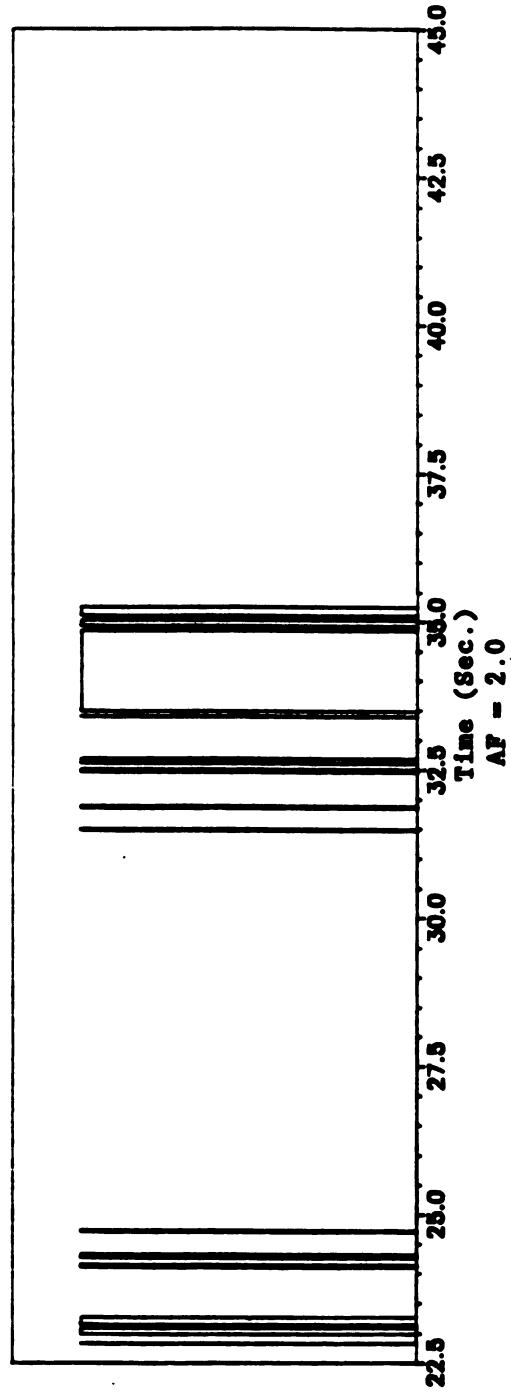
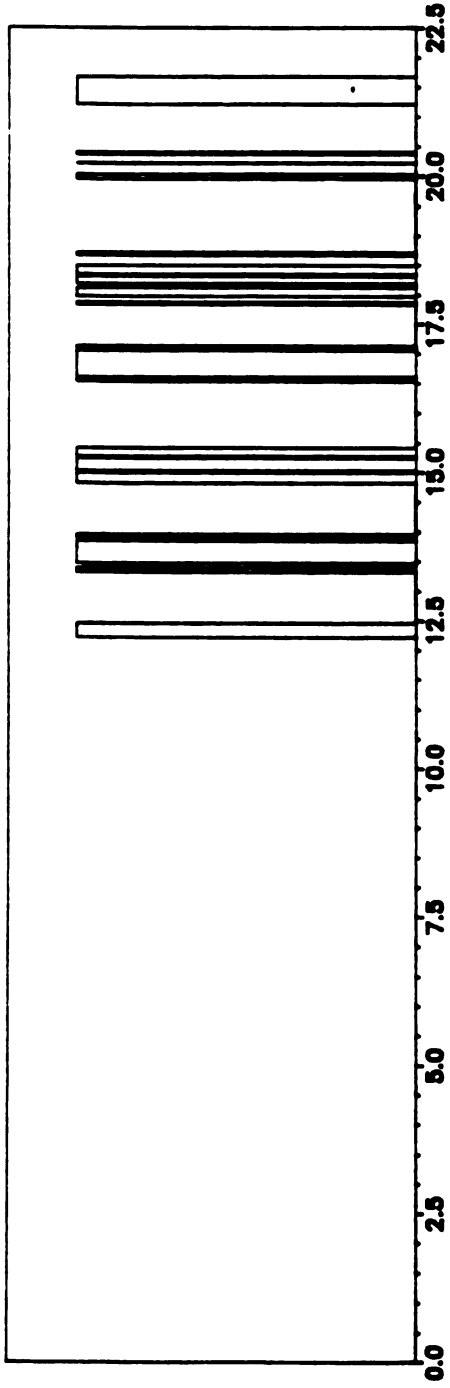


Figure 3-12. Time Intervals with Inelastic Response (MSB)

AF - 2.0

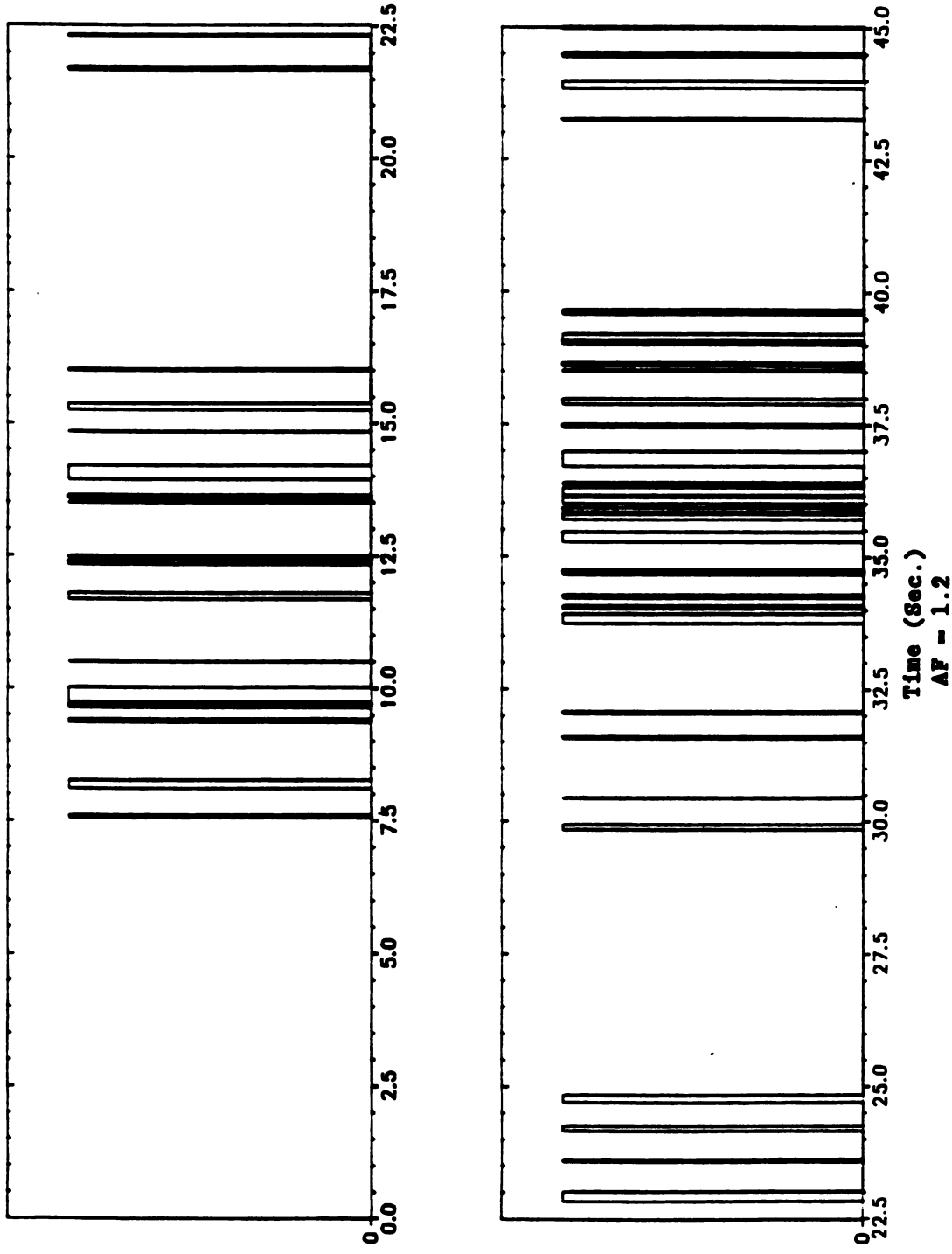


Figure 3-13. Time Intervals with Inelastic Response (SSB)
AF = 1.2

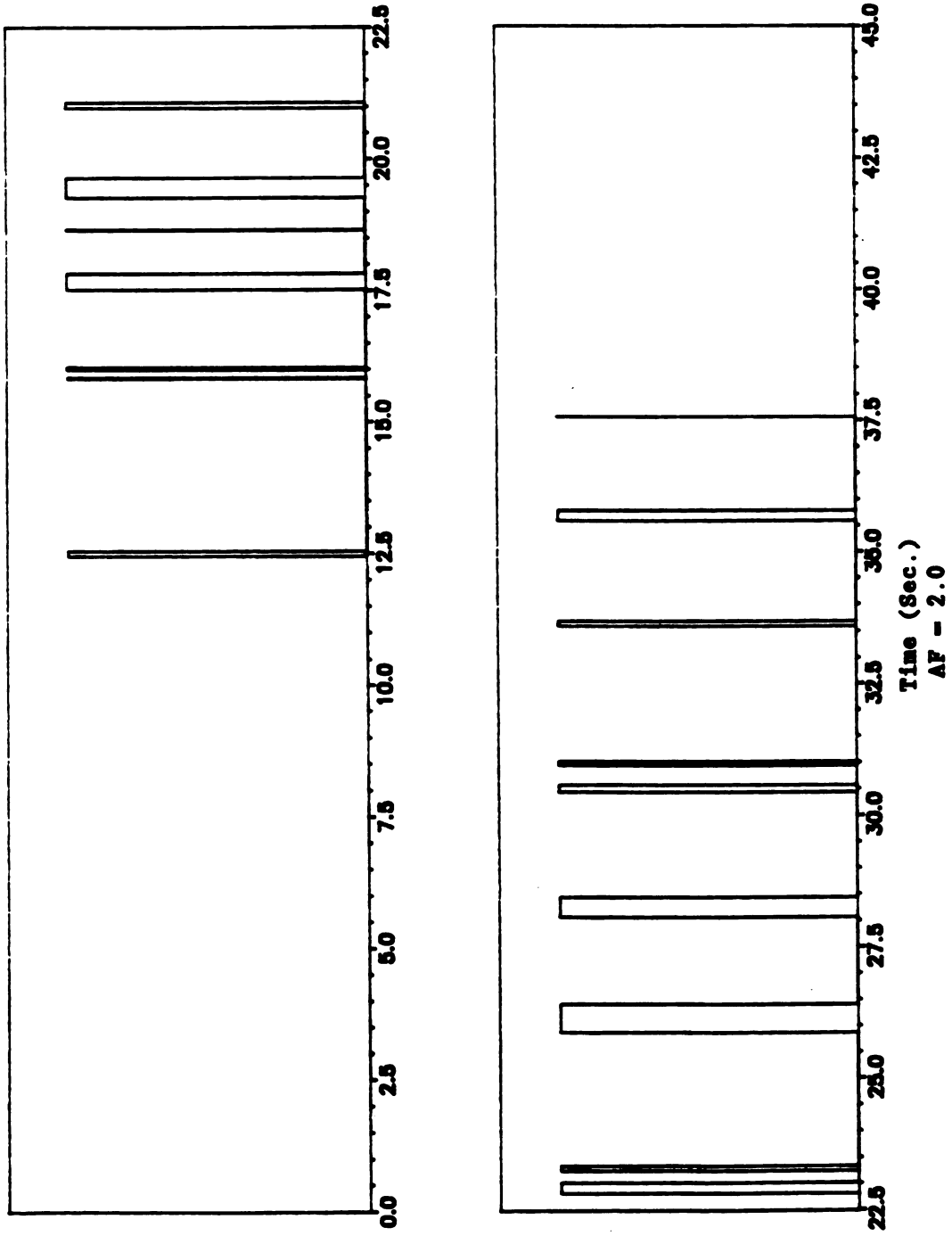


Figure 3-14. Time Intervals with Inelastic Response (LSB)
AF - 2.0

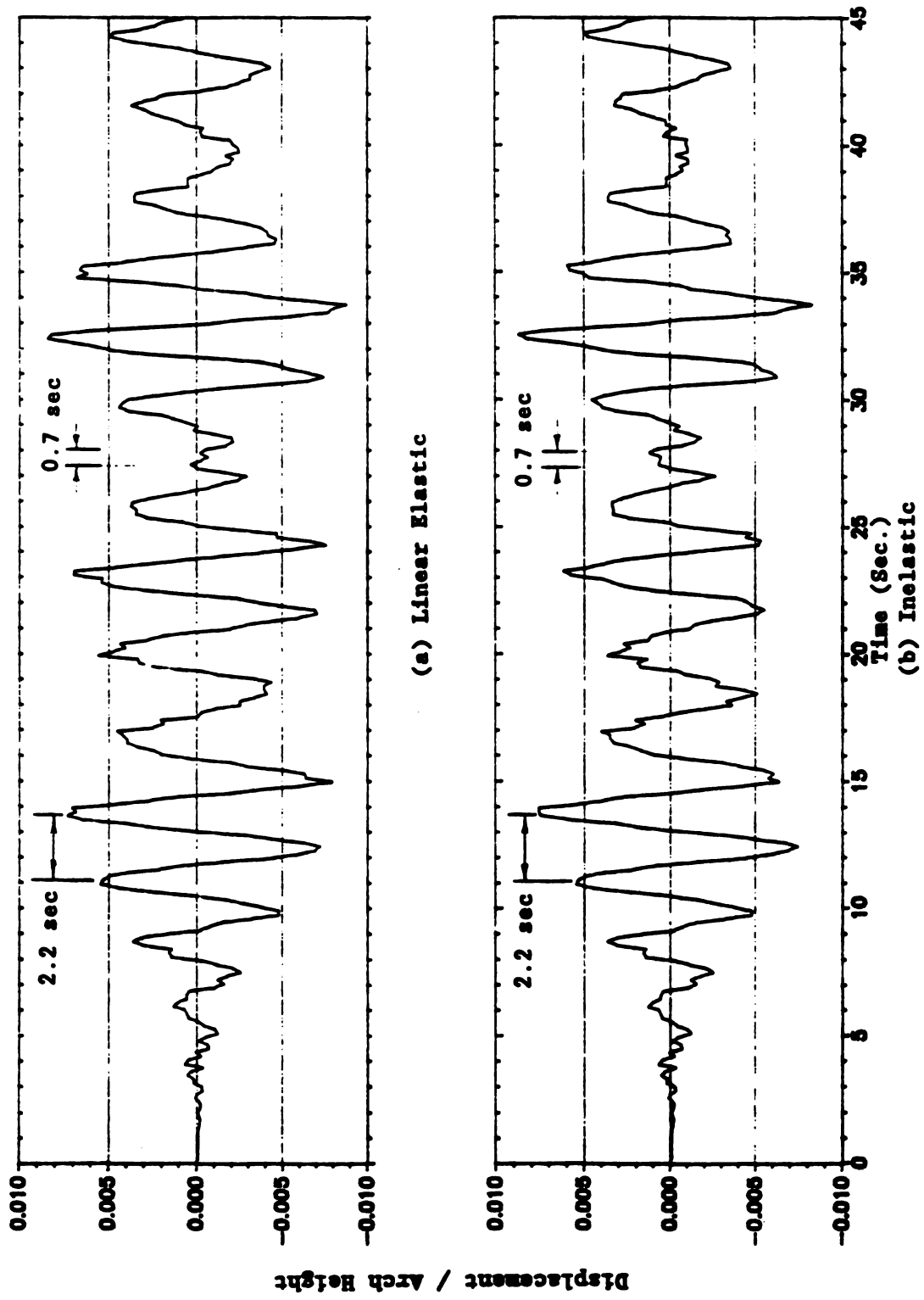


Figure 3-15. Node 5 Horizontal (X) Displacement Time History for MSB

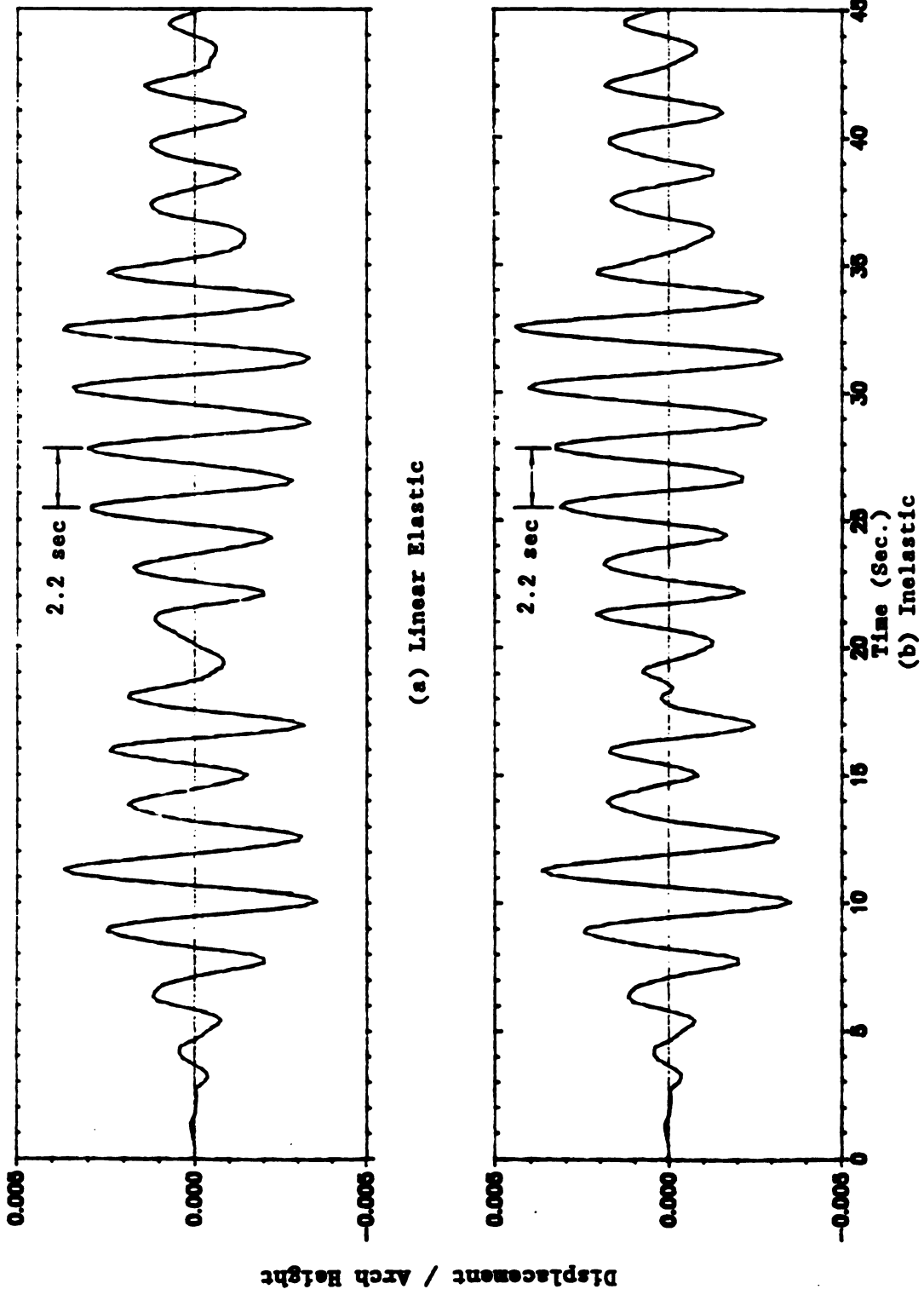
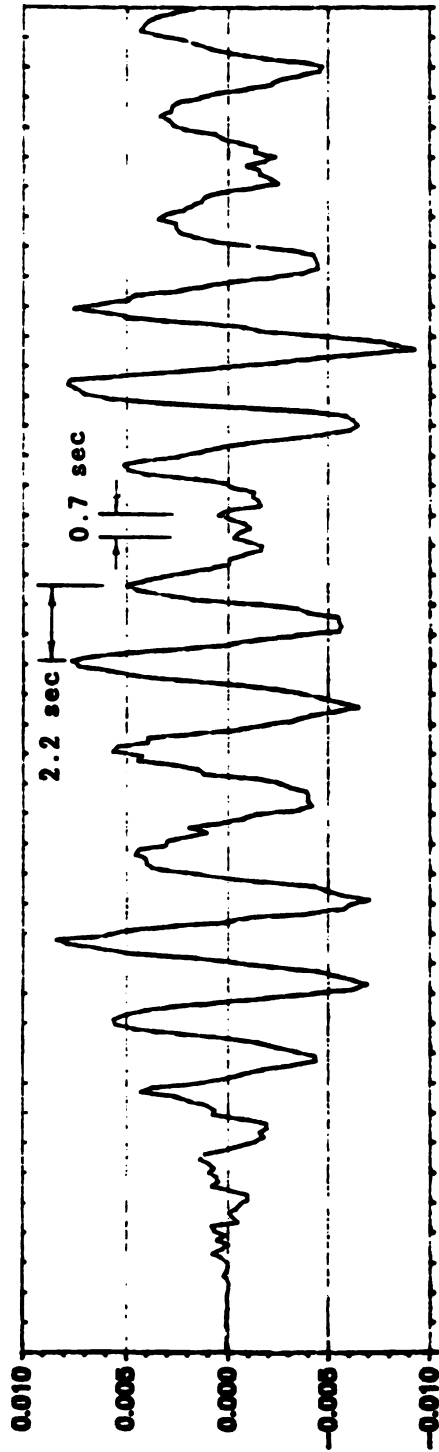
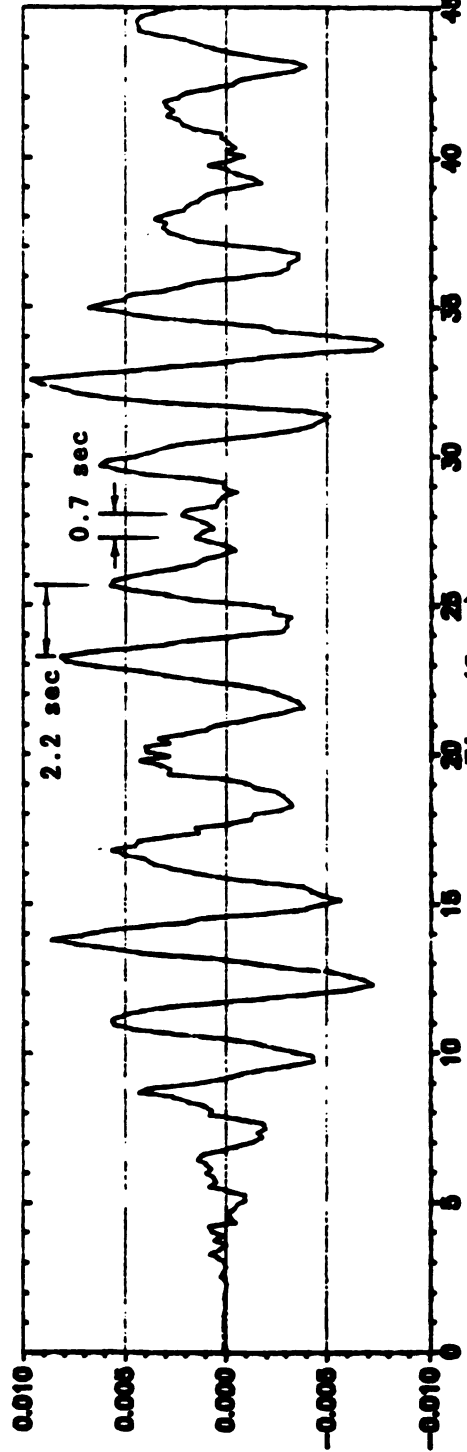


Figure 3-16. Node 17 Horizontal (X) Displacement Time History for MSB



(a) Linear Elastic



(b) Inelastic

Figure 3-17. Node 31 Horizontal (X) Displacement Time History for MSB

Displacement / Arch Height

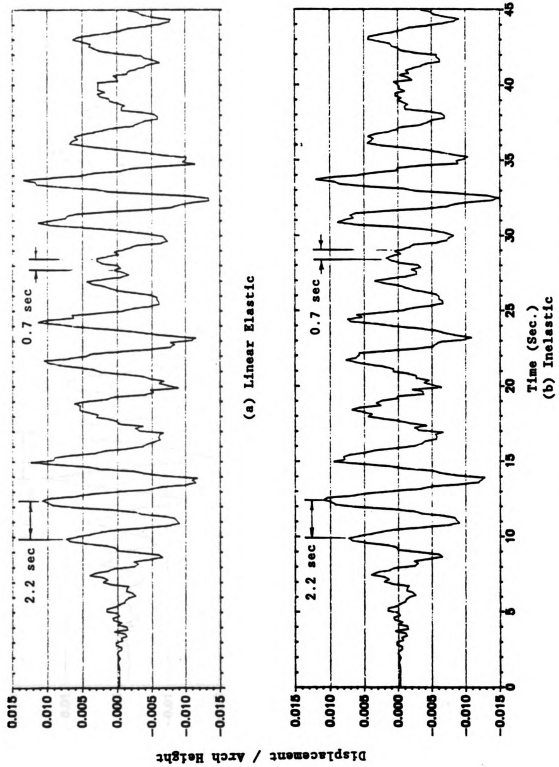
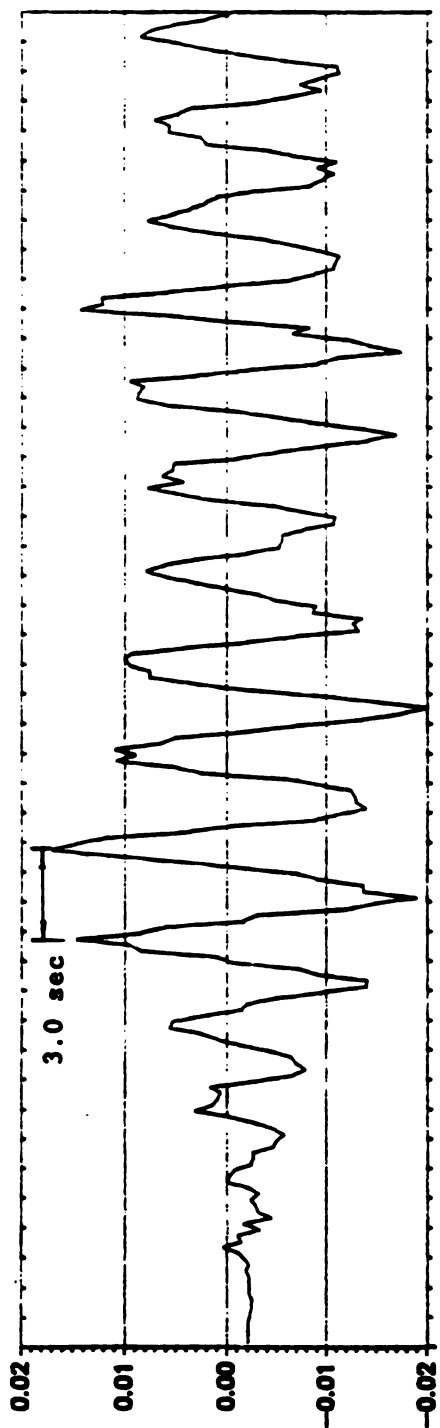
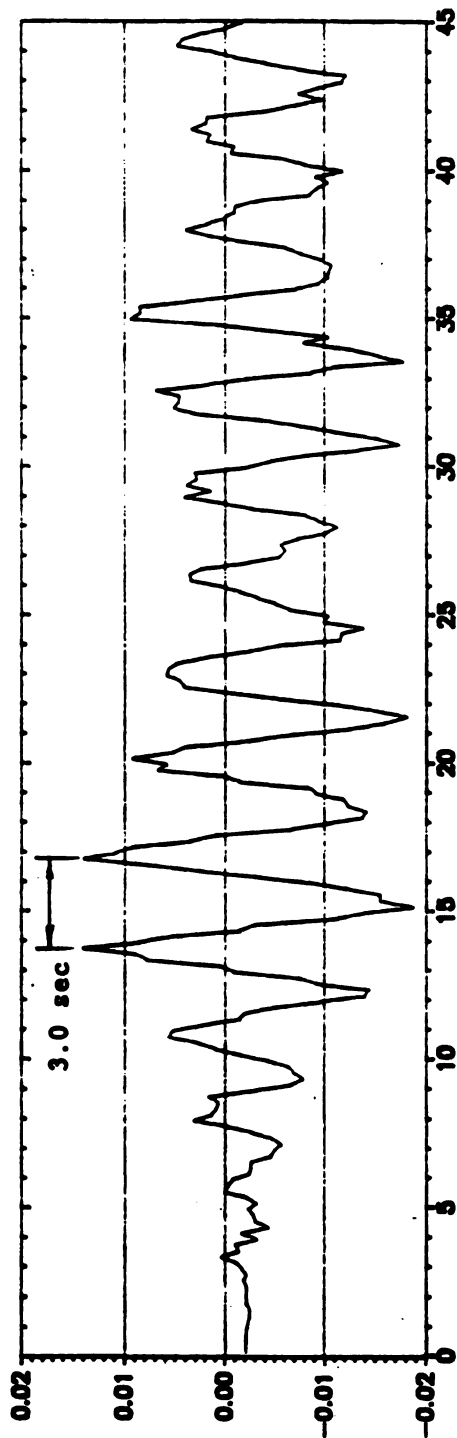


Figure 3-18. Node 5 Vertical (Y) Displacement Time History for MSE



(a) Linear Elastic



(b) Inelastic

Figure 3-19. Node 17 Vertical (Y) Displacement Time History for MSB

Displacement / Arch Height

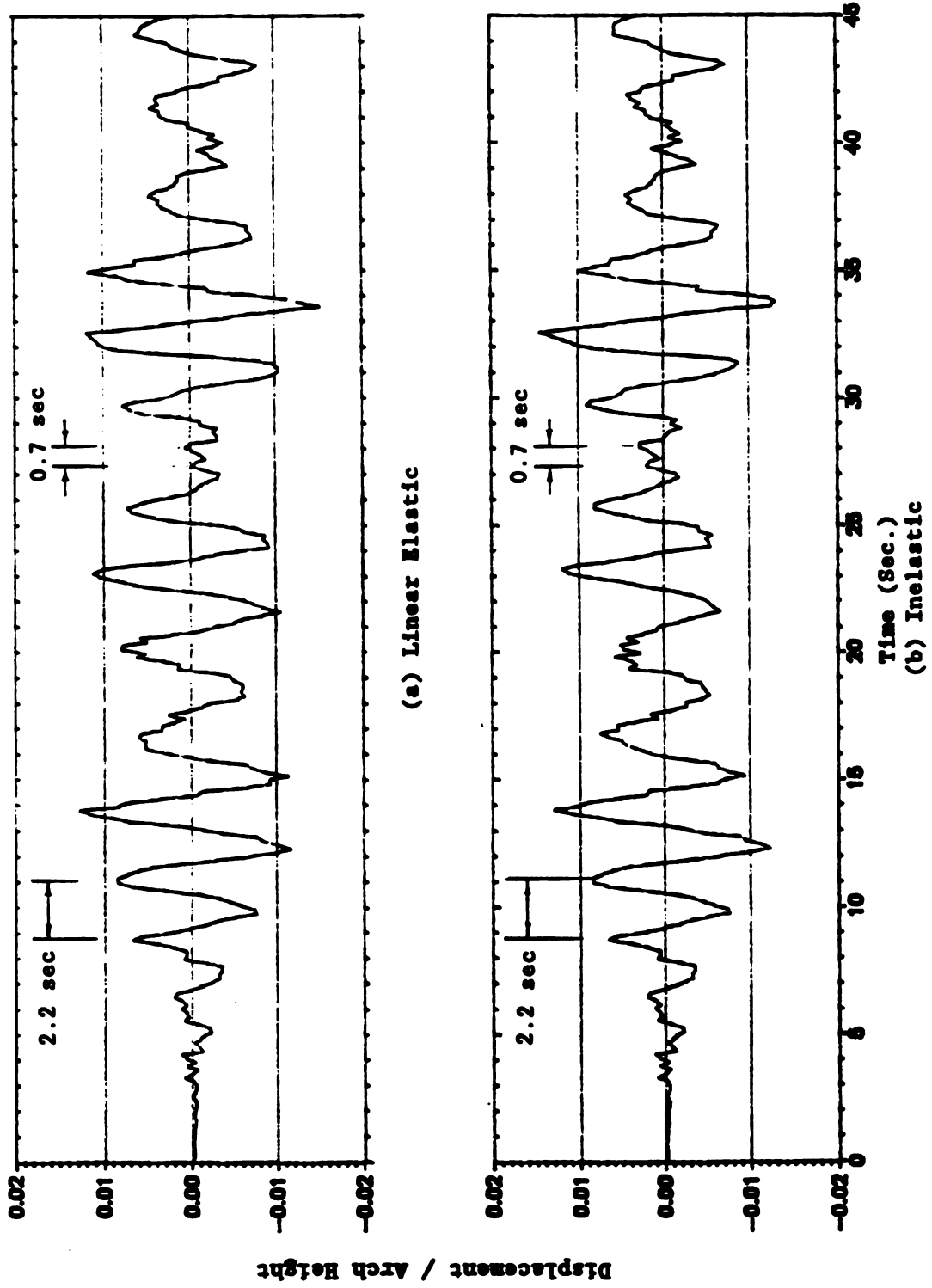


Figure 3-20. Node 31 Vertical (Y) Displacement Time History for MSB

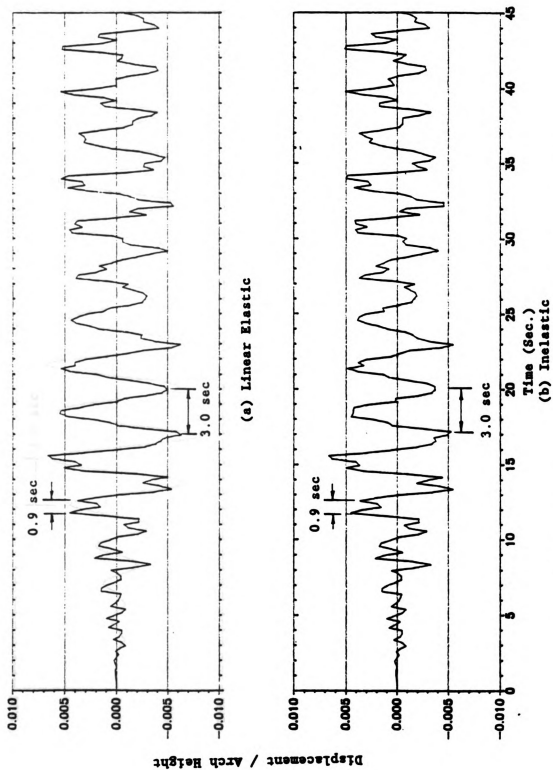
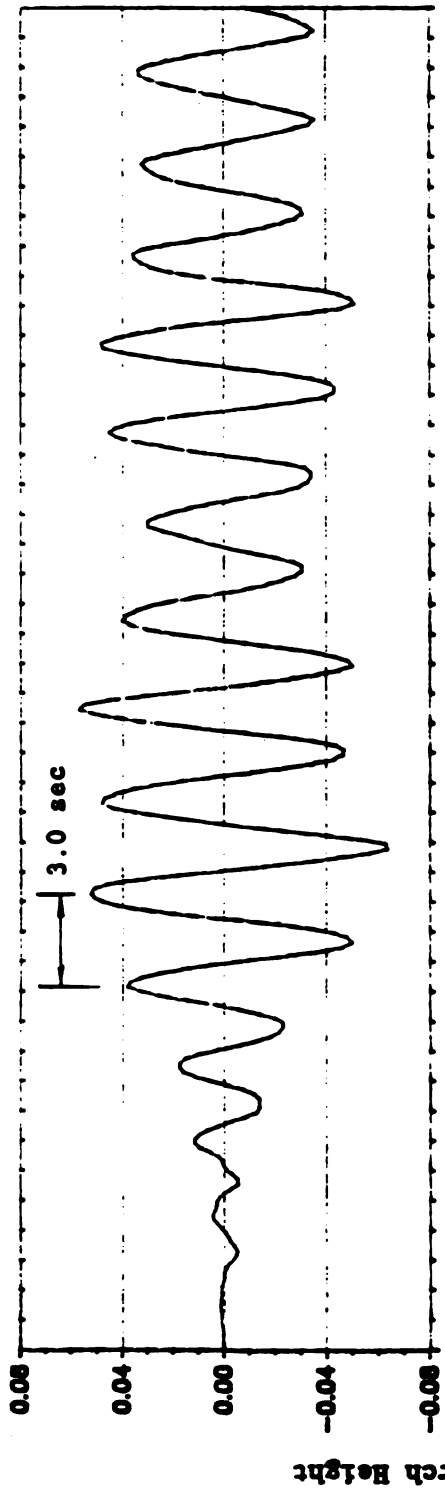
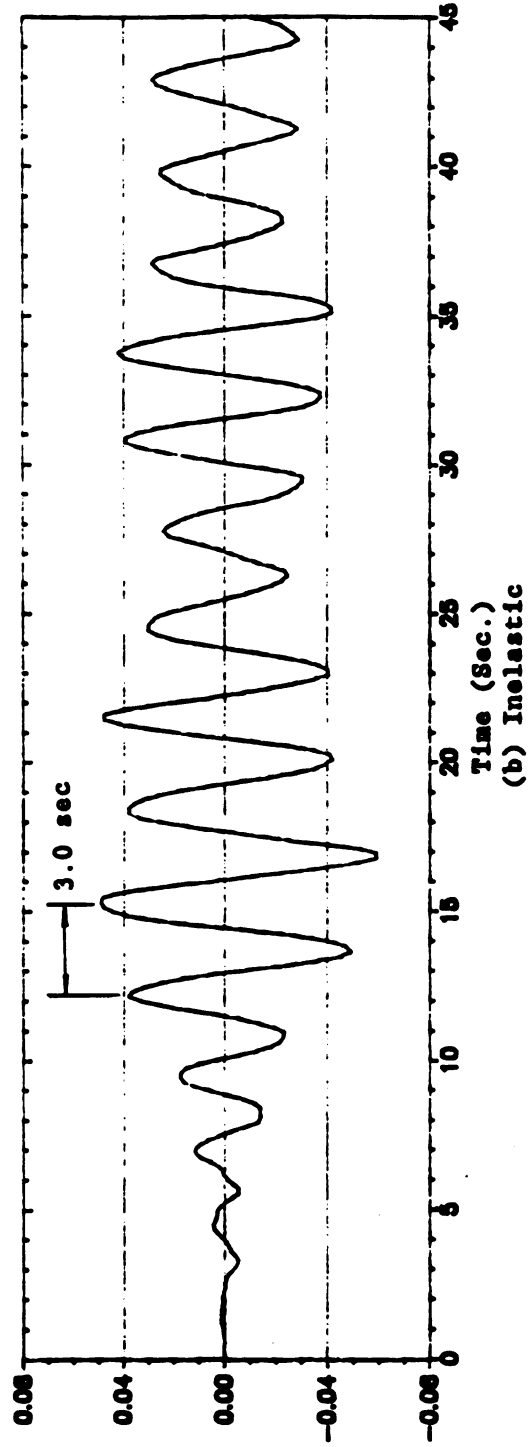


Figure 3-21. Node 5 Lateral (Z) Displacement Time History for MSB



(a) Linear Elastic



(b) Inelastic

Figure 3-22. Node 17 Lateral (Z) Displacement Time History for MSB

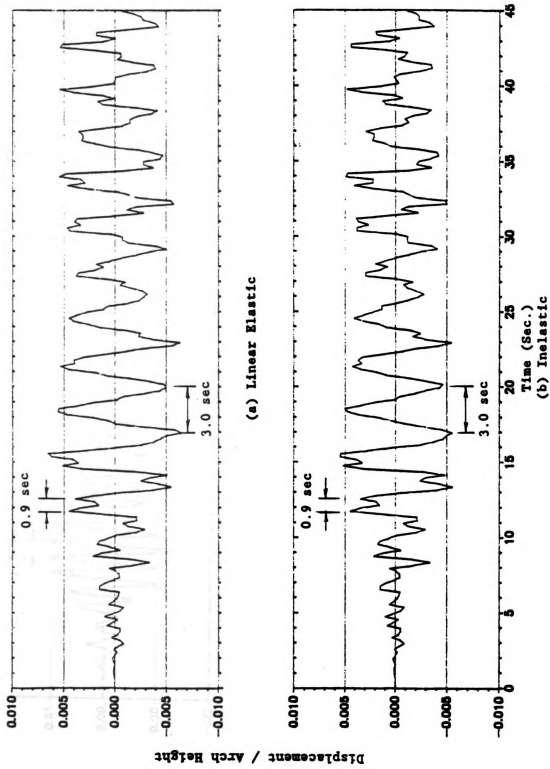
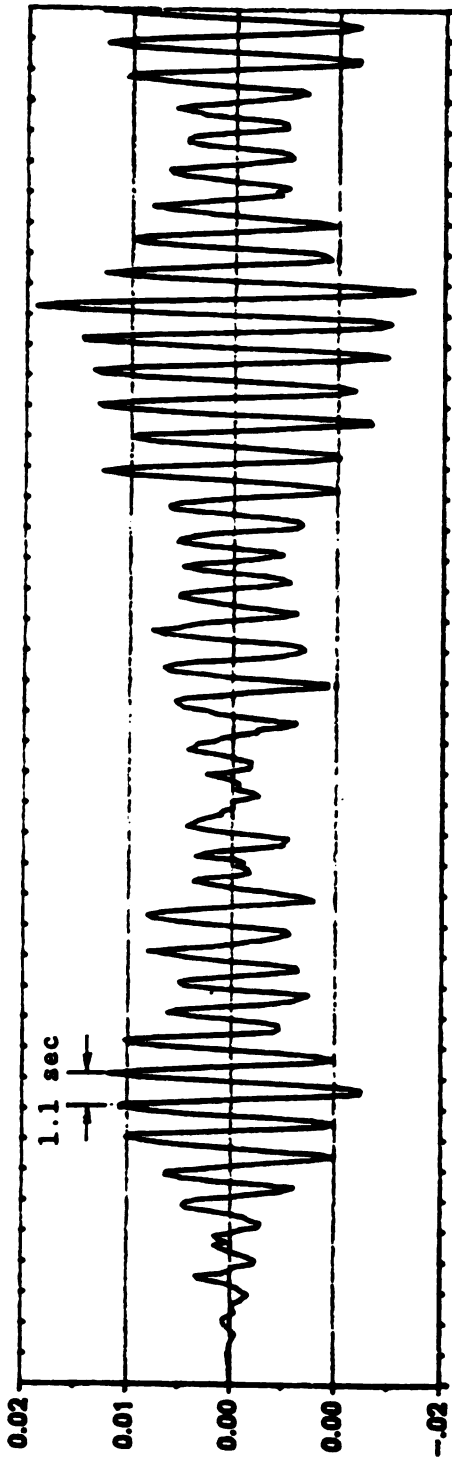
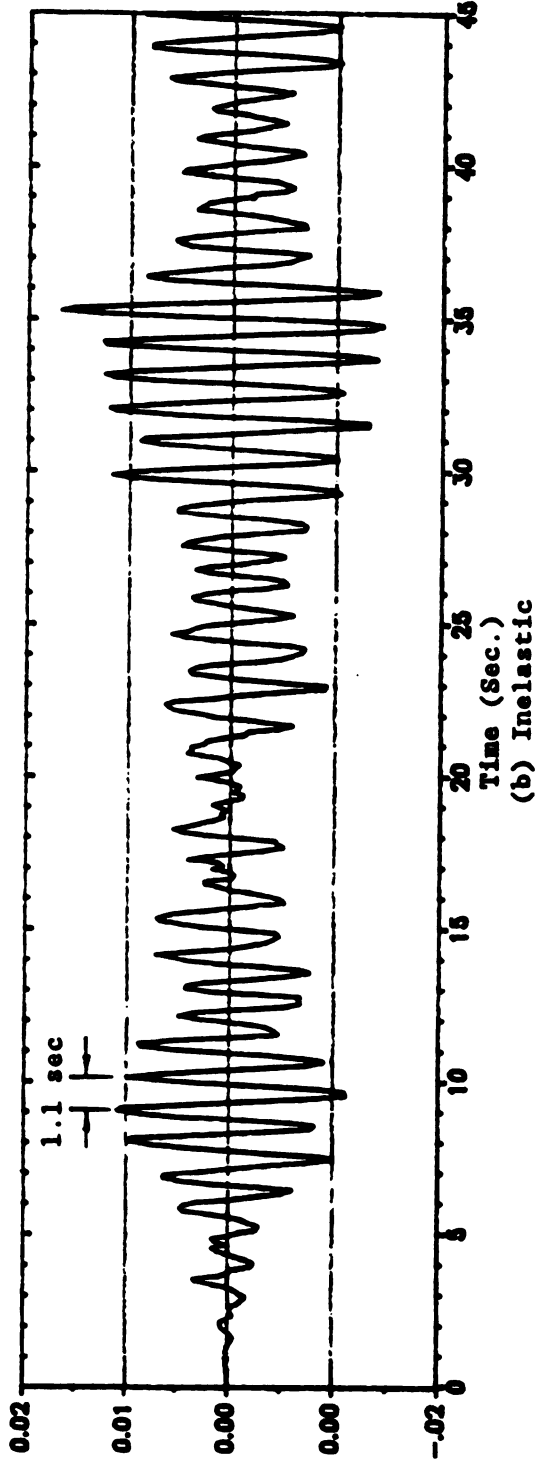


Figure 3-23. Node 31 Lateral (Z) Displacement Time History for MSB



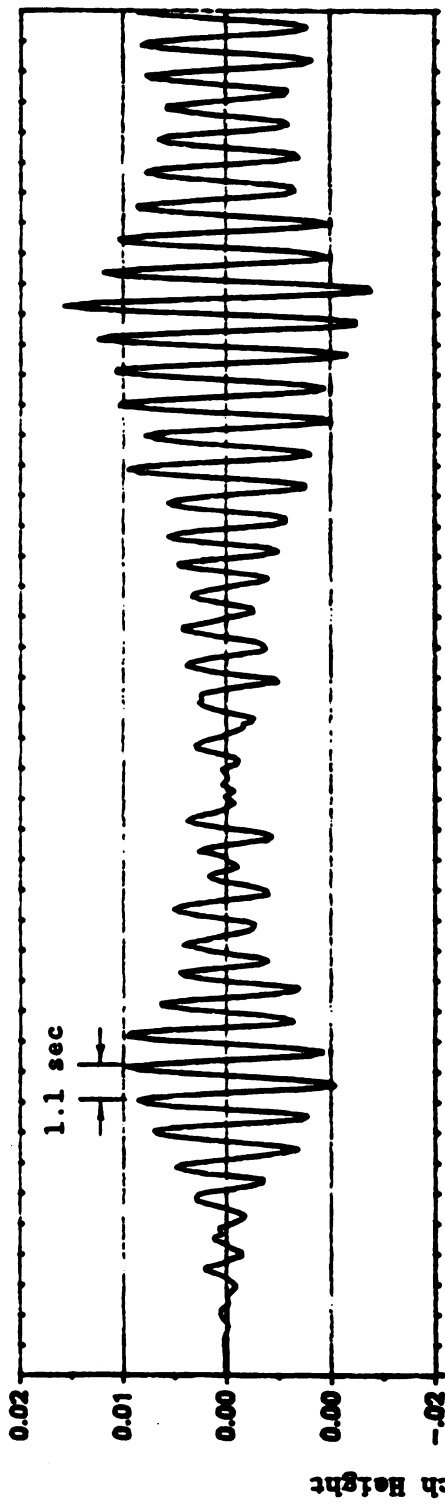
(a) Linear Elastic



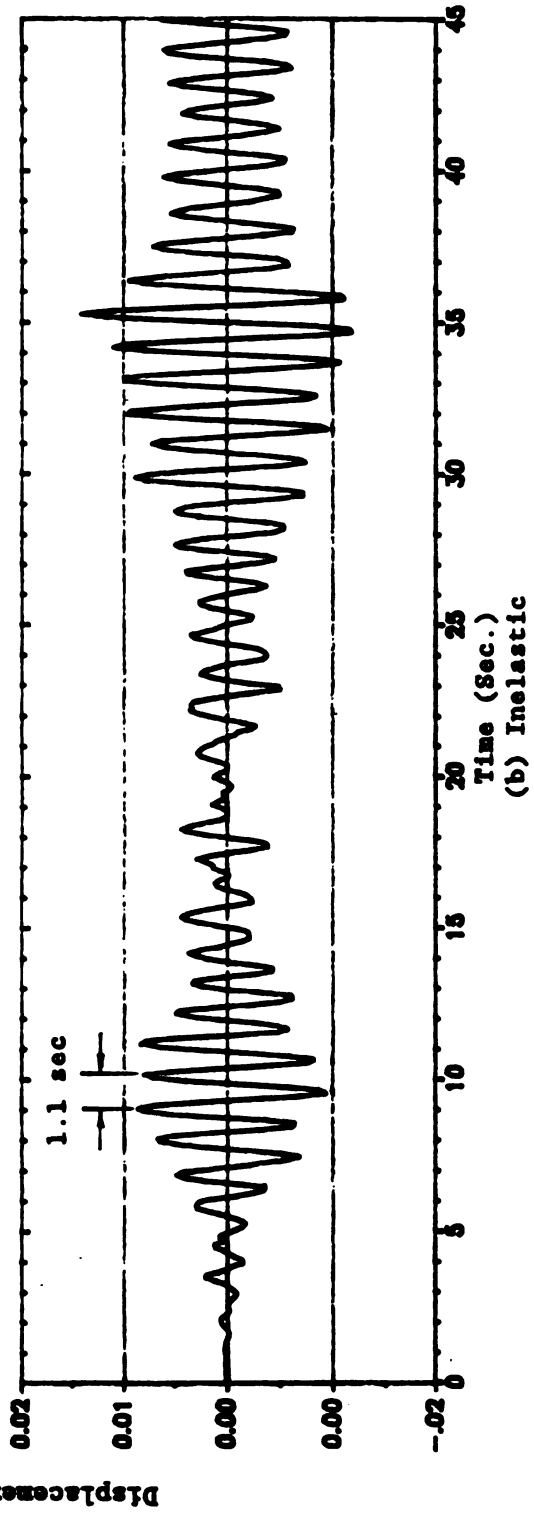
(b) Inelastic

Figure 3-24. Node 11 Horizontal (X) Displacement Time History for SSB

Displacement / Arch Height

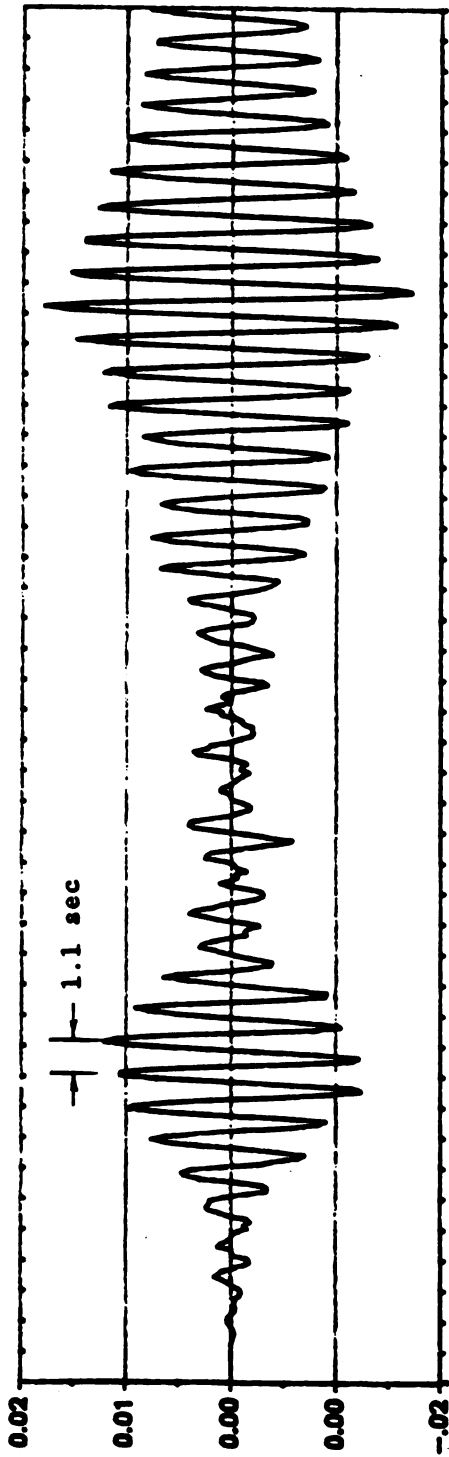


(a) Linear Elastic

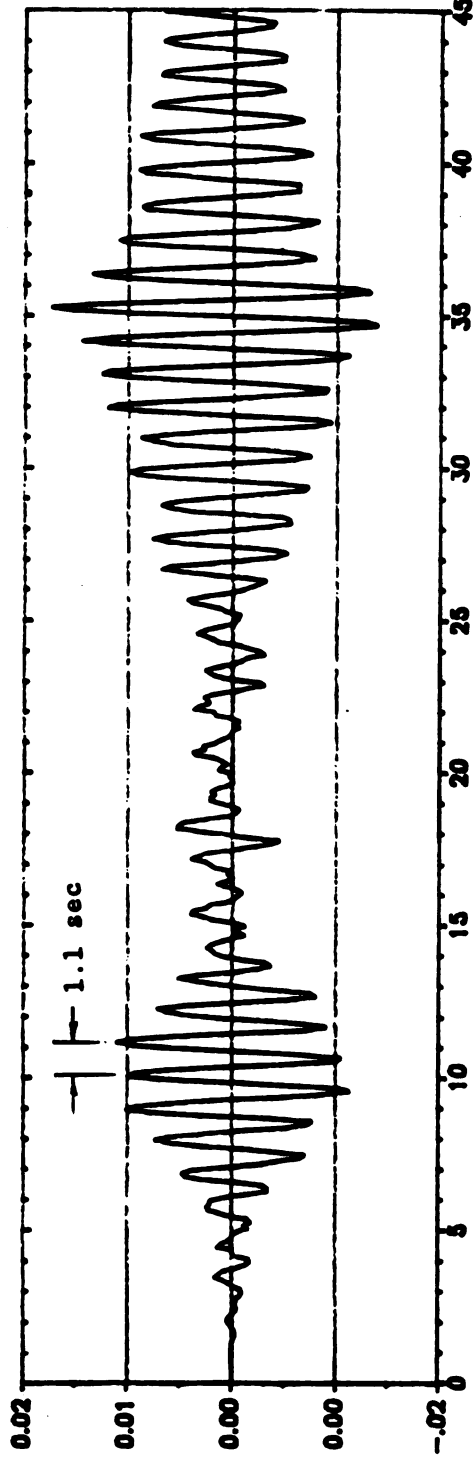


(b) Inelastic

Figure 3-25. Node 13 Horizontal (X) Displacement Time History for SSB



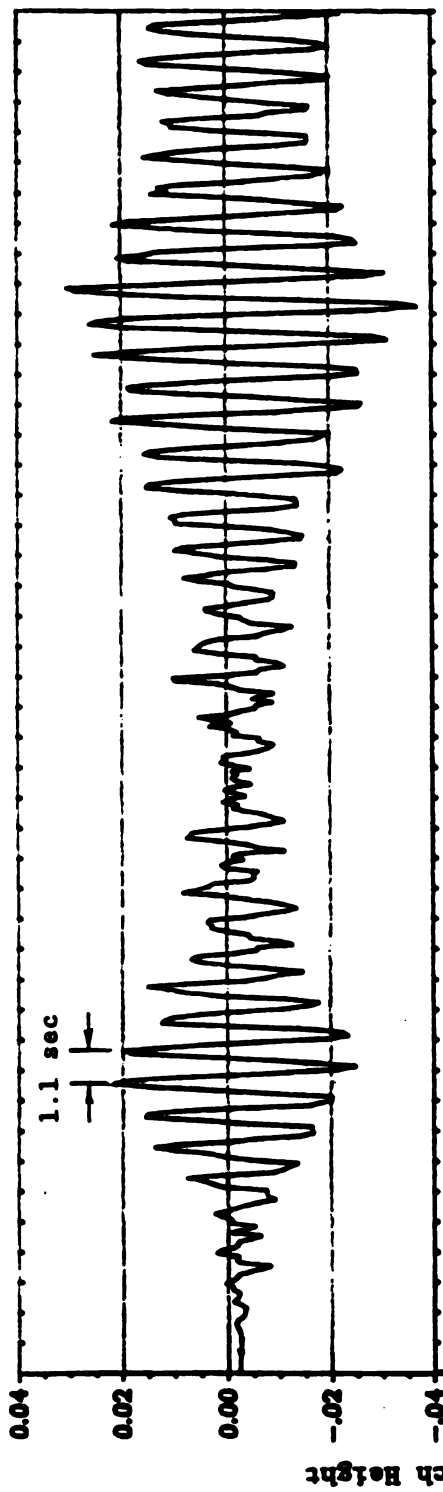
(a) Linear Elastic



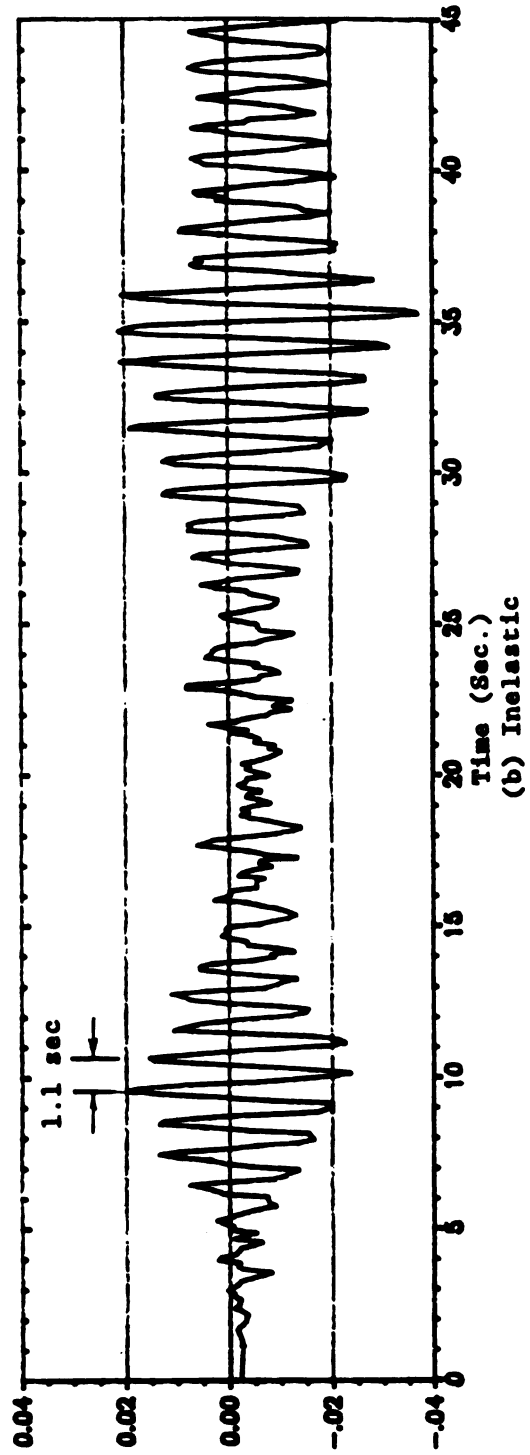
(b) Inelastic

Figure 3-26. Node 23 Horizontal (X) Displacement Time History for SSB

Displacement / Arch Height



(a) Linear Elastic



(b) Inelastic

Figure 3-27. Node 11 Vertical (Y) Displacement Time History for SSB

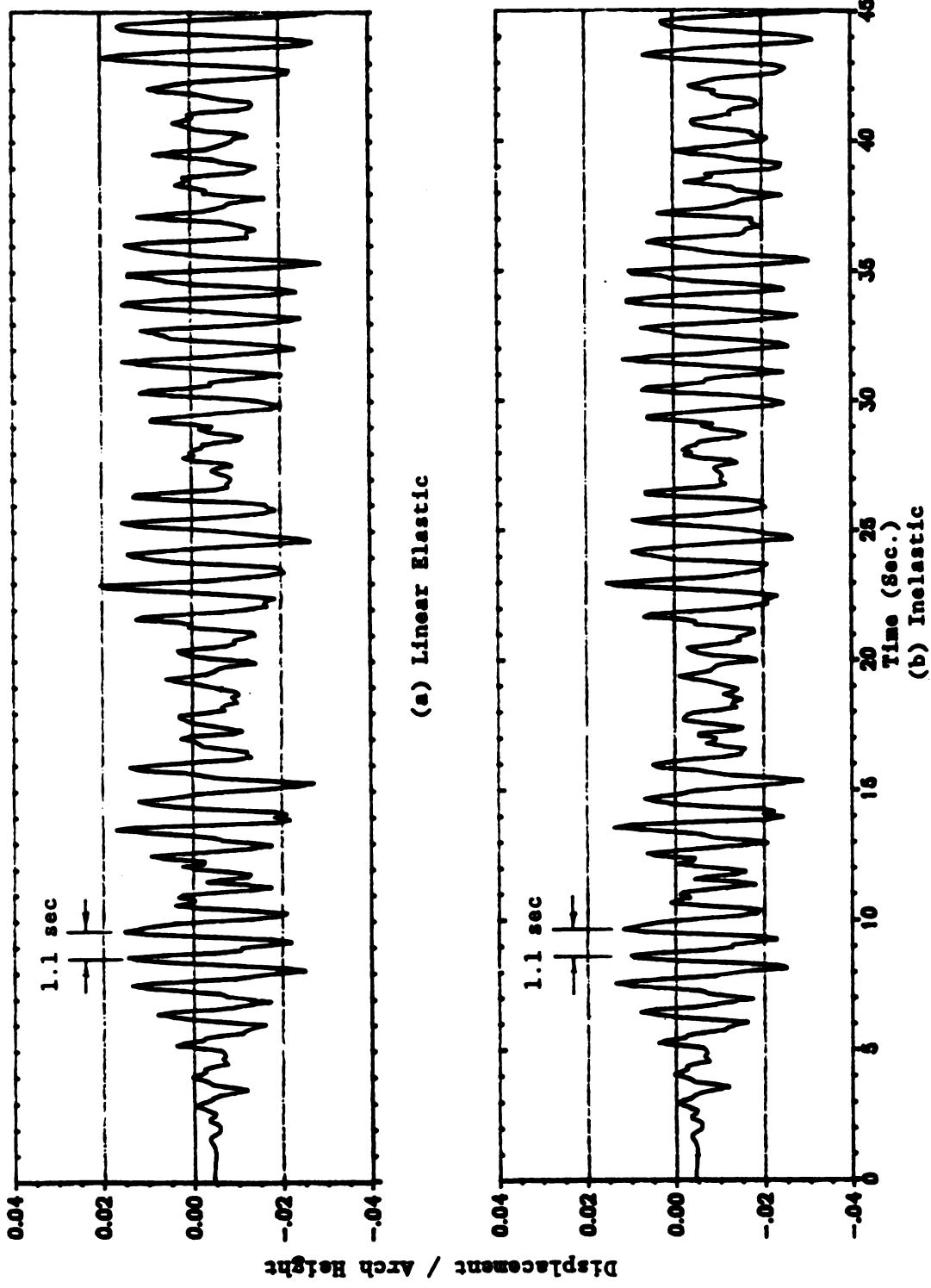


Figure 3-28. Node 13 Vertical (Y) Displacement Time History for SSB

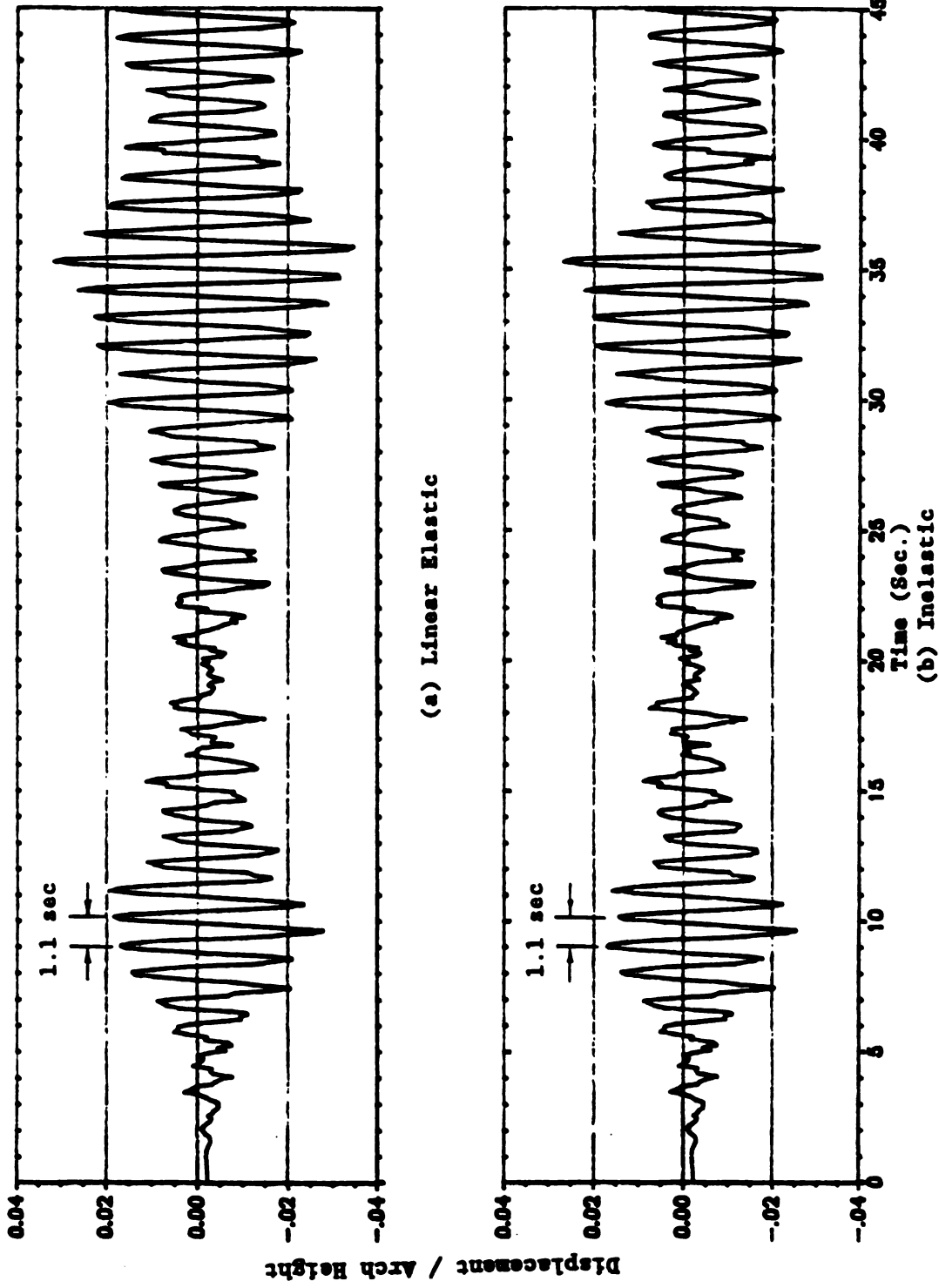


Figure 3-29. Node 23 Vertical (Y) Displacement Time History for SBB

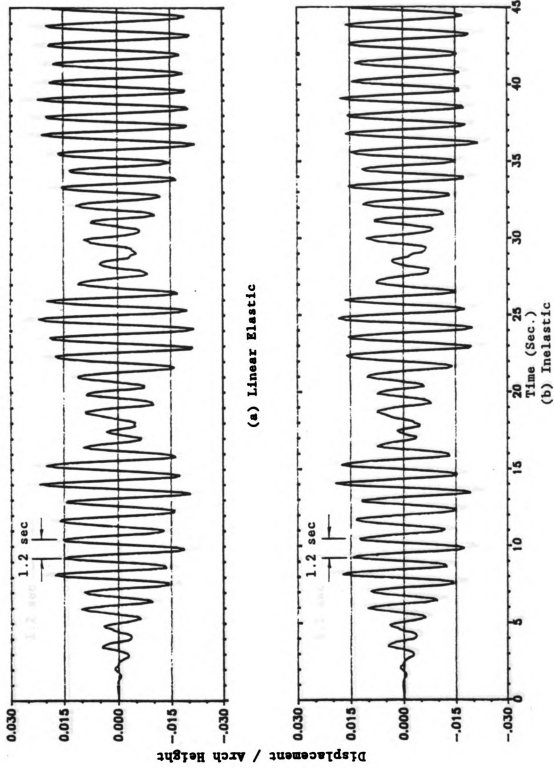


Figure 3-30. Node 11 Lateral (Z) Displacement Time History for SSB

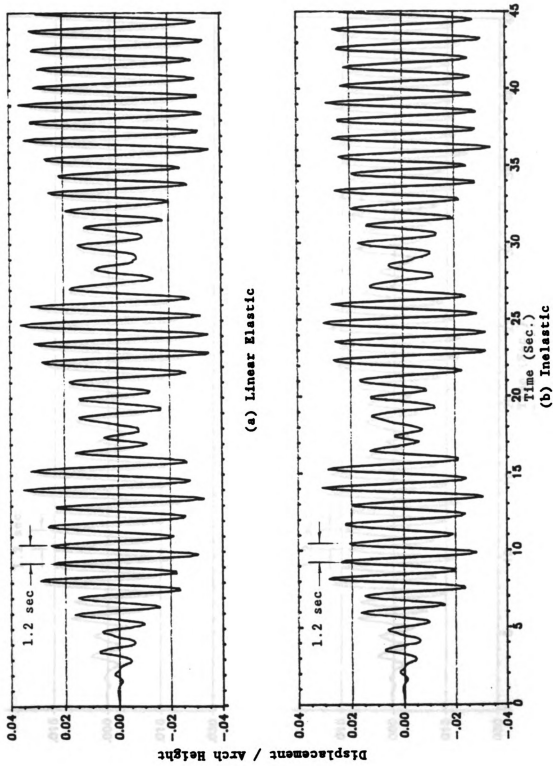


Figure 3-31. Node 13 Lateral (Z) Displacement Time History for SSB

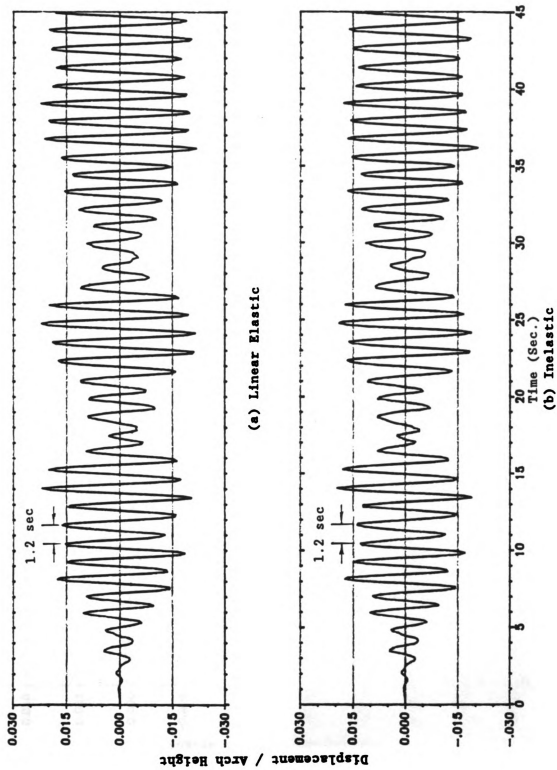
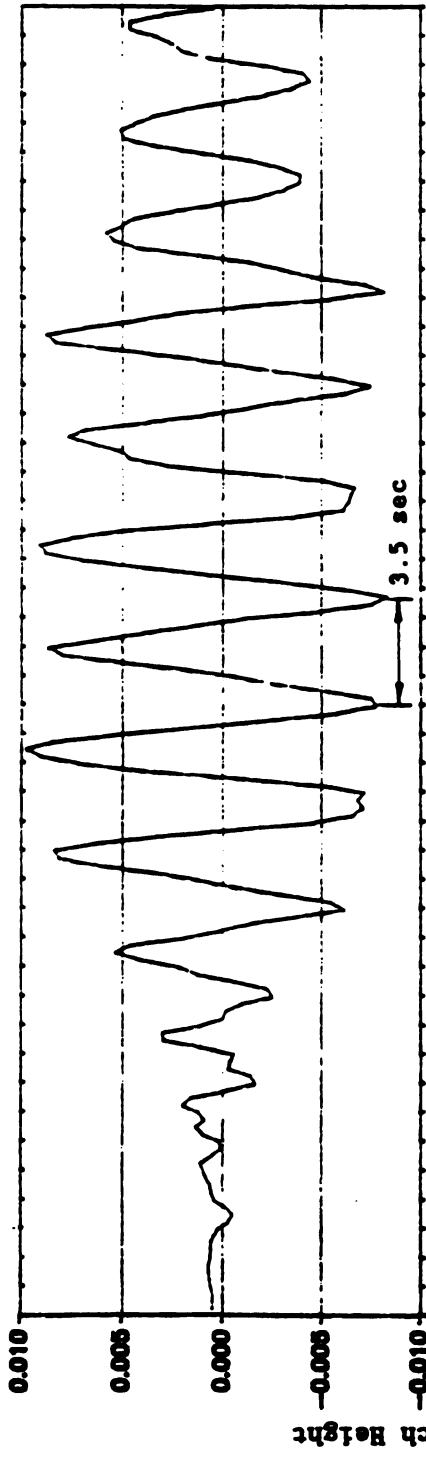
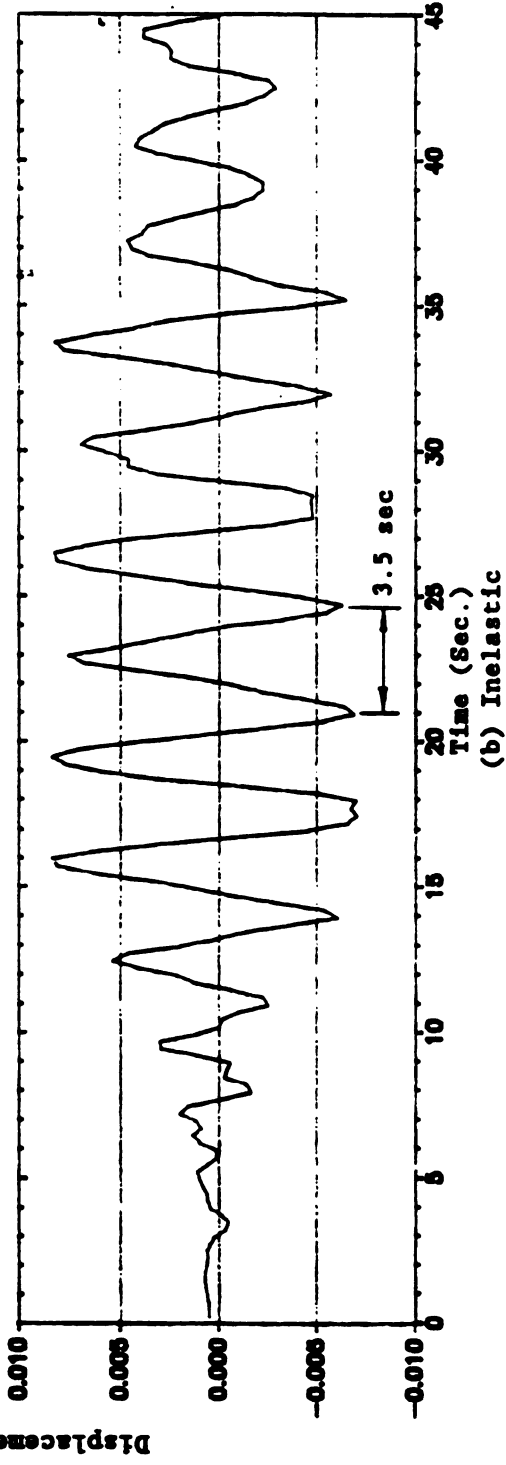


Figure 3-32. Node 23 Lateral (Z) Displacement Time History for SSB



(a) Linear Elastic



(b) Inelastic

Figure 3-33. Node 12 Horizontal (X) Displacement Time History for LSB

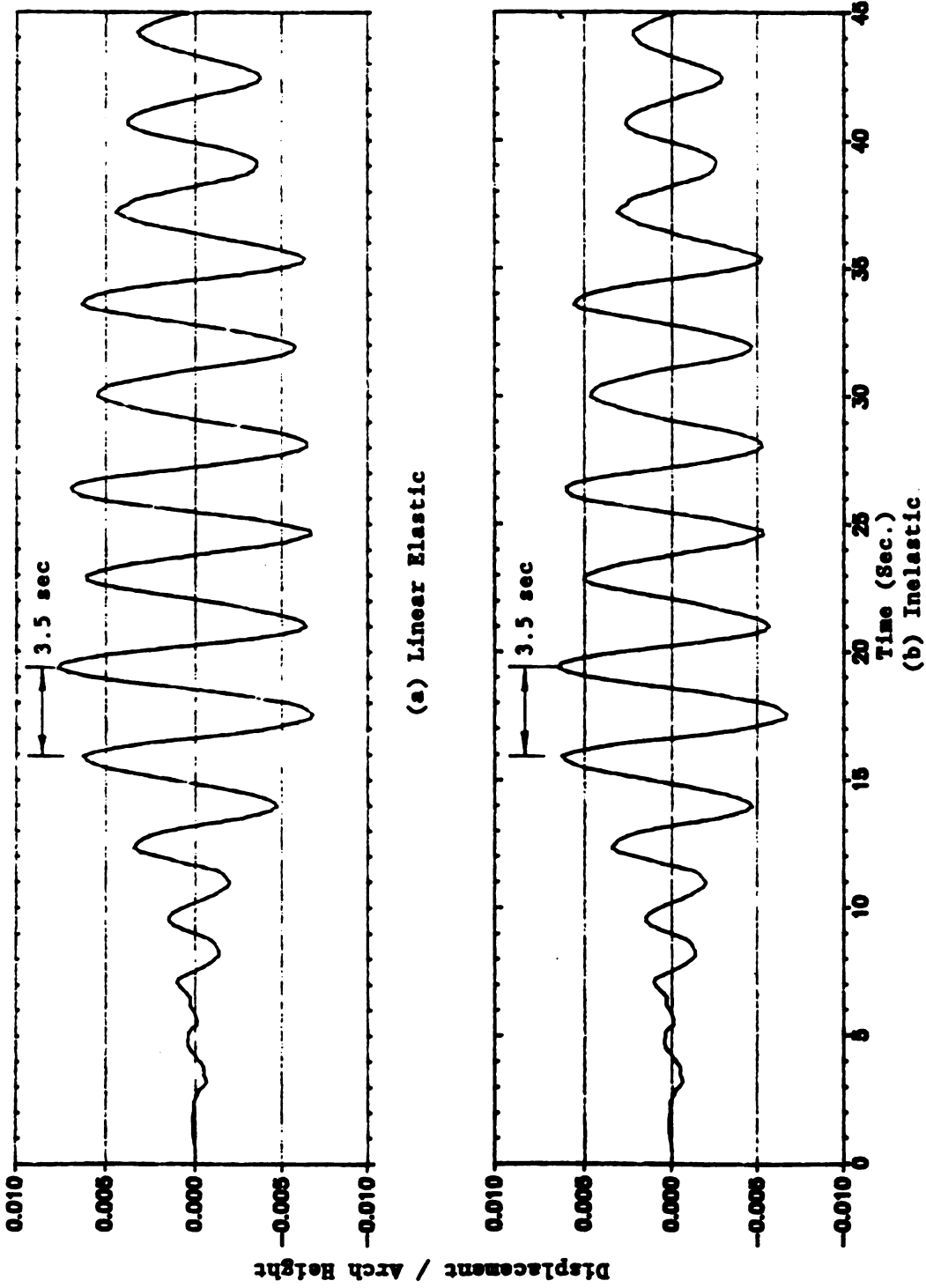
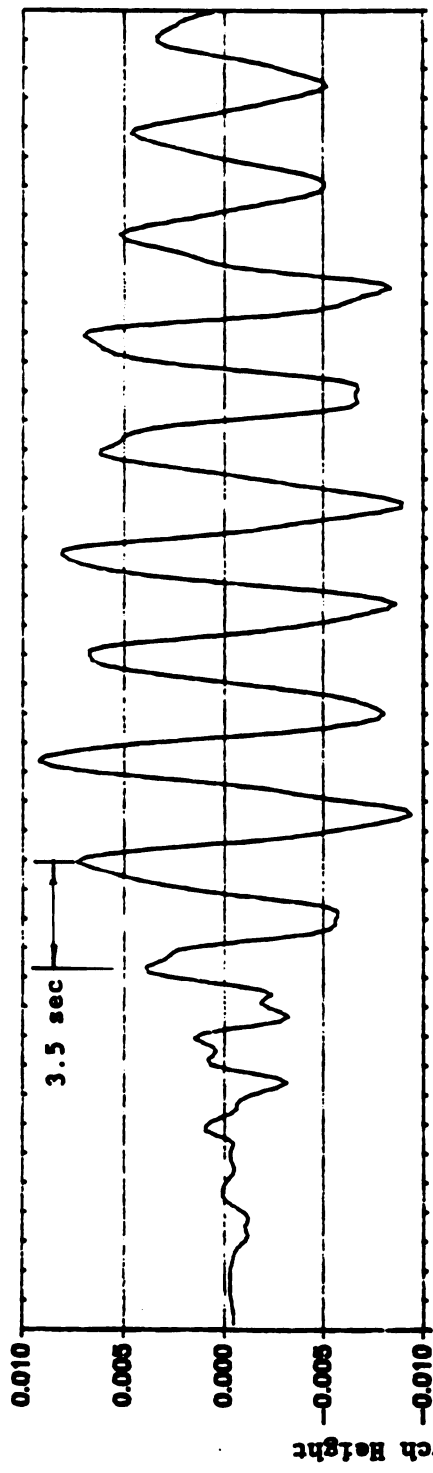
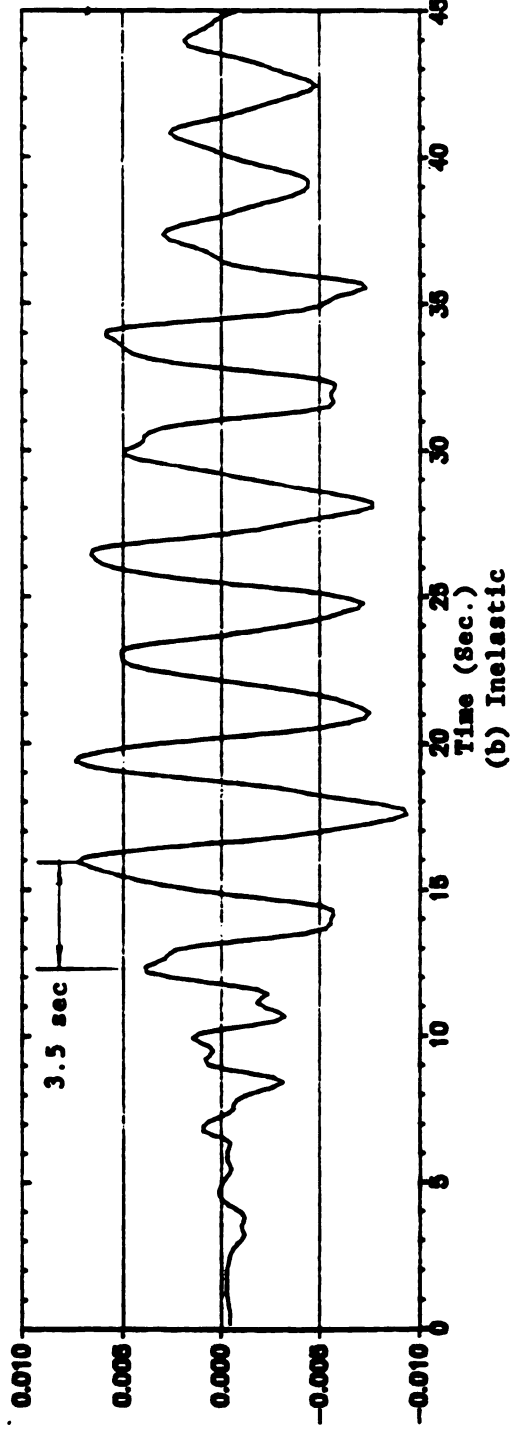


Figure 3-34. Node 18 Horizontal (X) Displacement Time History for LSB



(a) Linear Elastic



(b) Inelastic

Figure 3-35. Node 24 Horizontal (X) Displacement Time History for LSB

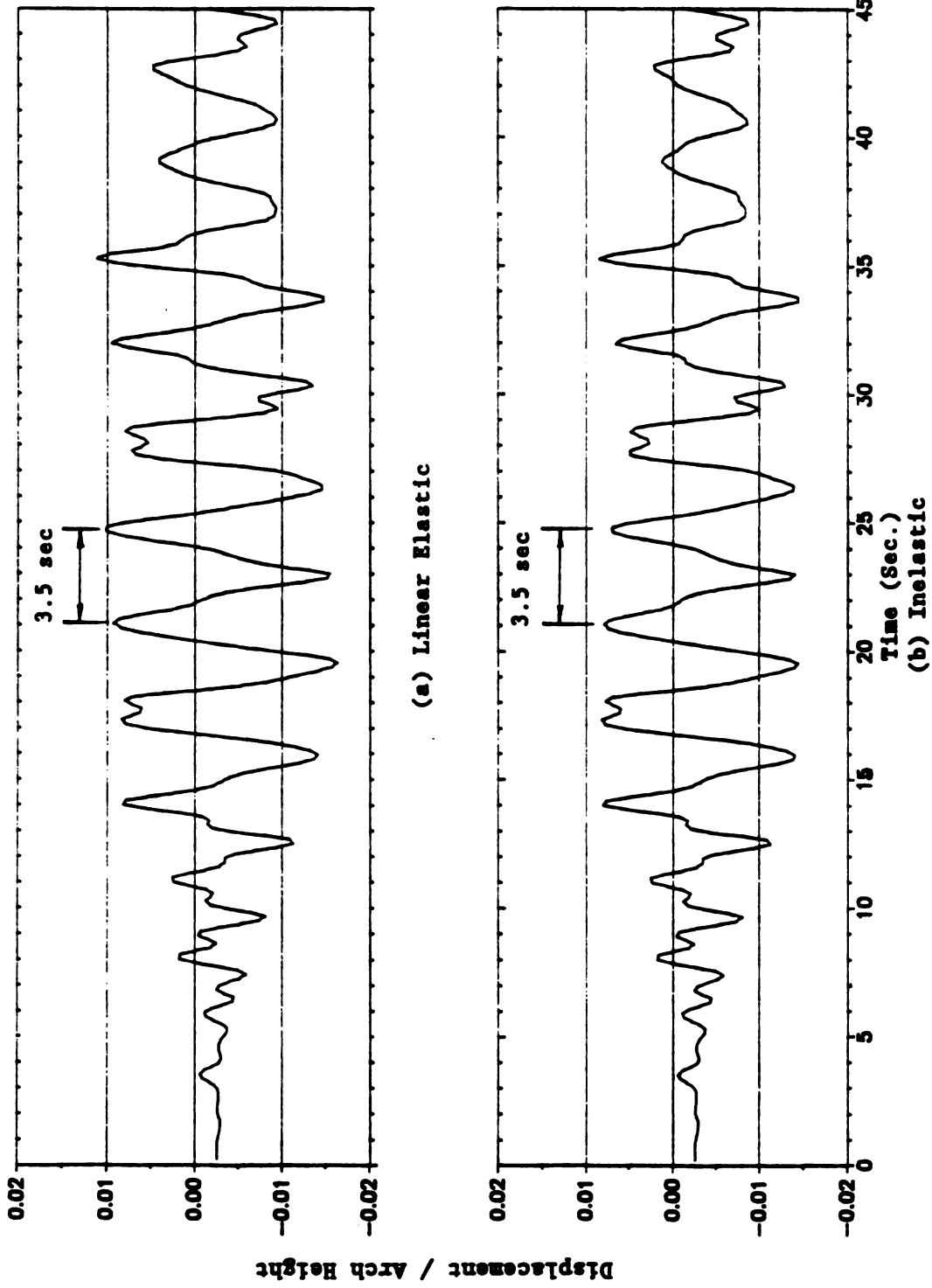


Figure 3-36. Node 12 Vertical (Y) Displacement Time History for LSB

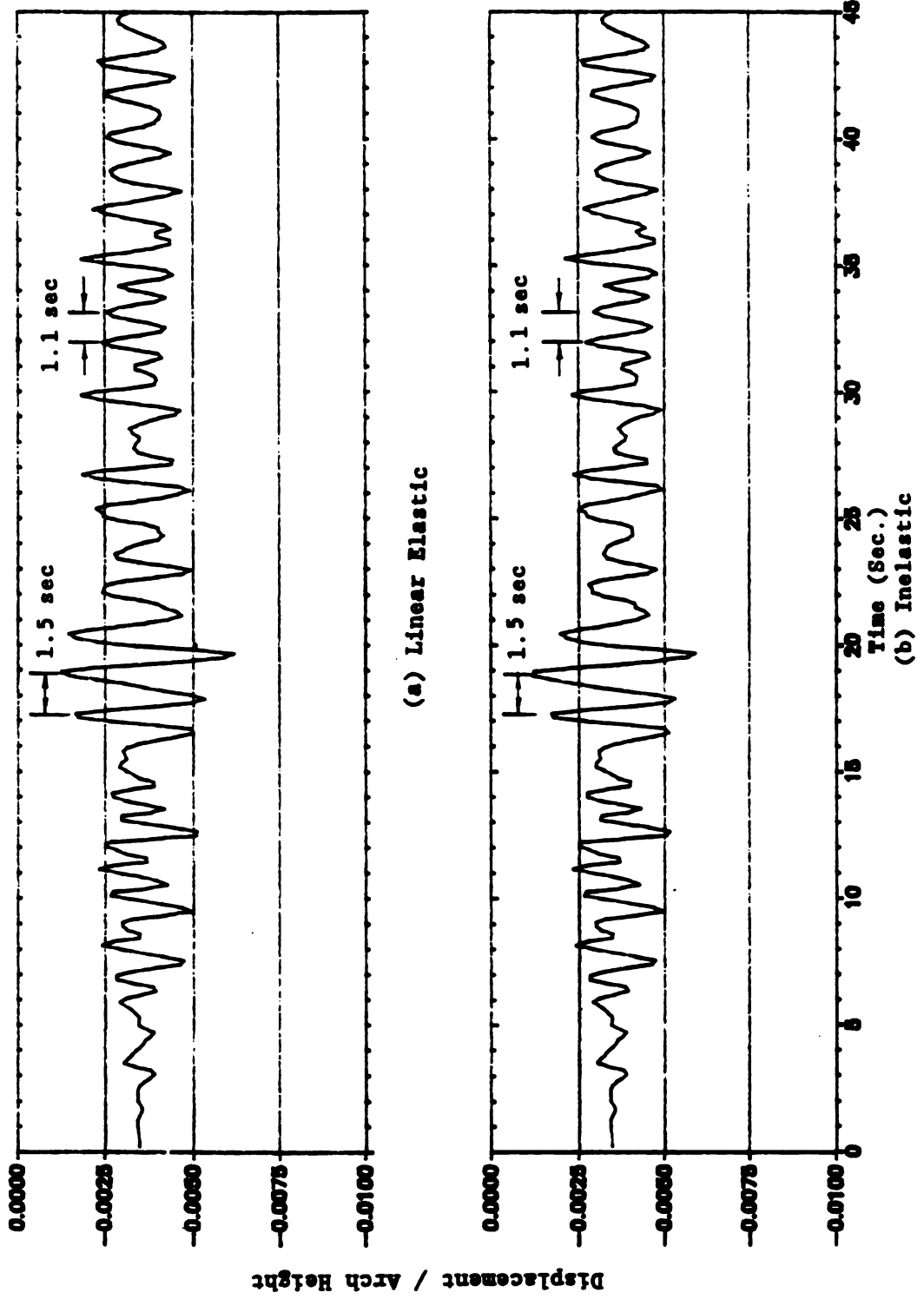


Figure 3-37. Node 18 Vertical (Y) Displacement Time History for LSB

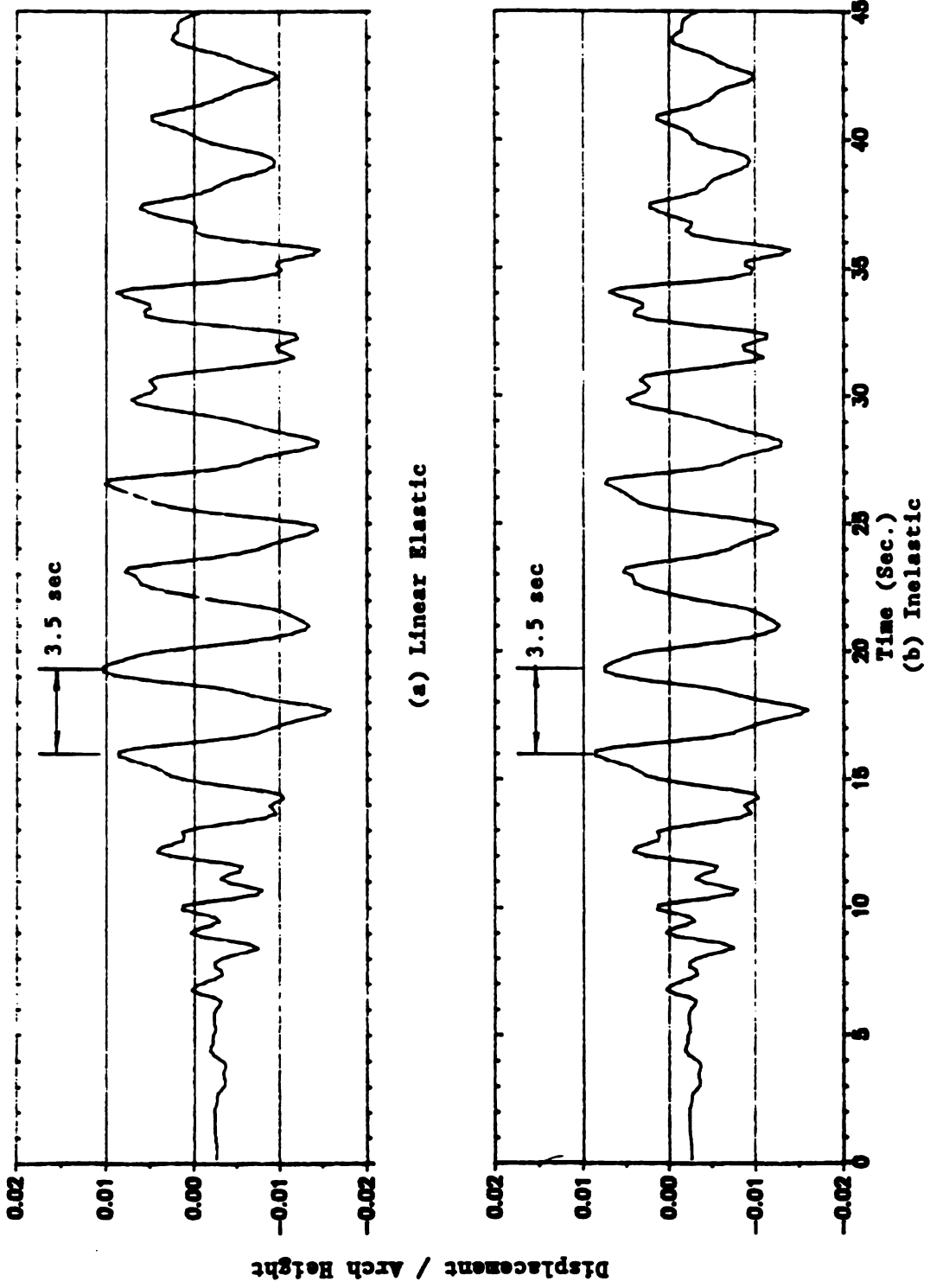


Figure 3-38. Node 24 Vertical (Y) Displacement Time History for LSB

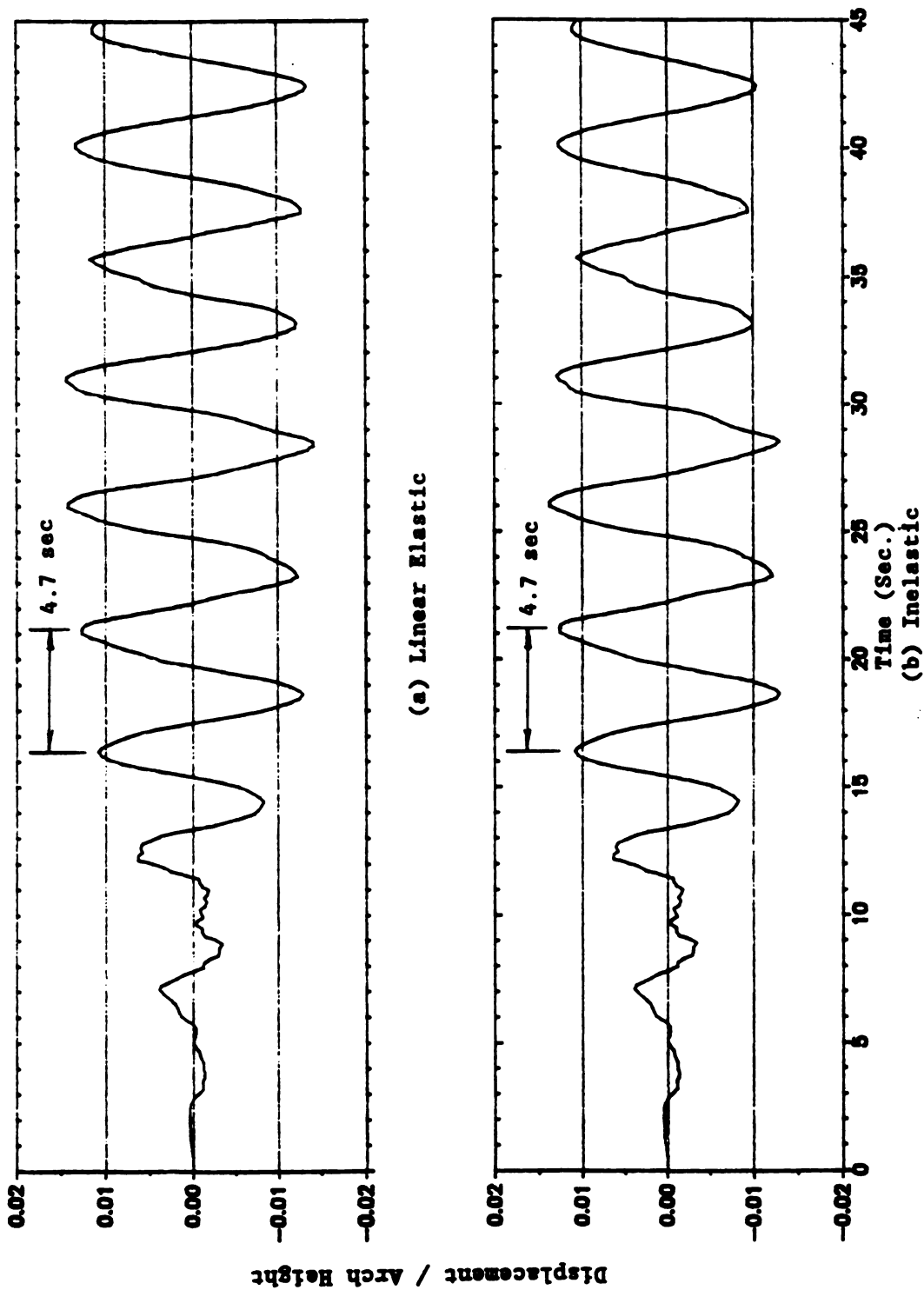


Figure 3-39. Node 12 Lateral (Z) Displacement Time History for LSB

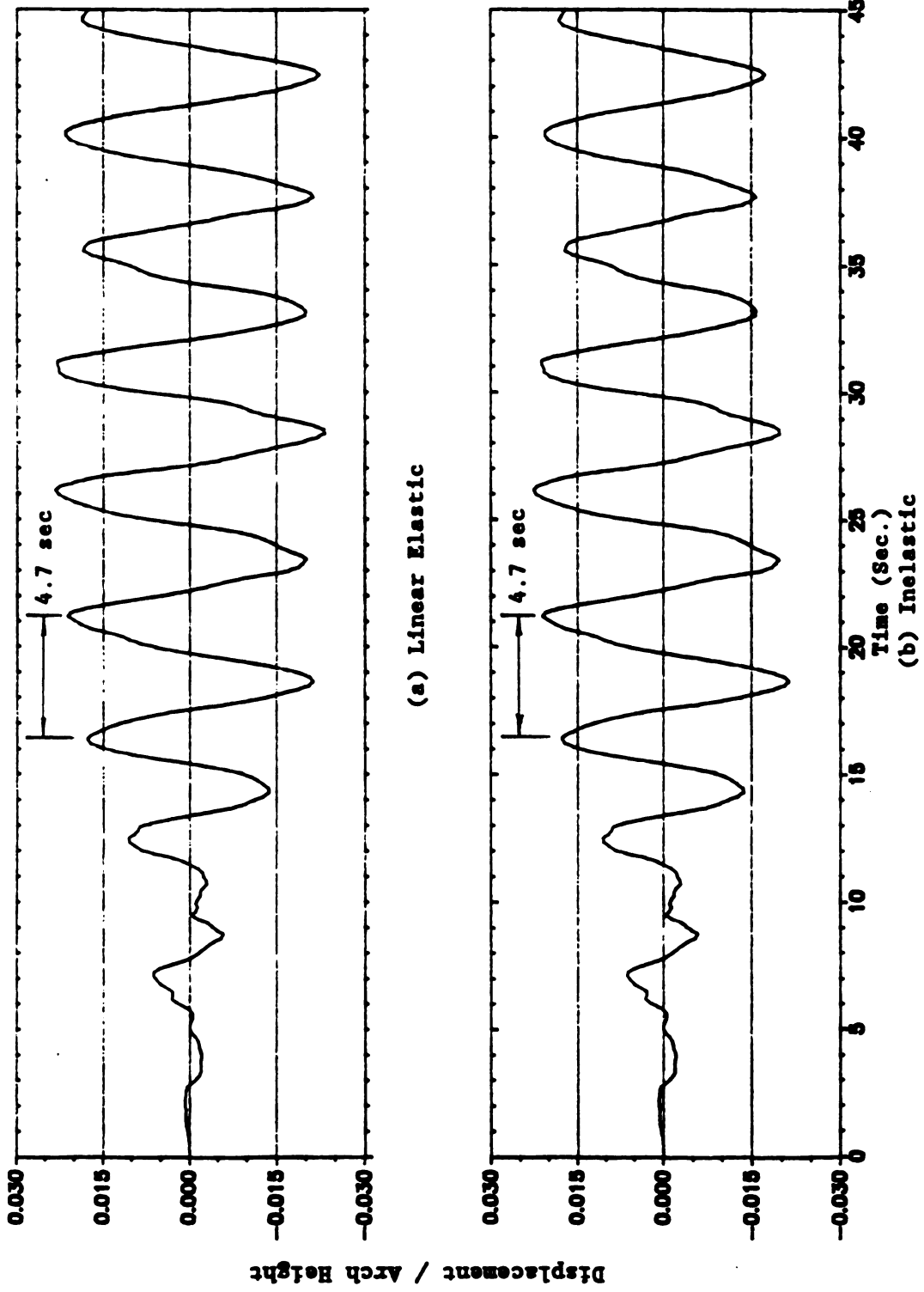
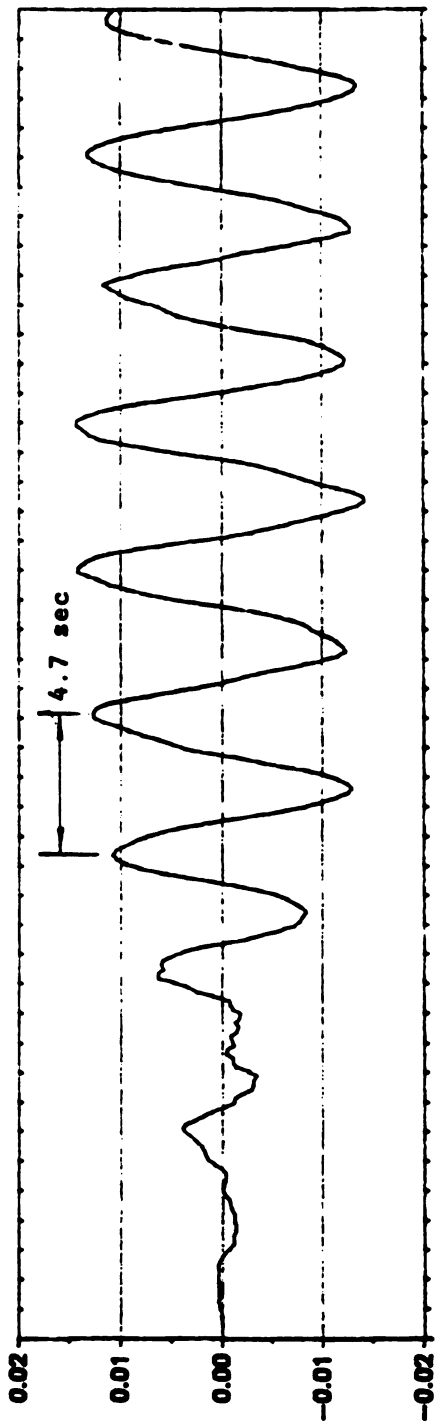
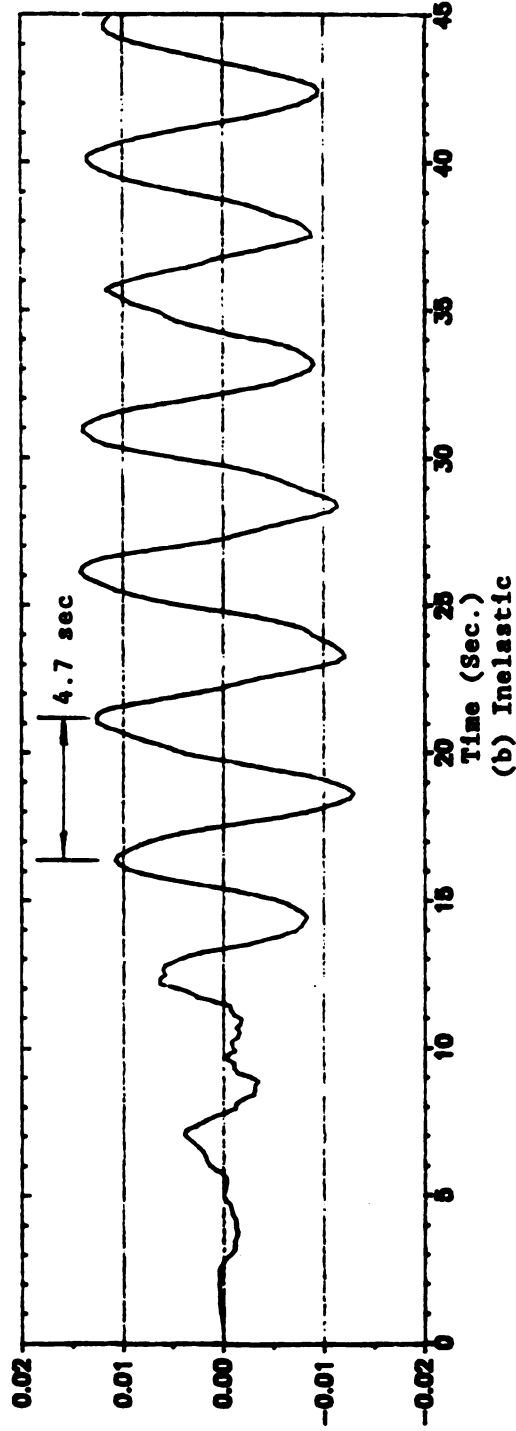


Figure 3-40. Node 18 Lateral (Z) Displacement Time History for LSB



(a) Linear Elastic



(b) Inelastic

Figure 3-41. Node 24 Lateral (Z) Displacement Time History for LSB

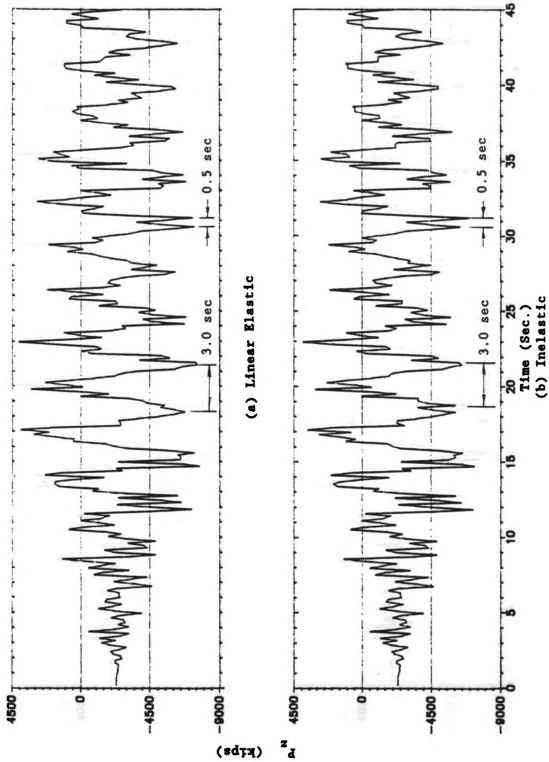


Figure 3-42. Member 1 End J (Node 5) Axial Force Time History for MSB

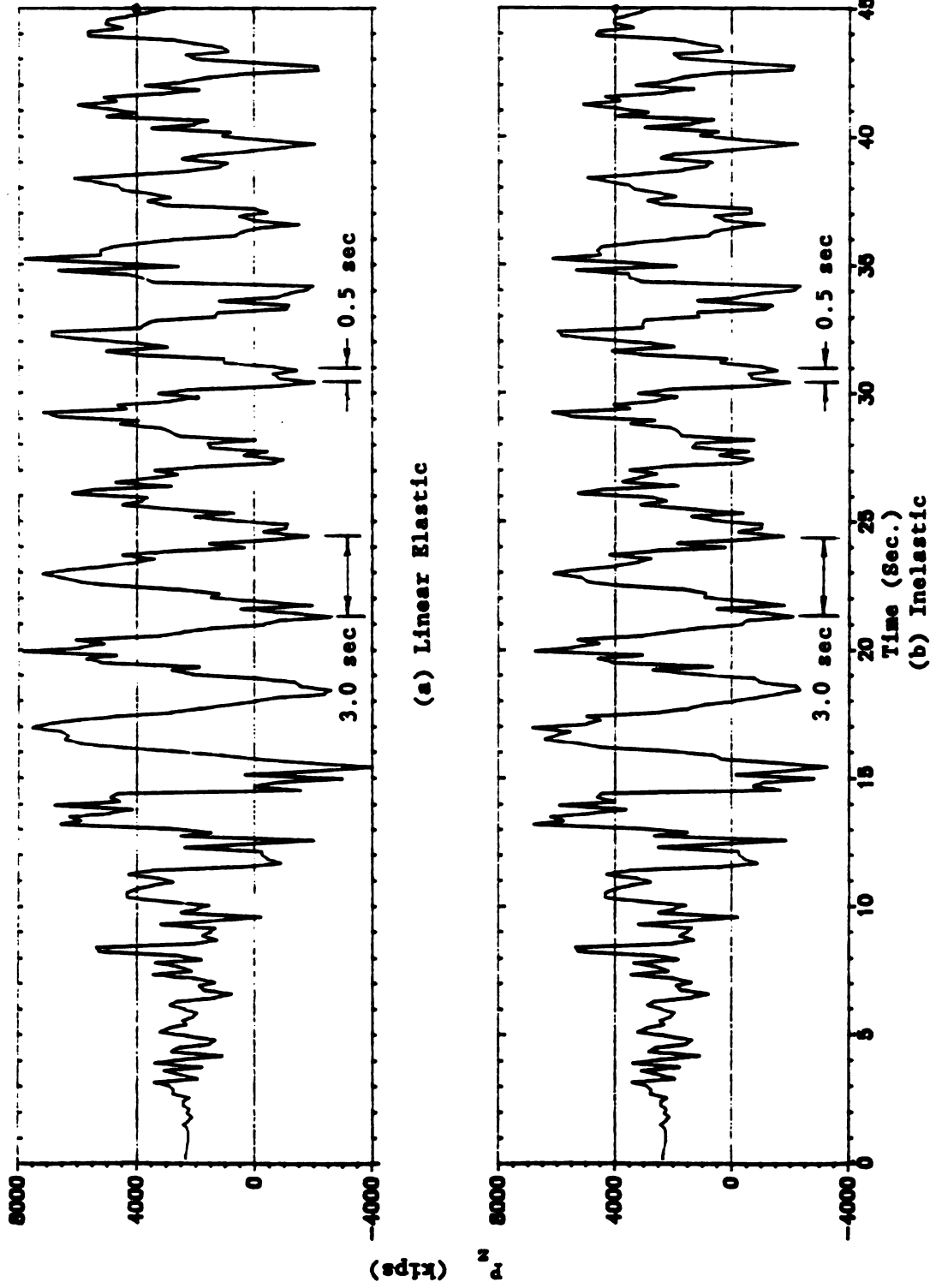


Figure 3-43. Member 16 End I (Node 31) Axial Force Time History for MSB

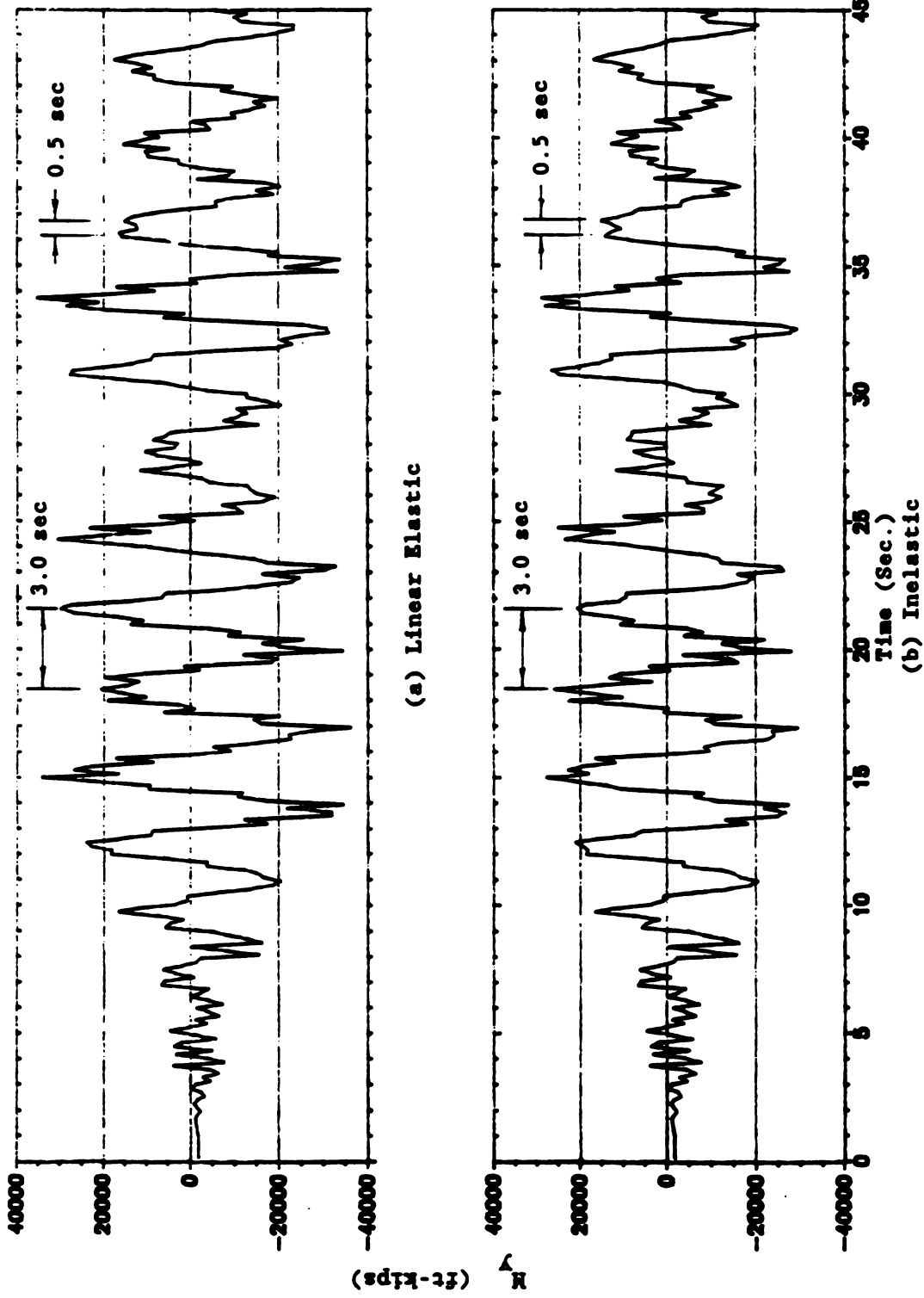


Figure 3-44. Member 1 End J (Node 5) In-Plane Bending Time History for MSB

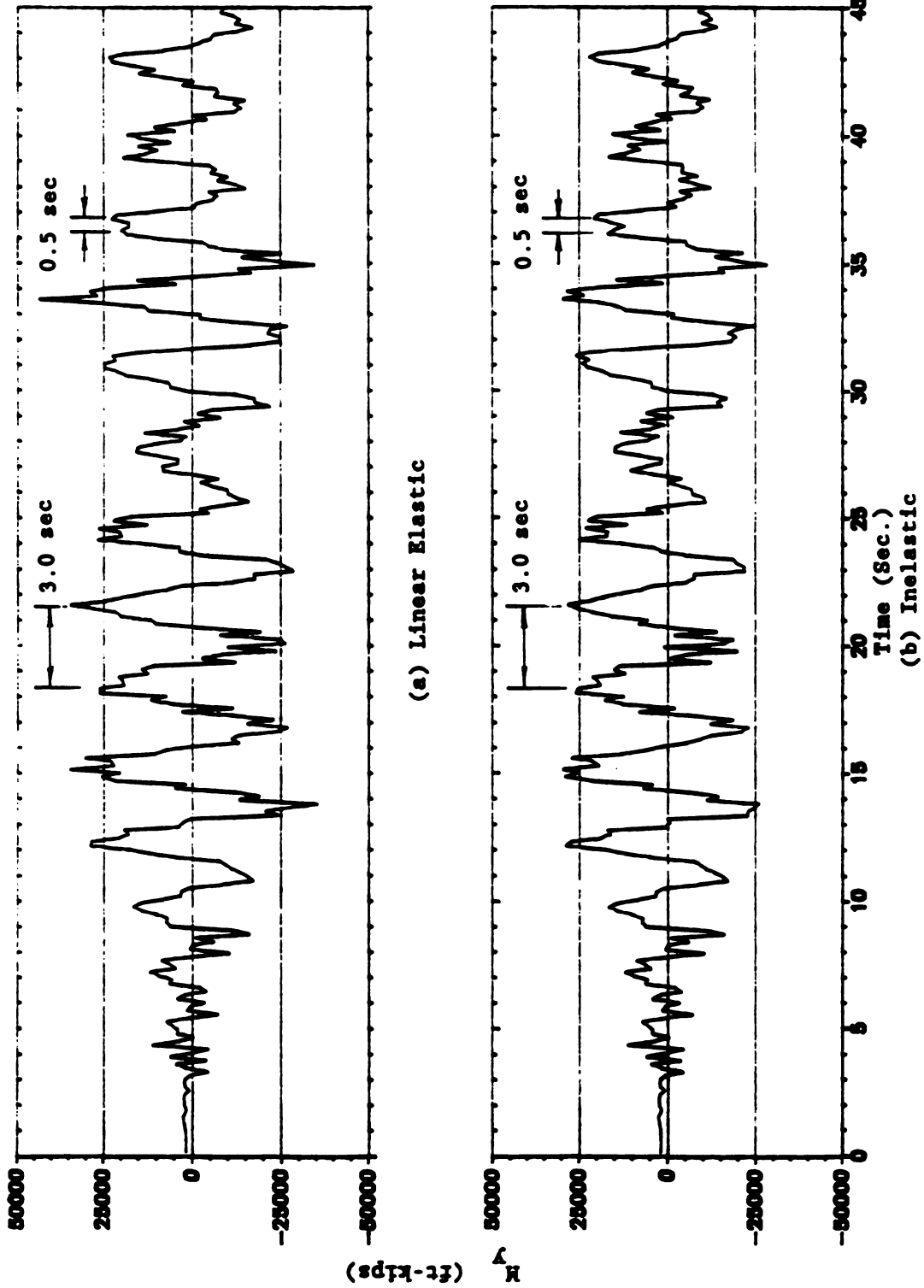
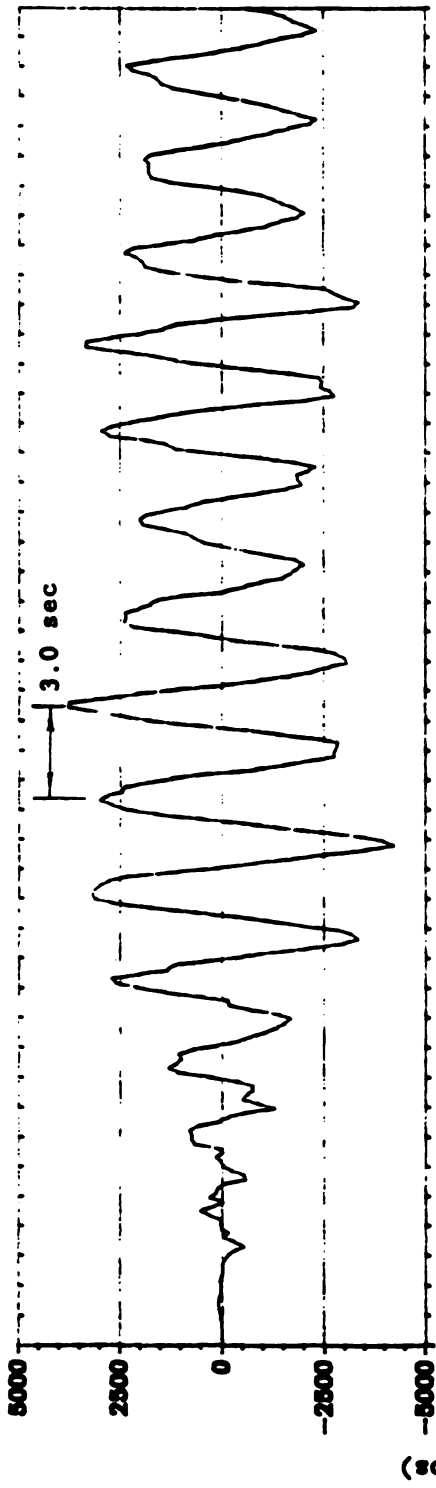
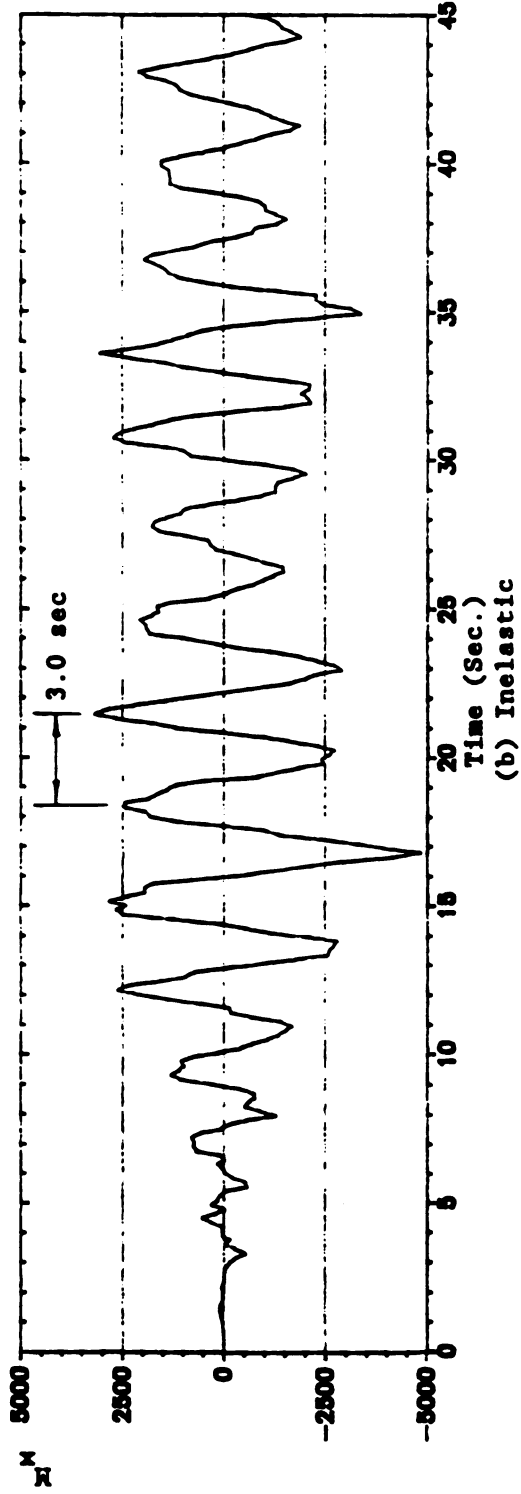


Figure 3-45. Member 16 End I (Node 31) In-Plane Bending Time History for MSB

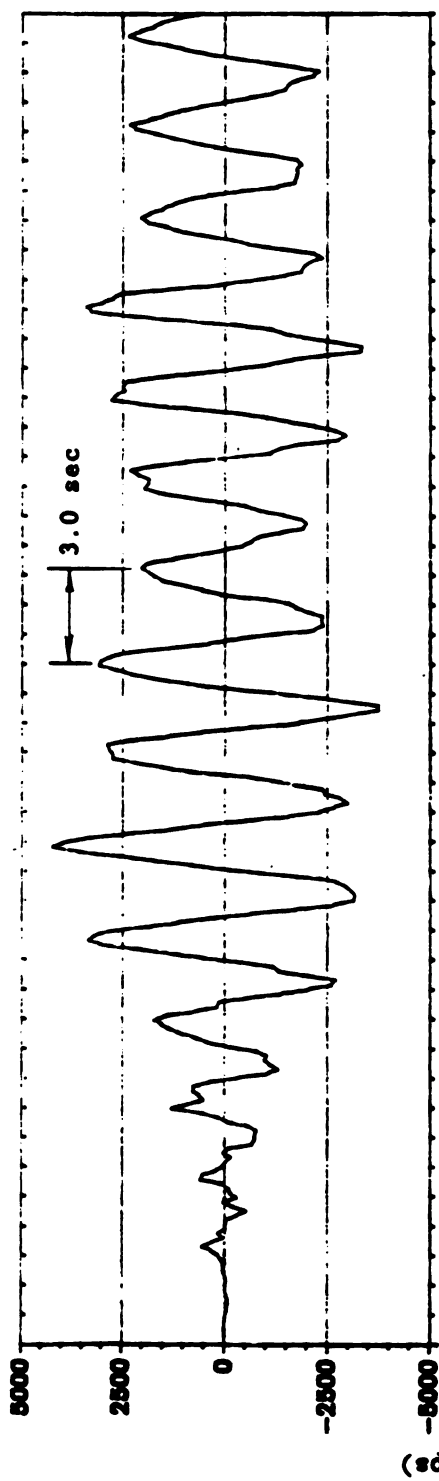


(a) Linear Elastic

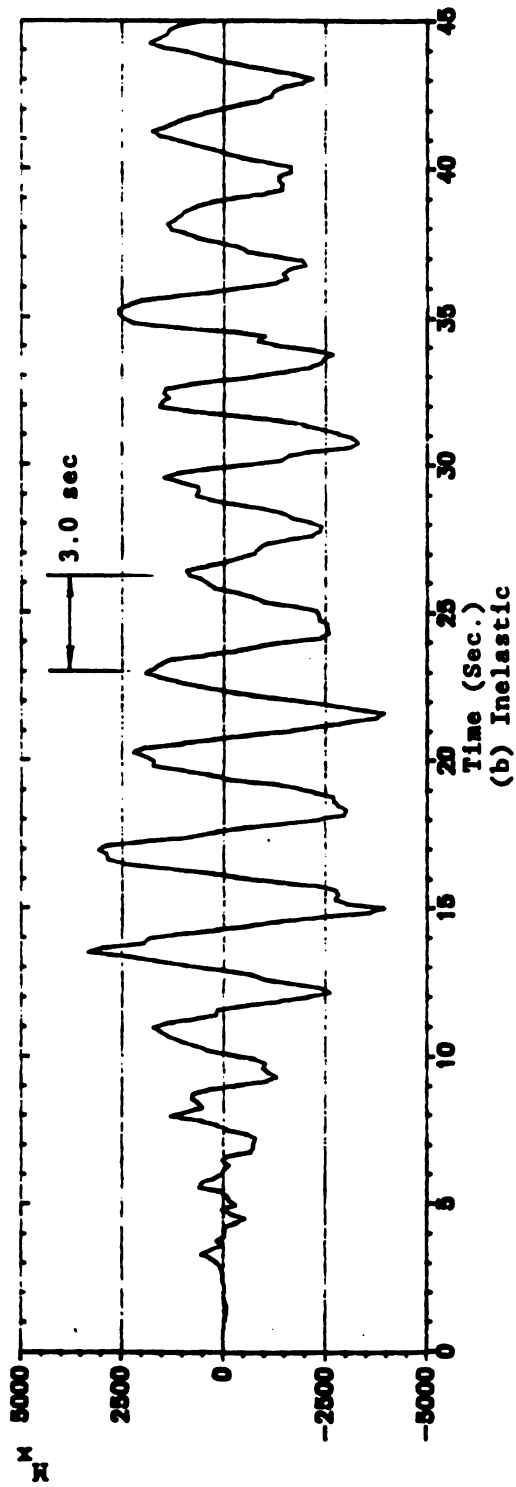


(b) Inelastic

Figure 3-46. Member 1 End J (Node 5) Out-of-Plane Bending Time History for MSB



(a) Linear Elastic



(b) Inelastic

Figure 3-47. Member 16 End I (Node 31) Out-of-Plane Bending Time History for MSB

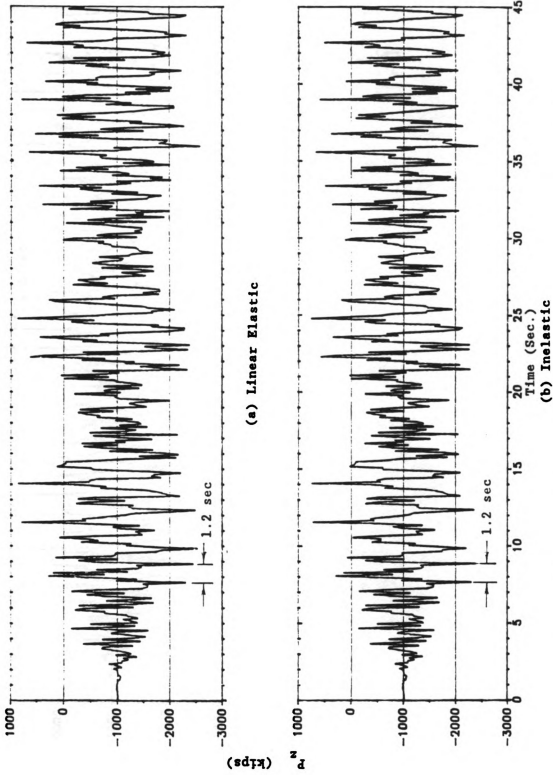


Figure 3-48. Member 9 End J (Node 11) Axial Force Time History for SSB

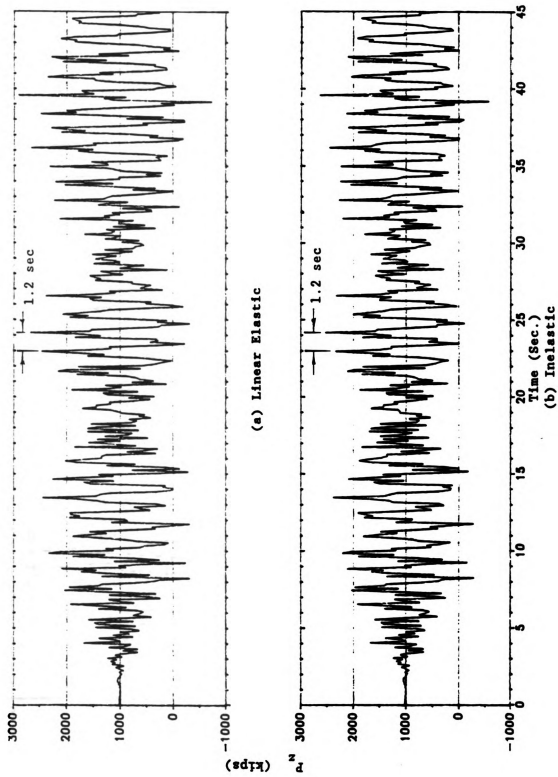


Figure 3-49. Member 13 End I (Node 23) Axial Force Time History for SSB

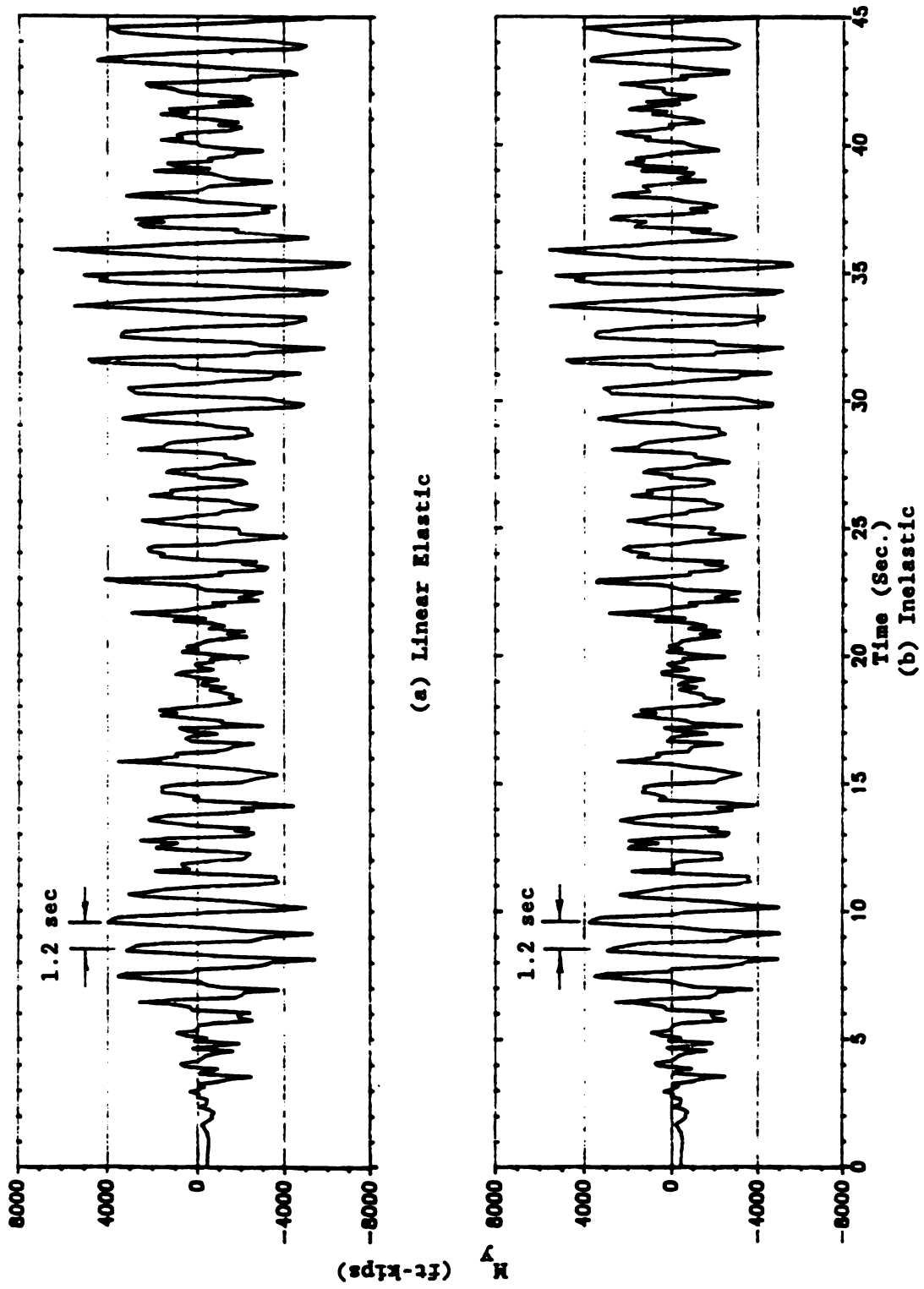


Figure 3-50. Member 9 End J (Node 11) In-Plane Bending Time History for SSB

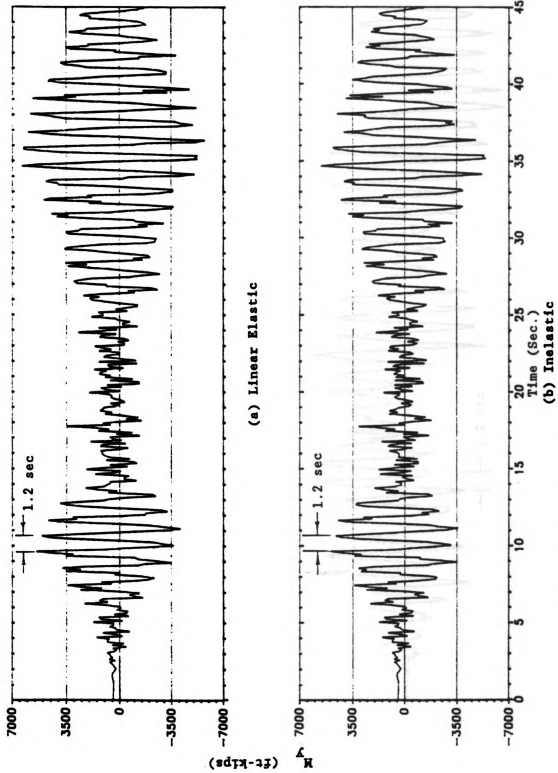


Figure 3-51. Member 13 End I (Node 23) In-Plane Bending Time History for SSB

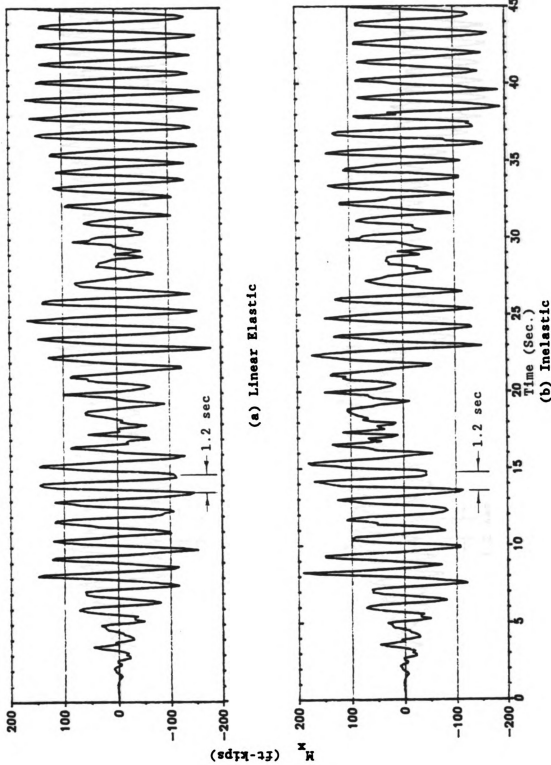


Figure 3-52. Member 9 End J (Node 11) Out-of-Plane Bending Time History for SSB

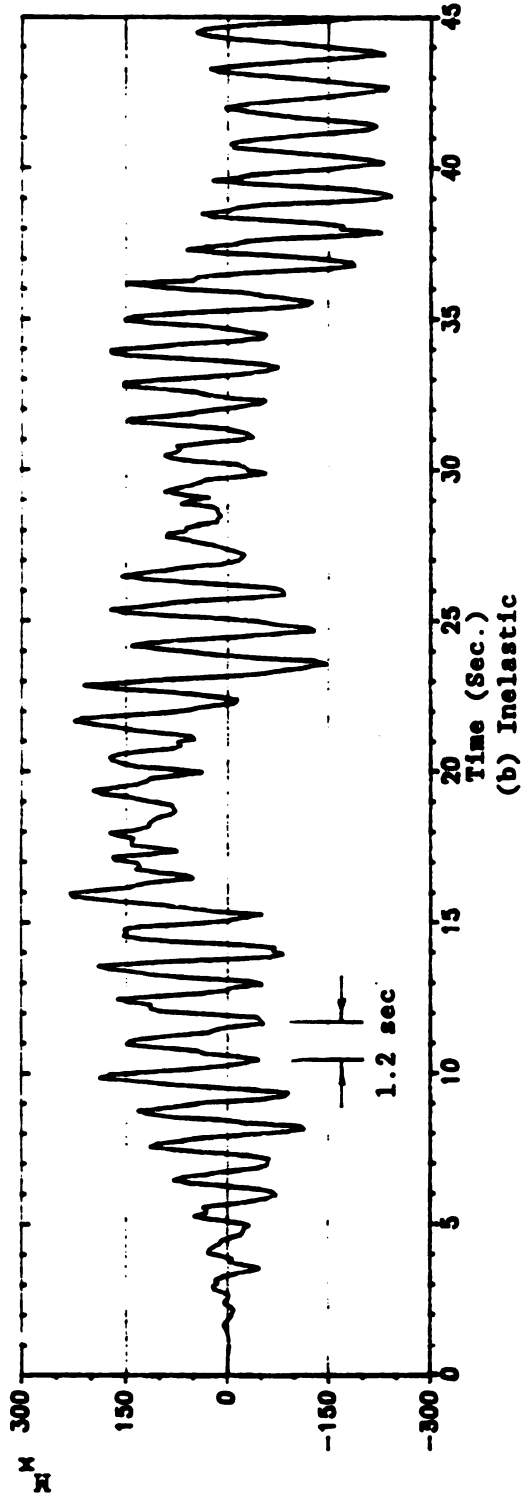
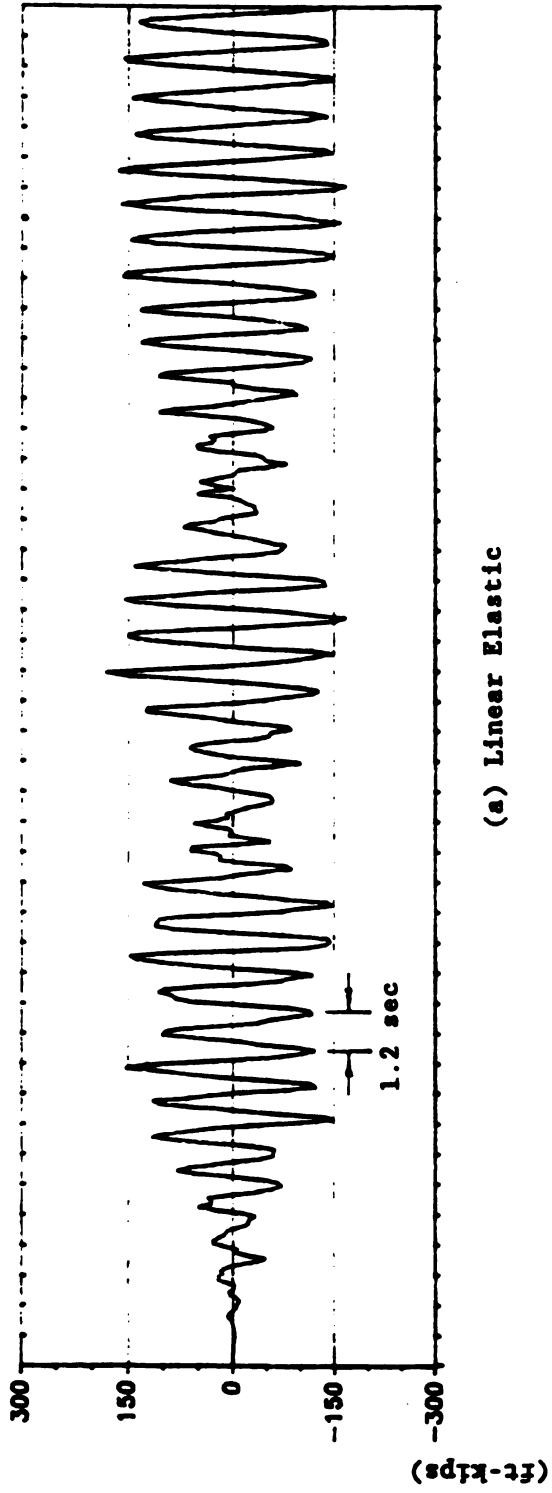


Figure 3-53. Member 13 End I (Node 23) Out-of-Plane Bending Time History for SSB

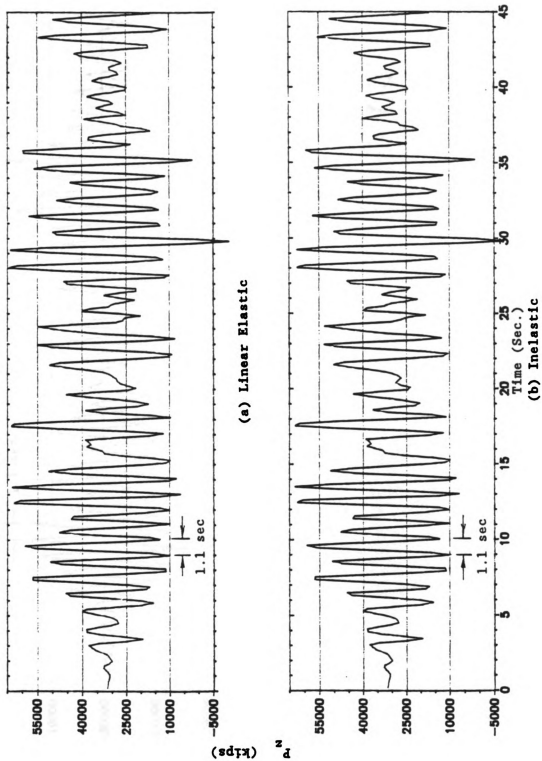
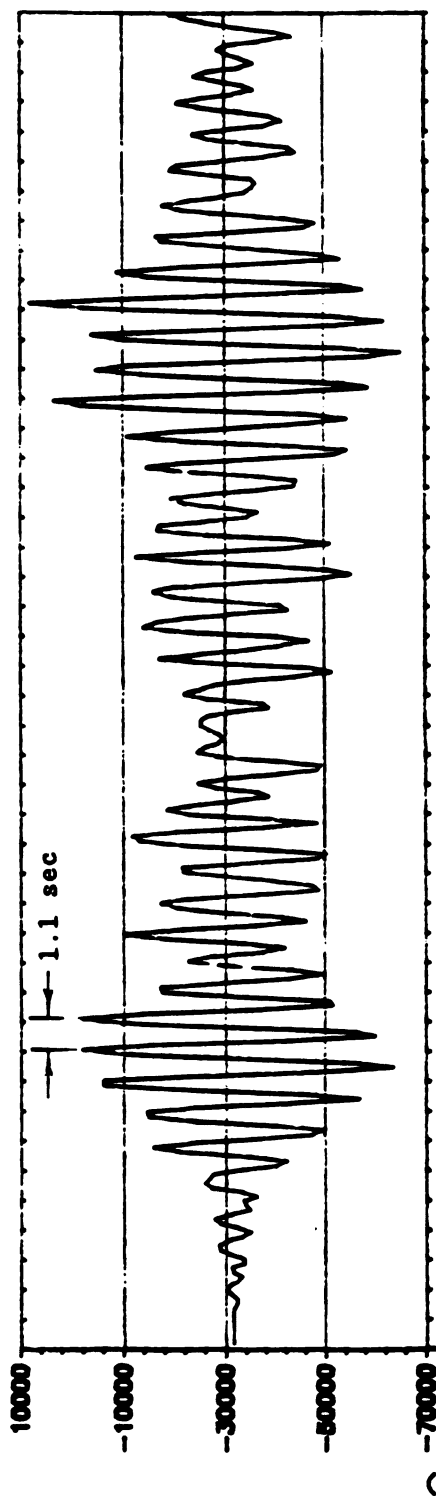
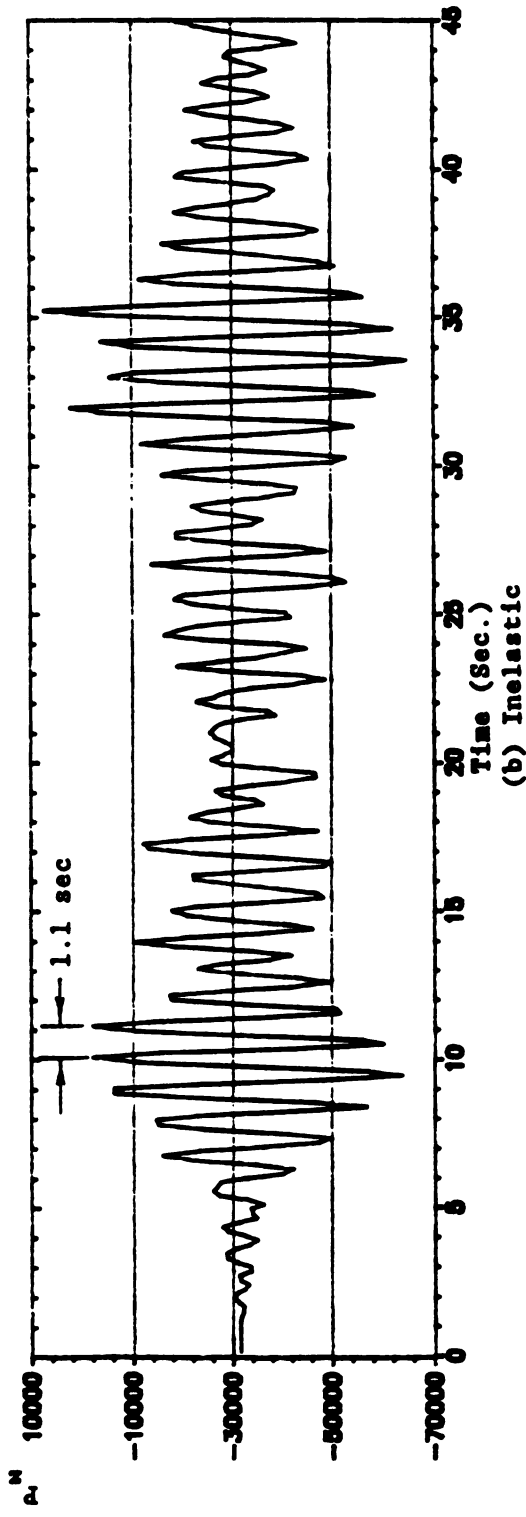


Figure 3-54. Member 5 End I (Node 12) Axial Force Time History for LSB

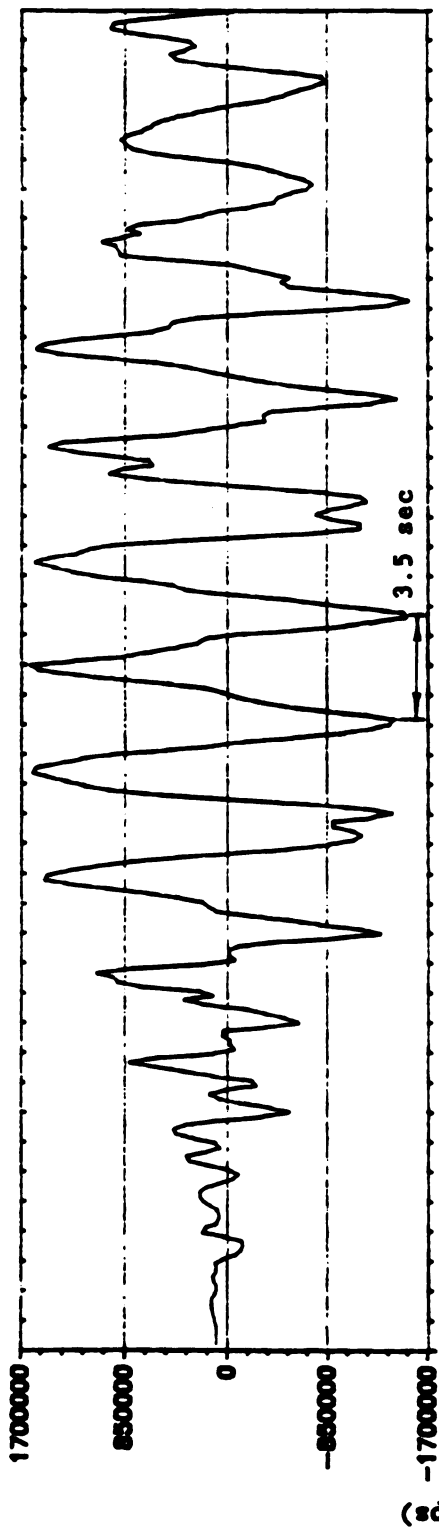


(a) Linear Elastic

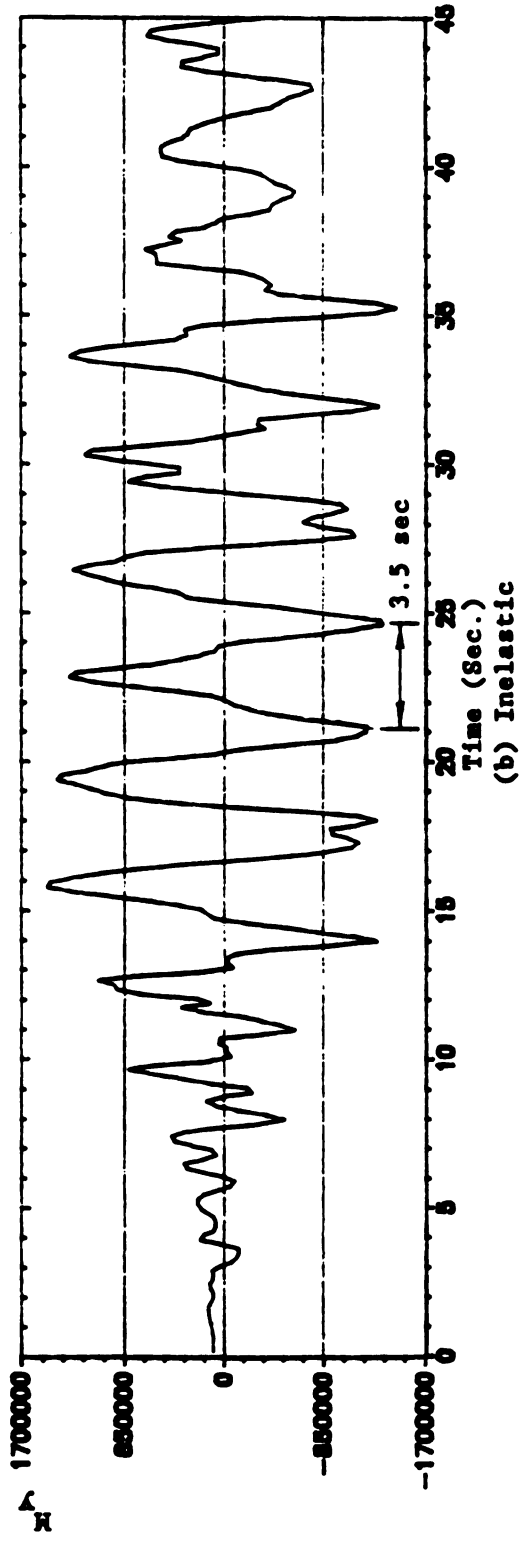


(b) Inelastic

Figure 3-55. Member 10 End J (Node 24) Axial Force Time History for LSB



(a) Linear Elastic



(b) Inelastic

Figure 3-56. Member 5 End I (Node 12) In-Plane Bending Time History for LSB

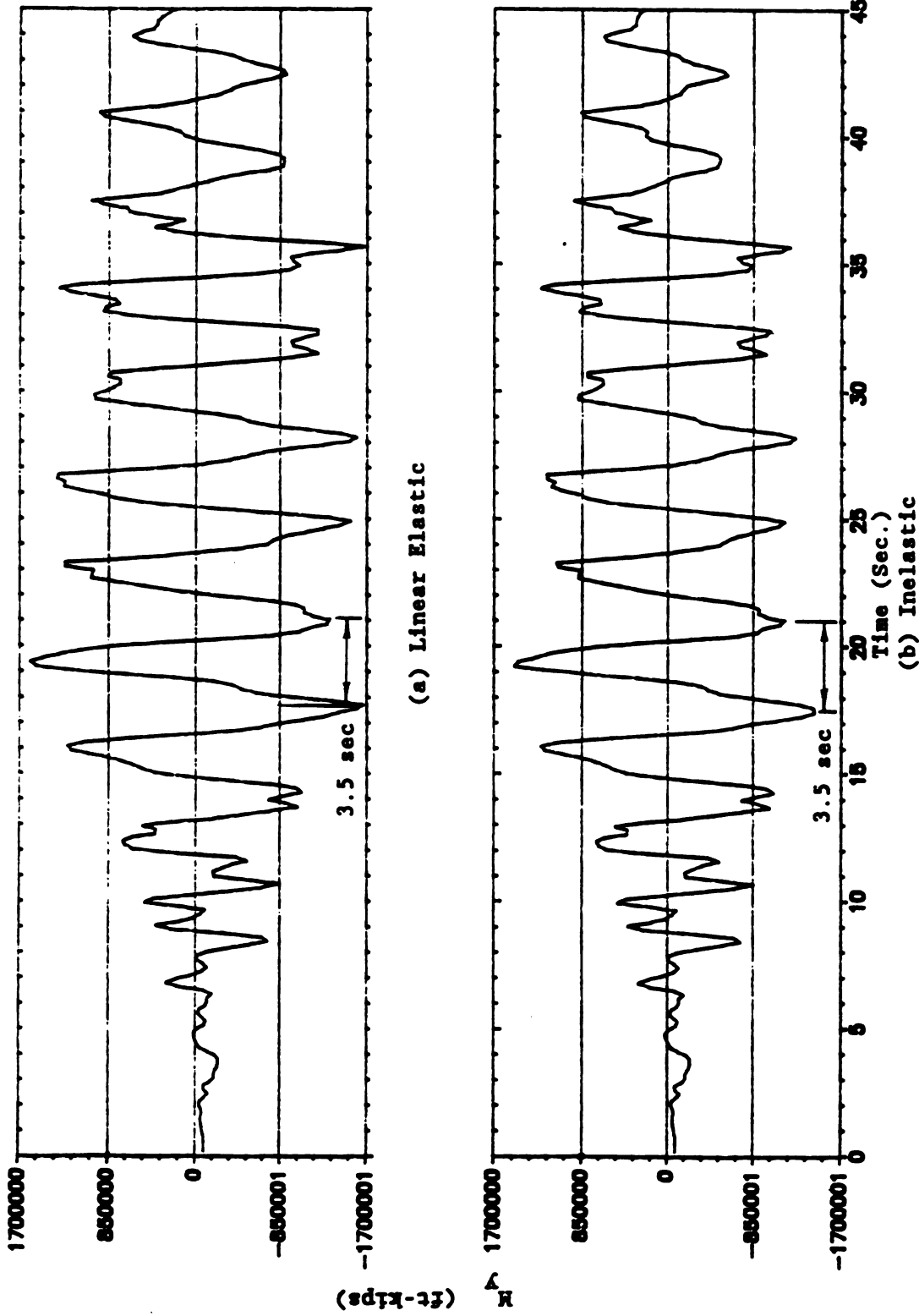


Figure 3-57. Member 10 End J (Node 24) In-Plane Bending Time History for LSB

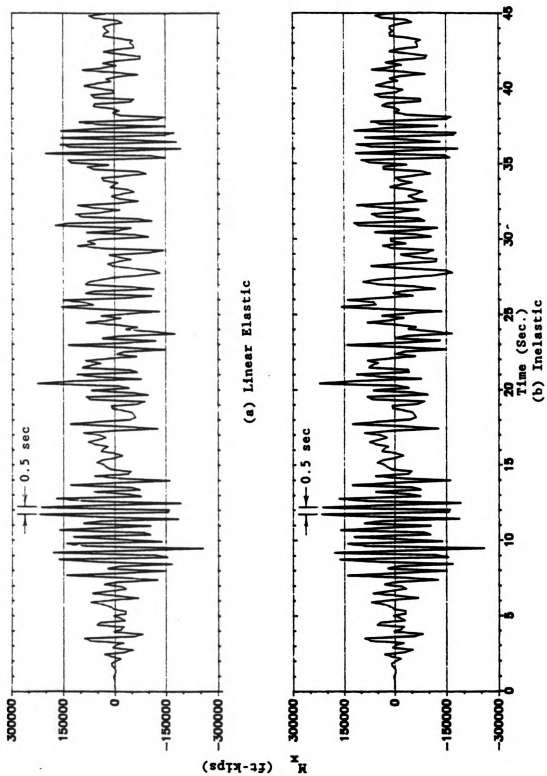


Figure 3-58. Member 5 End I (Node 12) Out-of-Plane Bending Time History for LSB

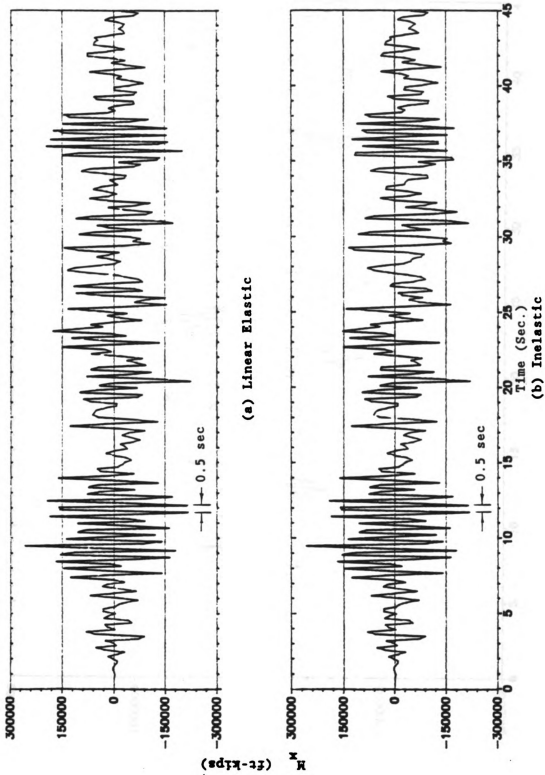


Figure 3-59. Member 10 End J (Node 24) Out-of-Plane Bending Time History for LSB

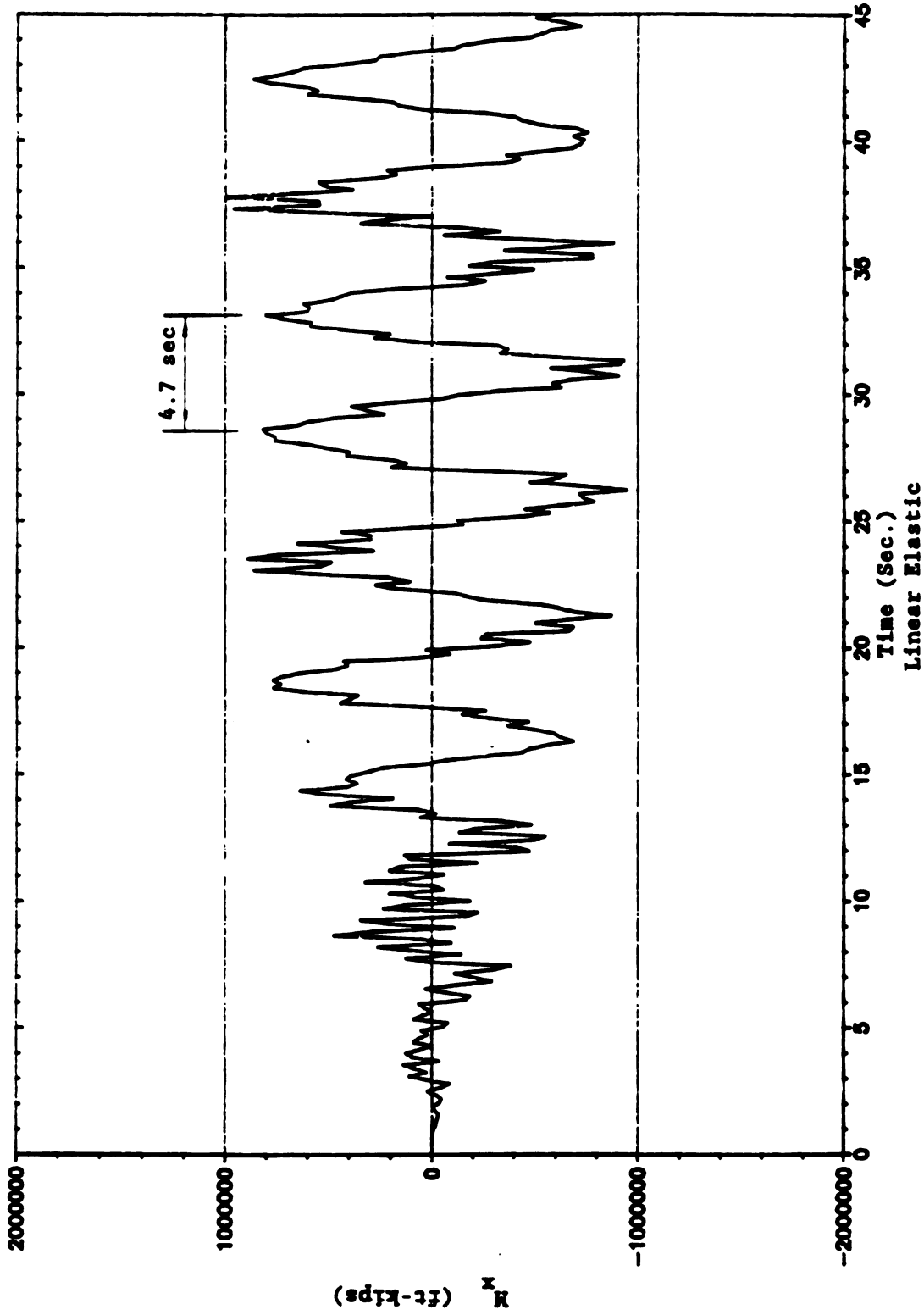


Figure 3-60. Member 4 End I (Node 10) Out-of-Plane Bending Time History for LSB

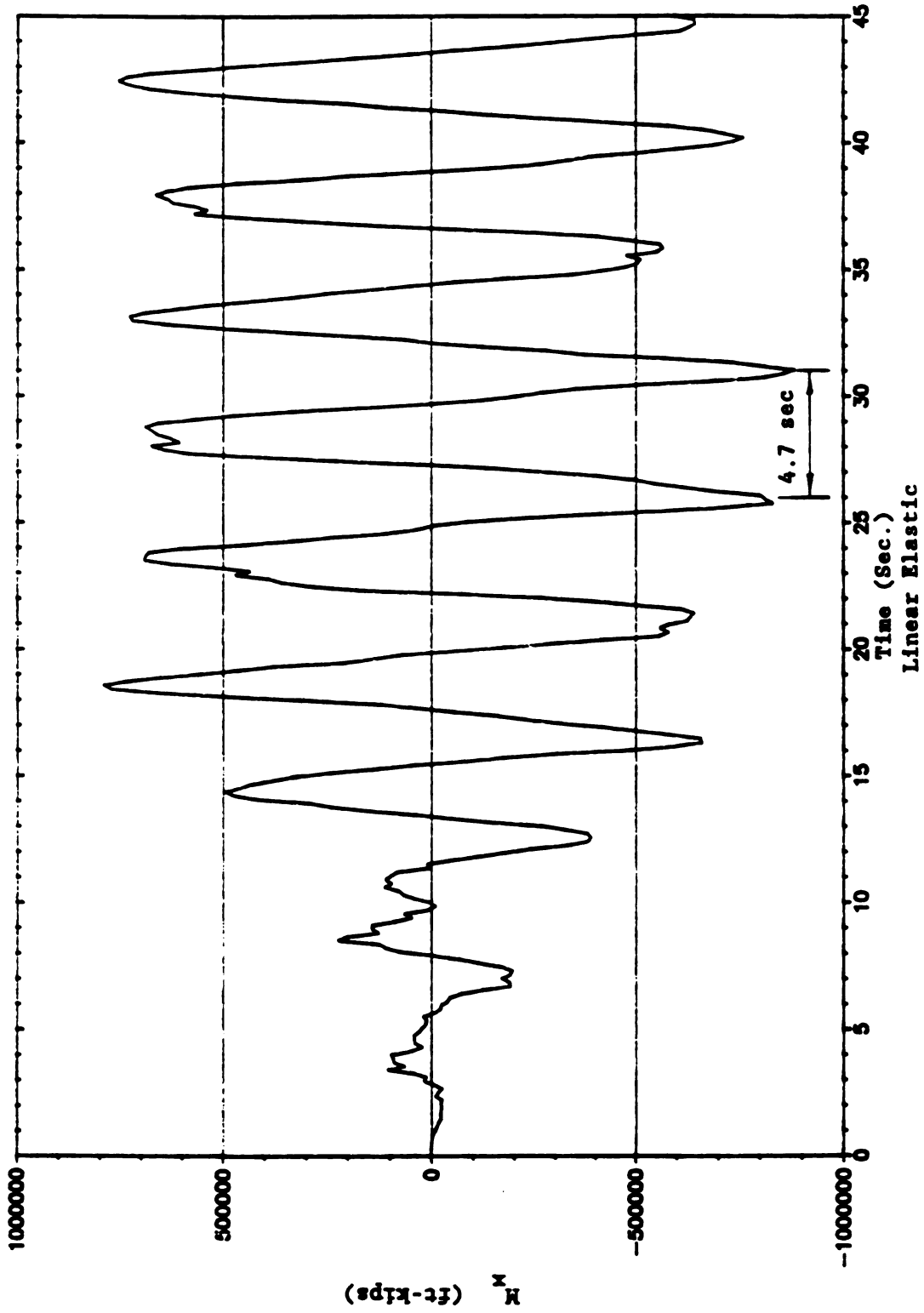


Figure 3-61. Member 5 End J (Node 14) Out-of-Plane Bending Time History for LSB

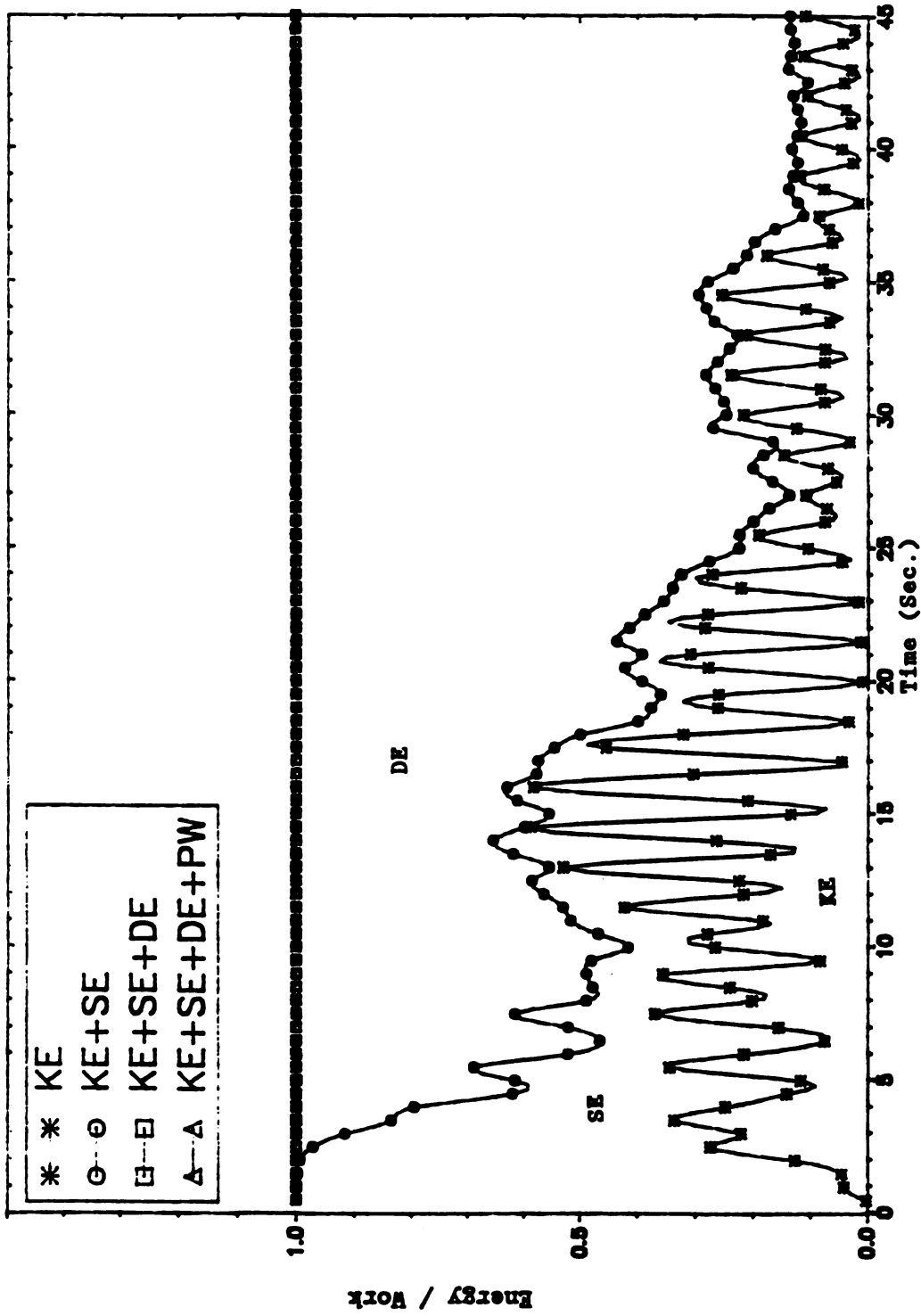


Figure 3-62. Work and Energy Distribution Time History for MSB (Linear Elastic)

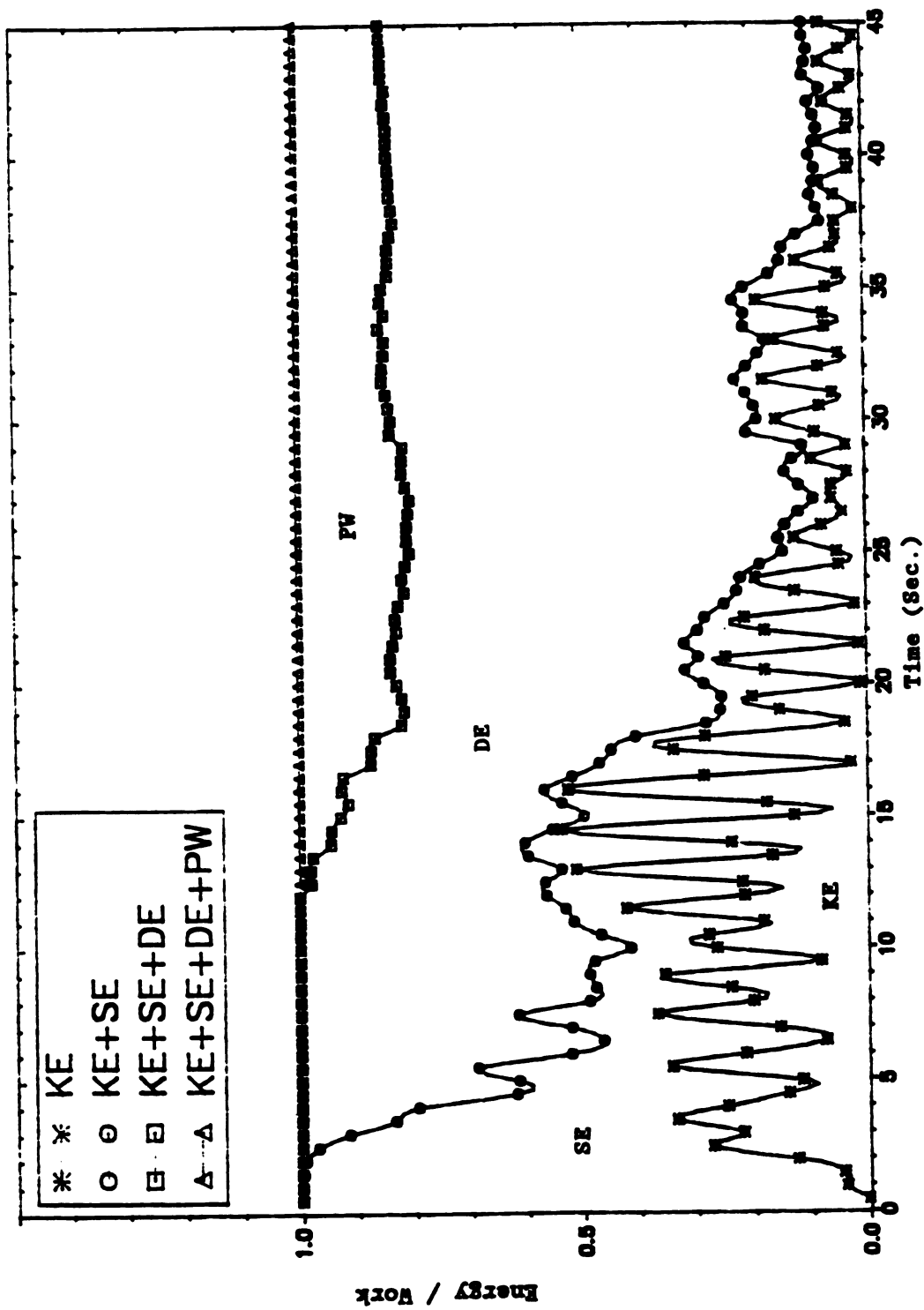


Figure 3-63. Work and Energy Distribution Time History for MSB (Inelastic)

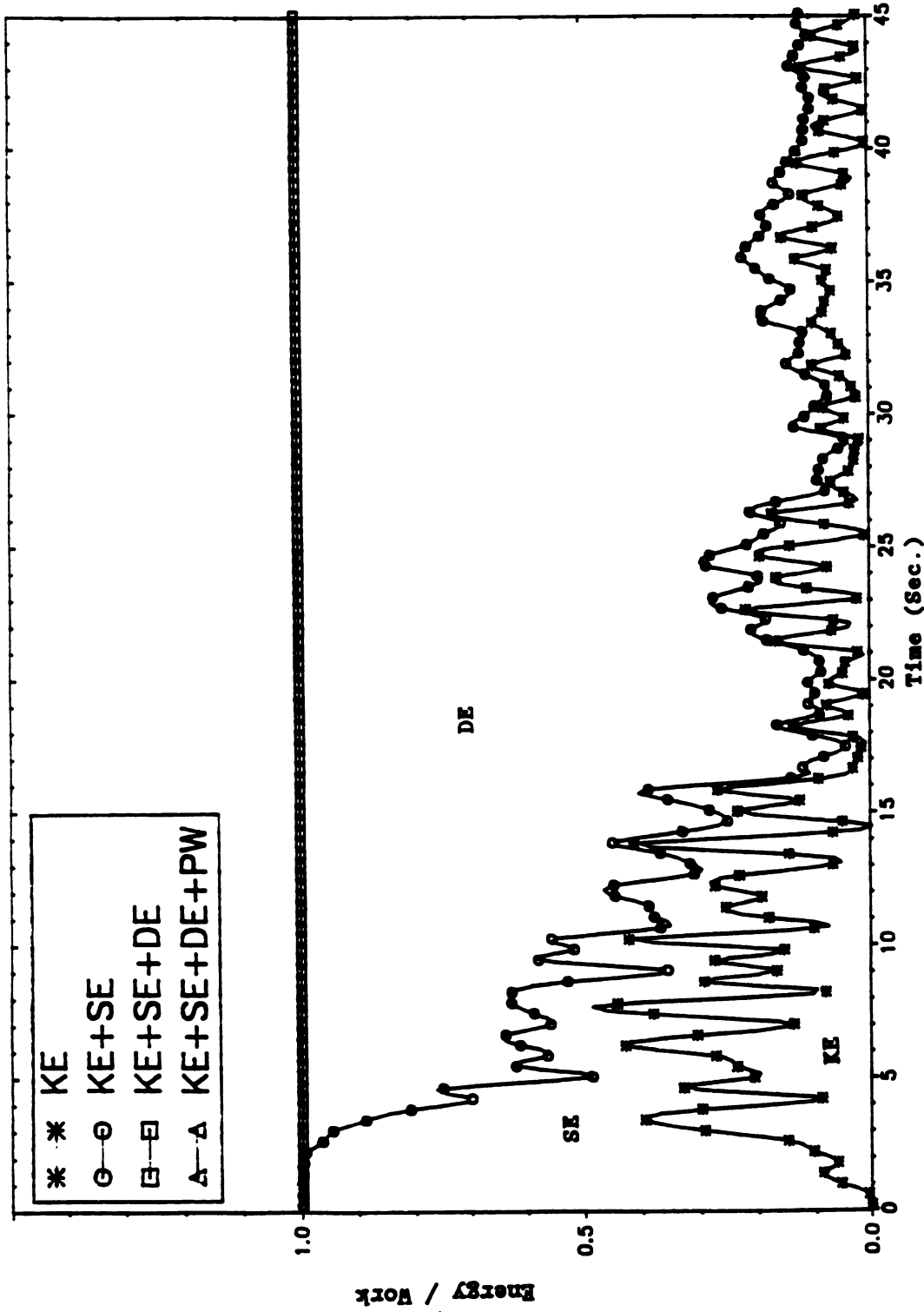


Figure 3-64. Work and Energy Distribution Time History for SSB (Linear Elastic)

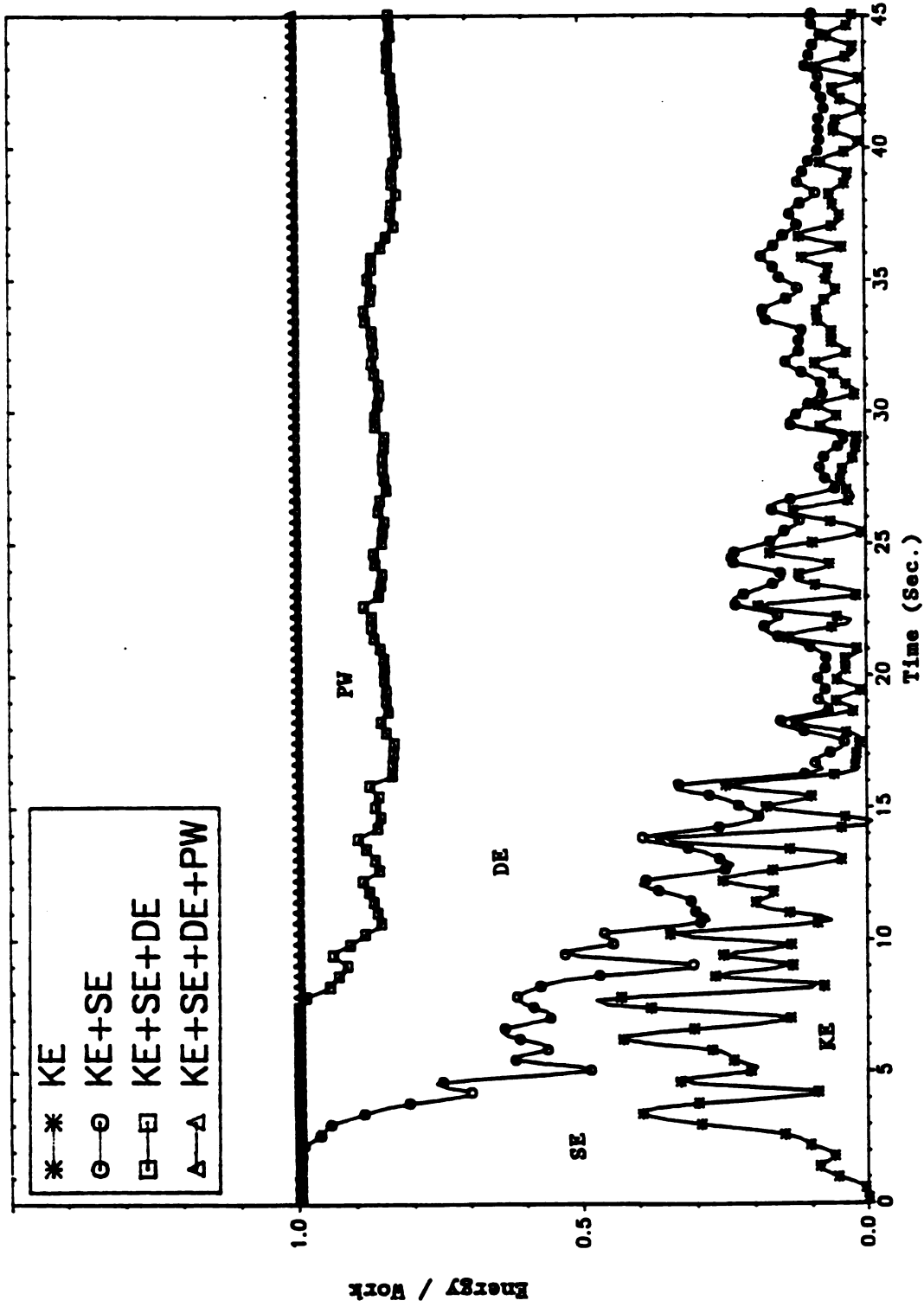


Figure 3-65. Work and Energy Distribution Time History for SSB (Inelastic)

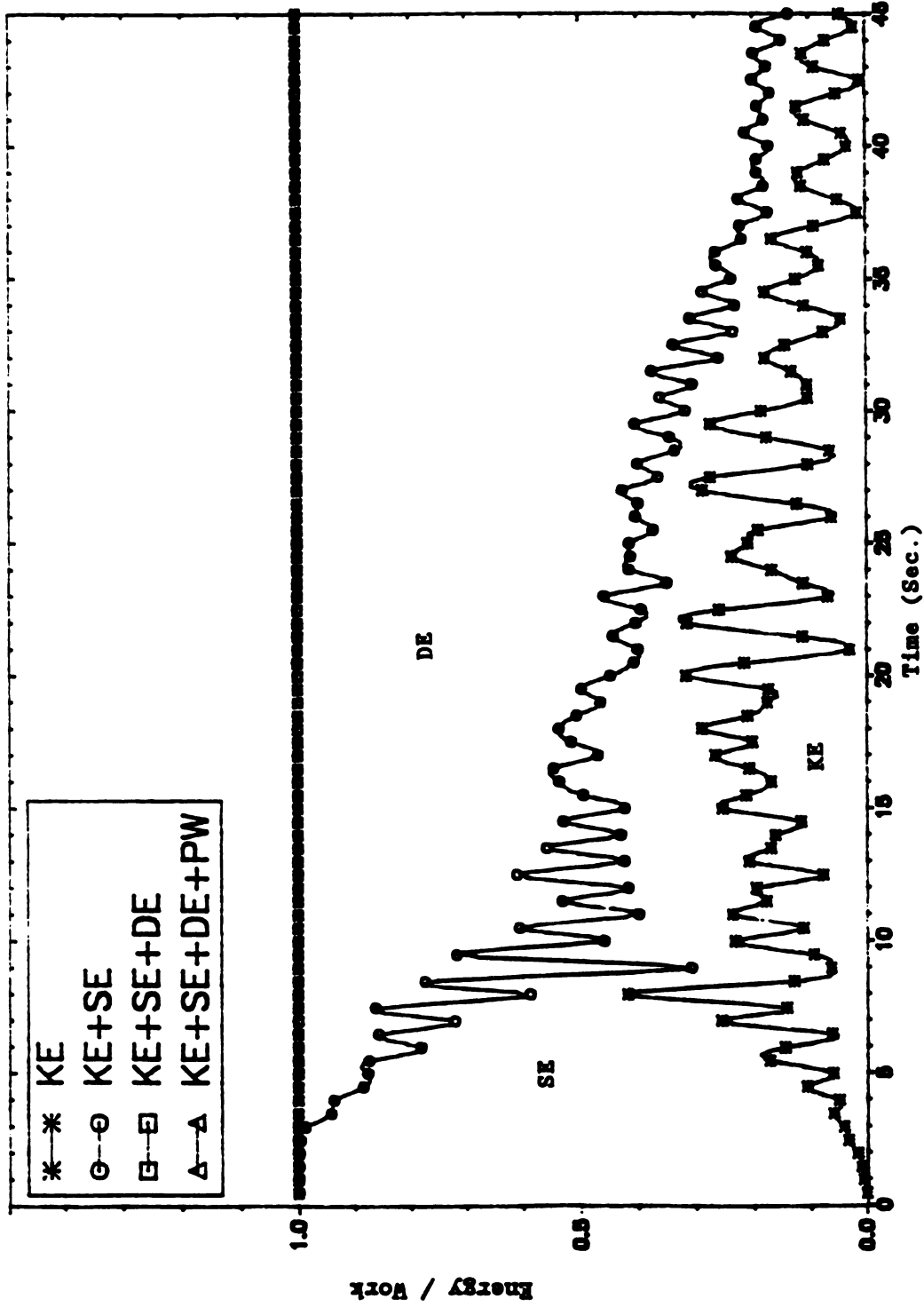


Figure 3-66. Work and Energy Distribution Time History for LSB (Linear Elastic)

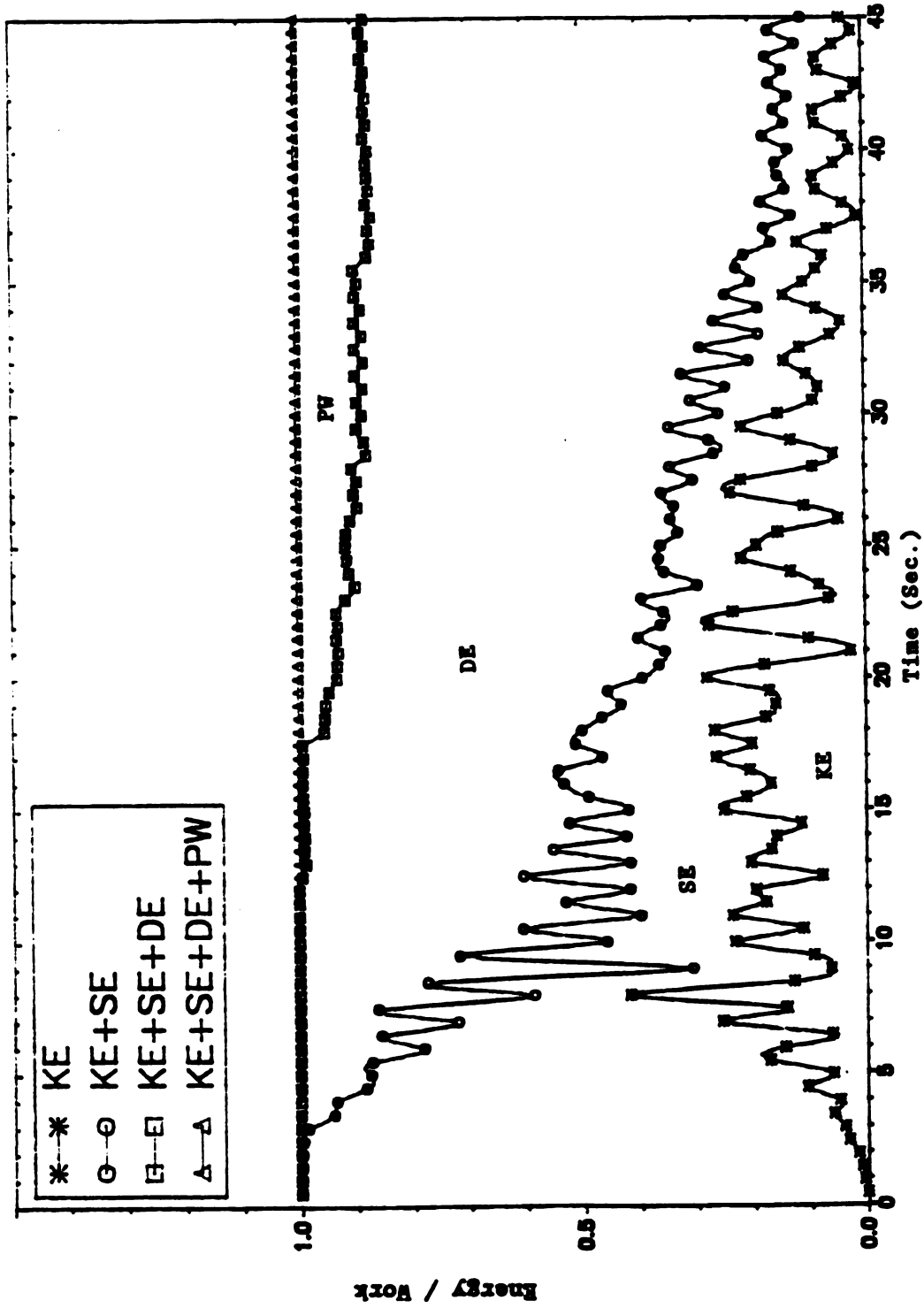


Figure 3-67. Work and Energy Distribution Time History for LSB (Inelastic)

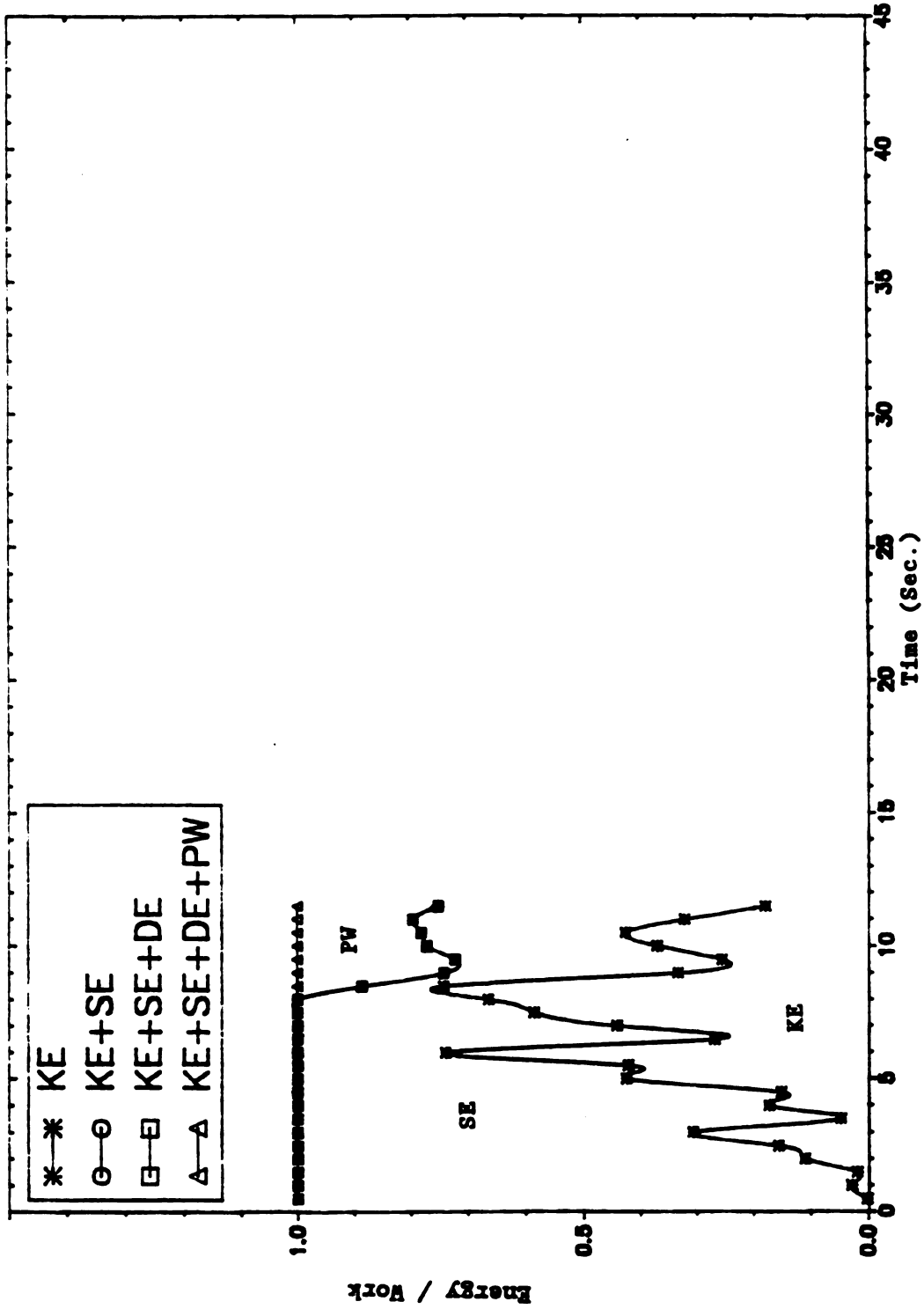


Figure 3-68. Work and Energy Distribution Time History for MSB (2-D Model) with 0.0% Damping Ratio (Inelastic)

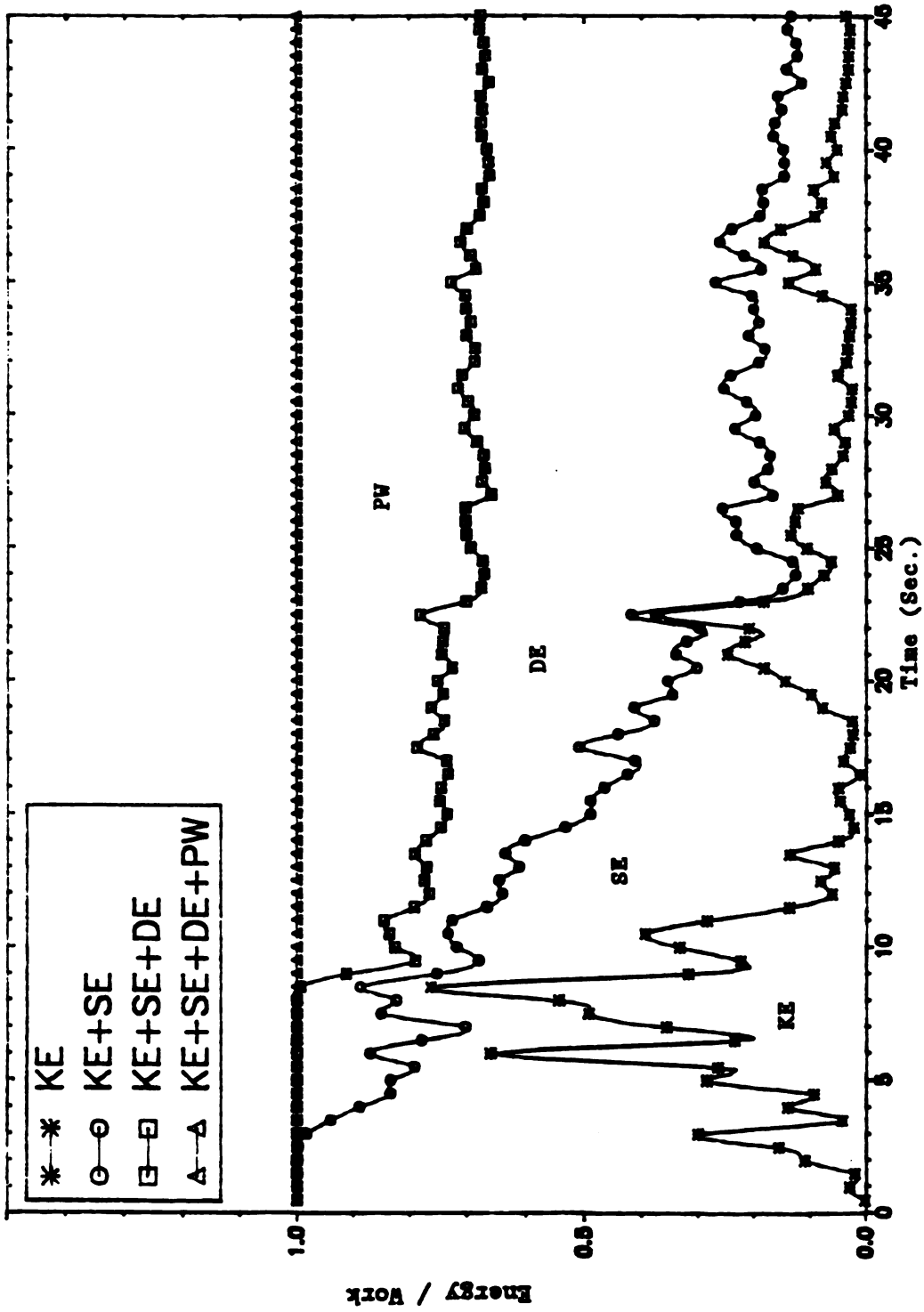


Figure 3-69. Work and Energy Distribution Time History for MSB (2-D Model) with 0.25% Damping Ratio (Inelastic)

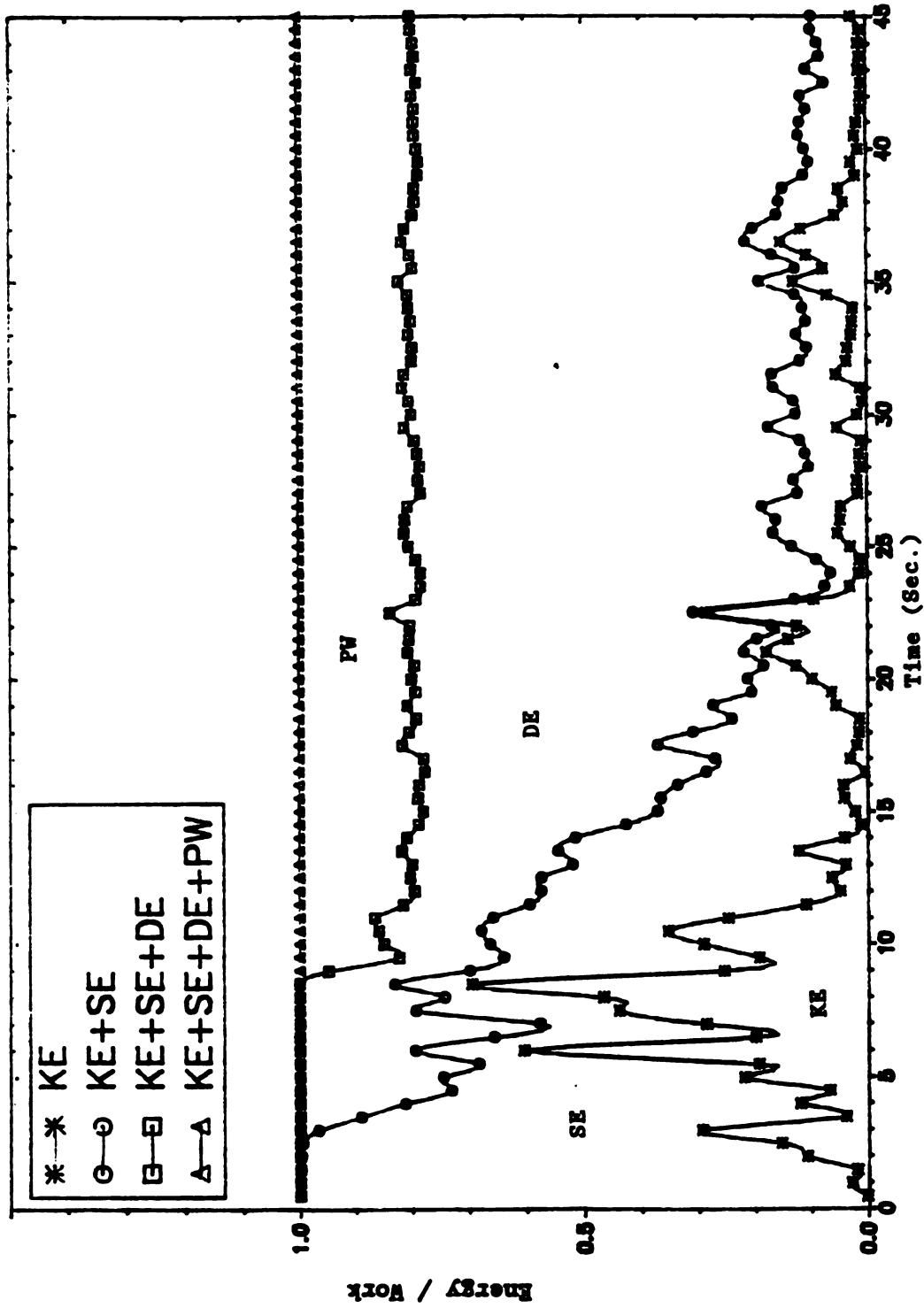


Figure 3-70. Work and Energy Distribution Time History for MSB (2-D Model) with 0.5% Damping Ratio (Inelastic)

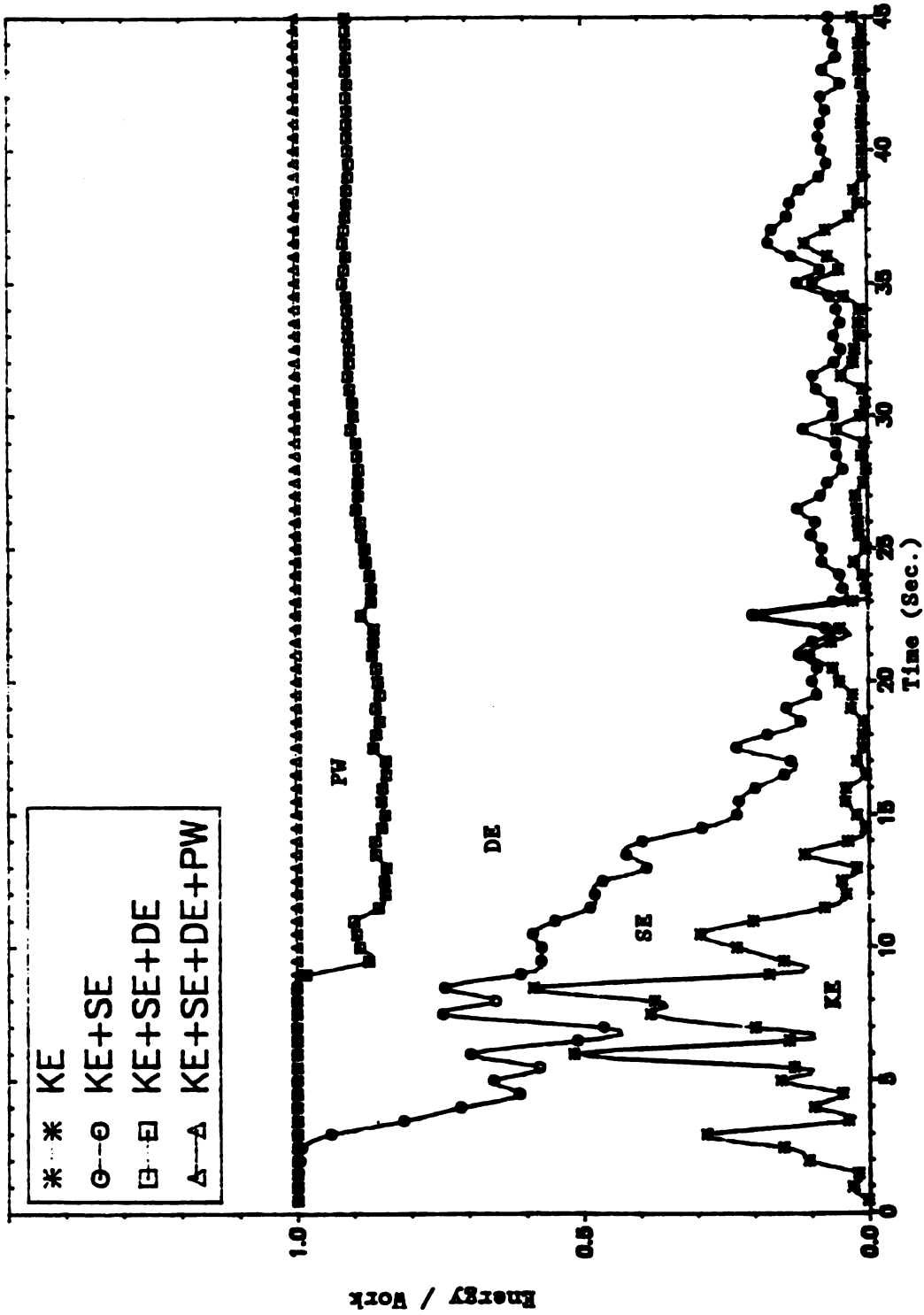
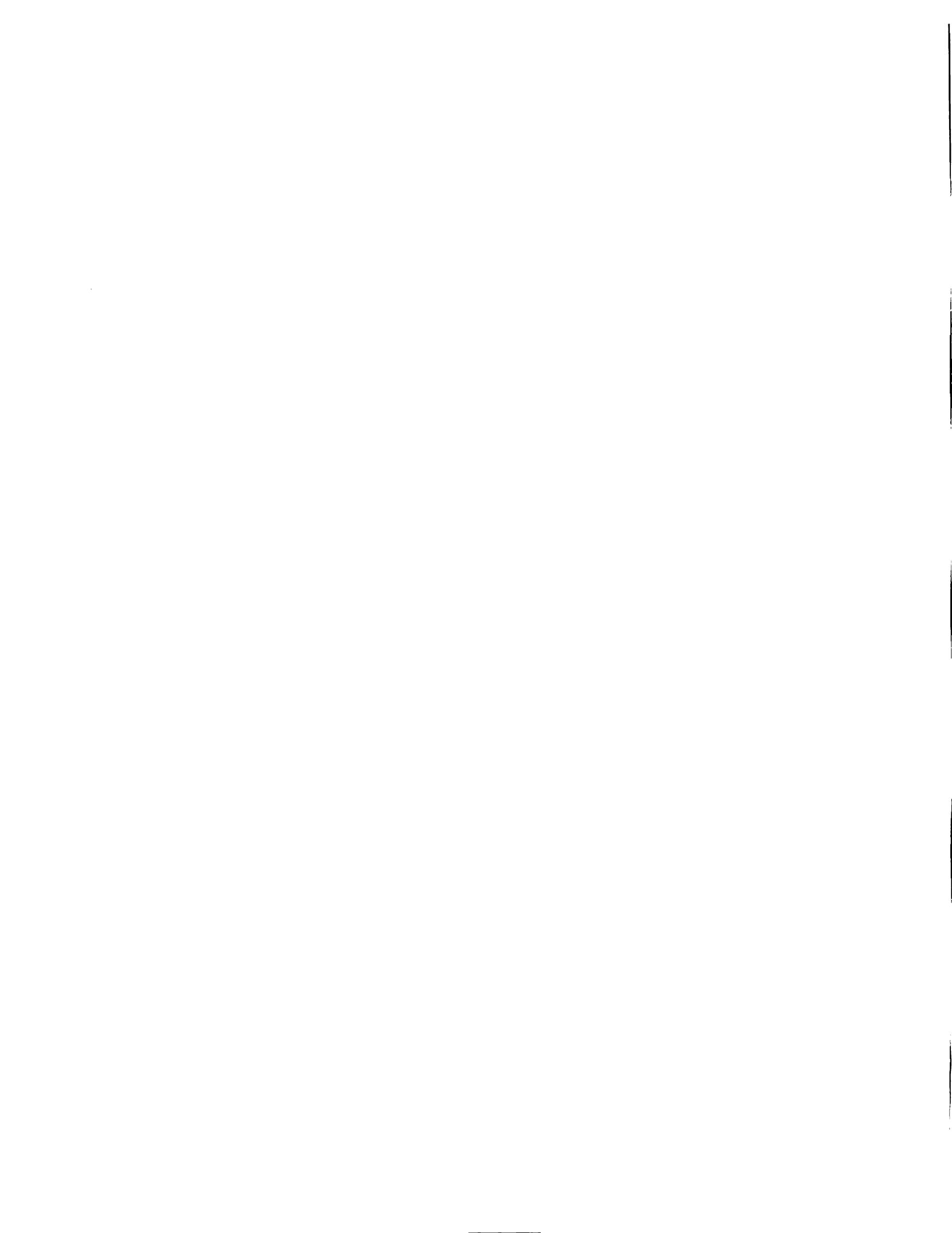


Figure 3-71. Work and Energy Distribution Time History for MSB (2-D Model) with 1.0% Damping Ratio (Inelastic)



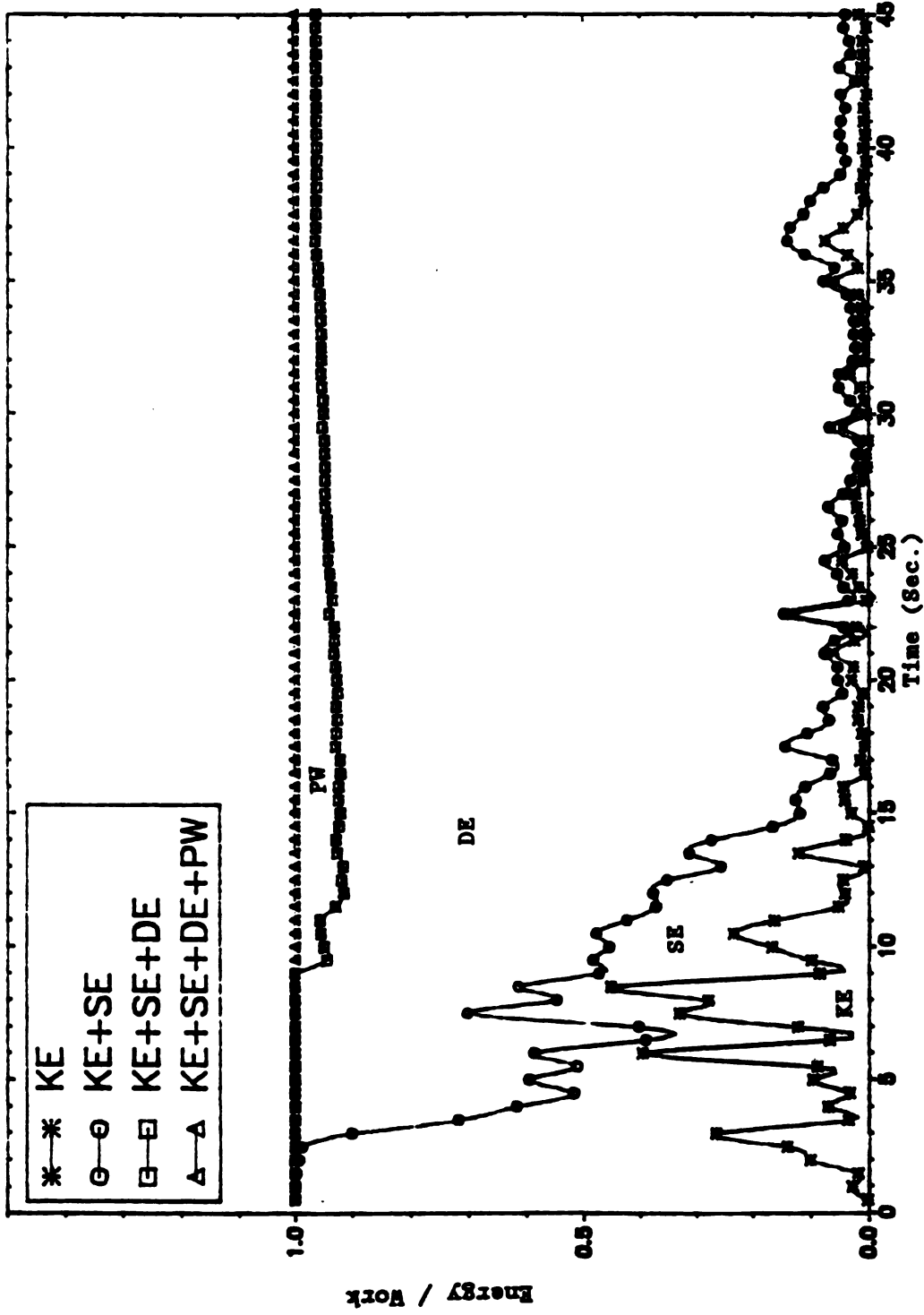


Figure 3-72. Work and Energy Distribution Time History for MSB (2-D Model) with 2.0% Damping Ratio (Inelastic)

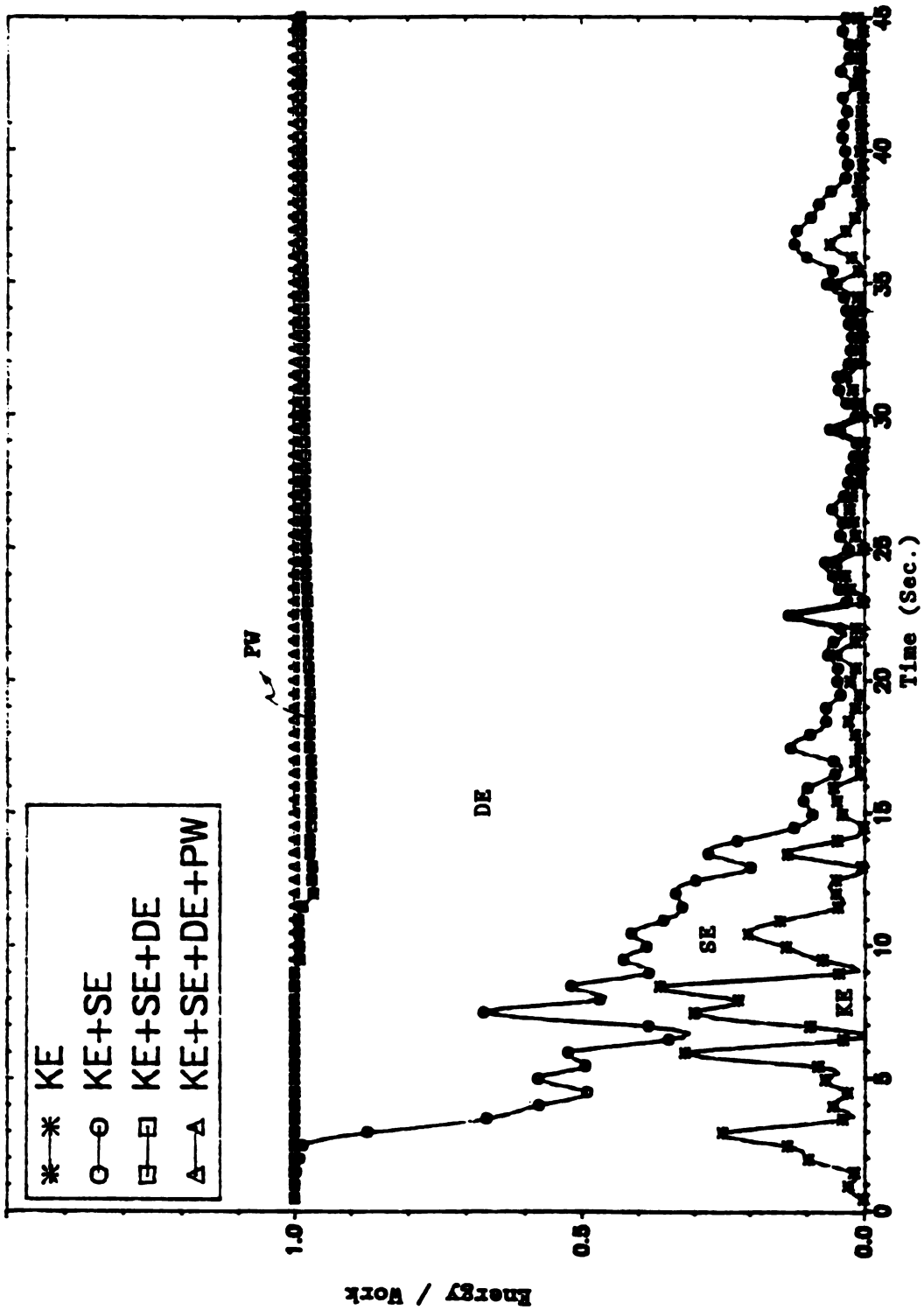


Figure 3-73. Work and Energy Distribution Time History for MSB (2-D Model) with 3.0% Damping Ratio (Inelastic)

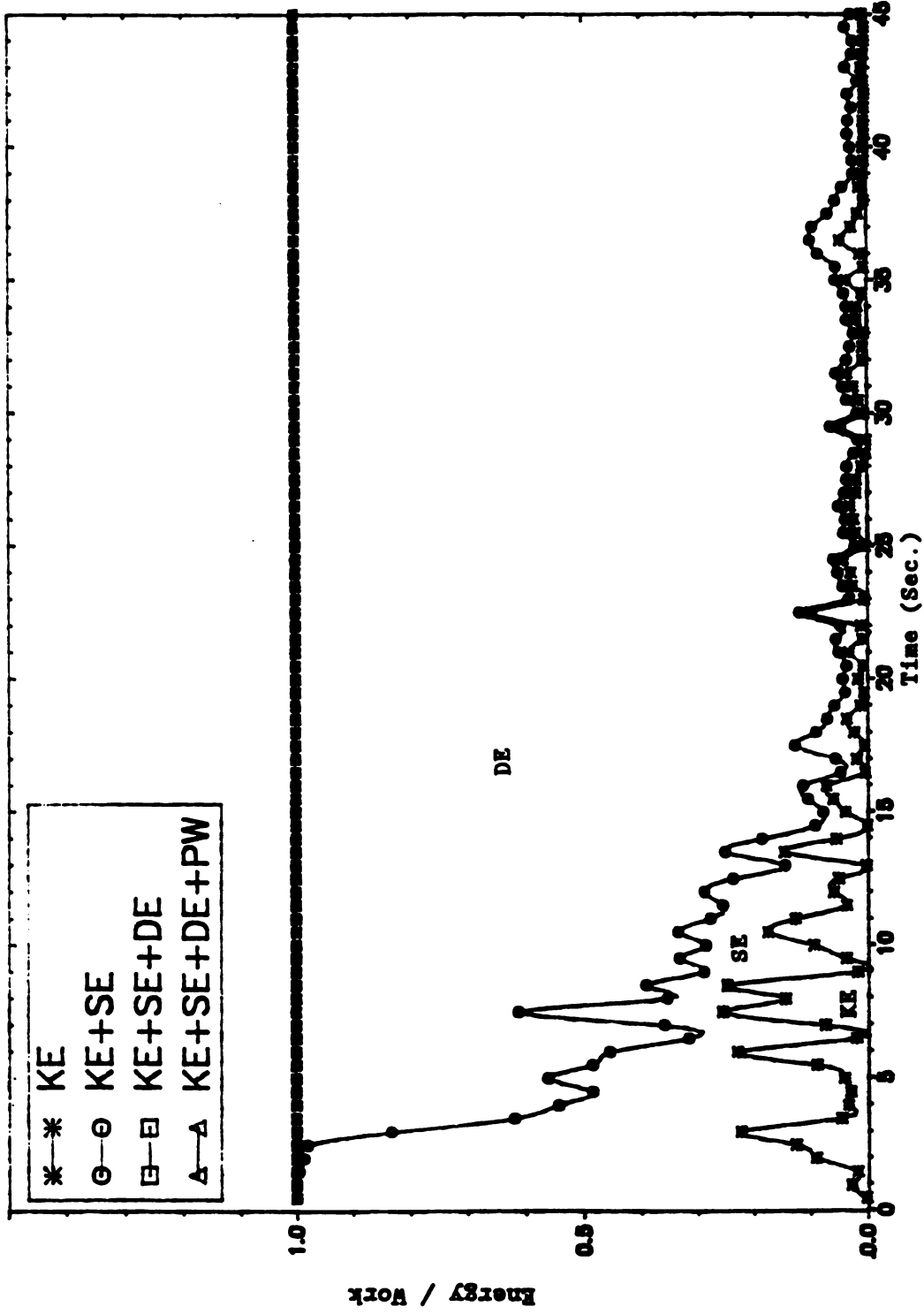


Figure 3-74. Work and Energy Distribution Time History for MSB (2-D Model) with 5.0% Damping Ratio (Inelastic)

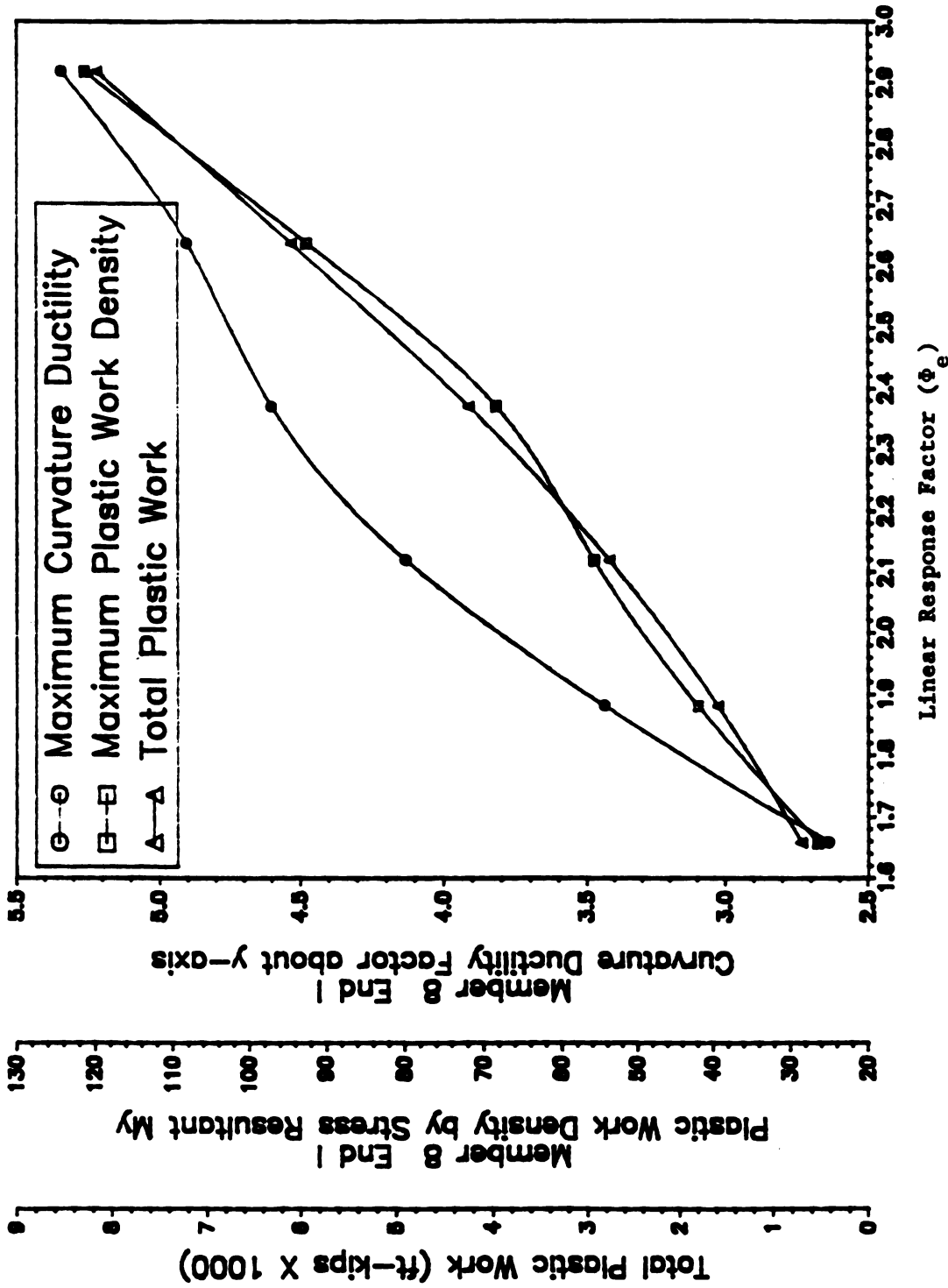


Figure 3-75. Inelastic Responses Versus Linear Response Factor for MSB

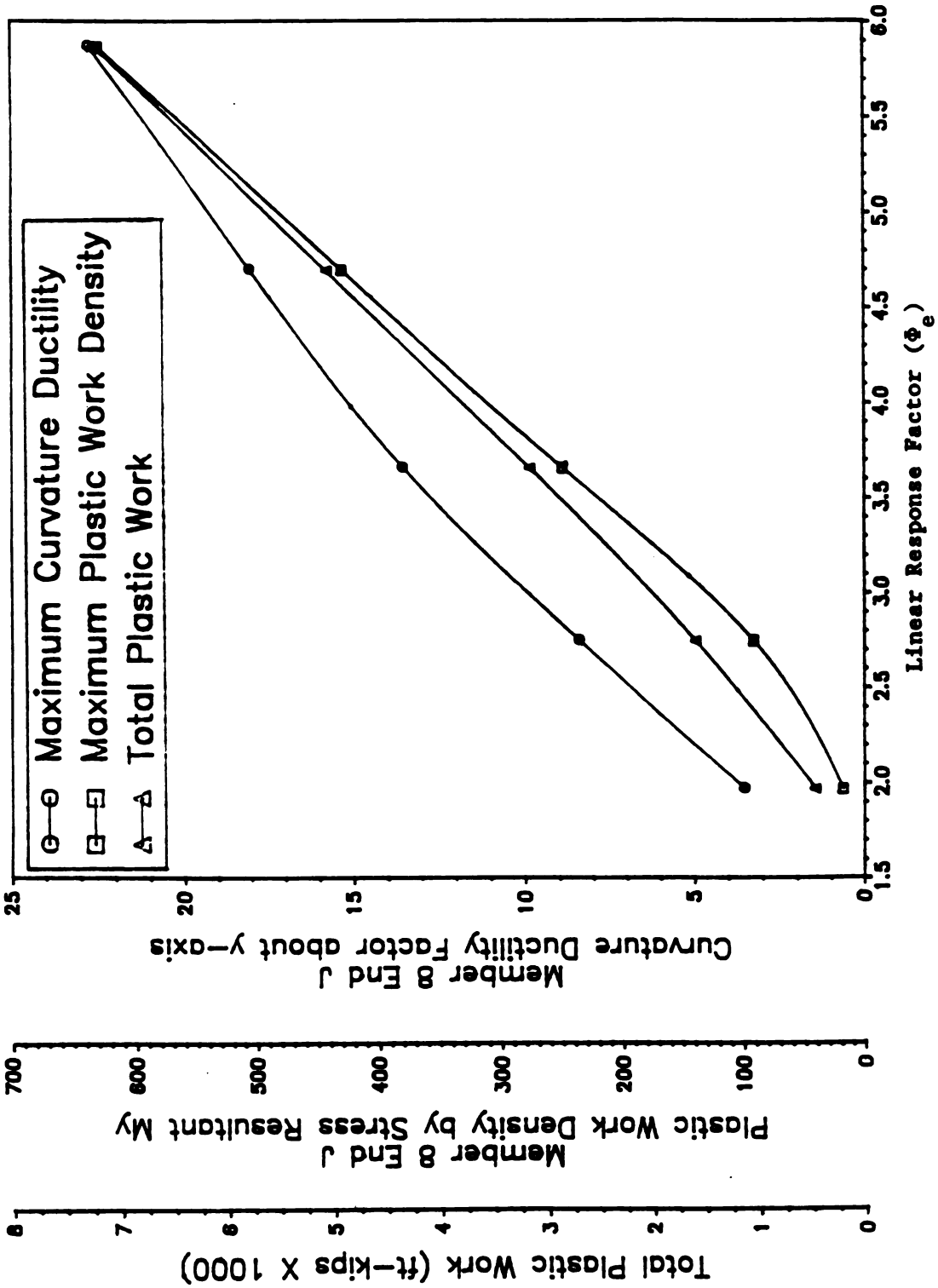


Figure 3-76. Inelastic Responses Versus Linear Response Factor for SSB

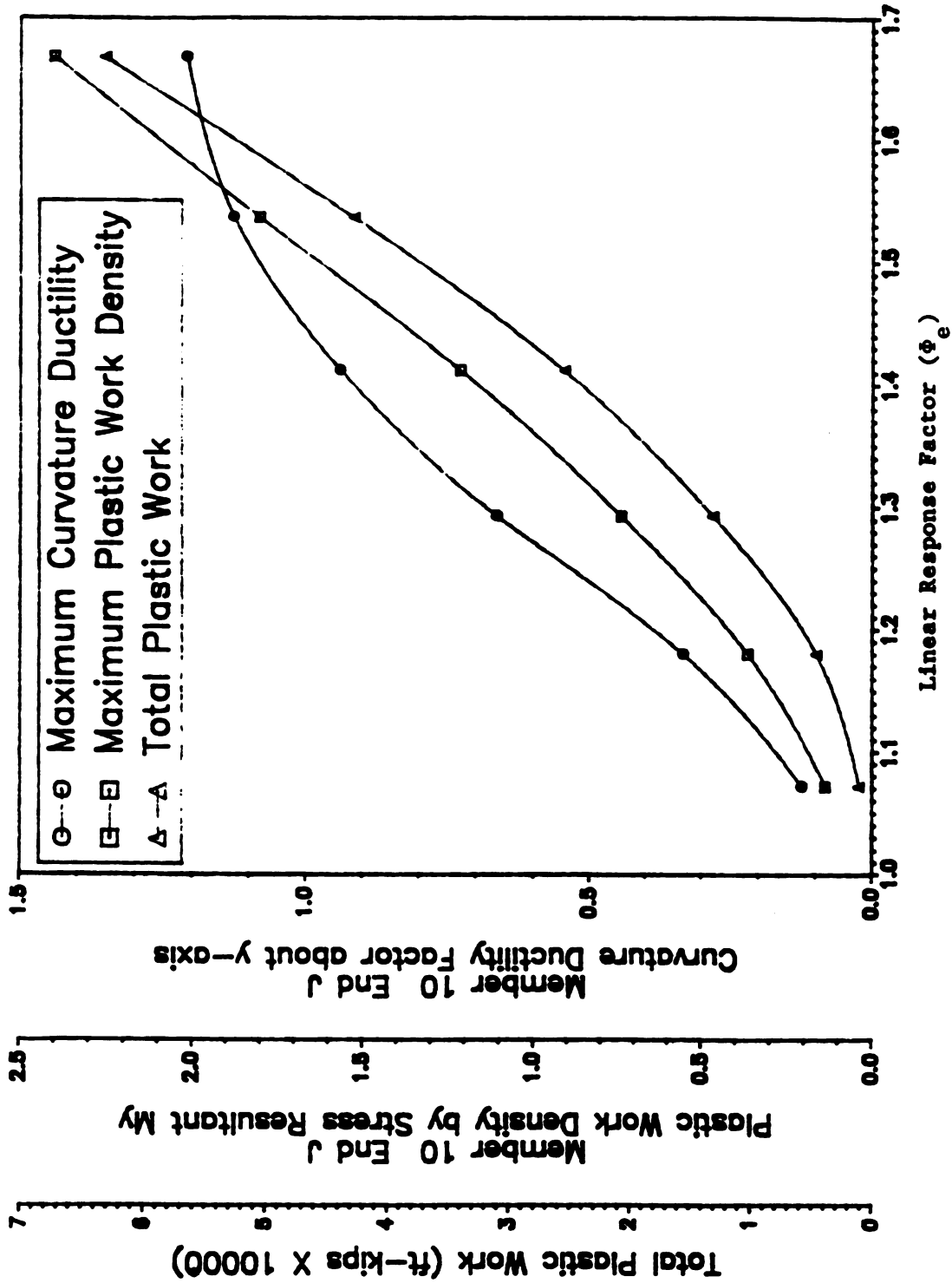
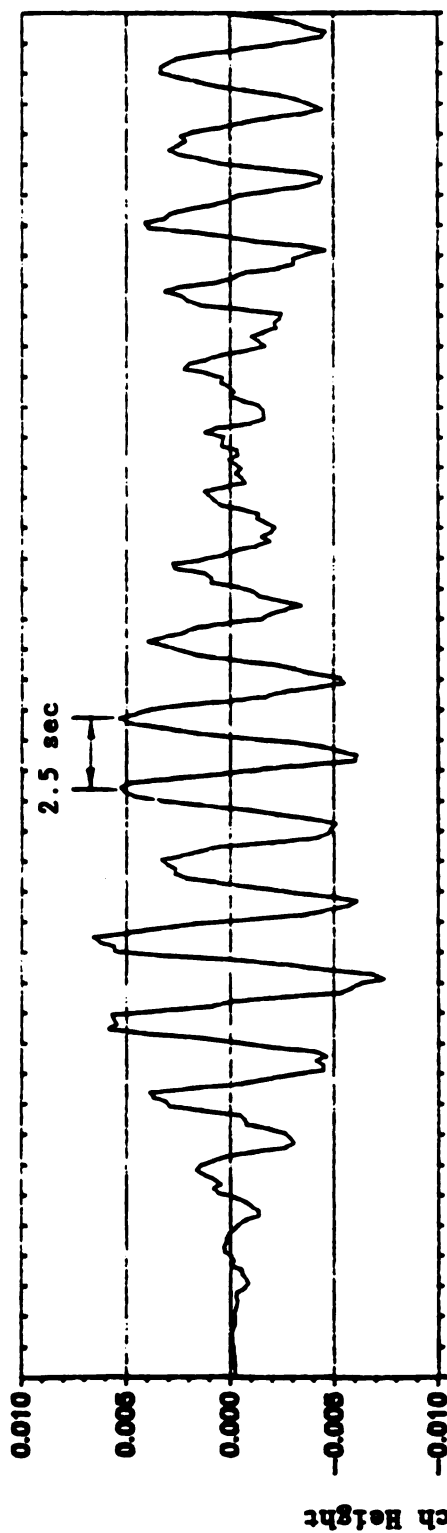
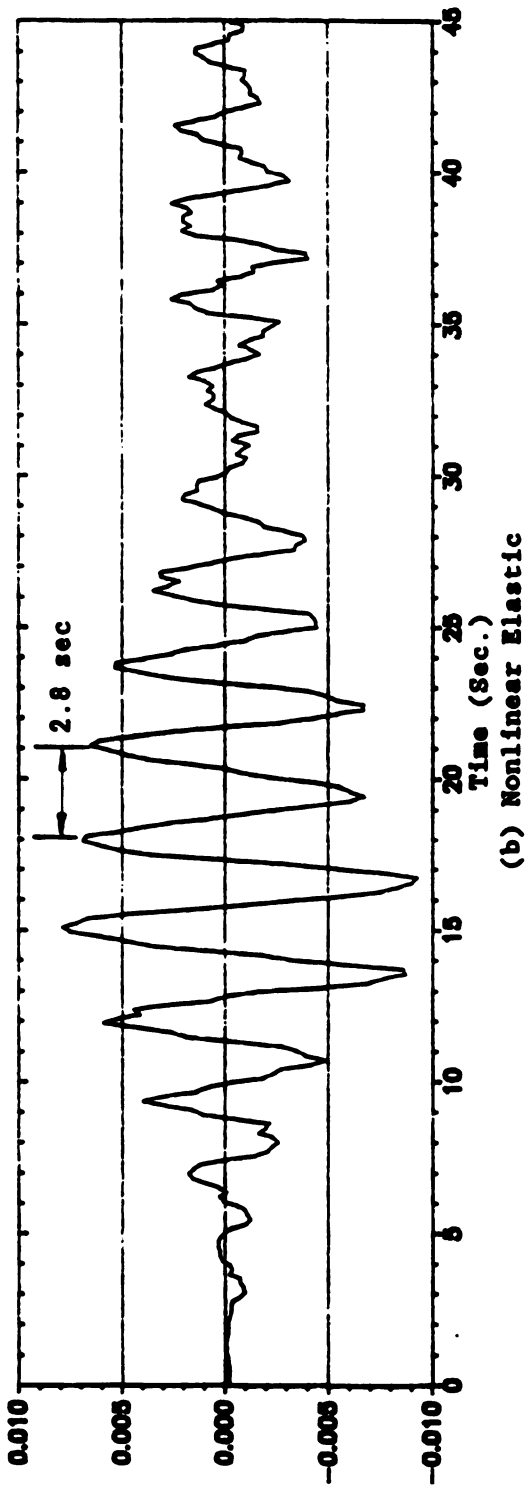


Figure 3-77. Inelastic Responses Versus Linear Response Factor for LSB

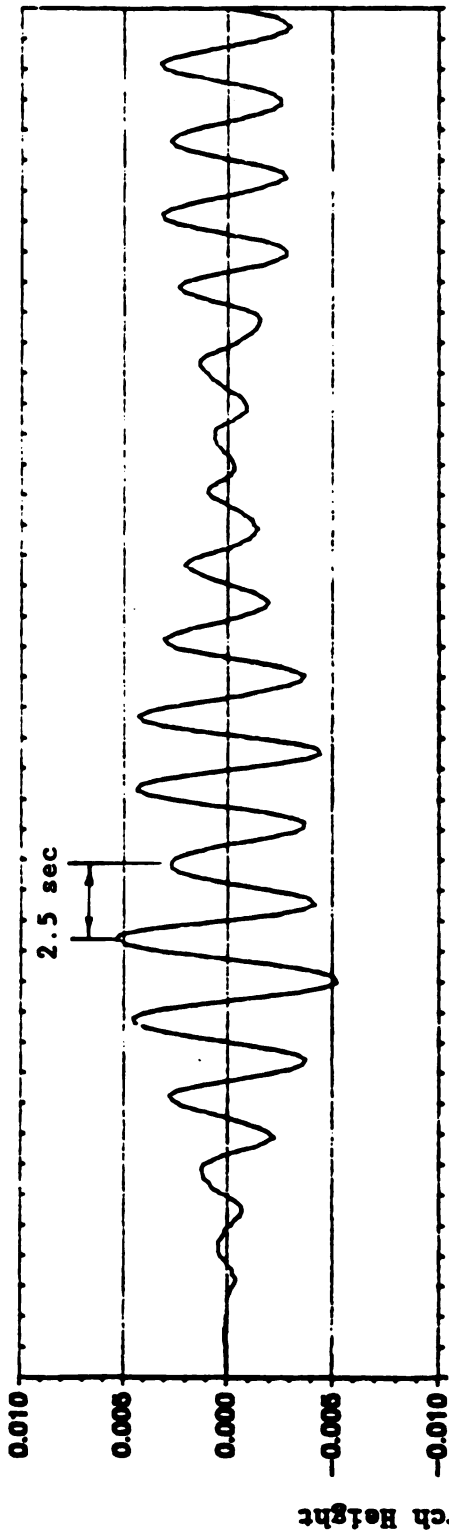


(a) Linear Elastic

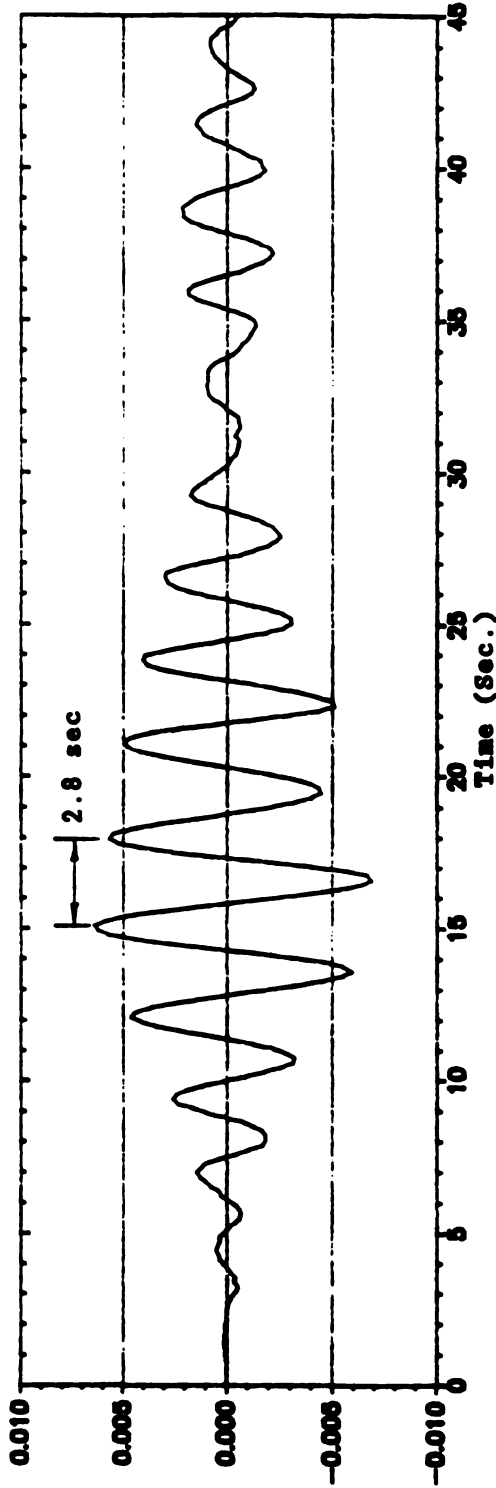


(b) Nonlinear Elastic

Figure 3-78. Node 3 Horizontal (X) Displacement Time History for MSB



(a) Linear Elastic



(b) Nonlinear Elastic

Figure 3-79. Node 5 Horizontal (X) Displacement Time History for MSB

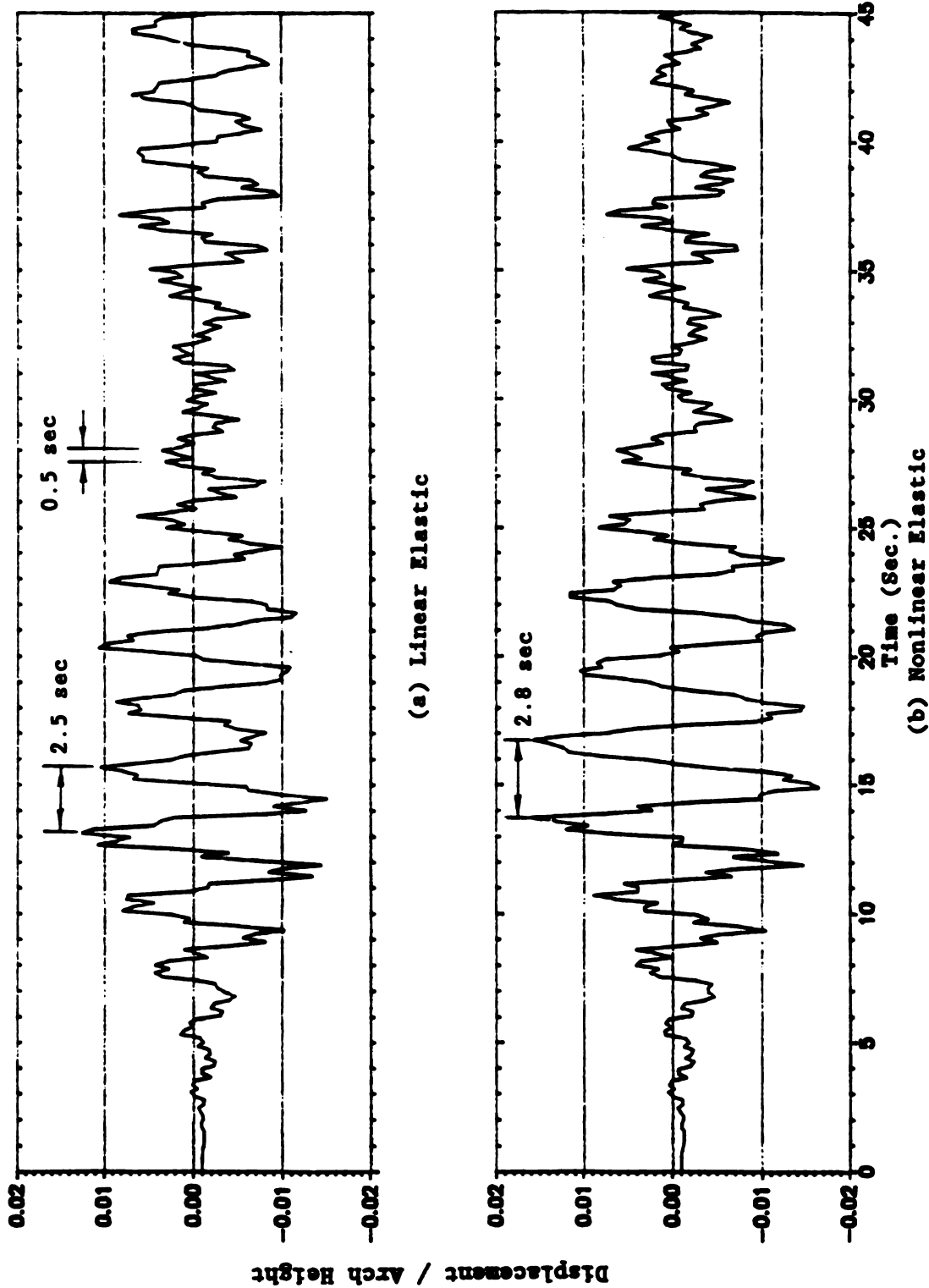


Figure 3-80. Node 3 Vertical (Y) Displacement Time History for MSB

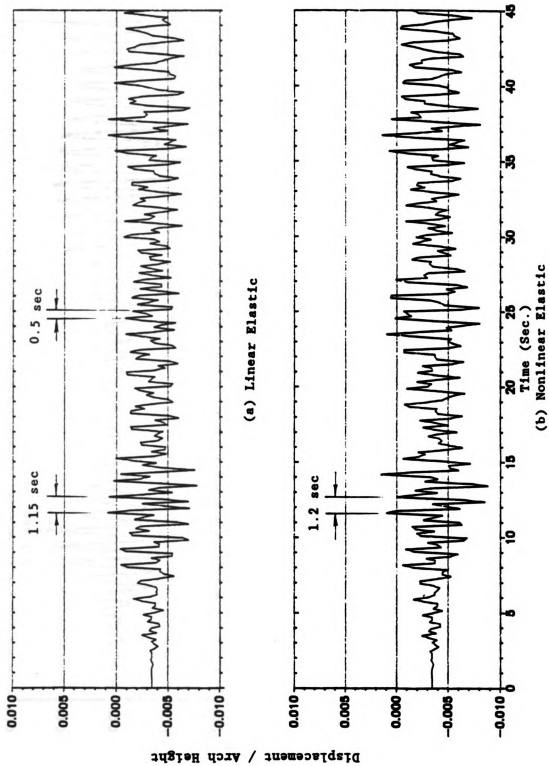
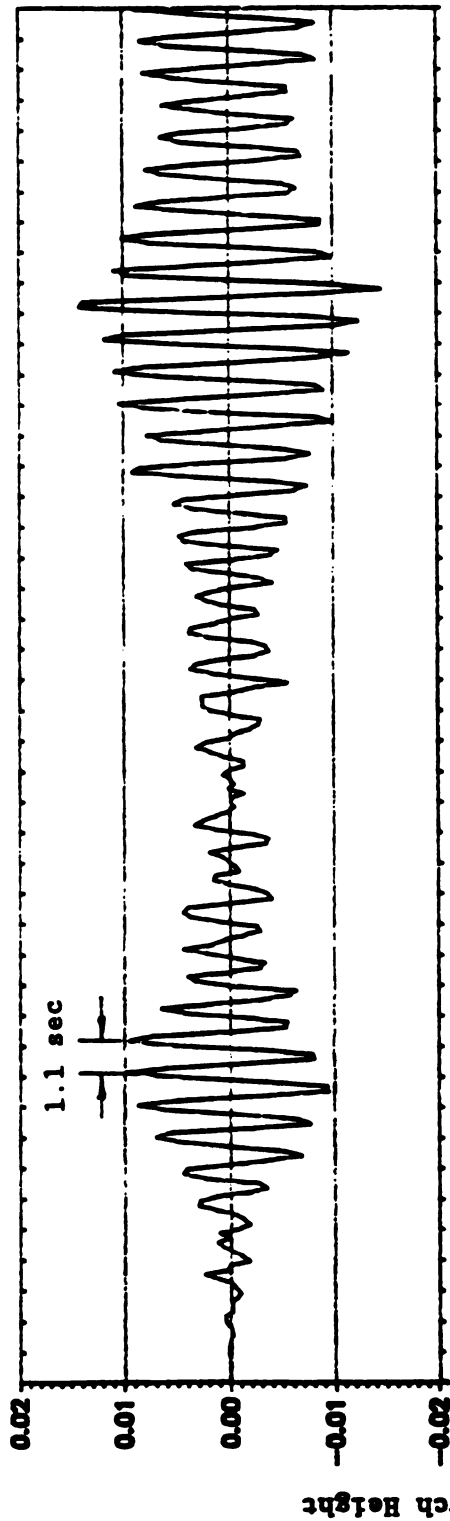
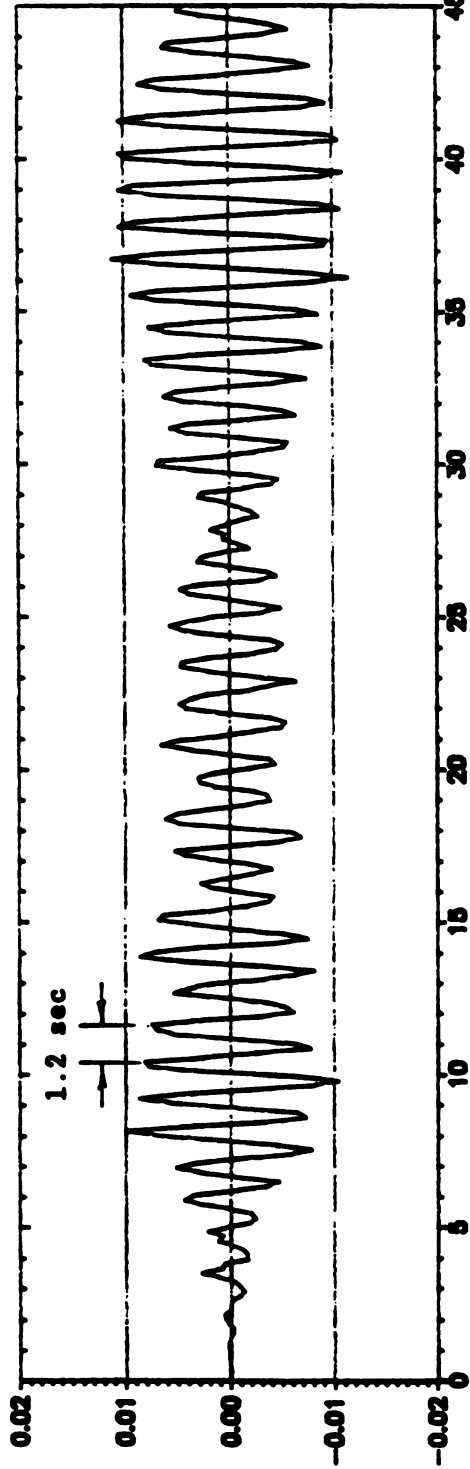


Figure 3-81. Mode 5 Vertical (Y) Displacement Time History for MSB



(a) Linear Elastic



(b) Nonlinear Elastic

Figure 3-82. Node 9 Horizontal (X) Displacement Time History for SSB

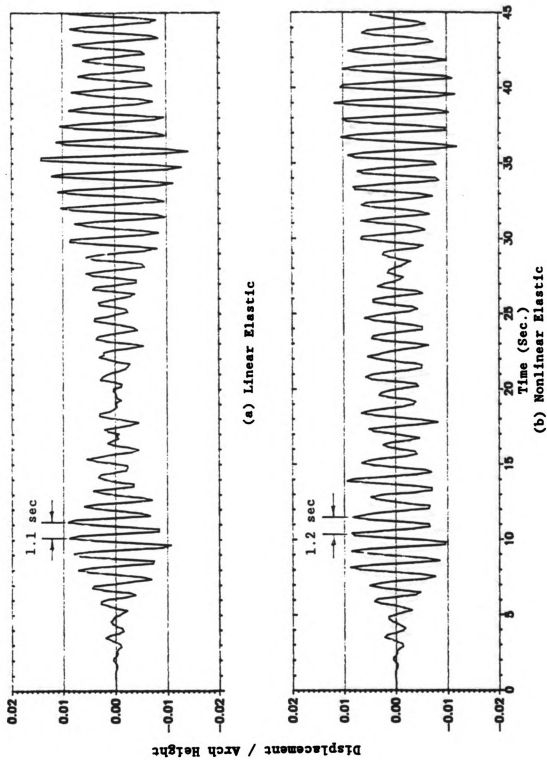


Figure 3-83. Node 21 Horizontal (X) Displacement Time History for SSB

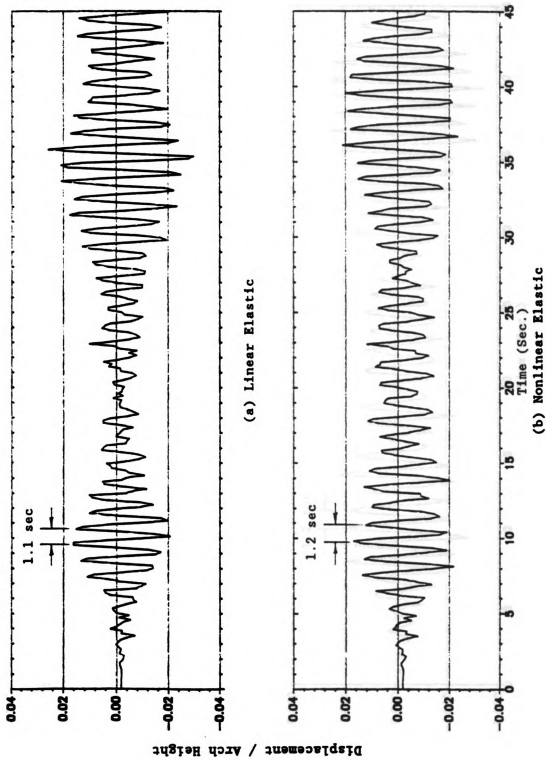


Figure 3-84. Node 9 Vertical (Y) Displacement Time History for SSB

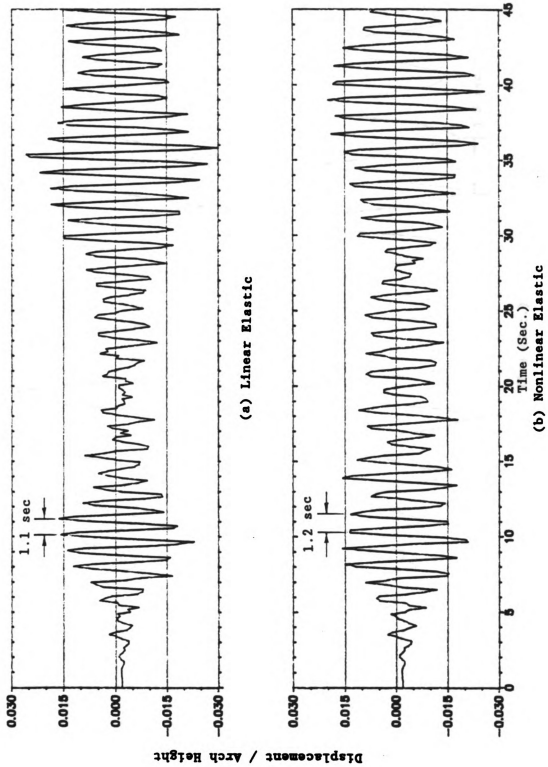
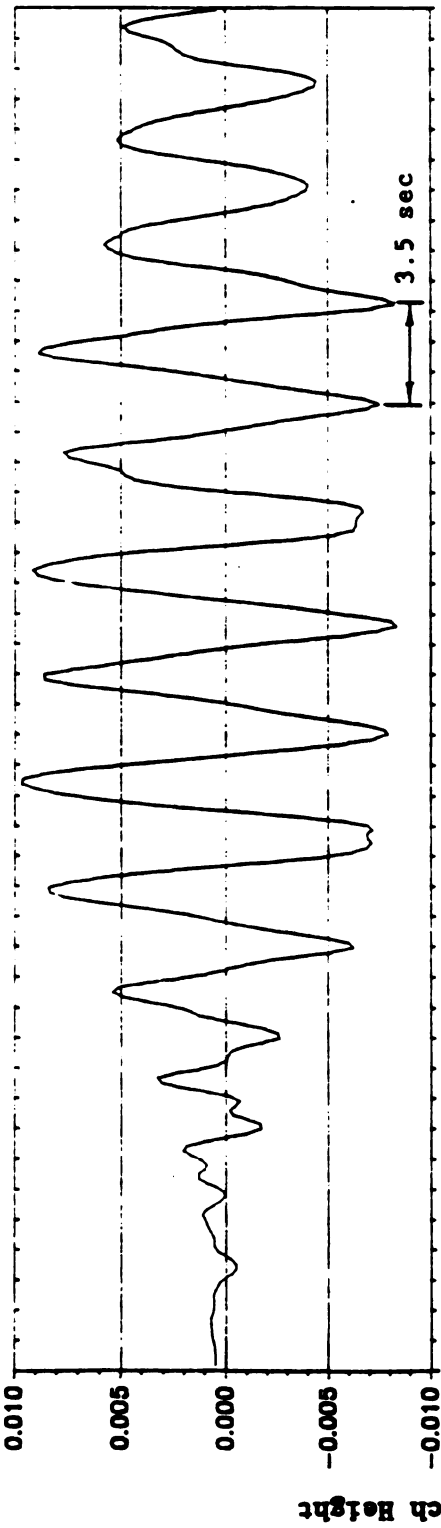
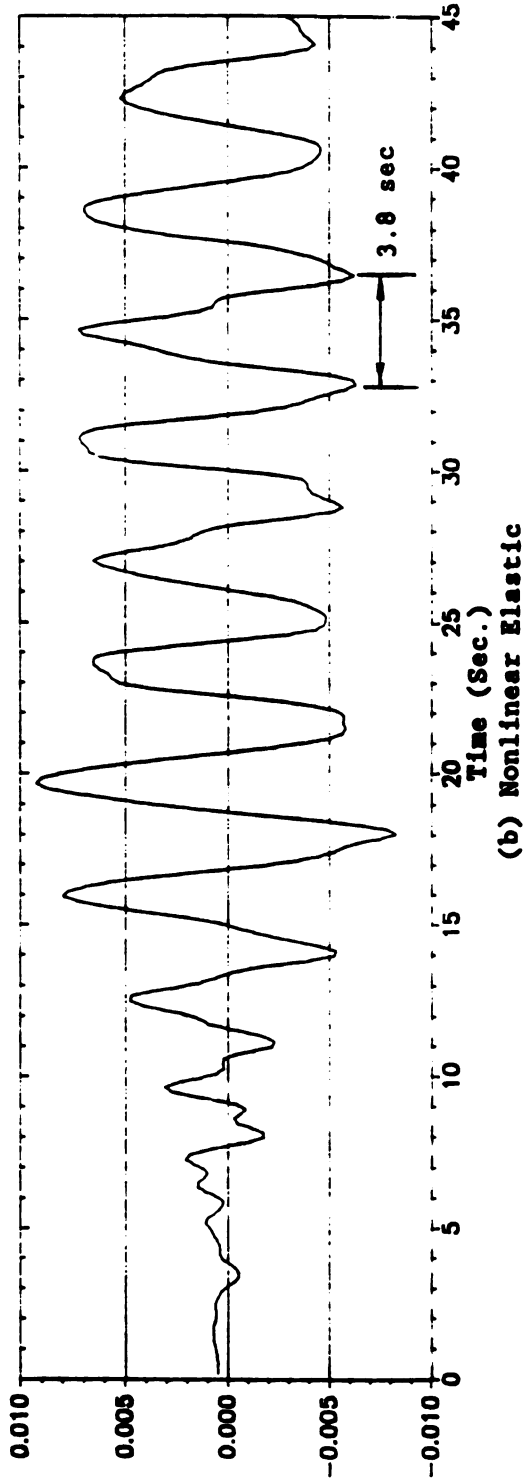


Figure 3-85. Node 21 Vertical (Y) Displacement Time History for SSB



(a) Linear Elastic



(b) Nonlinear Elastic

Figure 3-86. Node 12 Horizontal (X) Displacement Time History for LSB

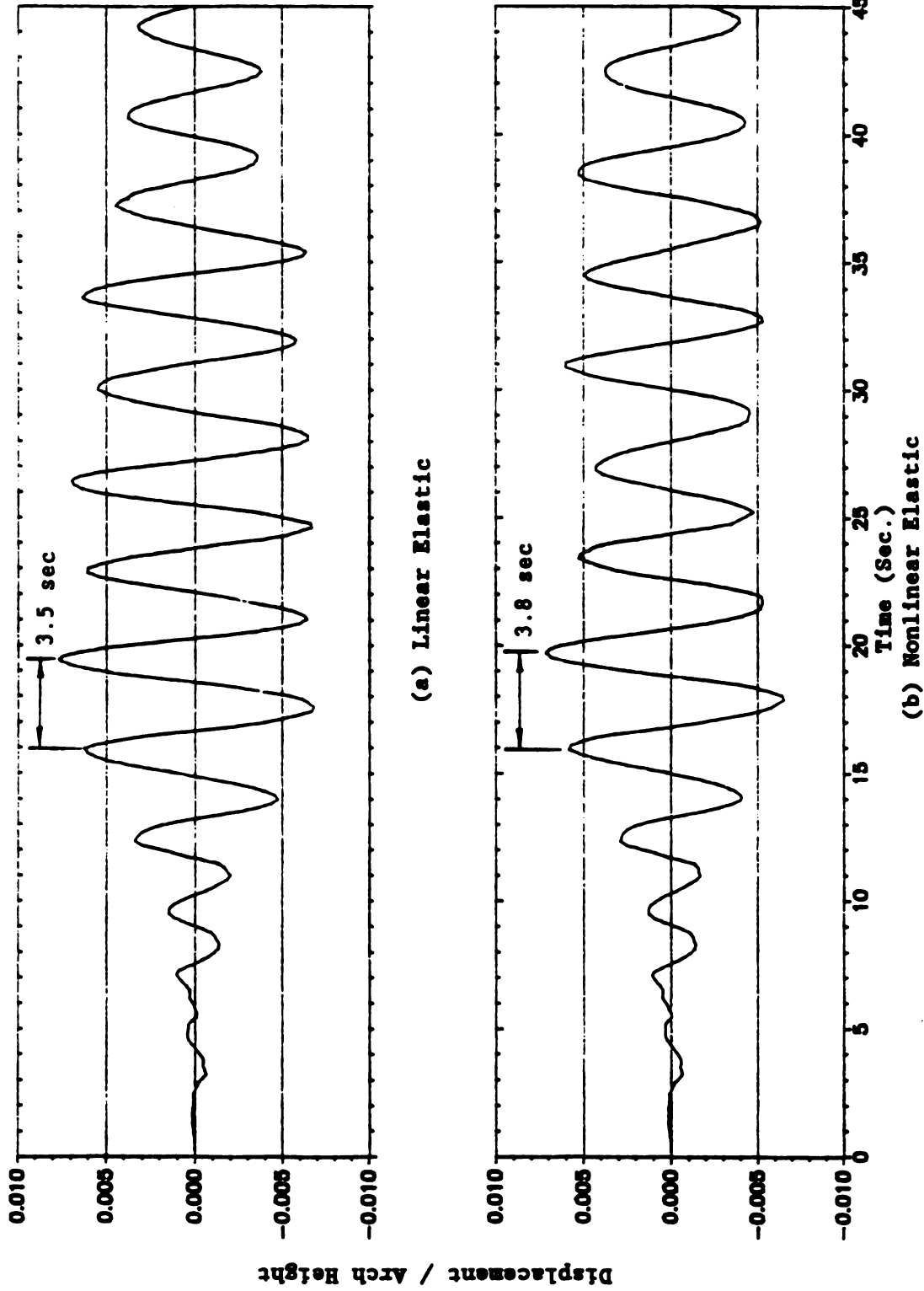


Figure 3-87. Node 18 Horizontal (X) Displacement Time History for LSB

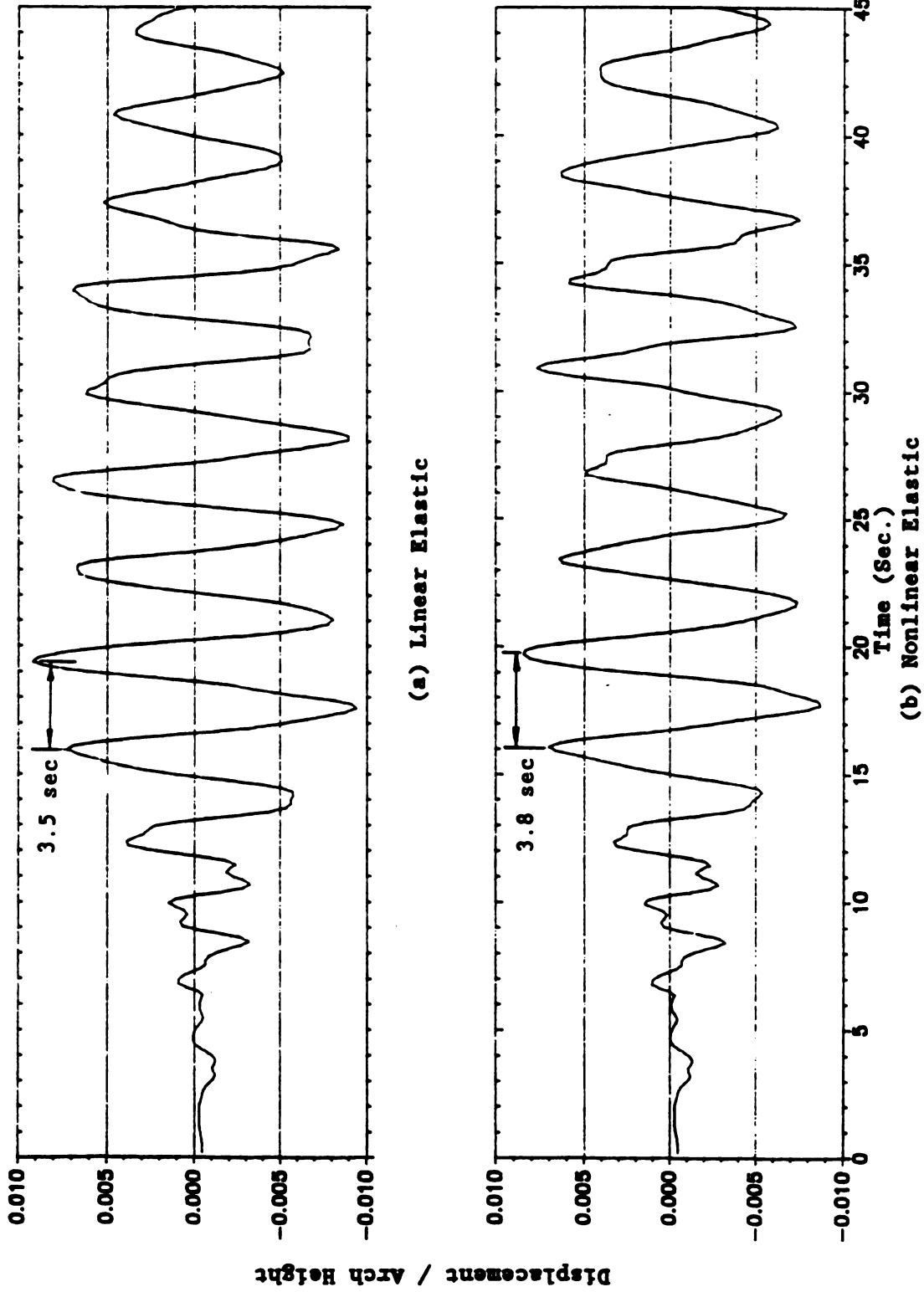
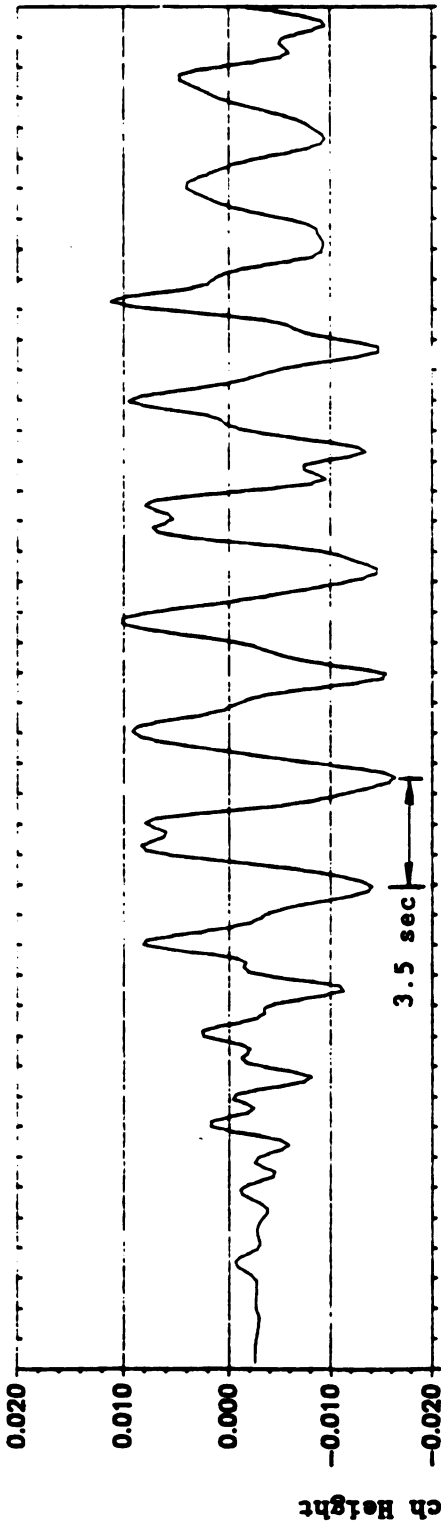
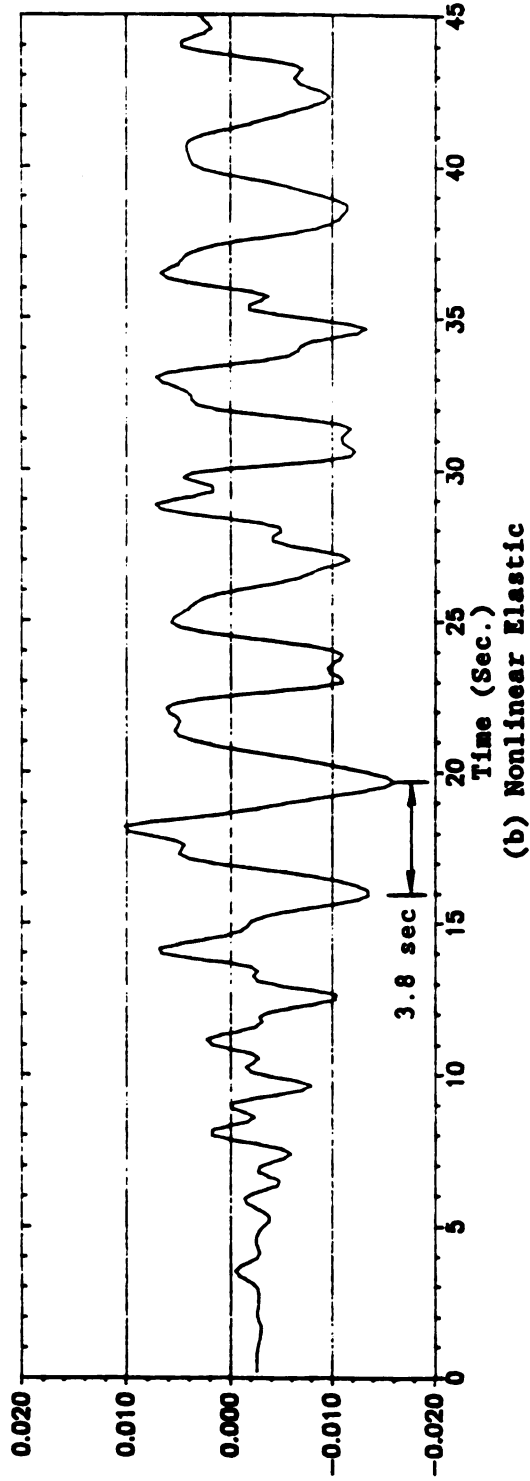


Figure 3-88. Node 24 Horizontal (X) Displacement Time History for LSB



(a) Linear Elastic



(b) Nonlinear Elastic

Figure 3-89. Node 12 Vertical (Y) Displacement Time History for LSB

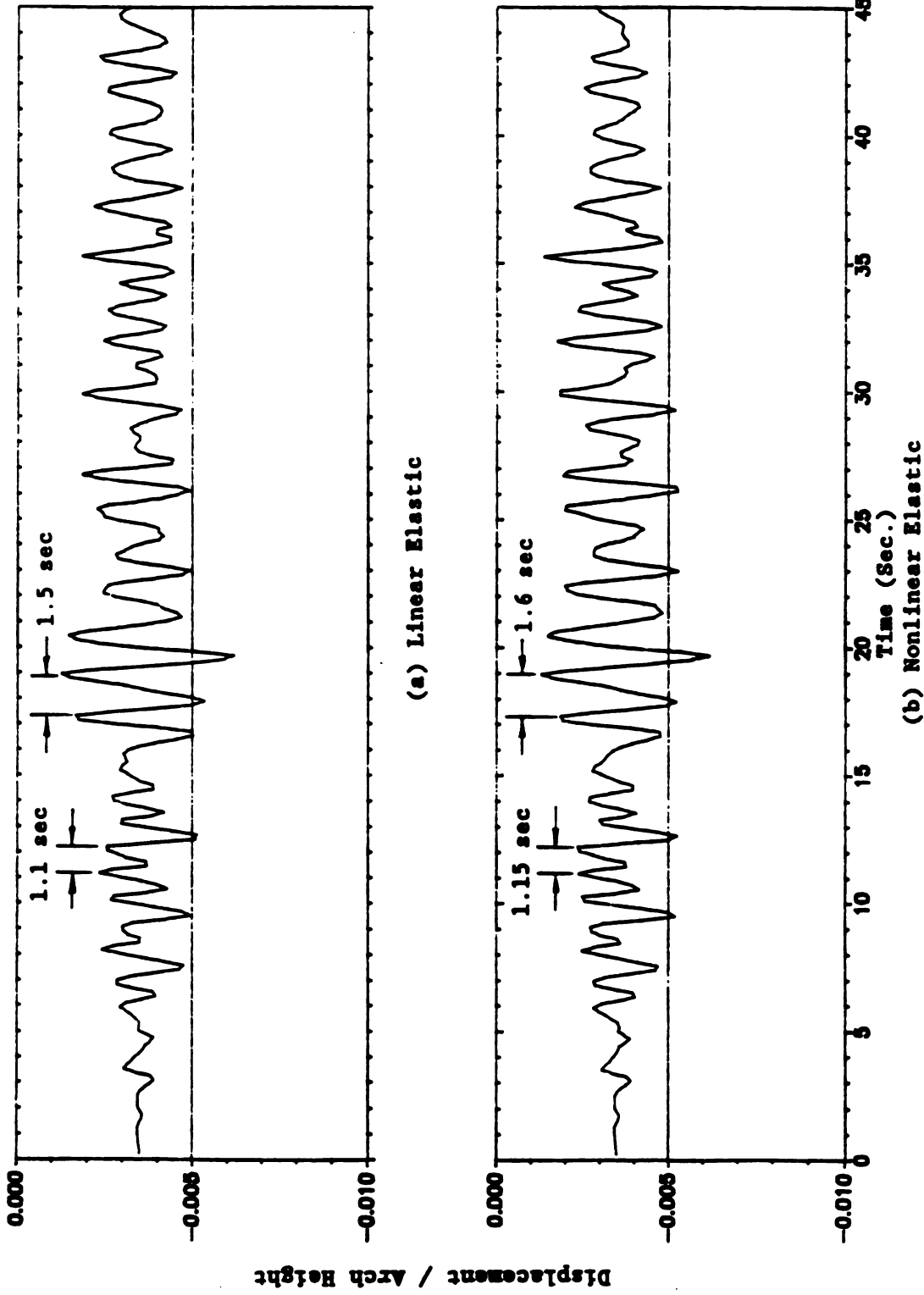


Figure 3-90. Node 18 Vertical (Y) Displacement Time History for LSB

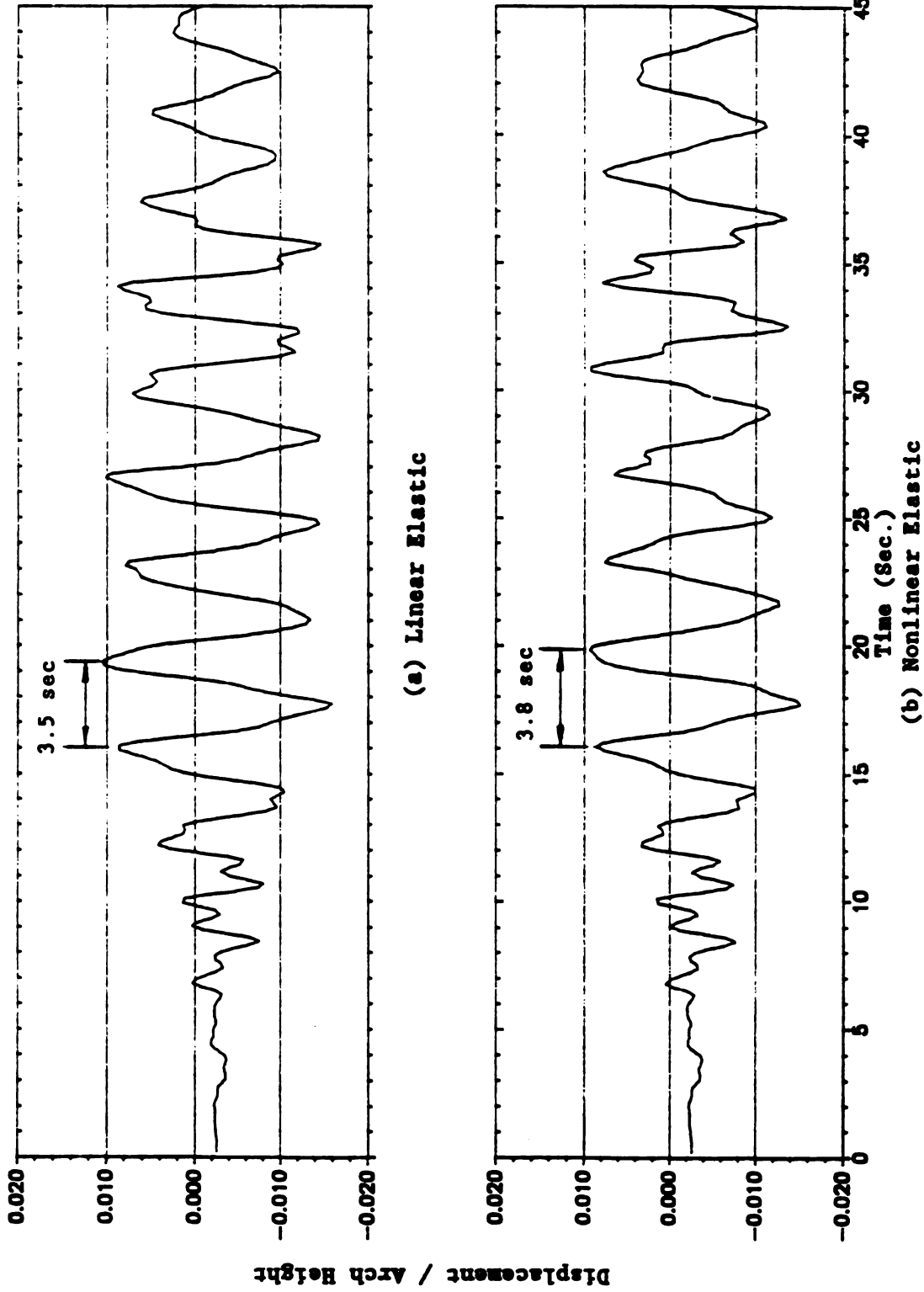


Figure 3-91. Node 24 Vertical (Y) Displacement Time History for LSB

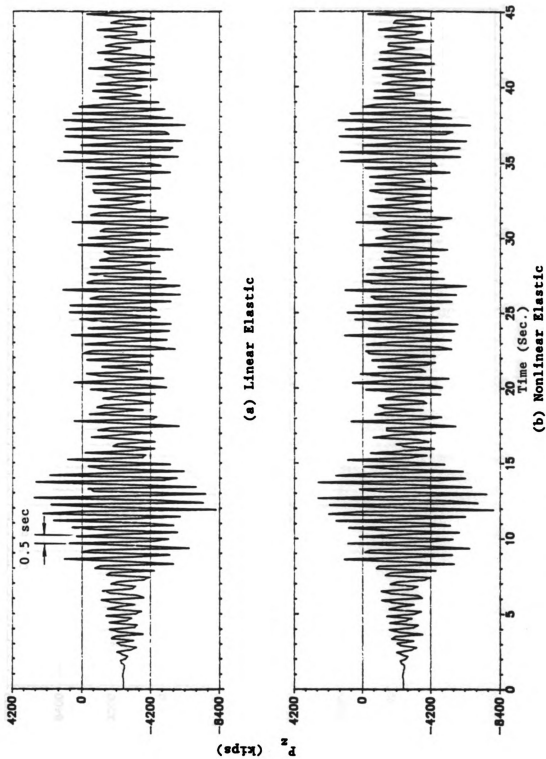


Figure 3-92. Member 1 End J (Node 3) Axial Force Time History for MSB

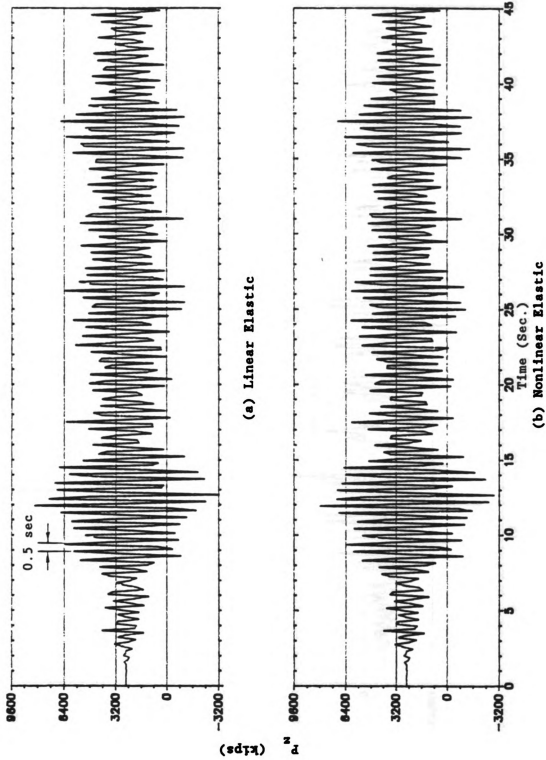
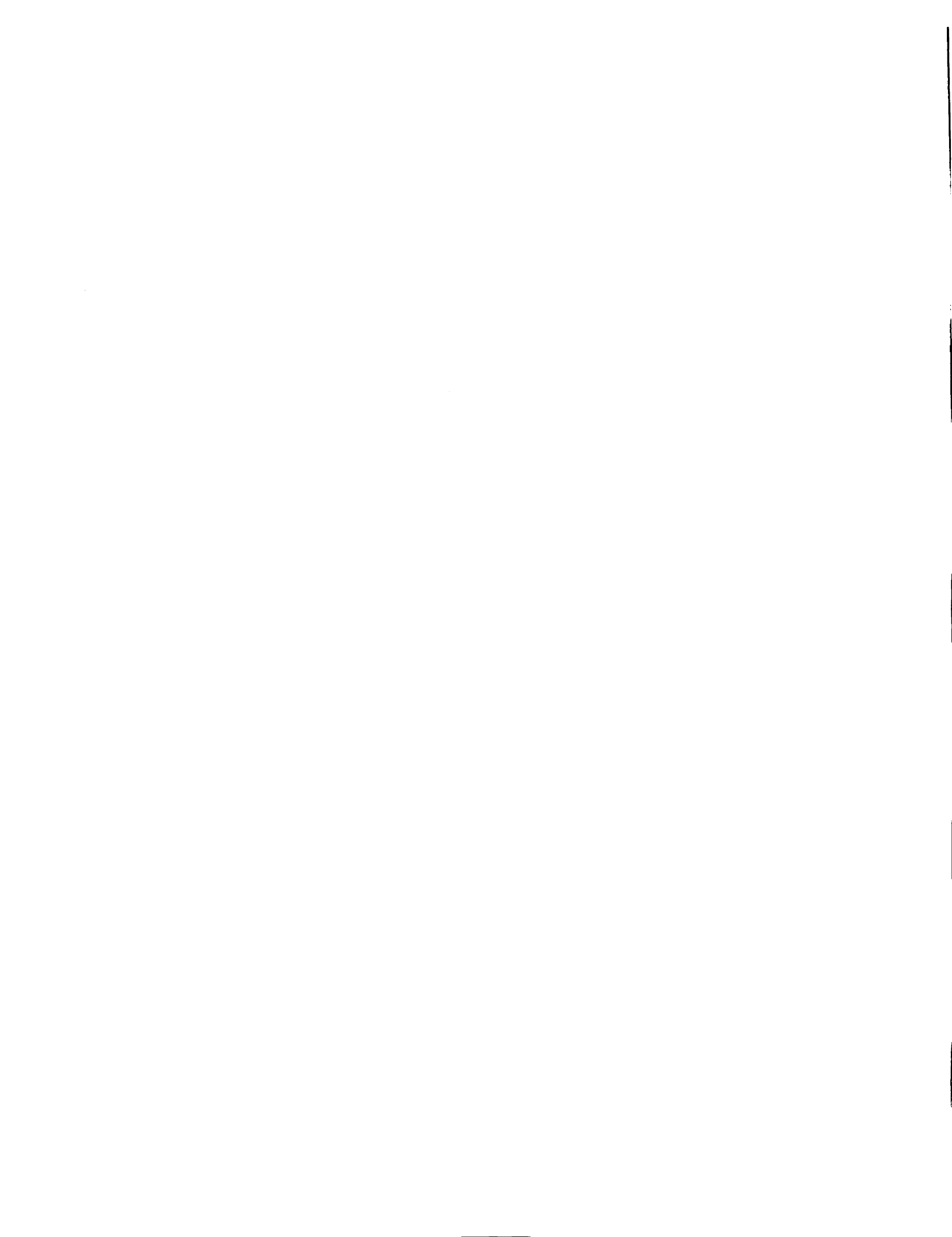


Figure 3-93. Member 4 End I (Node 7) Axial Force Time History for MSB



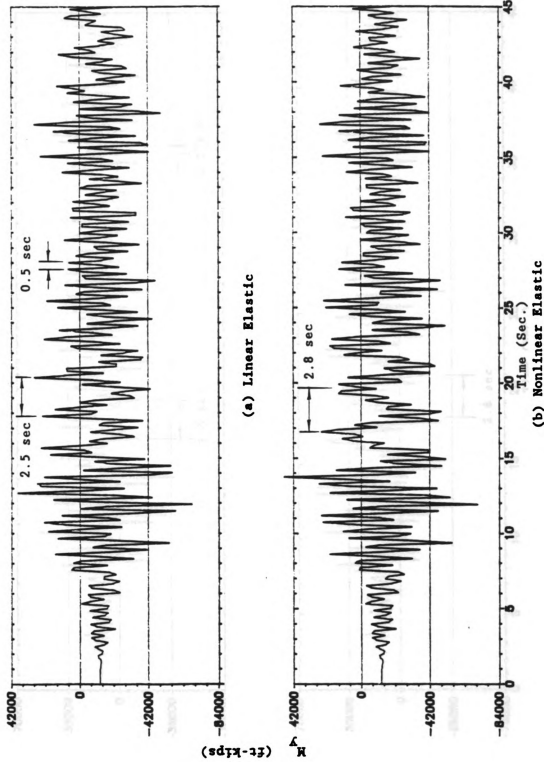
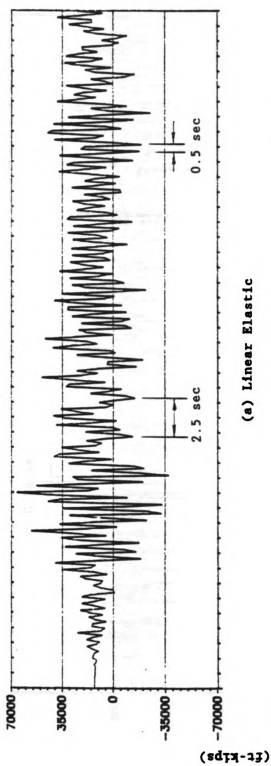
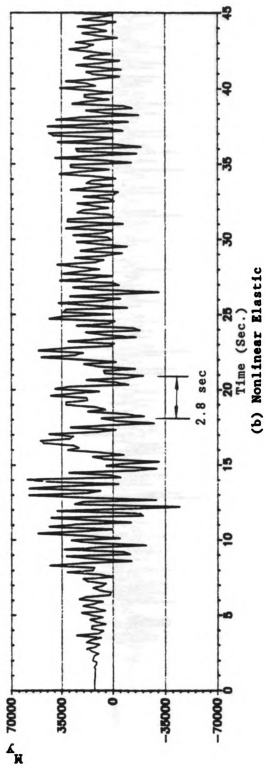


Figure 3-94. Member 1 End J (Node 3) In-Plane Bending Time History for MSB



(a) Linear Elastic



(b) Nonlinear Elastic

Figure 3-95. Member 4 End I (Node 7) In-Plane Bending Time History for MSB

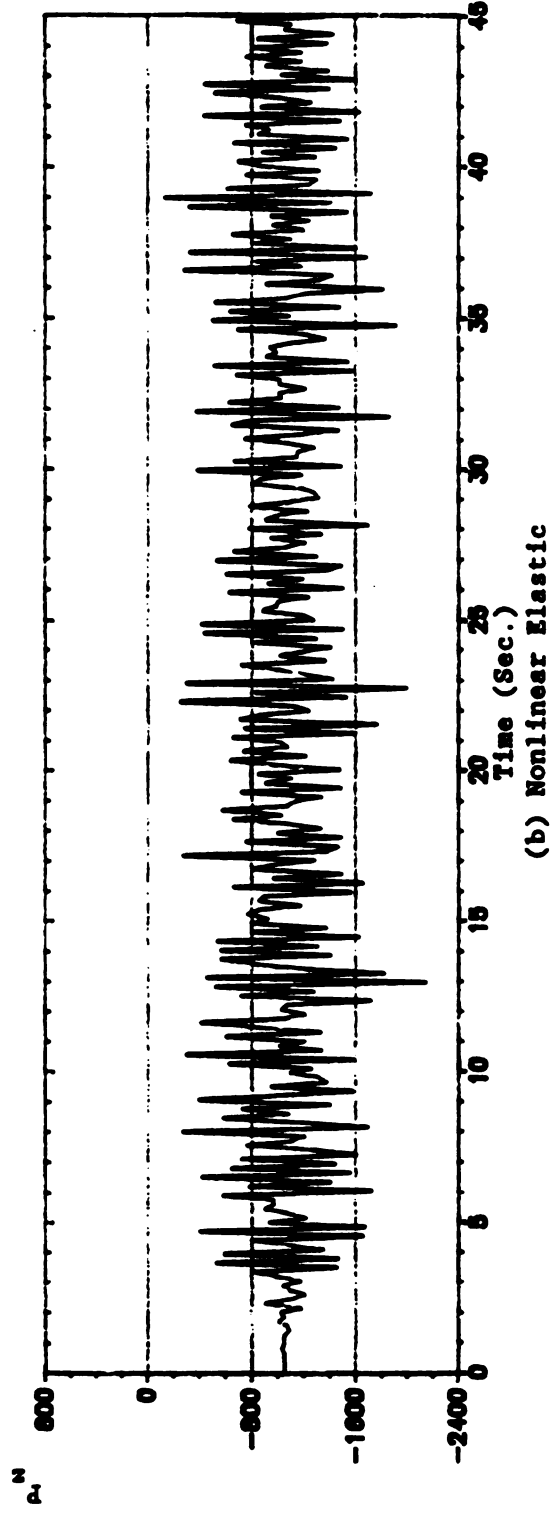
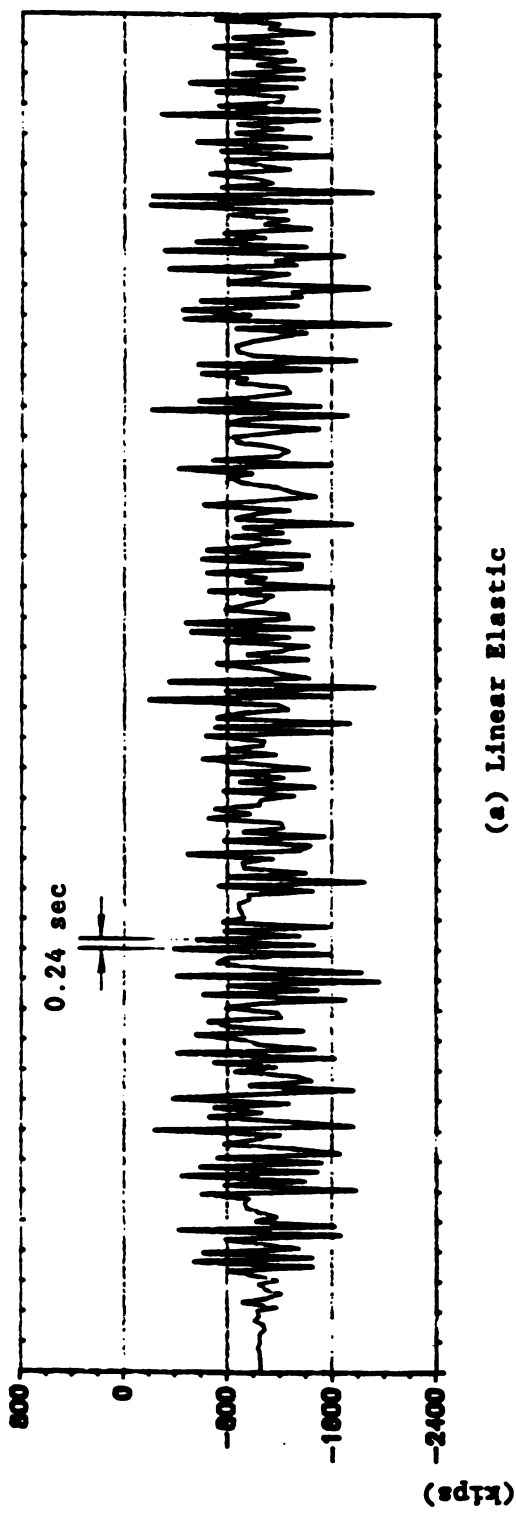


Figure 3-96. Member 2 End J (Node 9) Axial Force Time History for SSB

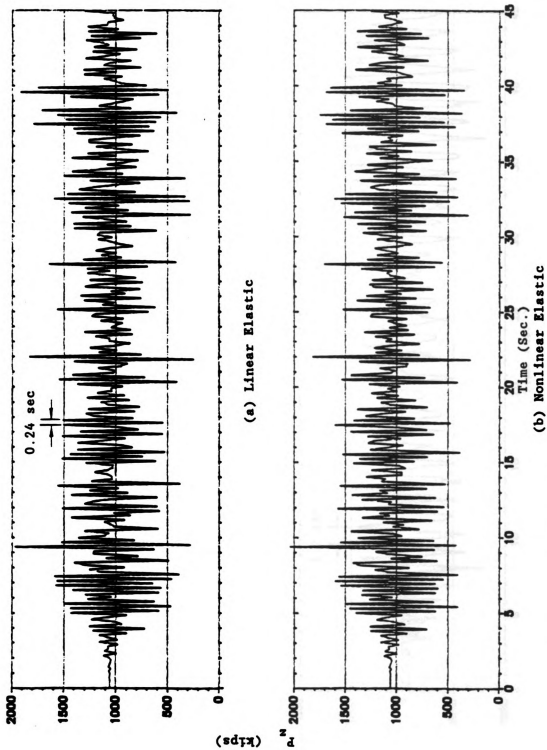


Figure 3-97. Member 6 End I (Node 21) Axial Force Time History for SSB

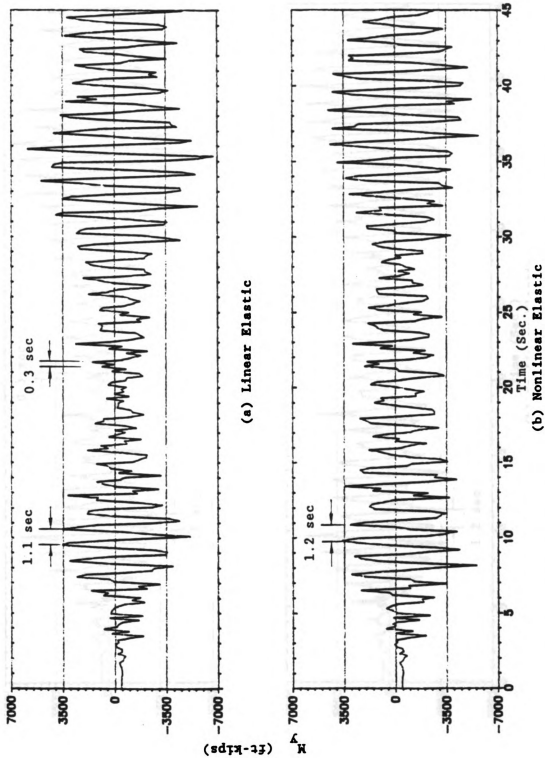


Figure 3-98. Member 2 End J (Node 9) In-Plane Bending Time History for SSB

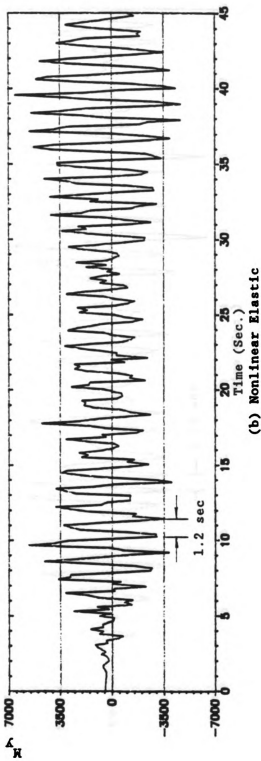
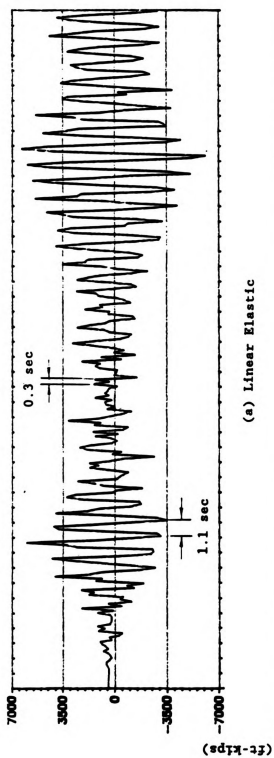


Figure 3-99. Member 6 End I (Node 21) In-Plane Bending Time History for SSB

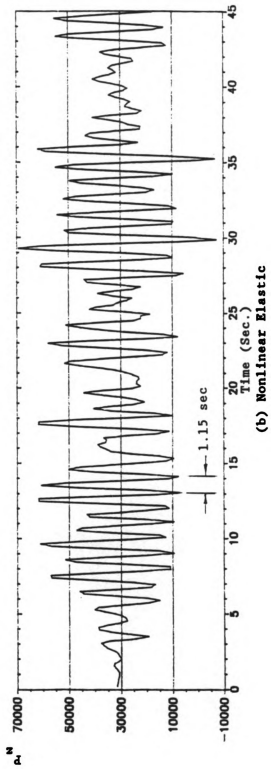
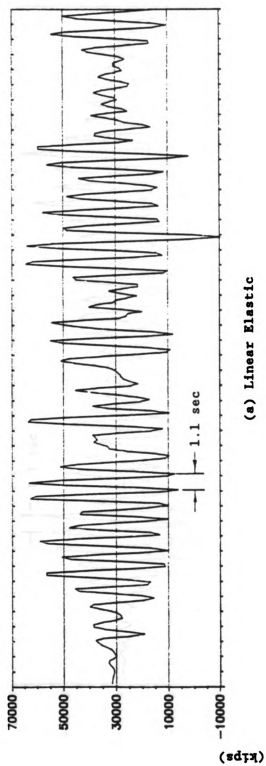


Figure 3-100. Member 5 End I (Node 12) Axial Force Time History for LSB

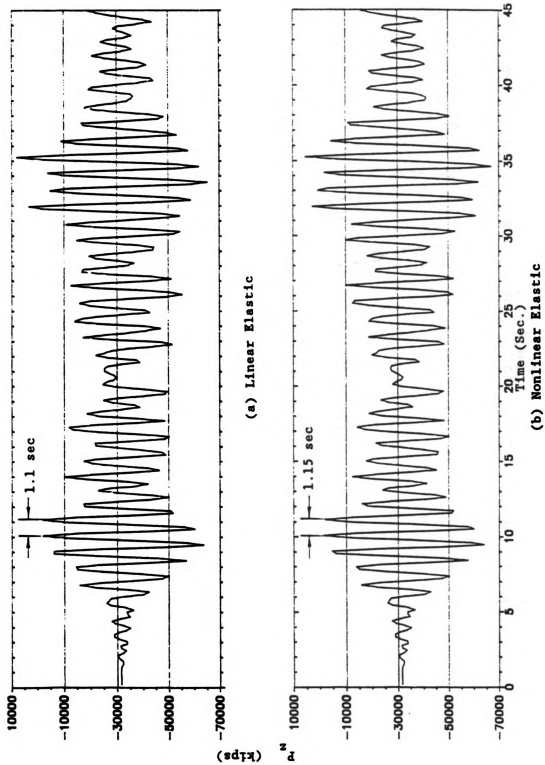
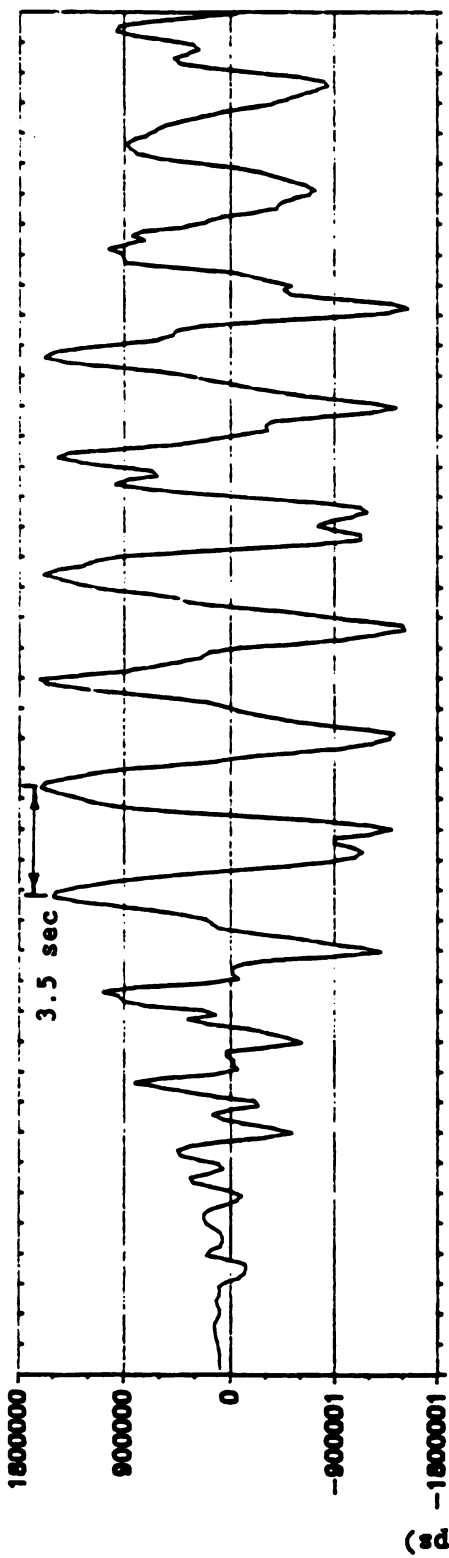
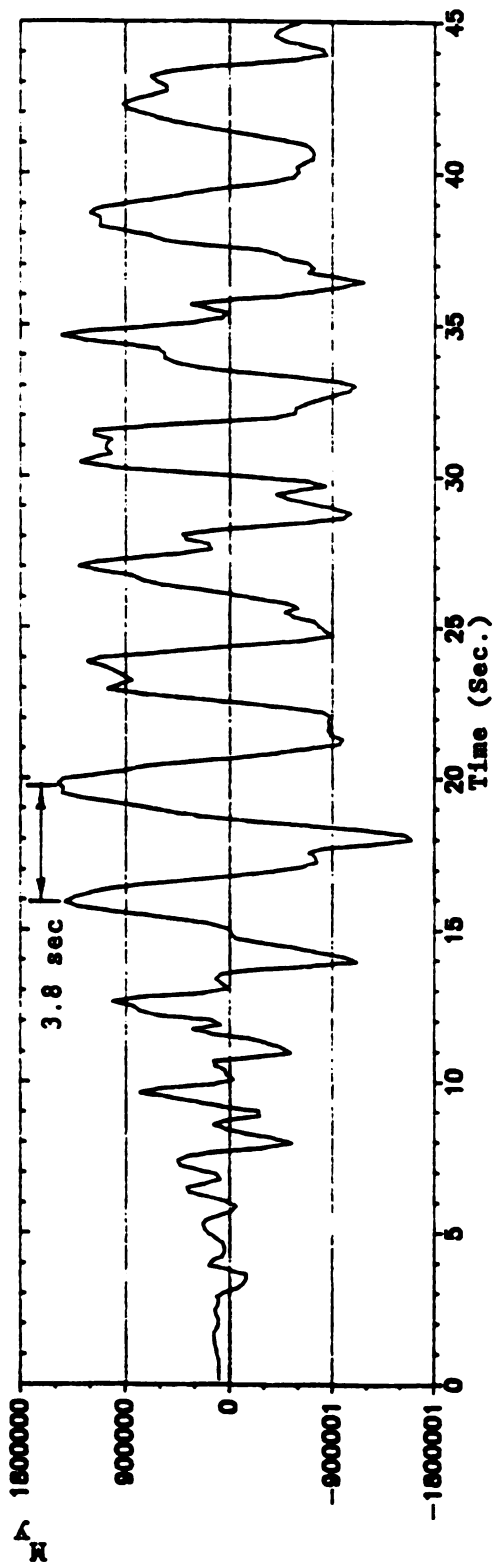


Figure 3-101. Member 10 End J (Node 24) Axial Force Time History for LSB

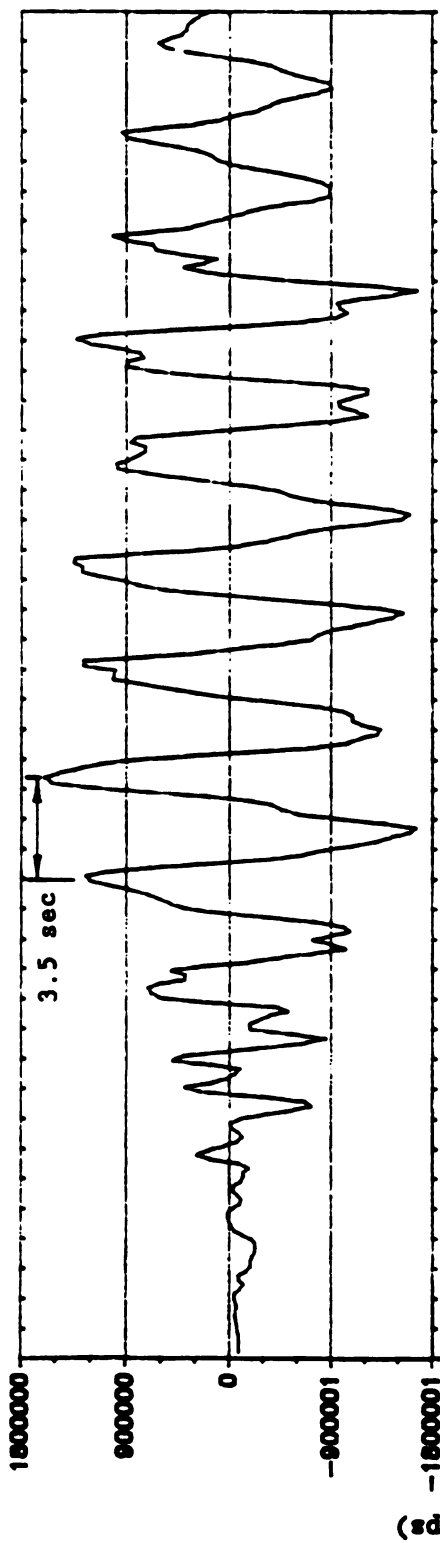


(a) Linear Elastic

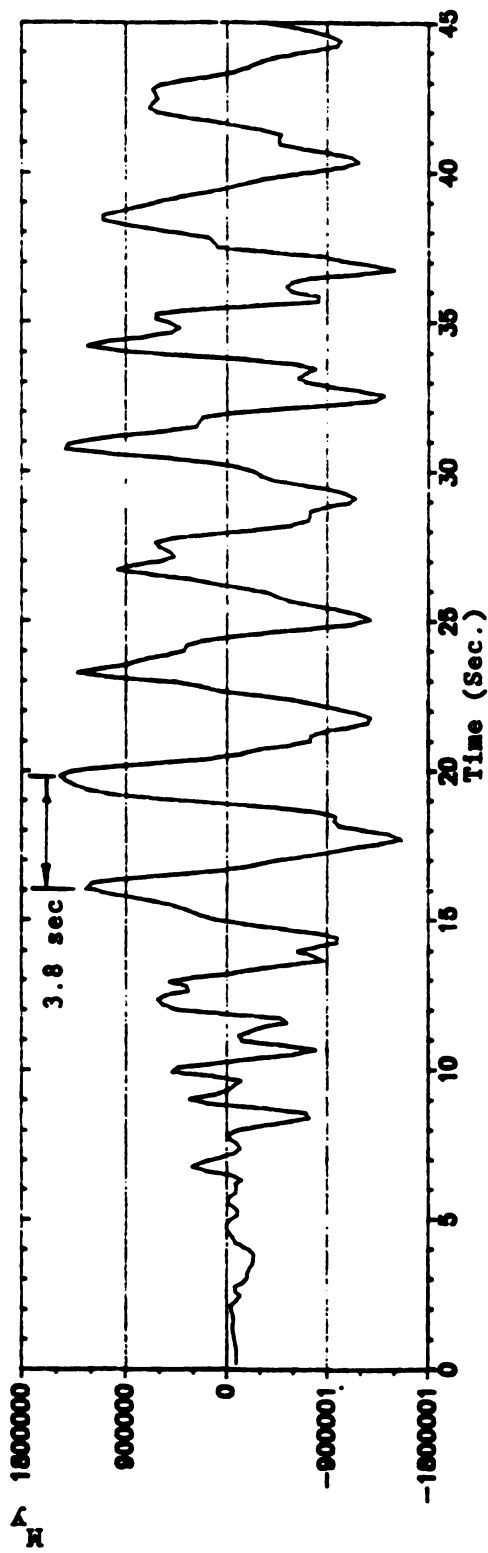


(b) Nonlinear Elastic

Figure 3-102. Member 5 End I (Node 12) In-Plane Bending Time History for LSB



(a) Linear Elastic



(b) Nonlinear Elastic

Figure 3-103. Member 10 End J (Node 24) In-Plane Bending Time History for LSB

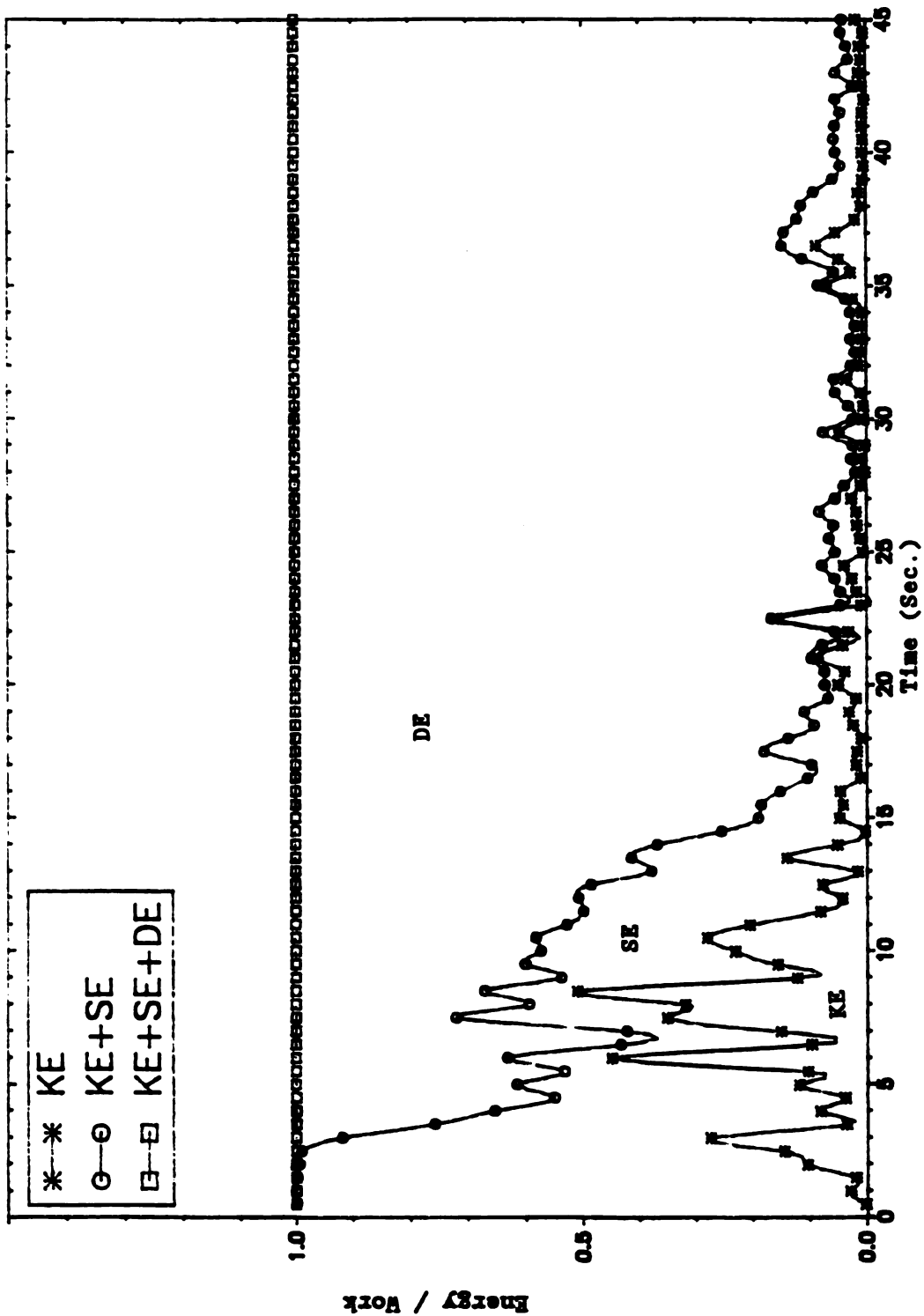


Figure 3-104. Work and Energy Distribution Time History for MSB (Linear Elastic)

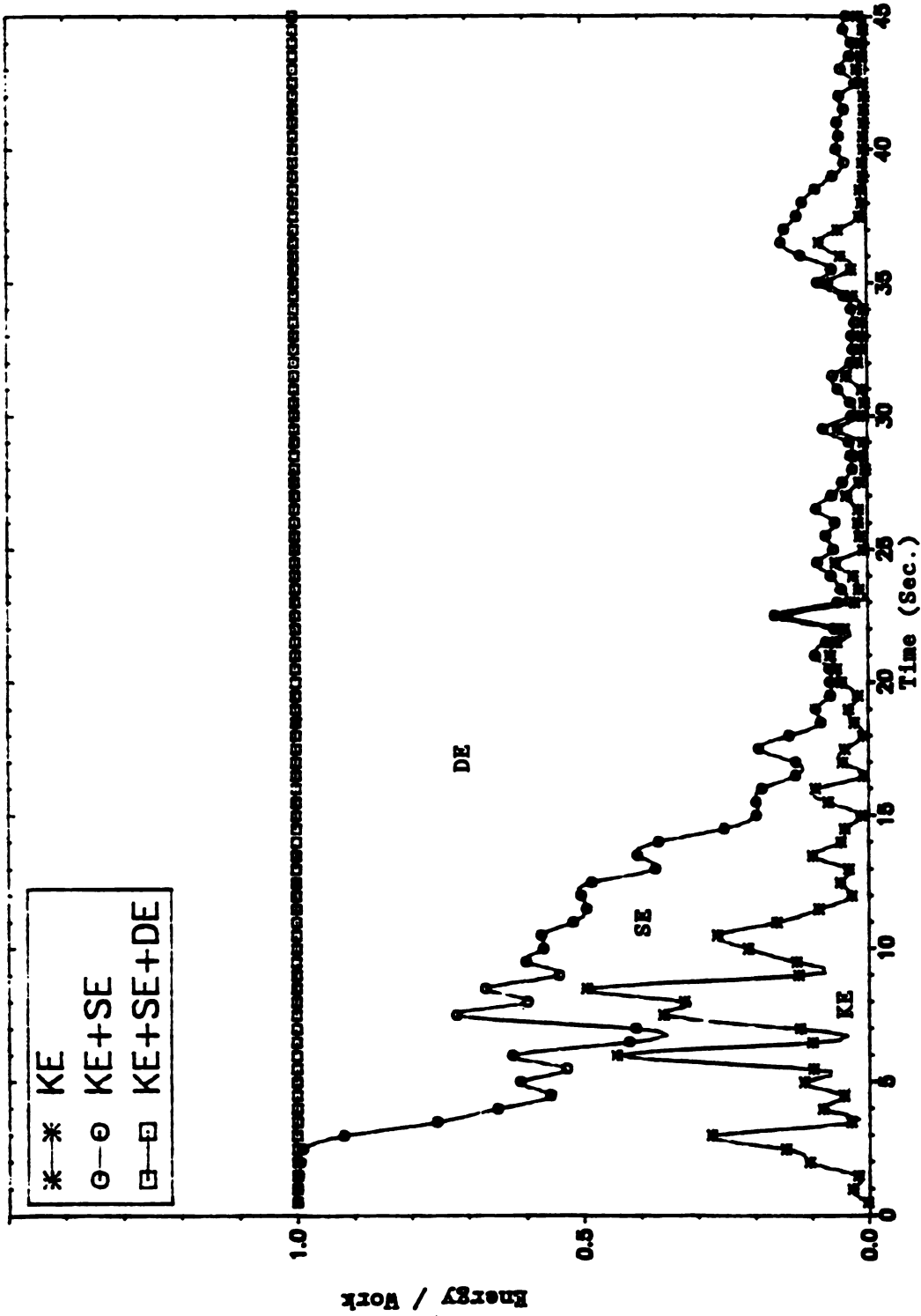


Figure 3-105. Work and Energy Distribution Time History for MSB (Nonlinear Elastic)

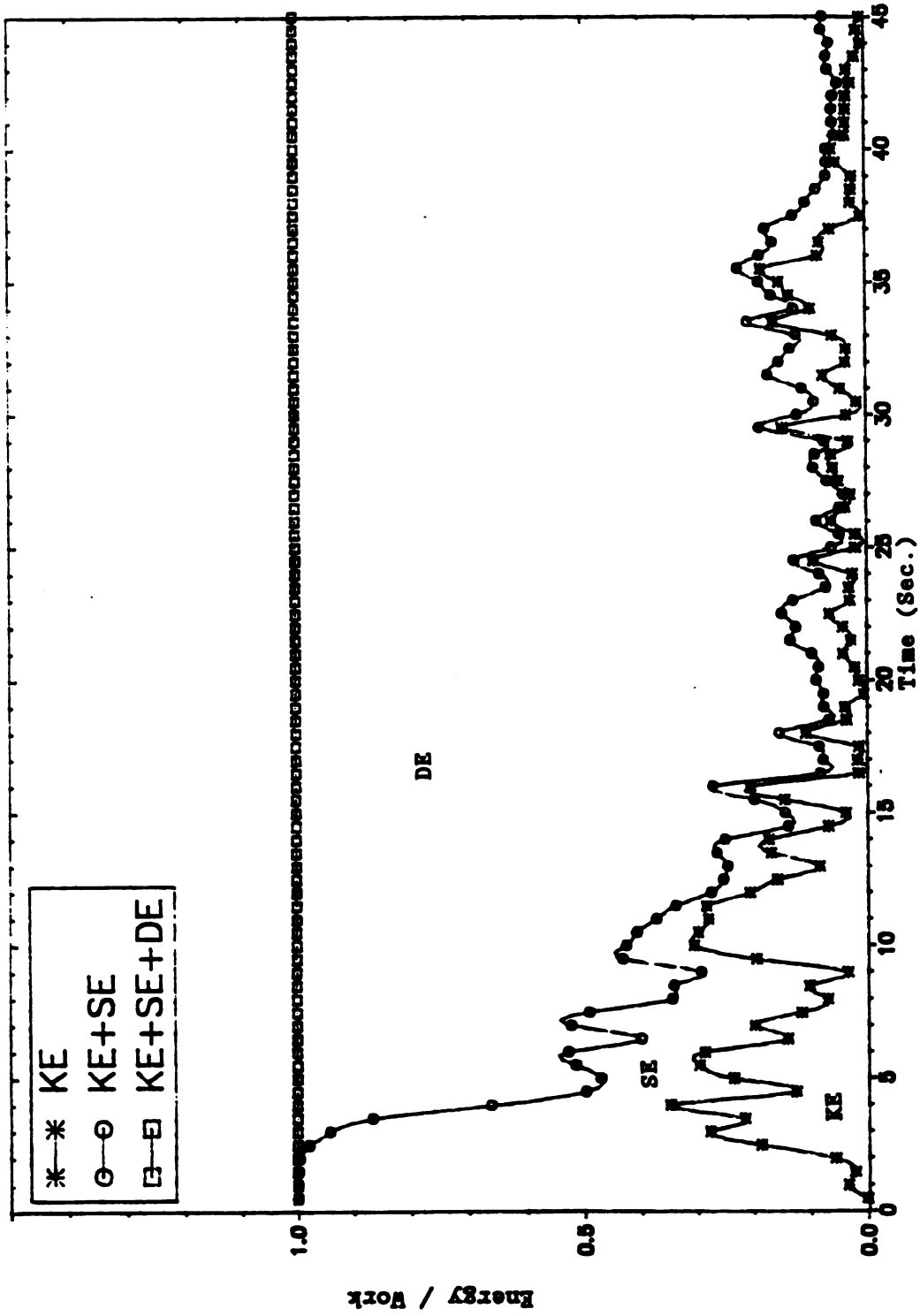


Figure 3-106. Work and Energy Distribution Time History for SSB (Linear Elastic)

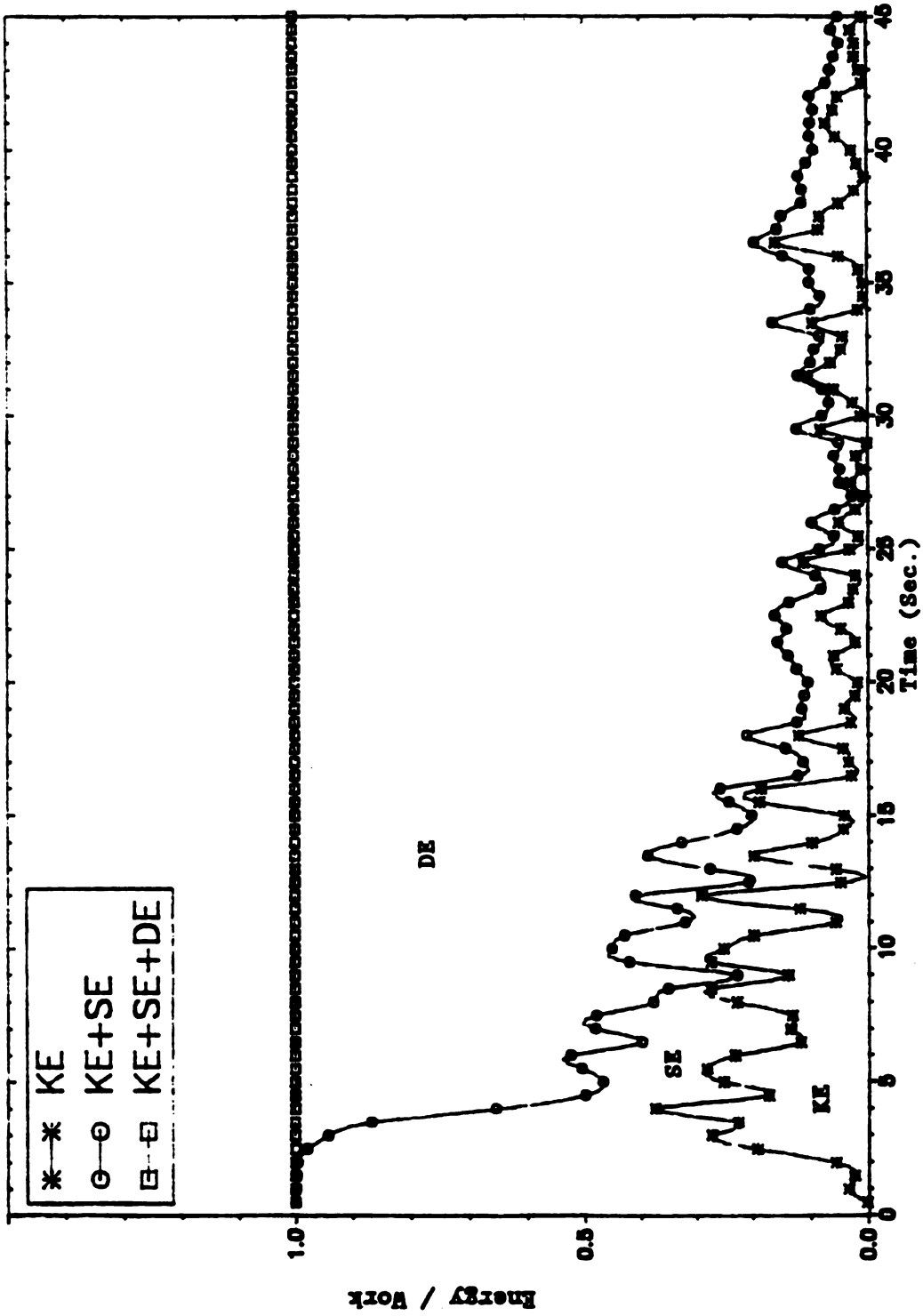


Figure 3-107. Work and Energy Distribution Time History for SSB (Nonlinear Elastic)

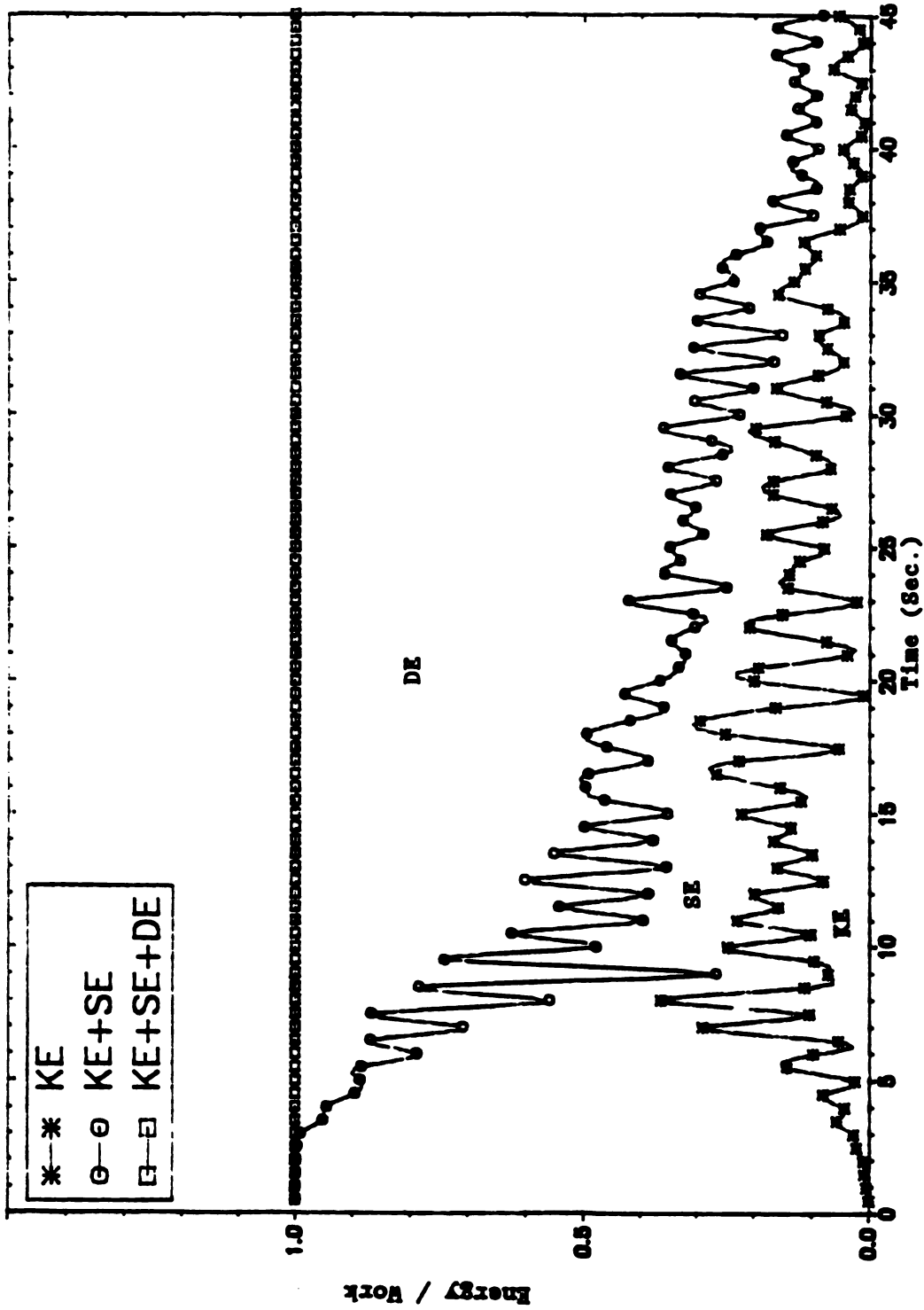


Figure 3-108. Work and Energy Distribution Time History for LSB (Linear Elastic)

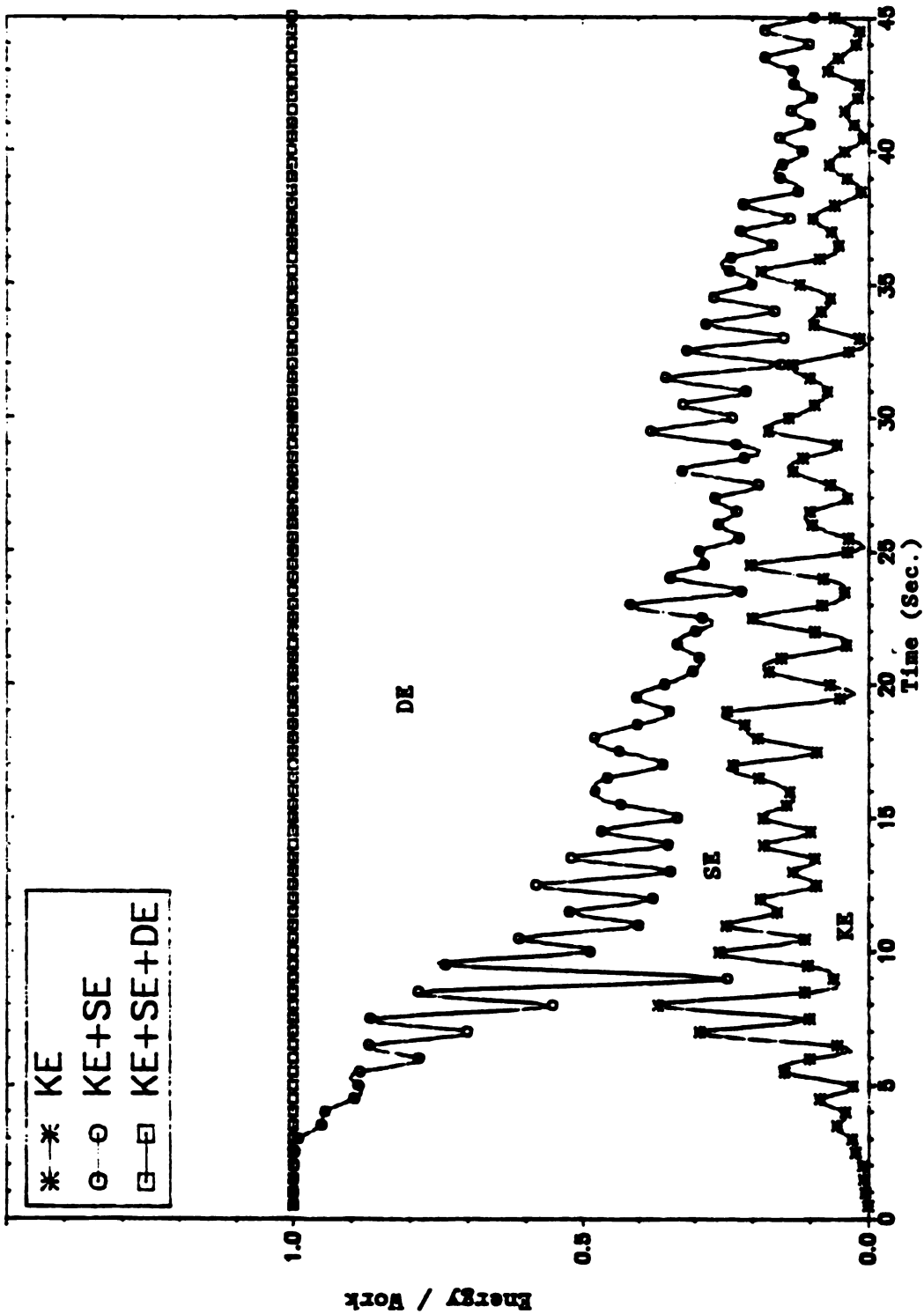


Figure 3-109. Work and Energy Distribution Time History for LSB (Nonlinear Elastic)

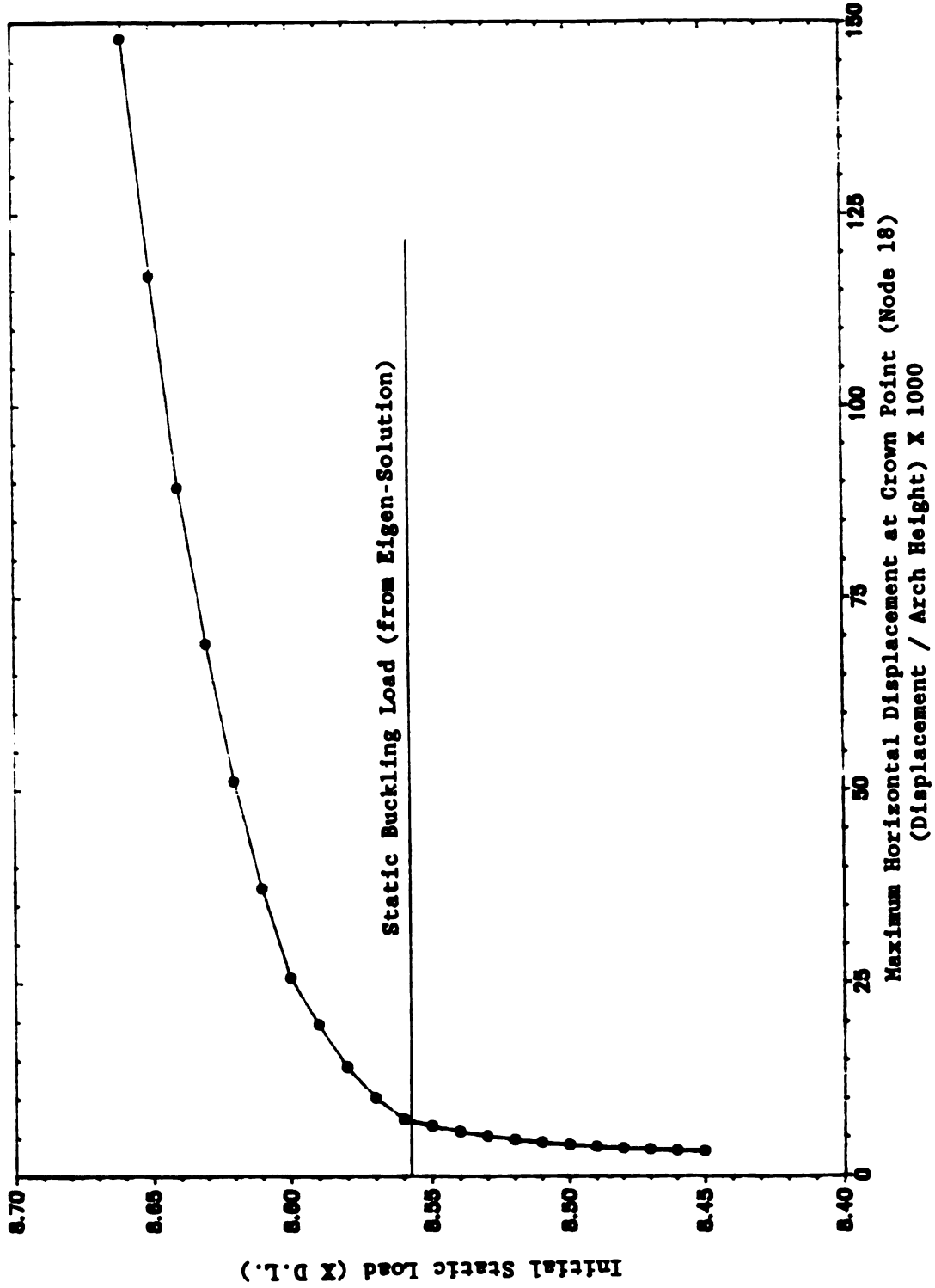


Figure 3-110. "Instability" Effects for LSB

CHAPTER IV

SUMMARY AND CONCLUSION

4.1 SUMMARY

This study has presented a method for the nonlinear dynamic analysis of arch bridges. For the analysis, mass is lumped at the nodes. The effects of either geometric or material nonlinearity have been taken into account. The effects of such nonlinearities enter in the analysis through the computation of the "resistance" of the arch ribs.

For the inelastic effects, a method of analysis based on the "plastic hinge" concept has been developed for the elasto-plastic resistance of a curved beam element in the three-dimensional space. The yield function is based on the three stress resultants (axial force P , in-plane bending moment M_y , and out-of-plane bending moment M_x). For the analysis of nonlinear elastic effects, a twelve degrees of freedom incremental stiffness matrix $[n_1]$ was also derived.

Other features of the analysis included the use of "mixed nodal coordinate systems": cartesian coordinates for the nodes on the deck, and curvilinear coordinates for the nodes on the arch ribs, and the use of various constraints such as those that would result in infinitely large axial stiffness for the cross-beams and/or columns. All these features were motivated by a desire to make the model more computationally effective by reducing the number of degrees of freedom. For seismic analysis, the load input is a uniform ground acceleration in

all three directions in space. The system equation consists of the equations of motion for the unconstrained degrees of freedom of the nodes.

The method of analysis is one of a step-by-step numerical integration in the time domain. Within a time increment, the solution is essentially of the Newton-Raphson type implying an outer loop of iteration for the equilibrium of the system equation. For each elastoplastic element (curved beam element), an inner loop of iteration is needed because of the material nonlinearity. The validity of the analysis was corroborated by checking the balance of the various energies in the system and the work done on the system in each time increment.

For interpretation of the results on inelastic behavior, the quantities "ductility factors" and "plastic work densities" are defined. A computer program has been developed for the implementation of the three-dimensional nonlinear seismic analyses described above.

Three bridge models, MSB, SSB and LSB, based on three prototype bridges: CSCB (700 ft), SSB (193 ft) and NRCB (1700 ft), respectively, were used to obtain the numerical results. Three-dimensional models were employed to consider the nonlinear inelastic effects. Results for nonlinear elastic solution were based on two-dimensional models. The ground motion used were the artificially generated motion CIT-A2 with different amplification factors applied to the amplitude of the ground acceleration.

For the maximum displacement responses involving material nonlinearity, there is no appreciable difference between the linear and nonlinear analysis. But plasticity limited the magnitude of the internal

force response to that as defined by the yield function. It follows that if plastic deformations are allowed, the design forces may be reduced from that which would be required if the design is to be done on a linearly elastic basis. For example, this reduction factor, as discussed in Section 3.4.8 and illustrated in Figures 3-75 through 3-77 and applied to the linear response factor, would be 1.0/1.88 if the "damage" represented by a curvature ductility factor of 3.5 was accepted.

Both the maximum displacements and internal forces of nonlinear elastic responses did not vary a great deal from the linear solution. The history curves, however, exhibited different periods of vibration. In general, the dominant period increased by 5% to 10%.

According to work and energy distribution time histories, the dissipated damping energy (for a 1.5% damping ratio) is over 70% of the work done for three bridge models. From Section 3.4.7, the results show that almost 50% of the work done was dissipated by damping if the damping ratio is equal to 0.25%. There was no nonlinear inelastic effects if the damping ratio is equal to (or, presumably, exceeds) 5%. These observations emphasize the importance of damping in the response.

4.2 CONCLUSION

This study as summarized in the previous section has developed a method of analysis, prepared a computer program and obtained a significant amount of numerical results that provide much understanding of the behavior of deck-type arch bridges subjected to earthquake ground motions.

Because of the capabilities of supercomputer, the arch bridge structures could be modelled in sufficient detail and subjected to

strong earthquake ground motions of a realistic duration. The nonlinear analyses had yielded responses that are more realistic than those obtainable using linear models of earlier studies, particularly when applied to models of the true three-dimensional kind.

The method of analysis described herein can provide a good basis for the development of design procedures. For consideration of design, the following improvements seem worthwhile for future study.

The results on nonlinear behavior obtained in this report are either for geometric nonlinearity (nonlinear elastic effects) only, or for material nonlinearity (nonlinear inelastic effects) only. Obviously, it is more realistic to consider both nonlinearities simultaneously.

For applications to the design of steel structures, the "octahedral yield surface" (which is linear or consists of planar surfaces) seems more appropriate than the spherical yield surface. The latter may over-estimate the strength of the element, and hence could err on the unconservative side.

The numerical results of this study have concentrated on steel deck-type arch bridges. They are only one kind of arch bridges. The other two types of steel arch bridges are tied through and tied half-through steel arch bridges. The responses of these types of arch bridges could be quite different from the responses of the deck-type. The analysis and the computer program developed in this study can, of course, be applied to these types of arch bridges.

The artificially generated ground motion CIT-A2 was used in this study. For purposes of design studies, additional ground motions should be used. A variety of other ground acceleration histories such as the type B, C and D artificially generated accelerograms (Ref. [18]) and the

records of actual earthquake ground motion such as the 1941 El Centro and 1971 San Fernando earthquakes may be used.

Another limitation of the study presented here is the assumption that the motions of all bridge supports are the same. The validity of this assumption obviously decreases with an increase in the span length of the bridge. Thus, effects of non-uniform motion of the supports would be a significant topic for future study. In Ref. [12], these effects were presented in a linearly elastic setting. Future work may consider non-uniform motion of the supports in a nonlinear response framework.

LIST OF REFERENCES

LIST OF REFERENCES

1. Abdel-Ghaffer, A. M., "Dynamic Analysis of Suspension Bridge Structures," California Institute of Technology, Report No. EERL 76-01, Earthquake Engineering Research Laboratory, Pasadena, California, May 1976.
2. Abdel-Ghaffar, A. M., "Free Torsional Vibrations of Suspension Bridges," Journal of the Structural Division, ASCE, April, 1979, pp. 767-788.
3. Abdel-Ghaffar, A. M., and Rood, J. D., "Simplified Earthquake Analysis of Suspension Bridge Towers," Journal of Engineering Mechanics Division, ASCE, April, 1982, pp. 291-308.
4. Abdel-Ghaffar, A. M., and Rubin, L. I., "Suspension Bridge Response to Multiple-Support Excitations," Journal of Engineering Mechanics Division, ASCE, April, 1982, pp. 419-435.
5. Abdel-Ghaffar, A. M., and Rubin, L. I., "Lateral Earthquake Response of Suspension Bridges," Preprint 82-051, American Society of Civil Engineers Convention, April, 1982, Las Vegas, Nevada.
6. Chen, W. F., and Atsuta, T., "Theory of Beam-Columns, Volume II: Space Behavior and Design," McGraw-Hill Book Company, 1977.
7. Cheng, F. Y., and Kitipitayangkul, P., "Investigation of the Effect of 3-D Parametric Earthquake Motions on Stability of Elastic and Inelastic Building Systems," Report to the National Sci. Foun., Dept. of Civil Eng., Univ. of Missouri-Rolla, Missouri, August, 1979.
8. Conner, J. J., Logcher, R. D., and Chan, S., "Nonlinear Analysis of Elastic Framed Structures," Journal of the Structural Division, ASCE, Vol. 94, No. ST6, June, 1968, pp. 1525-1547.
9. Drucker, D. C., "A More Fundamental Approach to Plastic Stress Strain Relations," Proceedings, 1st U. S. National Congress on Applied Mechanics, Chicago, 1951, pp. 487-491.
10. Dusseau, R. A., "Seismic Analysis of Two Steel Deck Arch Bridges," M.S. Thesis, Department of Civil Engineering, Michigan State University, 1981.
11. Dusseau, R. A., and Wen, R. K., "Seismic Responses of Two Deck Arch Bridges," Pre-print 82-010, American Society of Civil Engineers

Convention, Las Vegas, Nevada, April, 1982.

12. Dusseau, R. A., "Unequal Seismic Support of Steel Deck Arch Bridges," Ph.D. Thesis, Department of Civil and Environmental Engineering, Michigan State University, 1985.
13. Dusseau, R. A., and Wen, R. K., "Seismic Responses of Deck-Type Arch Bridges," *Earthquake Engineering and Structural Dynamics*, Vol. 18, 1989, pp. 701-715.
14. Gates, J. M., "Factors Considered in the Development of the California Seismic Design Criteria," *Proceedings of a Workshop on Earthquake Resistance of Highway Bridges*, Applied Technological Council, Palo Alto, California, January, 1979.
15. Hodge, H. G., "Plastic Analysis of Structures," McGraw-Hill Book Company, 1959.
16. Imbsen, R. A., Nutt, R. V., and Penzien, J., "Seismic Response of Bridges--Case Studies," UCB/EERC - 78/14, *Earthquake Engineering Research Center*, University of California, Berkeley, June, 1978.
17. Irvine, H. M., "The Estimation of Earthquake Generated Additional Tension in a Suspension Bridge Cable," *Earthquake Engineering and Structural Dynamics*, 1980, pp. 267-273.
18. Jennings, P. C., Housner, G. W., and Tsai, N. C., "Simulated Earthquake Motions," Report to the National Science Foundation, California Institute of Technology, Earthquake Engineering Research Laboratory, Pasadena, California, April, 1968.
19. Kuranishi, S., and Nakajima, A., "Strength Characteristics of Steel Arch Bridges Subjected to Longitudinal acceleration," *Structural Engineering Earthquake Engineering*, JSCE, Vol. 3, 1986, 287s-295s.
20. Mallett, R. H., and Marcal, P. V., "Finite Element Analyses of Nonlinear structures," *Journal of the Structural Division*, ASCE, Vol. 94, No. ST9, Sept., 1968, pp. 2081-2105.
21. Morris, G. A., and Fenves, S. J., "Approximate Yield Surface Equations," *Journal of the Engineering Mechanics Division*, ASCE, Vol. 95, No. EM4, August, 1969, pp. 937-954.
22. Morris, G. A., and Fenves, S. J., "Elastic-Plastic Analysis of Frameworks," *Journal of the Structural Division*, ASCE, Vol. 96, No. ST5, May, 1970, pp. 931-946.
23. Nigam, N. C., "Yielding in Framed Structures under Dynamic Loads," *Journal of the Engineering Mechanics Division*, ASCE, Vol. 96, No. EM5, October, 1970, pp. 687-709.
24. Oran, C., "Tangent Stiffness in Space Frames," *Journal of the Structural Division*, ASCE, Vol. 99, No. ST6, June, 1973, pp. 987-

1001.

25. Orbison, J., McQuire, W., and Abel, J., "Yield Surface Applications in Nonlinear Steel Frame Analysis," *Computer Methods in Applied Mechanics and Engineering*, Vol. 33, 1982, pp. 557-573.
26. Porter, F. L., and Powell, G. H., "Static and Dynamic Analysis of Inelastic Frame Structures," Report No. EERC 71-3, Earthquake Engineering Research Center, University of California, Berkeley, California, 1971.
27. Powell, G. H., "Theory of Nonlinear Elastic Structures," *Journal of the Structural Division, ASCE*, Vol. 95, No. ST12, December, 1969, pp. 2687-2701.
28. Riahi, A., Powell, G. H., and Mondkar, D. P., "3d Beam-Column Element (Type 2-Parallel Element Theory) for ANSR-II Program," Report No. UCB/EERC-79/31, Earthquake Engineering Research Center, University of California, Berkeley, California, 1980.
29. Row, D. G., Powell, G. H., and Mondkar, D. P., "2D Beam-Column Element (Type 5-Parallel Element Theory) for the ANSR-II Program," Report No. UCB/EERC-79/30, Earthquake Engineering Research Center, University of California, Berkeley, California, 1979.
30. Sakimoto, T., and Komatsu, S., "Ultimate Strength of Arches with Bracing Systems," *Journal of the Structural Division, ASCE*, Vol. 108, No. ST5, May, 1982, pp. 1064-1076.
31. Tebedge, N., and Chen, W. F., "Design Criteria for H-columns under Bi-axial Loading," *Journal of the Structural Division, ASCE*, Vol. 100, No. ST3, March, 1974, pp. 579-598.
32. Tezcan, S. S., and Mahapatra, B. C., "Tangent Stiffness Matrix for Space Frame Members," *Journal of the Structural Division, ASCE*, Vol. 95, No. ST6, June, 1969, pp. 1257-1270.
33. Thakkar, S. K., and Arya, A., "Dynamic Response of Arches Under Seismic Forces," proceedings, Fifth World Conference on Earthquake Engineering, Rome, Italy, 1973, pp. 952-956.
34. Toridis, T. G., and Khozeimeh, K., "Bifurcation, Pre- and Post-Buckling Analysis of Frame Structures," *Computers and Structures*, Vol. 8, 1978, pp. 667-678.
35. Tseng, W. S., and Penzien, J., "Analytical Investigations of the Seismic Response of Long Multiple Span Highway Bridges," Earthquake Engineering Research Center, Report No. EERC 73-12, June, 1973, University of California, Berkeley, California.
36. Tseng, W. S., and Penzien, J., "Seismic Analysis of Long Multi-span Highway Bridges," *Earthquake Engineering and Structural Dynamics*, Vol. 4, 1975, pp. 1-24.

37. Tseng, W. S., and Penzien, J., "Seismic Response of Long Multi-span Highway Bridges," *Earthquake Engineering and Structural Dynamics*, Vol. 4, 1975, pp. 25-48.
38. Wen, R. K., and Farhoomand, F., "Dynamic Analysis of Inelastic Space Frames," *Journal of the Engineering Mechanics Division, ASCE*, Vol. 96, No. EM5, October, 1970, pp. 667-686.
39. Wen, R. K., and Lange, J., "Curved Beam Element for Arch Buckling Analysis," *Journal of the Structural Division, ASCE*, November, 1981, pp. 2053-2069.
40. Wen, R. K., and Rahimzadeh, J., "Nonlinear Elastic Frame Analysis by Finite Element," *Journal of the Structural Division, ASCE*, Vol. 109, No. ST8, August, 1983, pp. 1952-1971.
41. Wen, R. K., Lee, C. M., and Alhamad, A., "Incremental Resistance and Deformation of Elasto-Plastic Beams," *Technical Notes, Journal of the Structural Division, ASCE*, Vol. 115, No. 5, May, 1989, pp. 1267-1271.
42. Yabuki, T., and Vinnakota, S., "Stability of Steel Arch-Bridges a State-of-the-Art Report," *S.M. Archives*, Vol. 9, 1984, pp. 115-158.

APPENDIX
PROPERTIES OF BRIDGE MODELS

APPENDIX
PROPERTIES OF BRIDGE MODELS

A.1 GENERAL

This appendix includes the description of the three bridge models in both the three- and two-dimensional cases as depicted in Figures 3-1 through 3-4. In conjunction with these figures, the data presented below completely define the bridge models used.

A.2 MEDIUM SPAN BRIDGE (TRUE 3-D)

A.2.1 NODAL DATA

In each line, the first value is node number (see Figure 3-1). The next six values are the boundary condition codes. (a "0" (zero) denotes "free" and "1" denotes "restrained".) The order is X translation, Y translation, Z translation, rotation about X, rotation about Y, and rotation about Z in standard cartesian coordinates system. The following three values are X, Y, and Z coordinate in feet.

1	1	1	1	1	0	0	0.0	0.0	26.0
2	0	0	0	1	0	0	0.0	133.5	26.0
3	1	1	1	1	0	0	0.0	0.0	0.0
4	0	0	0	1	0	0	0.0	133.5	0.0
5	0	0	0	0	0	0	87.5	53.047	26.0
6	0	0	0	0	0	0	87.5	133.5	26.0
7	0	0	0	0	0	0	87.5	53.047	0.0
8	0	0	0	0	0	0	87.5	133.5	0.0
9	0	0	0	0	0	0	175.0	90.937	26.0
10	0	0	0	0	0	0	175.0	133.5	26.0
11	0	0	0	0	0	0	175.0	90.937	0.0
12	0	0	0	0	0	0	175.0	133.5	0.0
13	0	0	0	0	0	0	262.5	113.672	26.0
14	0	0	0	0	0	0	262.5	133.5	26.0
15	0	0	0	0	0	0	262.5	113.672	0.0

16	0	0	0	0	0	0	262.5	133.5	0.0
17	0	0	0	0	0	0	350.0	121.25	26.0
18	0	0	0	0	0	0	350.0	133.5	26.0
19	0	0	0	0	0	0	350.0	121.25	0.0
20	0	0	0	0	0	0	350.0	133.5	0.0
21	0	0	0	0	0	0	437.5	113.672	26.0
22	0	0	0	0	0	0	437.5	133.5	26.0
23	0	0	0	0	0	0	437.5	113.672	0.0
24	0	0	0	0	0	0	437.5	133.5	0.0
25	0	0	0	0	0	0	525.0	90.937	26.0
26	0	0	0	0	0	0	525.0	133.5	26.0
27	0	0	0	0	0	0	525.0	90.937	0.0
28	0	0	0	0	0	0	525.0	133.5	0.0
29	0	0	0	0	0	0	612.5	53.047	26.0
30	0	0	0	0	0	0	612.5	133.5	26.0
31	0	0	0	0	0	0	612.5	53.047	0.0
32	0	0	0	0	0	0	612.5	133.5	0.0
33	1	1	1	1	0	0	700.0	0.0	26.0
34	0	0	0	1	0	0	700.0	133.5	26.0
35	1	1	1	1	0	0	700.0	0.0	0.0
36	0	0	0	1	0	0	700.0	133.5	0.0
37	1	1	1	1	1	1	0.0	133.5	-20.0
38	1	1	1	1	1	1	700.0	133.5	-20.0
39	1	1	1	1	1	1	-182.0	133.5	26.0
40	1	1	1	1	1	1	-182.0	133.5	0.0

A.2.2 TRUSS ELEMENTS

The four values in each line of this group are element number, global nodal number of end I, global nodal number of end J, and cross section area (ft²).

1	2	8	3.78
2	4	6	3.78
3	6	12	3.78
4	8	10	3.78
5	10	16	3.78
6	12	14	3.78
7	14	20	3.78
8	16	18	3.78
9	18	24	3.78
10	20	22	3.78
11	22	28	3.78
12	24	26	3.78
13	26	32	3.78
14	28	30	3.78
15	30	36	3.78
16	32	34	3.78
17	1	7	0.3881
18	3	5	0.3881
19	5	11	0.3881

20	7	9	0.3881
21	9	15	0.3881
22	11	13	0.3881
23	13	19	0.3881
24	15	17	0.3881
25	17	23	0.3881
26	19	21	0.3881
27	21	27	0.3881
28	23	25	0.3881
29	25	31	0.3881
30	27	29	0.3881
31	29	35	0.3881
32	31	33	0.3881
33	37	4	0.00489
34	38	36	0.00489
35	1	2	1.623
36	5	6	0.3264
37	9	10	0.3264
38	13	14	0.3264
39	17	18	0.3264
40	21	22	0.3264
41	25	26	0.3264
42	29	30	0.3264
43	34	33	1.623
44	3	4	1.623
45	7	8	0.3264
46	11	12	0.3264
47	15	16	0.3264
48	19	20	0.3264
49	23	24	0.3264
50	27	28	0.3264
51	31	32	0.3264
52	36	35	1.623
53	14	17	0.0144
54	17	22	0.0144
55	16	19	0.0144
56	19	24	0.0144
57	17	20	0.0144
58	18	19	0.0144
59	39	2	2.44
60	40	4	2.44

A.2.3 STRAIGHT BEAM ELEMENTS

The five values are property set number, axial area (ft^2), local x-x moment of inertia (ft^4), local y-y moment of inertia (ft^4), and torsion constant (ft^4).

1	0.78	2.18	3.72	1.36
---	------	------	------	------

The values in each line are element number, global nodal number

of end I, global nodal number of end J, and corresponding property set number of the straight beam element.

1	2	6	1
2	6	10	1
3	10	14	1
4	14	18	1
5	18	22	1
6	22	26	1
7	26	30	1
8	30	34	1
9	4	8	1
10	8	12	1
11	12	16	1
12	16	20	1
13	20	24	1
14	24	28	1
15	28	32	1
16	32	36	1

A.2.4 CURVED BEAM ELEMENTS

In this group of data, every four lines form a set of one kind of properties for a curved beam element. In each set, the four values in the first line are property set number, axial area (ft^2), local x-x moment of inertia (ft^4), local y-y moment of inertia (ft^4), and torsion constant (ft^4). The three values in the second line are axial yield force (kips), local y-y yield moment (kips-ft), and local x-x yield moment (kips-ft), respectively equal to P_0 , M_{y0} and M_{x0} in Eq. 2-20. The three values in the third line are local x-x yield rotation, local y-y yield rotation, and axial yield displacement (ft), respectively equal to θ_{xp} , θ_{yp} and Δ_p in Section 2.6.2. The two value in the last line are volume of the plastic hinge (ft^3) corresponding to local x-x bending and that to local y-y bending (ft^3), respectively equal to V_{hx} and V_{hy} in Section 2.6.1.

1	2.1180	3.4830	23.497	24.70
	10064.34	30034.75	12169.45	
	0.0025102	0.0027548	0.0068276	
	6.750	4.221		

2	2.5920	3.8020	32.397	25.010
	12316.52	39794.21	13770.57	
	0.0026019	0.0026473	0.0068276	
	11.250	4.221		
3	2.8290	3.9620	36.719	25.170
	13442.62	44603.56	14571.13	
	0.0026422	0.0026179	0.0068276	
	13.500	4.221		
4	2.3550	3.6420	27.990	24.850
	11190.43	34937.93	12970.01	
	0.0025581	0.0026902	0.0068276	
	9.000	4.221		

The values in each of the following lines are element number, global nodal number of end I, global nodal number of end J, and corresponding property set number of the curved beam element.

1	1	5	1
2	5	9	2
3	9	13	3
4	13	17	4
5	17	21	4
6	21	25	3
7	25	29	2
8	29	33	1
9	3	7	1
10	7	11	2
11	11	15	3
12	15	19	4
13	19	23	4
14	23	27	3
15	27	31	2
16	31	35	1

A.2.5 MASS

The four values in each line are global nodal number, mass in X direction, mass in Y direction, and mass in Z direction (kip-second²/ft).

2	3.8825	3.8825	3.8825
4	3.8825	3.8825	3.8825
6	7.765	7.765	7.765
8	7.765	7.765	7.765
10	7.765	7.765	7.765
12	7.765	7.765	7.765
14	7.765	7.765	7.765
16	7.765	7.765	7.765
18	7.765	7.765	7.765

20	7.765	7.765	7.765
22	7.765	7.765	7.765
24	7.765	7.765	7.765
26	7.765	7.765	7.765
28	7.765	7.765	7.765
30	7.765	7.765	7.765
32	7.765	7.765	7.765
34	3.8825	3.8825	3.8825
36	3.8825	3.8825	3.8825
5	5.125	5.125	5.125
7	5.125	5.125	5.125
9	5.125	5.125	5.125
11	5.125	5.125	5.125
13	5.125	5.125	5.125
15	5.125	5.125	5.125
17	5.125	5.125	5.125
19	5.125	5.125	5.125
21	5.125	5.125	5.125
23	5.125	5.125	5.125
25	5.125	5.125	5.125
27	5.125	5.125	5.125
29	5.125	5.125	5.125
31	5.125	5.125	5.125

A.2.6 DAMPING COEFFICIENTS

The Rayleigh damping constants α and β are equal to, respectively, 0.0483000 and 0.0039000.

A.3 SHORT SPAN BRIDGE (TRUE 3-D)

A.3.1 NODAL DATA

1	1	1	1	1	0	0	0.0	0.0	22.0
2	0	0	0	1	0	0	0.0	30.75	22.0
3	1	1	1	1	0	0	0.0	0.0	0.0
4	0	0	0	1	0	0	0.0	30.75	0.0
5	0	0	0	0	0	0	24.0	13.281	22.0
6	0	0	0	0	0	0	24.0	30.75	22.0
7	0	0	0	0	0	0	24.0	13.281	0.0
8	0	0	0	0	0	0	24.0	30.75	0.0
9	0	0	0	0	0	0	53.0	23.509	22.0
10	0	0	0	0	0	0	53.0	30.75	22.0
11	0	0	0	0	0	0	53.0	23.509	0.0
12	0	0	0	0	0	0	53.0	30.75	0.0
13	0	0	0	0	0	0	82.0	28.398	22.0
14	0	0	0	0	0	0	82.0	30.75	22.0
15	0	0	0	0	0	0	82.0	28.398	0.0
16	0	0	0	0	0	0	82.0	30.75	0.0
17	0	0	0	0	0	0	111.0	28.398	22.0
18	0	0	0	0	0	0	111.0	30.75	22.0
19	0	0	0	0	0	0	111.0	28.398	0.0
20	0	0	0	0	0	0	111.0	30.75	0.0

21	0	0	0	0	0	0	140.0	23.509	22.0
22	0	0	0	0	0	0	140.0	30.75	22.0
23	0	0	0	0	0	0	140.0	23.509	0.0
24	0	0	0	0	0	0	140.0	30.75	0.0
25	0	0	0	0	0	0	169.0	13.281	22.0
26	0	0	0	0	0	0	169.0	30.75	22.0
27	0	0	0	0	0	0	169.0	13.281	0.0
28	0	0	0	0	0	0	169.0	30.75	0.0
29	1	1	1	1	0	0	193.0	0.0	22.0
30	0	0	0	1	0	0	193.0	30.75	22.0
31	1	1	1	1	0	0	193.0	0.0	0.0
32	0	0	0	1	0	0	193.0	30.75	0.0
33	1	1	1	1	1	1	0.0	30.75	-10.0
34	1	1	1	1	1	1	193.0	30.75	-10.0

A.3.2 TRUSS ELEMENTS

1	1	7	0.064
2	3	5	0.064
3	5	11	0.064
4	7	9	0.064
5	9	15	0.064
6	11	13	0.064
7	13	19	0.064
8	15	17	0.064
9	17	23	0.064
10	19	21	0.064
11	21	27	0.064
12	23	25	0.064
13	25	31	0.064
14	27	29	0.064
15	2	8	0.303
16	4	6	0.303
17	6	12	0.303
18	8	10	0.303
19	10	16	0.303
20	12	14	0.303
21	14	20	0.303
22	16	18	0.303
23	18	24	0.303
24	20	22	0.303
25	22	28	0.303
26	24	26	0.303
27	26	32	0.303
28	28	30	0.303
29	13	18	0.048
30	14	17	0.048
31	15	20	0.048
32	16	19	0.048
33	1	2	0.1662
34	5	6	0.1662
35	9	10	0.1662
36	13	14	0.1662
37	17	18	0.1662

38	21	22	0.1662
39	25	26	0.1662
40	30	29	0.1662
41	3	4	0.1662
42	7	8	0.1662
43	11	12	0.1662
44	15	16	0.1662
45	19	20	0.1662
46	23	24	0.1662
47	27	28	0.1662
48	32	31	0.1662
49	14	15	0.303
50	13	16	0.303
51	17	20	0.303
52	18	19	0.303
53	33	4	0.000288
54	34	32	0.000288

A.3.3 STRAIGHT BEAM ELEMENTS

1	0.746	0.10	0.24	0.0002
1	2	6	1	
2	6	10	1	
3	10	14	1	
4	14	18	1	
5	18	22	1	
6	22	26	1	
7	26	30	1	
8	4	8	1	
9	8	12	1	
10	12	16	1	
11	16	20	1	
12	20	24	1	
13	24	28	1	
14	28	32	1	

A.3.4 CURVED BEAM ELEMENTS

1	0.9583	0.5465	1.726	1.168
	4554.000	5696.625	3112.313	
	0.0027275	0.0026023	0.0030108	
	1.9201390	0.8229166		
1	1	5	1	
2	5	9	1	
3	9	13	1	
4	13	17	1	
5	17	21	1	
6	21	25	1	
7	25	29	1	
8	3	7	1	
9	7	11	1	
10	11	15	1	
11	15	19	1	

12	19	23	1
13	23	27	1
14	27	31	1

A.3.5 MASS

2	1.91	1.91	1.91
4	1.91	1.91	1.91
6	4.21	4.21	4.21
8	4.21	4.21	4.21
10	4.61	4.61	4.61
12	4.61	4.61	4.61
14	4.61	4.61	4.61
16	4.61	4.61	4.61
18	4.61	4.61	4.61
20	4.61	4.61	4.61
22	4.61	4.61	4.61
24	4.61	4.61	4.61
26	4.21	4.21	4.21
28	4.21	4.21	4.21
30	1.91	1.91	1.91
32	1.91	1.91	1.91
5	1.08	1.08	1.08
7	1.08	1.08	1.08
9	1.18	1.18	1.18
11	1.18	1.18	1.18
13	1.18	1.18	1.18
15	1.18	1.18	1.18
17	1.18	1.18	1.18
19	1.18	1.18	1.18
21	1.18	1.18	1.18
23	1.18	1.18	1.18
25	1.08	1.08	1.08
27	1.08	1.08	1.08

A.3.6 DAMPING COEFFICIENTS
0.115000 0.0028000

A.4 LONG SPAN BRIDGE (ONE-PLANE 3-D)

A.4.1 NODAL DATA

1	1	1	1	1	1	0	0.0	0.0	0.0
2	0	0	0	0	0	0	0.0	416.0	0.0
3	1	1	1	1	1	1	-10.0	416.0	0.0
4	1	1	1	1	1	1	0.0	416.0	-10.0
5	1	1	1	1	1	1	0.0	0.0	0.0
6	0	0	0	0	0	0	121.43	98.164	0.0
7	0	0	0	0	0	0	121.43	416.0	0.0
8	0	0	0	0	0	0	242.86	181.226	0.0
9	0	0	0	0	0	0	242.86	416.0	0.0
10	0	0	0	0	0	0	364.29	249.186	0.0
11	0	0	0	0	0	0	364.29	416.0	0.0
12	0	0	0	0	0	0	485.71	302.039	0.0
13	0	0	0	0	0	0	485.71	416.0	0.0

14	0	0	0	0	0	0	607.14	339.795	0.0
15	0	0	0	0	0	0	607.14	416.0	0.0
16	0	0	0	0	0	0	728.57	362.449	0.0
17	0	0	0	0	0	0	728.57	416.0	0.0
18	0	0	0	0	0	0	850.00	370.0	0.0
19	0	0	0	0	0	0	850.00	416.0	0.0
20	0	0	0	0	0	0	971.43	362.449	0.0
21	0	0	0	0	0	0	971.43	416.0	0.0
22	0	0	0	0	0	0	1092.86	339.795	0.0
23	0	0	0	0	0	0	1092.86	416.0	0.0
24	0	0	0	0	0	0	1214.29	302.039	0.0
25	0	0	0	0	0	0	1214.29	416.0	0.0
26	0	0	0	0	0	0	1335.71	249.186	0.0
27	0	0	0	0	0	0	1335.71	416.0	0.0
28	0	0	0	0	0	0	1457.14	181.226	0.0
29	0	0	0	0	0	0	1457.14	416.0	0.0
30	0	0	0	0	0	0	1578.57	98.164	0.0
31	0	0	0	0	0	0	1578.57	416.0	0.0
32	1	1	1	1	1	0	1700.00	0.0	0.0
33	0	0	0	0	0	0	1700.00	416.0	0.0
34	1	1	1	1	1	1	1710.00	416.0	0.0
35	1	1	1	1	1	1	1700.00	416.0	-10.0
36	1	1	1	1	1	1	1700.00	0.0	0.0

A.4.2 TRUSS ELEMENTS

1	6	7	3.529
2	8	9	3.437
3	10	11	3.395
4	12	13	4.061
5	14	15	4.914
6	16	17	5.922
7	18	19	3.042
8	20	21	5.922
9	22	23	4.914
10	24	25	4.061
11	26	27	3.395
12	28	29	3.437
13	30	31	3.529
14	17	18	1.956
15	18	21	1.956
16	1	2	3.6279
17	33	32	3.6279
18	4	2	0.0028
19	35	33	0.0028

A.4.3 STRAIGHT BEAM ELEMENTS

1	1.00	1304.52	80.6544	12.804
2	0.00	0.00	0.00	347.475
3	3.04	12024.00	0.00	3960.96

1	2	7	1
2	7	9	1
3	9	11	1

4	11	13	1
5	13	15	1
6	15	17	1
7	17	19	1
8	19	21	1
9	21	23	1
10	23	25	1
11	25	27	1
12	27	29	1
13	29	31	1
14	31	33	1
15	3	2	2
16	33	34	2
17	19	18	3

A.4.4 CURVED BEAM ELEMENTS

1	14.428	24947.0	9775.0	1355.0
	103620.0	2678184.0	3730340.0	
	0.00258	0.0033	0.1054	
	1385.9	777.3		
2	13.840	23921.0	8823.0	1277.0
	97932.0	2368498.0	3525540.0	
	0.00254	0.0031	0.1031	
	1328.9	741.4		
3	13.080	22608.0	7606.0	1177.0
	92643.0	2096060.0	3335160.0	
	0.00254	0.0030	0.1008	
	1256.0	677.6		
4	12.370	21378.0	6464.0	1083.0
	87643.0	1853374.0	3155160.0	
	0.00255	0.0029	0.0984	
	1187.7	612.7		
5	11.690	20206.0	5378.0	994.0
	82849.0	1634933.0	2982580.0	
	0.00255	0.0029	0.0961	
	1122.6	544.6		
6	11.040	19077.0	4330.0	908.0
	78198.0	1435822.0	2815140.0	
	0.00254	0.0029	0.0938	
	1059.8	470.6		
7	10.400	17973.0	3307.0	824.0
	73624.0	1251613.0	2650480.0	
	0.00254	0.0031	0.0915	
	998.5	387.9		

1	1	6	1
2	6	8	2
3	8	10	3
4	10	12	4
5	12	14	5
6	14	16	6
7	16	18	7
8	18	20	7

9	20	22	6
10	22	24	5
11	24	26	4
12	26	28	3
13	28	30	2
14	30	32	1

A.4.5 MASS

2	30.9315	30.9315	30.9315
7	61.863	61.863	61.863
9	61.863	61.863	61.863
11	61.863	61.863	61.863
13	61.863	61.863	61.863
15	61.863	61.863	61.863
17	61.863	61.863	61.863
19	61.863	61.863	61.863
21	61.863	61.863	61.863
23	61.863	61.863	61.863
25	61.863	61.863	61.863
27	61.863	61.863	61.863
29	61.863	61.863	61.863
31	61.863	61.863	61.863
33	30.9315	30.9315	30.9315
6	55.963	55.963	55.963
8	55.963	55.963	55.963
10	55.963	55.963	55.963
12	55.963	55.963	55.963
14	55.963	55.963	55.963
16	55.963	55.963	55.963
18	55.963	55.963	55.963
20	55.963	55.963	55.963
22	55.963	55.963	55.963
24	55.963	55.963	55.963
26	55.963	55.963	55.963
28	55.963	55.963	55.963
30	55.963	55.963	55.963

A.4.6 DAMPING COEFFICIENTS

0.0406 0.0086

A.5 MEDIUM SPAN BRIDGE (2-D)A.5.1 NODAL DATA

1	1	1	1	1	1	0	0.0	0.0	0.0
2	0	0	1	1	1	0	0.0	133.5	0.0
3	0	0	1	1	1	0	175.0	90.937	0.0
4	0	0	1	1	1	0	175.0	133.5	0.0
5	0	0	1	1	1	0	350.0	121.25	0.0
6	0	0	1	1	1	0	350.0	133.5	0.0
7	0	0	1	1	1	0	525.0	90.937	0.0
8	0	0	1	1	1	0	525.0	133.5	0.0
9	1	1	1	1	1	0	700.0	0.0	0.0
10	0	0	1	1	1	0	700.0	133.5	0.0

11	1	1	1	1	1	1	1	-182.0	133.5	0.0
----	---	---	---	---	---	---	---	--------	-------	-----

A.5.2 TRUSS ELEMENTS

1	1	2	1.623
2	3	4	0.3264
3	5	6	0.3264
4	7	8	0.3264
5	10	9	1.623
6	11	2	2.44

A.5.3 STRAIGHT BEAM ELEMENTS

1	0.78	2.18	3.72	1.36
---	------	------	------	------

1	2	4	1
2	4	6	1
3	6	8	1
4	8	10	1

A.5.4 CURVED BEAM ELEMENTS

1	2.6559	3.939	35.990	21.01
	13768.186	48670.998	14413.960	
	0.0024828	0.0024828	0.0065172	
	11.250	4.221		
2	2.9058	4.126	41.580	24.75
	15063.667	56230.623	15098.248	
	0.0024828	0.0024828	0.0065172	
	11.81	4.430		

1	1	3	1
2	3	5	2
3	5	7	2
4	7	9	1

A.5.5 MASS

2	7.765	7.765	7.765
3	10.25	10.25	10.25
4	15.53	15.53	15.53
5	10.25	10.25	10.25
6	15.53	15.53	15.53
7	10.25	10.25	10.25
8	15.53	15.53	15.53
10	7.765	7.765	7.765

A.5.6 DAMPING COEFFICIENTS

0.048300	0.0039000
----------	-----------